NASA Technical Memorandum 78745

FLIGHT DEMONSTRATIONS OF CURVED, DESCENDING APPROACHES AND AUTOMATIC LANDINGS USING TIME REFERENCE SCANNING BEAM GUIDANCE

COMPILED BY:
WILLIAM F. WHITE

May 1978

NASA
National Aeronautics and Space Administration

Langley Research Center
Hampton, Virginia 23665

NASA Technical Memorandum 78745

FLIGHT DEMONSTRATIONS OF CURVED, DESCENDING APPROACHES AND AUTOMATIC LANDINGS USING TIME REFERENCE SCANNING BEAM GUIDANCE

Compiled by William F. White

May 1978

National Aeronautics and
Space Administration

Langley Research Center
Hampton, Virginia 23665

CONTENTS

Chapter

Chapter

Chapter

DEMONSTRATION OF AUTOMATIC CURVED, DESCENDING APPROACHES AND LANDINGS USING MICROWAVE LANDING SYSTEM GUIDANCE

Compiled by William F. White
Langley Research Center

SUMMARY

The NASA Langley Research Center's Terminal Configured Vehicle (TCV) program operates a Boeing 737 modified to include a second, research, cockpit and a large amount of experimental navigation, guidance and control equipment for research on advanced avionic systems. In the spring of 1975 the Federal Aviation Administration (FAA) requested that NASA use the TCV B-737 to provide a demonstration of the Time Referenced Scanning Beam (TRSB) microwave landing system which was being proposed by the United States to the International Civil Aviation Organization (ICAO) as a new international standard landing guidance system. This demonstration was to include curved approaches and automatic landings. Because of the short time available before the demonstration, it was not practical to develop new control laws optimized for the TRSB guidance. Instead, it was decided to use the existing control laws and aircraft systems with the least possible modifications.

Hardware changes to the aircraft included the addition of TRSB receiving equipment and antennas, and a separate digital computer to process the TRSB data along with interfaces to accept data from the TRSB equipment and transmit the processed data to the aircraft computers. The TRSB signals were first filtered using an α-β prefilter, then transformed from the conical TRSB coordinate system to a rectangular runway-based system. Estimates of position, velocity and acceleration were then generated by third order complementary filters. The processed data was then transformed into the several coordinate systems required by the navigation and flight control computers and transmitted to those computers.

All flight hardware and software (except for the TRSB receivers) was checked out and debugged to the extend practical in a laboratory simulation prior to installation of the new equipment in the aircraft. About two dozen flights were then conducted to check out the systems and adjust filter gains. Most of these flights were conducted at the demonstration site, the National Aviation Facilities Experimental Center (NAFEC) at Atlantic City, New Jersey. Development flights were conducted from late March through early May, 1976, often under adverse weather and wind conditions.

During May, 1976, 11 demonstration flights were made for members of ICAO, industry and government officials, and representatives of the media. Some of these flights were subject to adverse winds gusting to over 30 knots, large wind shears and moderate to severe turbulence. Analysis of onboard

recorded data from the inertial systems showed that the average flight was conducted with a 15 knot quartering tailwind at the flare point. All of the flights were tracked by the NAFEC phototheodolite system and the results have been statistically analyzed. For 50 approaches during the demonstration flights, the following results were obtained: the navigation system, using TRSB guidance, delivered the aircraft onto the 3 nautical mile final approach leg with an average overshoot of 25 feet past centerline, subject to a 2-σ dispersion of 90 feet. Lateral tracking data showed a mean error of 4.6 feet left of centerline at the Category I decision height (200 feet) and 2.7 feet left of centerline at the Category II decision height (100 feet). These values were subject to a 2-σ dispersion of about 10 feet. Finally, the glidepath tracking errors were 2.5 feet and 3.0 feet high at the Category I and II decision heights, respectively, with a 2-σ value of 6 feet.

INTRODUCTION

By William F. White

In the fall of 1977 the International Civil Aviation Organization (ICAO) is scheduled to meet and select a new international standard landing guidance system to replace the present Instrument Landing System (ILS) and Precision Approach Radar (PAR). Various types of microwave landings systems have been proposed by the United States, Australia, Britain, France and Germany. The United States has proposed a Time Reference Scanning Beam (TRSB) system.

Working Group A of the ICAO All Weather Operations Panel was given the responsibility of evaluating technical proposals for the landing system and making a recommendation to the parent body. As part of its technical presentation and demonstration to the AWOP group, the Federal Aviation Administration (FAA) requested that the Boeing 737 used in Langley Research Center's Terminal Configured Vehicle Program be modified to allow a demonstration of the use of the U. S. TRSB system by a transport type aircraft.

The demonstration provided by NASA included automatic area navigation (RNAV) flights into the TRSB coverage area, transition to TRSB guidance, curved descending approaches to a 3 mile final approach leg, and automatic landings with rollout under TRSB guidance. Two types of curved approaches were flown which were typical of the ICAO operational requirements. One was an S turn and the other a 130^{0} turn to final approach. Observer seating was rotated such that each person was able to watch one approach from the front cockpit and one approach from the aft research cockpit, where the automatic controls and the electronic displays were located. Observers who were not aboard a given flight could watch the path-following performance of the aircraft by means of real-time tracking data plots at the NAFEC range control station operated by the FAA.

The TCV B-737 automatic control systems were designed to use only conventional navigation aids and there was insufficient time for a development program to provide an optimized control system for TRSB. Therefore the changes to the existing navigation and guidance systems were kept to a minimum and the TRSB signal processing was done in a separate computer which was added to the aircraft. The TRSB data was processed and converted into the parameters which were normally used by the aircraft navigation and guidance equations. The main modifications to the existing systems were thus involved with the elimination of the smoothing which was normally done with Inertial Navigation System (INS) data.

Many people were involved in the design, development and testing which was required in order to prepare for the demonstration, and in its satisfactory

conduct. In this report they have described such aspects as airborne antennas and hardware, signal processing requirements and software, and modifications to the existing aircraft systems. Further, the entire system of airborne hardware and software had to be tested in a ground simulation facility in order to debug hardware interfaces and the software system as much as possible prior to flight testing. The design and construction of the ground simulation facility is also described. Other chapters describe the flight testing, airborne and ground data acquisition systems and data processing. A summary of the flight system performance during the ICAO demonstrations is also given.

I. Terminal Configured Vehicle Program Description

By Thomas M. Walsh

BACKGROUND

The growing congestion associated with the rapid expansion of air travel and the noise impact of the jet fleet on airport neighbors have led to technology developments in ground and airborne electronic systems and in noise suppression. In this area, the Department of Transportation (DOT) and the Federal Aviation Administration (FAA) have undertaken an effort to upgrade the air traffic control system. This revised system, know as the Upgraded Third-Generation Air Traffic Control System (UG3rd ATCS), has the following features (ref. I-1):

(1) Intermittent positive control
(2) Discrete address beacon system
(3) Area navigation
(4) Microwave landing system
(5) Upgraded air traffic control automation
(6) Airport surface traffic control
(7) Wake-vortex avoidance system
(8) Aeronautical satellites for transoceanic flight
(9) Automation of flight service stations

It is recognized that additional development and evaluation activities should make maximum use of the potential of these system developments. In formulating the joint DOT-NASA Civil Aviation Research and Development Policy Study Report (ref. I-2, p. 6-28) the question of U.S. Government conduct or support of demonstration programs in civil aviation is introduced with:

> "Demonstration programs are needed to prove out new systems and technologies, to assess market potentials, or to remove major institutional constraints temporarily. Demonstration programs are experiments designed to embrace new concepts, procedures, regulations, or the blending of new technologies into existing systems. These programs should collect information and required data in a real-world environment involving the ultimate users of the system. . "

In recognition of this need, the NASA Langley Research Center has implemented the Terminal Configured Vehicle (TCV) Program (ref. I-3). Its goal is to identify, evaluate, and demonstrate aircraft and flight management technology that will improve the efficiency and acceptability of conventional aircraft in terminal-area operations. The reason for

emphasis on terminal-area operations (fig. I-1) is that this region is recognized as the system bottleneck as well as the major area of possible unfavorable impact with the community environment.

GENERAL PROGRAM OVERVIEW

It has been recognized that new ATC equipment and procedures cannot solve the problems that they are intended to solve unless the airborne systems and flight procedures are developed to take full advantage of the capabilities of the ground-based facilities. The airborne system is considered to be the basic airframe and equipment, the flight-control systems (automatic and piloted modes), the displays for monitoring or pilot control, and the crew as manager and operator of the system. Because of the urgent need to develop the required airborne system capability, the NASA Langley Research Center has implemented a long-term research effort known as the Terminal Configured Vehicle Program. The program is conducting analytical, simulation, and flight-test work to develop advanced flight-control capability for

- 4-D RNAV and transition to MLS
- Precision, curved, steep, decelerating, and time-sequenced approaches utilizing MLS
- Zero-visibility landings through turnoff

This capability will be developed by means of

- Advanced automatic controls
- Advanced pilot displays for monitoring and control
- Reduced crew workload
- Improved interfaces of avionics, aircraft, and crew
- Advanced airframe configurations

The TCV Program is conducting analytical, simulation, and flight test research which will support improvements in (1) terminal-area capacity and efficiency, (2) approach and landing capability in adverse weather, and (3) operating procedures to reduce noise impact. The primary facility used in the flight research is a Boeing 737 airplane (fig. I-2) equipped with onboard reprogrammable all-digital integrated navigation, guidance, control, and display systems.

In the TCV Program research, major emphasis is being place on the development of advanced concepts for applications to avionics and displays for aircraft operations in the UG3rd and post-UG3rd ATCS's. Particular emphasis is being placed on operations in an MLS environment. One example of this effort is the participation of NASA through its TCV Program with the FAA in the demonstration of the U.S. national microwave landing system to the All Weather Operations Panel of the International Civil Aviation Organization (ICAO).

TCV B-737 DESCRIPTION

A cutaway view of the airplane, shown in figure I-3, illustrates the palletized installation of the experimental avionics and depicts a second cockpit for research (aft flight deck, AFD). The value of this system for research purposes is enhanced by several notable design features:

(a) The system functions are controllable and variable through software.

(b) The hardware is easily removed, modified, repaired, and installed.

(c) Flight station changes are readily accomplished in the research cockpit, which has a fly-by-wire implementation for control of the airplane.

The arrangement of the AFD is shown in the photograph of figure I-4. The center area of the cockpit is seen to resemble a conventional 737 cockpit, whereas the area immediately in front of the pilot and copilot has been opened up by removing the wheel and wheel column and replacing them with "brolly handle" controllers. This open area has been utilized as the location for advanced electronic displays. The displays illustrated in figure I-4 consist of an electronic attitude director indicator (EADI) at the top, the electronic horizontal situation indicator (EHSI) in the middle, and the navigation control display unit (NCDU) at the bottom. A control mode select panel is shown located at the top of the instrument panel and centered between the two pilots. The display system is all digital and can be readily reprogramed with regard to formats and symbology for research purposes. The NCDU is used to call up preplanned routes and flight profile information or for entering new or revised information to be displayed. Inserted information and flight progress information can be called up on the NCDU for review. The EADI instrument provides basic attitude information to control the airplane; the EHSI shows the horizontal plan of the flight, either with a heading-up or north-up mode, and the flight progress.

TCV PROGRAM GOALS

The basic goals of the TCV Program are illustrated in figure I-5. As seen in this figure, operations in the MLS environment can, perhaps with proper controls and displays, allow operators to take advantage of steep, decelerating curved approaches with close-in capture which result in shorter common paths. These paths can be planned for reduced noise over heavily populated areas and for increased airport capacity. Onboard precision navigation and guidance systems including displays are required for 3-D and 4-D navigation and for sequencing and closer lateral runway spacing. Displays are under development with the intent of achieving lower visibility operations in this future environment with sufficient confidence that they become routine. Finally, programmed turnoffs at relatively high speed should clear the runway to allow operations to proceed with perhaps 40 to 45 seconds between aircraft, should the vortex-wake problems be solved.

REFERENCES

I-1. An Overview of the FAA Engineering and Development Programs, 1973-1974. FAA-EM-73-2, Mar. 1973.

I-2. Joint DOT-NASA Civil Aviation Research and Development Policy Study-Supporting Papers. DOT TST-10-5, NASA SP-266, 1971.

I-3. Reeder, John P.; Taylor, Robert T.; and Walsh, Thomas M.: New Design and Operating Techniques and Requirements for Improved Aircraft Terminal Area Operations. NASA TM X-72006, 1974.

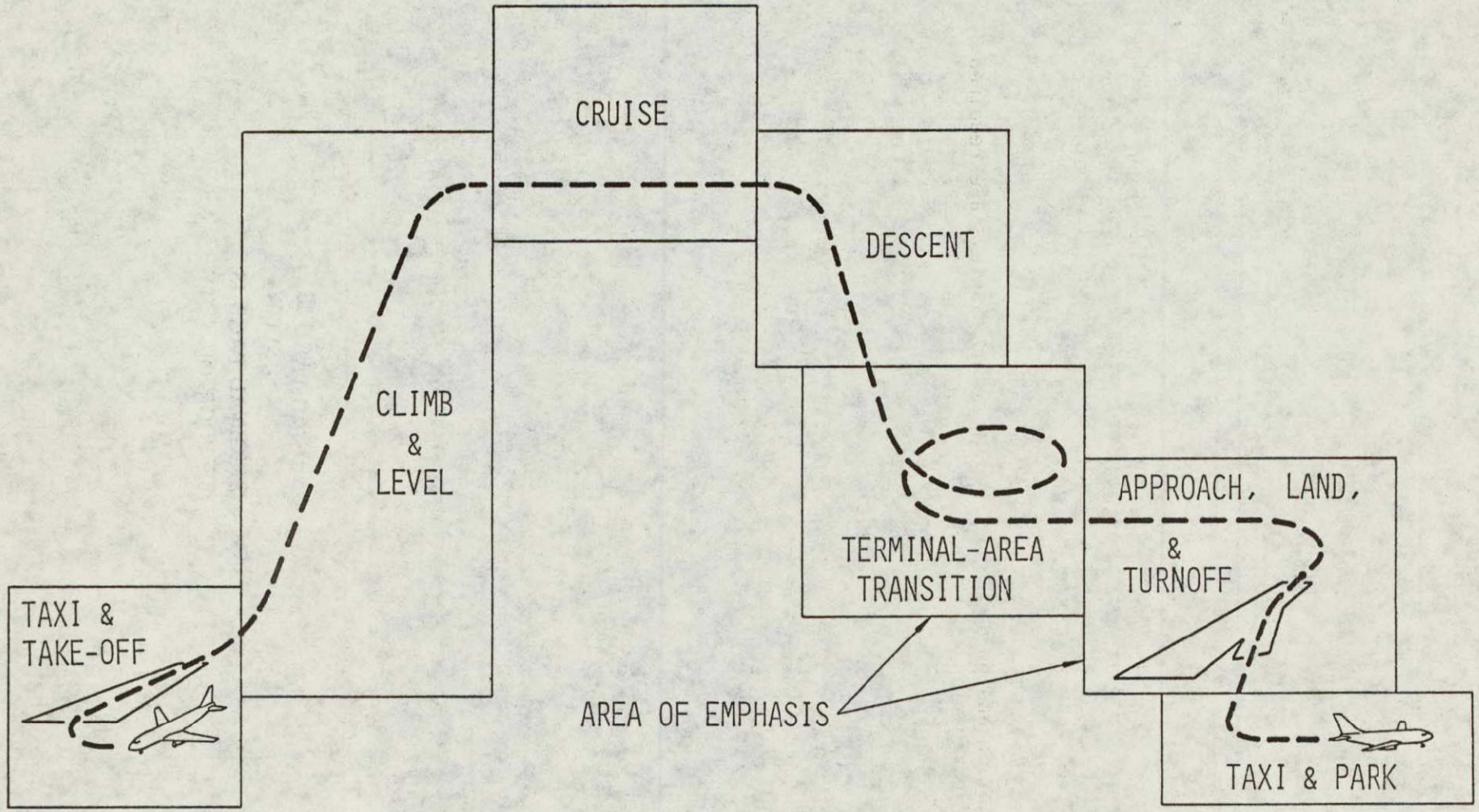

FIGURE I-1. FLIGHT MODES AND AREAS OF EMPHASIS
IN TERMINAL CONFIGURED VEHICLE PROGRAM

FIGURE I-2 TERMINAL CONFIGURED VEHICLE PROGRAM RESEARCH AIRPLANE

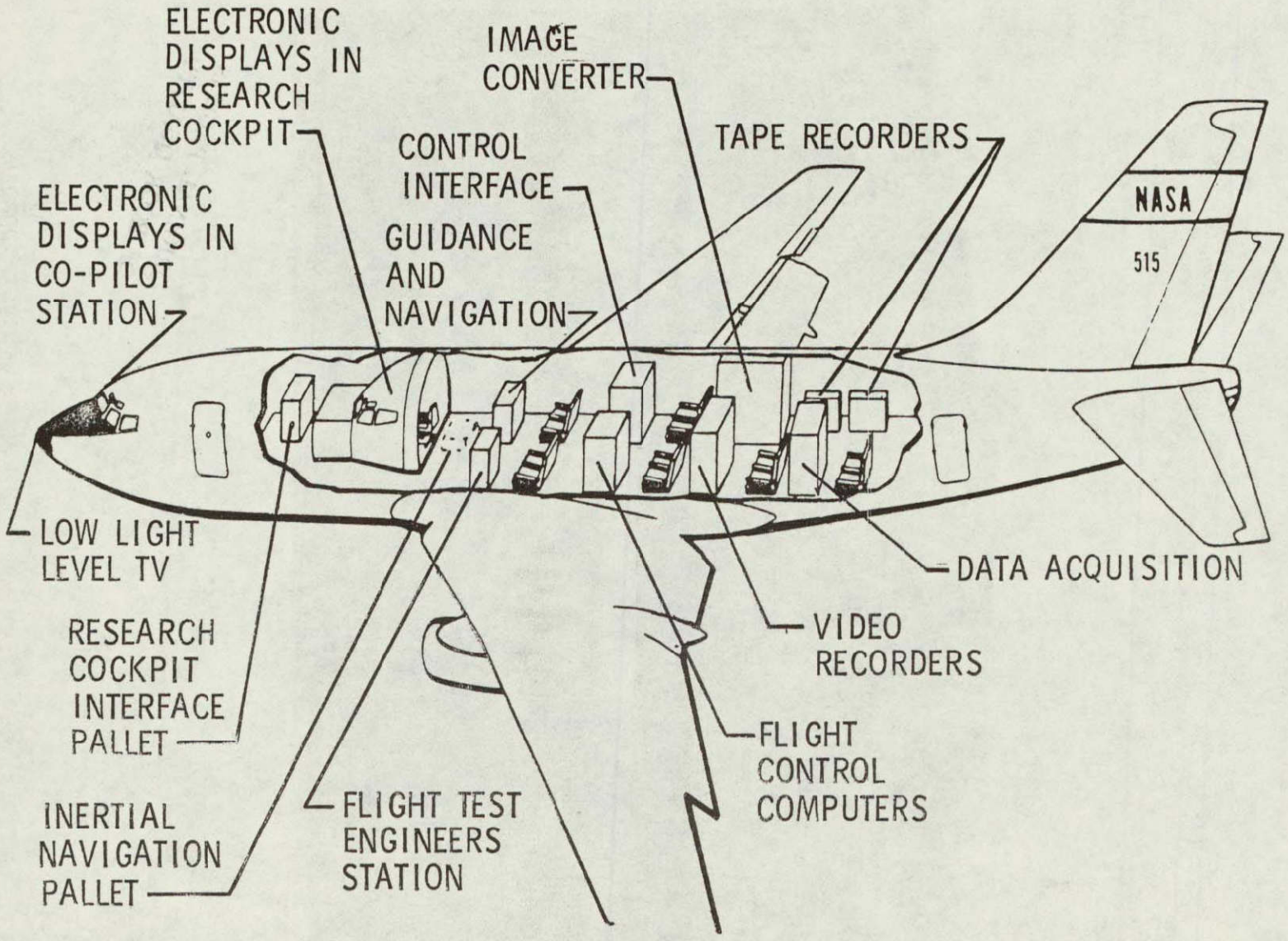

FIGURE I-3 RESEARCH SUPPORT FLIGHT SYSTEM INTERNAL ARRANGEMENT

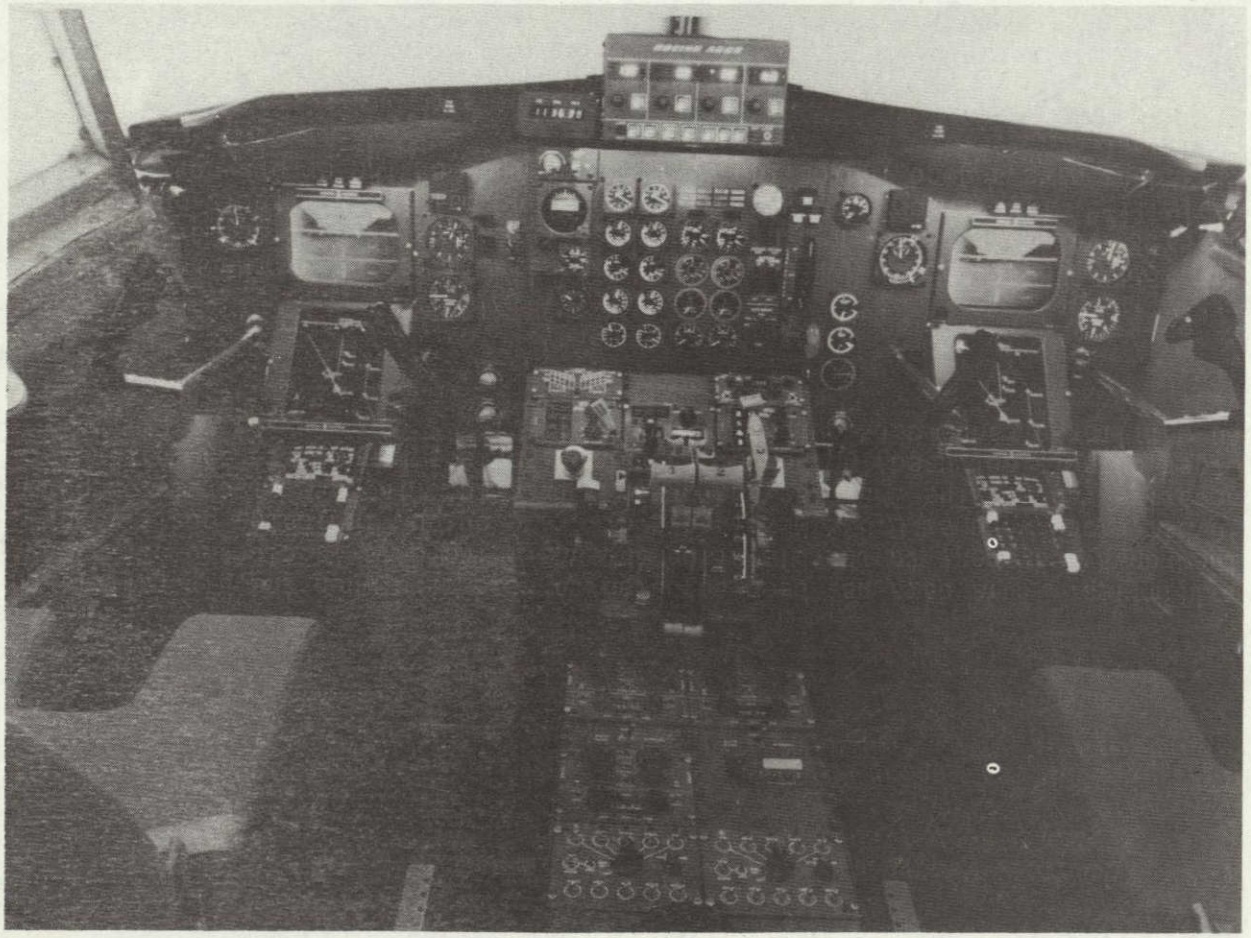

FIGURE I-4 AFT FLIGHT DECK DISPLAY ARRANGEMENT

IDENTIFY CTOL AIRCRAFT SYSTEMS AND FLIGHT MANAGEMENT TECHNOLOGY FOR HIGH CAPACITY TERMINAL AREA MANUAL AND AUTOMATIC OPERATIONS IN LOW VISIBILITY

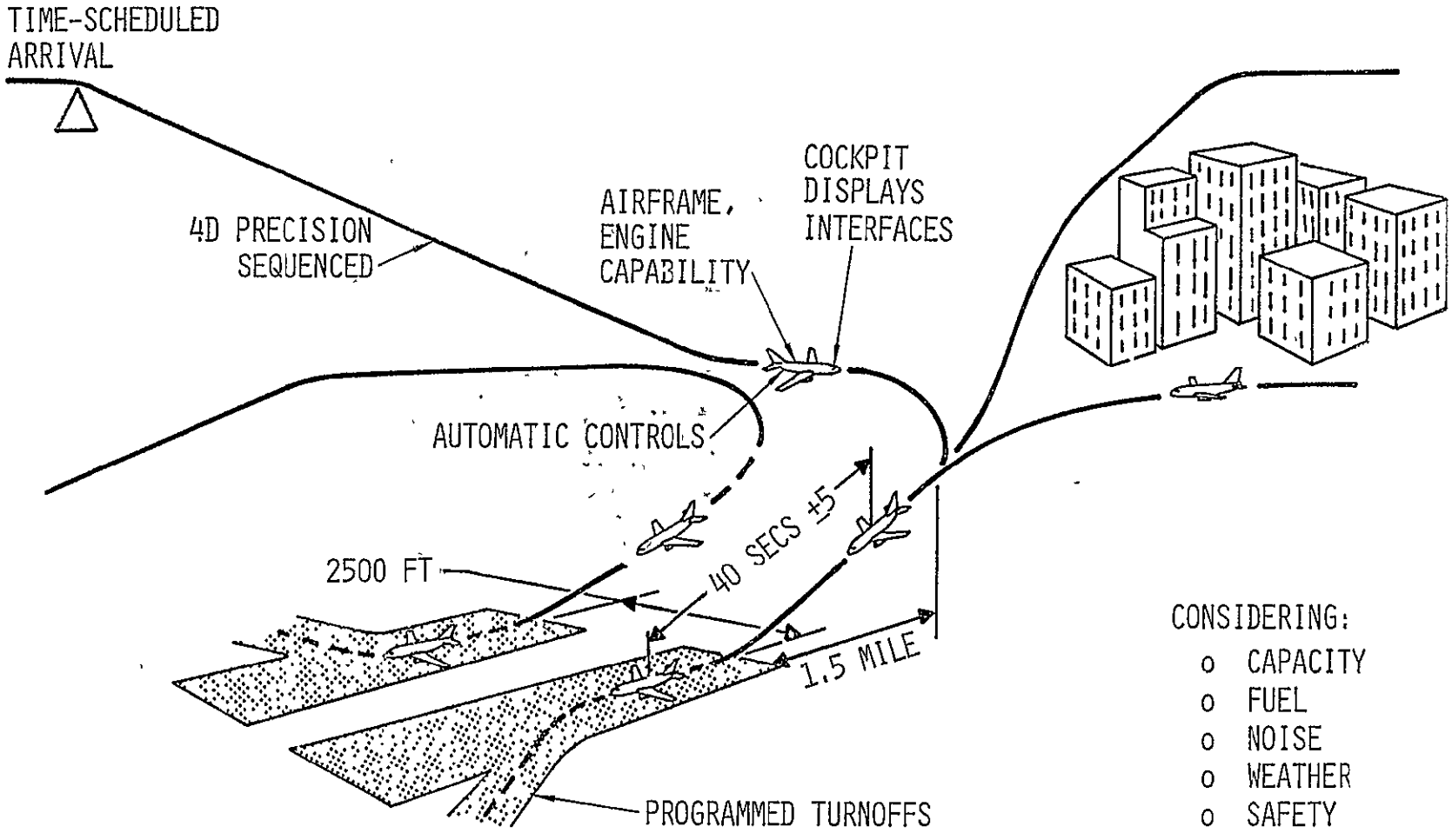

FIGURE I-5 TERMINAL CONFIGURED VEHICLE OPERATIONAL GOALS

II. THE TIME REFERENCE SCANNING BEAM MICROWAVE LANDING SYSTEM

By William T. Bundick

BACKGROUND

The U. S. candidate Microwave Landing System (MLS), the Time Reference Scanning Beam (TRSB) system, is being developed by the FAA in a three phase program which began in 1971. Phase I was a basic engineering design, or study, phase. In Phase II four companies (Hazeltine, ITT Gilfillan, Texas Instruments, and Bendix) each designed, fabricated, and tested a feasibility demonstration system. It was the Bendix Phase II system, after modification to the time reference format, that was utilized in the ICAO demonstration flights at NAFEC. In Phase III, currently underway, Bendix and Texas Instruments are each designing and fabricating prototype TRSB systems for testing at NAFEC, Crow's Landing, and several other sites.

GENERAL DESCRIPTION

The TRSB MLS is an air-derived system. By air-derived, it is meant that the position information is obtained by measurements made in the aircraft on a signal in space rather than by measurements made by the ground equipment and transmitted to the aircraft, as in GCA. By TRSB it is meant that the basic measurement is a measurement of the time between the passage of two scanning beams.

The signal in space is generated by transmitting an unmodulated signal via a narrow fan beam antenna while the antenna makes a to-fro scan through the desired volumetric coverage in space, as shown in Figure II-1. Assume an aircraft is located at an angle θ as illustrated in Figure II-2a. The angle θ is uniquely related to the time between passage of the "to" and "fro" beams, as shown in Figure II-2b. A pulse is received by the aircraft receiver each time the beam sweeps past, as shown in Figure II-2c, and the angle θ is determined by measuring the time Δt between the "to" and "fro" pulses.

The technique just described measures one angular coordinate of the aircraft. To uniquely determine aircraft position, two angular coordinates plus range are required. This is accomplished by employing two separate transmitters and antennas, one scanning in the azimuth direction and the other in the elevation direction. The azimuth antenna is normally located beyond the stop end of the runway to provide azimuth information during rollout, and the elevation (EL-1) antenna is located beside the runway next to the glide path intercept point (GPIP). The DME is located near the azimuth site and is similar in concept to a standard TACAN DME.

When an aircraft comes down the glide path and flares, it will pass the GPIP and thus fly out of the elevation antenna coverage before touchdown. To provide elevation guidance during flare, a flare (EL-2) transmitter and antenna are positioned beside the runway some 2000 feet beyond the elevation site at Category III installations. Also, Category III installations will include a Back Azimuth transmitter and antenna before threshold on the approach end of the runway to provide azimuth guidance during missed approaches and takeoffs.

The Azimuth, Elevation, Flare, and Back Azimuth functions are time multiplexed with the format shown in Figure II-3. Also included in the format are time slots for the transmission of such data as RVR, runway identification, and MLS/runway geometry, and for the future addition of 360^{o} azimuth function. The data rate for the azimuth function is 13.5 samples per second, and the rates for Elevation and Flare are each 40.5 samples per second. These rates are average. On a sample-to-sample basis the period is not constant, but jitter is introduced to reduce the effects of synchronous interference such as propellor modulation. At the beginning of each function time slot, a preamble is transmitted throughout the volumetric coverage via a sector-omni antenna using DPSK modulation. This preamble data includes a Barker code for synchronization and function identification. The DME is not time multiplexed with the angle information, but it is transmitted asynchronously at a different frequency. The nominal DME data rate is 40 Hz.

Background information on the MLS can be found in references II-1 through II-3, and further information on the TRSB system is contained in references II-4 through II-6.

THE NAFEC MLS

The TRSB system demonstrated for ICAO was the system installed at NAFEC. The characteristics of that system are listed in Table II-1.

TABLE II-1. - NAFEC TRSB SYSTEM CHARACTERISTICS

Parameter	Value
Approach Azimuth	
Scan coverage	$\pm 60^{o}$
Vertical coverage	0 to 20^{o}
Range coverage	>22 nautical miles
Beamwidth: scanned direction	1^{o}
orthogonal to scan	7.5^{o}
Data rate	13.5 updates/second
Vertical multipath reduction provisions	Sharp elevation pattern cutoff at horizon

-continued-

TABLE II-1. - NAFEC TRSB SYSTEM CHARACTERISTICS (cont.)

Parameter	Value
Transmitter frequency	5189.4 MHz
Transmitter power	20 watts
Approach Elevation	
Scan coverage	1^{o} to 20^{o}
Lateral coverage	120^{o}
Range coverage	>20 nautical miles
Beamwidth: scanned direction	1^{o}
orthogonal to scan	120^{o}
Data rate	40.5 updates/second
Scan rate	20^{o}/millisecond
Transmitter frequency	5189.4 MHz
Transmitter power	20 watts
Missed Approach Azimuth	
Scan coverage	$\pm 40^{o}$
Vertical coverage	1^{o} to 20^{o}
Range coverage	>7 nautical miles
Beamwidth: scanned direction	3^{o}
orthogonal to scan	7.5^{o}
Data rate	6.75 updates/second
Scan rate	20^{o}/millisecond
Vertical multipath reduction provision	Sharp elevation pattern cutoff at horizon
Transmitter frequency	5189.4 MHz
Transmitter power	20 watts
Flare Elevation	
Scan coverage	-0.5^{o} to 8.5^{o}
Lateral coverage	20^{o}
Range coverage	>7 nautical miles
Touchdown area coverage (abeam Flare Elevation position at runway centerline	500 to 3000 feet down to heights of 8 feet above runway
Beamwidth: scanned direction	0.5^{o}
orthogonal to scan	20^{o}
Data rate	40.5 updates/second
Scan rate	10^{o}/millisecond
Transmitter frequency	15,468.4 MHz
Transmitter power	20 watts

-continued-

TABLE II-1. - NAFEC TRSB SYSTEM CHARACTERISTICS (cont.)

Parameter		Value
Distance Measuring Equipment (DME)		
Angle coverage		120^{o} lateral, 20^{o} vertical
Range coverage		>22 nautical miles
Beamwidth: azimuth		120^{o}
elevation		7.5^{o}
Data rate		40 updates/second
Vertical multipath reduction provision		Sharp elevation pattern cutoff at horizon
Transmitter frequency:	G/A	5027 MHz
	A/G	5092 MHz
Transmitter power:	G/A	250 watts peak
	A/G	250 watts peak

Several items from the table are worthy of brief discussion. The one degree beamwidths for the AZ and EL antennas are the beamwidths planned for future use at long (13,000 feet) runways and at Category III installations. Wider beamwidths are planned for other installations. The NAFEC flare system operated at Ku-band, but future flare systems may operate at the same frequency (C-band) as AZ and EL. The DME was a special design, similar in concept to a standard DME, that operated at C-band. Phase III DME's will be L-band systems.

The azimuth scanning beam antenna was a 12 foot phased array whose 117 elements were 4 foot vertical slotted waveguides. This vertical aperture was used to obtain the desired radiation pattern in the vertical, or non-scan, direction. The AZ/DME installation is pictured in Figure II-4. The elevation scanning beam antenna was a 12 foot phased array whose 81 elements were dipoles with a metal plate along each side to shape the pattern in the horizontal plane. The EL-1 site is picture in Figure II-5. The flare antenna, pictured in Figure II-6, was an 8 foot phased array of 139 dipoles. The polarization was vertical in all cases.

Since the scanning beam antennas were linear phased arrays, the natural coordinate system was conical. As the antenna scanned off broadside, the fan beam assumed the shape of a sector of a cone rather than a plane, that is, the locus of constant angle (azimuth or elevation) is the surface of a cone with apex at the antenna and axis along the line of the linear array as in Figure II-7. The system was installed on runway 4. The geometry of the installation is shown in Figure II-8.

MLS AVIONICS

The MLS airborne equipment used in the ICA demonstration included an angle receiver, a DME interrogator/receiver, a DME power supply, and antennas. Characteristics of this equipment are listed in Table II-2.

TABLE II-2. - ANGLE RECEIVER CHARACTERISTICS

Parameter	Value
AZ, EL, BAZ (C-band)	
Noise figure	11 dB
IF bandwidth	150 kHz
Sensitivity[1]	-94 dBm
DPSK sensitivity[2]	-100.6 dBm
FL (Ku-band)	
Noise figure	15 dB
IF bandwidth[3]	150 kHz
Sensitivity[1]	-96 dBm

Notes:

1. Minimum signal at receiver input such that function flag is not displayed
2. Signal level for correctly decoding 11-bit preamble with probability of 0.998
3. Ku-band channel uses same IF section as C-band functions

The angle receiver contains a considerable amount of logic to reject multipath signals and to validate the data. Tracking gates are kept centered on the received "to-fro" pulses. The amplitudes of pulses received outside the tracking gates are continually compared with the amplitudes of the pulses within the tracking gates, the latter pulses normally being the direct signal. On a scan-by-scan basis if an outside pulse amplitude exceeds the inside pulse amplitude, a confidence counter is decremented; if the inside pulse amplitude is greater, the counter is incremented. Thus, whenever the outside amplitude is greater for more than 50 percent of the scans on the average, the counter will count down toward zero, and a function flag will be raised. There are separate counters and separate flags for each function (AZ, EL-1, and EL-2).

Any time that a valid function identification word is not decoded at the beginning of a preamble, a frame flag is raised. There is only one frame flag for all functions since the frame flag is raised and lowered on a scan-by-scan basis. The frame flag is also raised on any scan for which more than one beam (pulse) exceeded the beam threshold. The beam threshold is nominally 3 dB below the maximum peak within the tracking gate and is set on each scan. The frame flag is not a receiver output, but it does suppress one of the receiver clock outputs used to clock out data.

The filtered data output is slew rate limited, that is, any time the angular rate of the filtered angle data output exceeds 1 degree/second a slew rate flag is raised. This flag is not output.

There is a second counter for each function called an acquisition counter. The frame flag and the slew rate flag control the state of this counter, as shown in Figure II-9. If either flag is displayed, the counter decrements; otherwise it increments. If either flag is present continuously for longer than 1 second or if a flag is present for more than 50 percent of the time on the average, a function flag is generated.

The receiver angle data output is in the form of a 16 bit binary word, output once per scan, with the least significant bit representing 2.2552 millidegrees. A discrete output indicates positive or negative angles, and the data word is clocked out by a 16 bit clock at 1.108 MHz. This clock is suppressed on any scan for which there is a frame flag. All angle data is output on the same line, and separate discrete, or gate, outputs indicate which function is being output. Other angle receiver outputs, which were not used in the demonstration, include a filtered data output and the function flags. The filtered data is filtered by a digital low pass filter with a cut-off frequency of 10 radians/second.

The DME interrogator/receiver transmits a pulse pair to the ground transponder, which then transmits back a pulse pair reply. Range is determined by measuring the elapsed time between transmission and reception of the pulses. A range gate tracks the received pulses. The system will operate in the track mode as long as two valid replies are received within the range gate out of eight interrogations. If this criterion is not met, the DME tracking flag is raised, and the system begins searching for a valid reply. If the DME remains in the search mode for approximately 6.4 seconds, the DME flag is raised. During this time the output data is in a "flywheel" mode, that is, the output range is a predicted value based on the last good measurement of range and range rate.

The DME range output has been filtered by a digital moving window filter, which averages with equal weight the eight most recent range measurements. This same filter also estimates the range rate. The range output is in the form of a 16 bit binary word with a least significant bit representing 0.5

millimiles. This data has been adjusted to read zero when the aircraft is on the runway adjacent to the Elevation antenna. The data is clocked out by a 16 bit clock word at 0.632 MHz, and a discrete output indicates positive or negative range. The DME flag and the DME tracking flag are discrete outputs. Other outputs not used in the demonstration include range rate and altitude. An unfiltered range data output is not available.

TRSB ACCURACY

The TRSB system at NAFEC has been extensively tested by the FAA, and the overall system errors as measured in these tests are briefly summarized in Table II-3. The errors may vary with range and multipath effects but Table II-3 does give a good indication of the magnitude of the errors normally to be expected.

TABLE II-3. - SUMMARY OF NAFEC TRSB TEST RESULTS

Function	Bias error (2σ)	Noise error (2σ)
Azimuth	0.025^{o}	0.020^{o}
Elevation	0.025^{o}	0.020^{o}
Flare	1.2 ft	1.4 ft
DME[1]	15.0 ft	15.0 ft

1. In flare region

REFERENCES

II-1. Anon.: A New Guidance System for Approach and Landing. Report of Special Committee 117, Radio Technical Commission for Aeronautics, December 1970.

II-2. International Microwave Landing System (MLS) Symposium. Report No. FAA-RD-74-56, April 1974.

II-3. Technical Progress in the U. S. Development of a Microwave Landing System. Report No. FAA-RD-74-187, July 1974.

II-4. Del Balzo, Joseph M., and Jones, Stanley R.: United States Program to ICAO for a New Non-Visual Approach and Landing System. AGARD Conference Proceedings No. 188, Plans and Develpment for Air Traffic Systems.

II-5. Kelly, R. J.: Time Reference Microwave Landing System Multipath Control Techniques. J. of the Inst. of Nav., Vol. 23, No. 1, Spring 1976, pp. 42-58.

II-6. Kelly, Robert J.: Guidance Accuracy Consideration for the Microwave Landing System. NAECON '76.

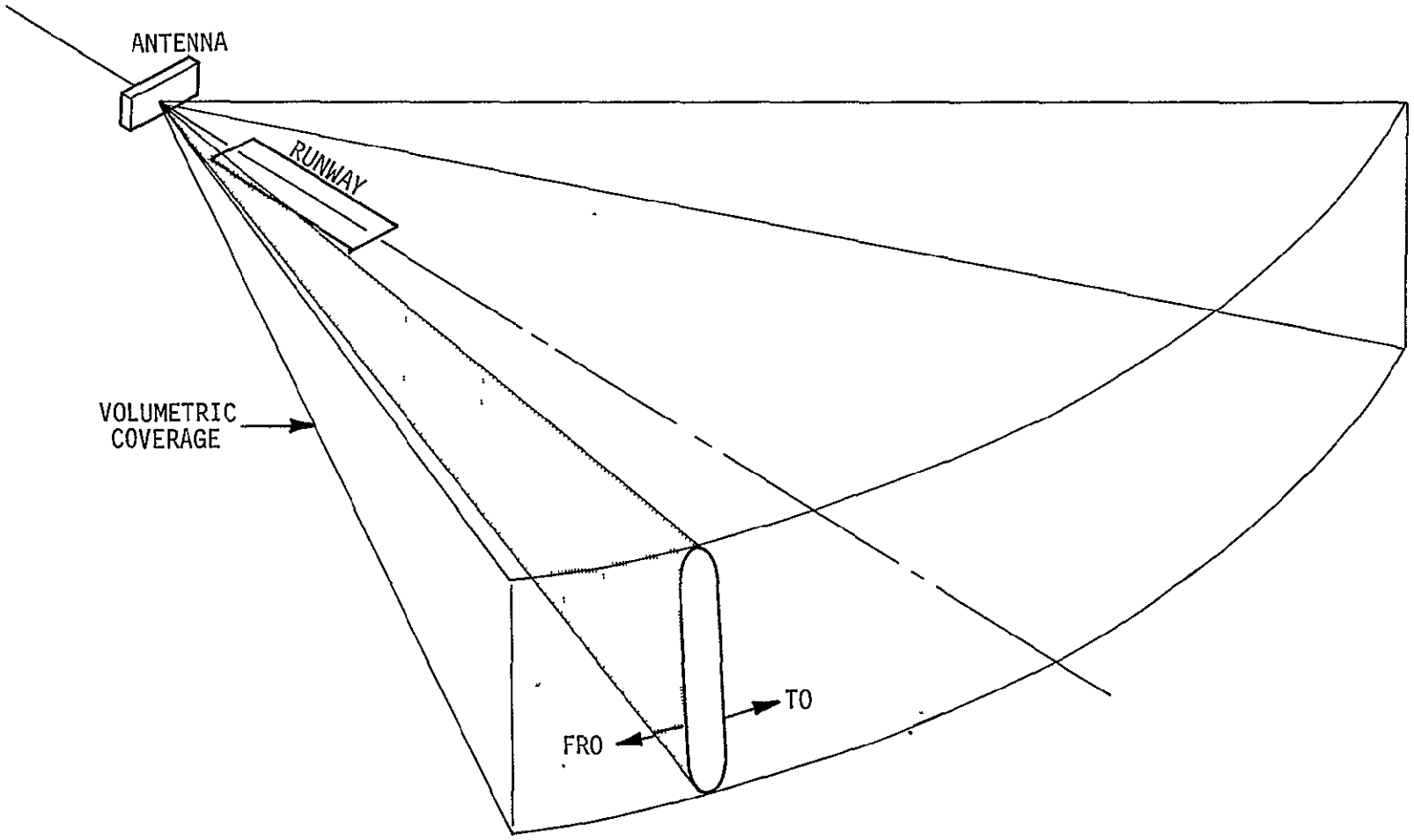

FIGURE II-1 TRSB "TO-FRO" SWEEP TECHNIQUE

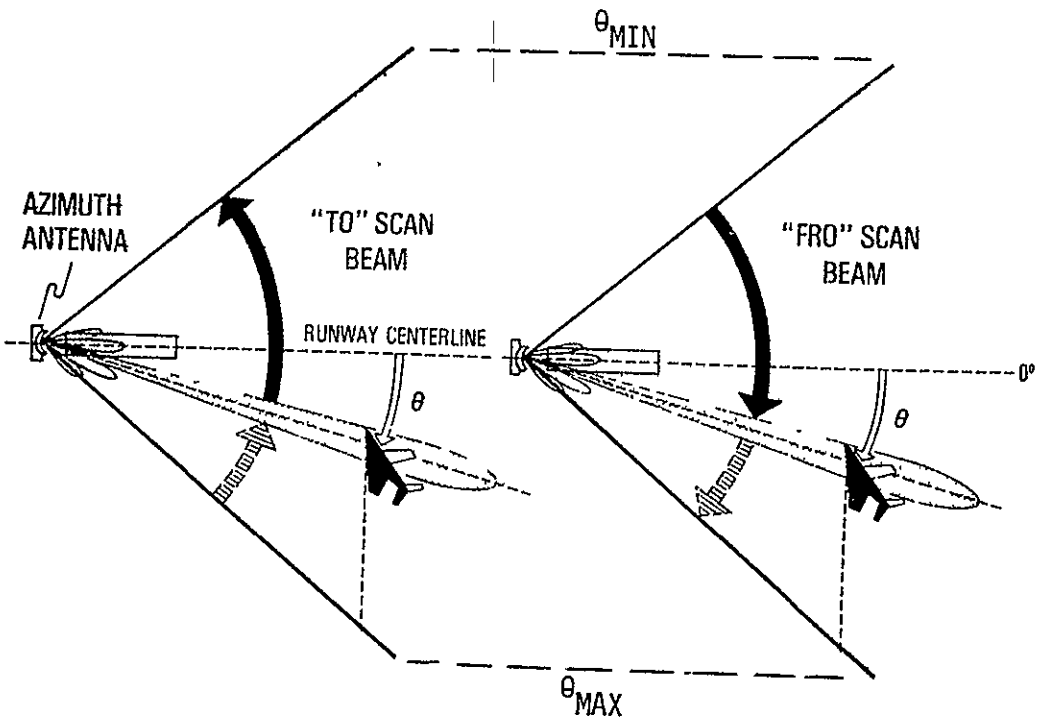

(A) AIRCRAFT AT AZIMUTH ANGLE θ

FIGURE II-2 TRSB TIME MEASUREMENT TECHNIQUE

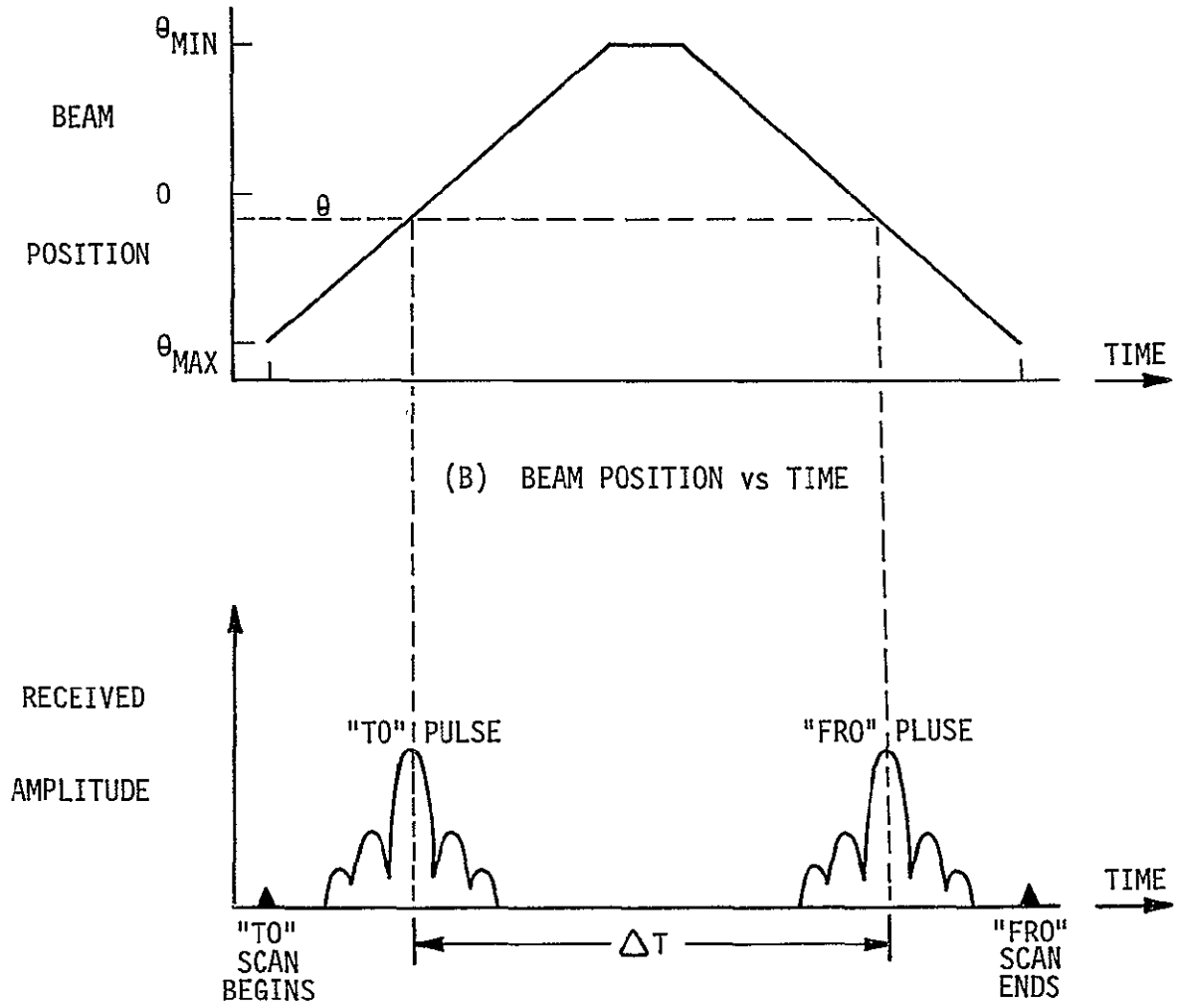

(B) RECEIVED PULSES vs TIME

FIGURE II-2 TRSB TIME MEASUREMENT TECHNIQUE - CONCLUDED

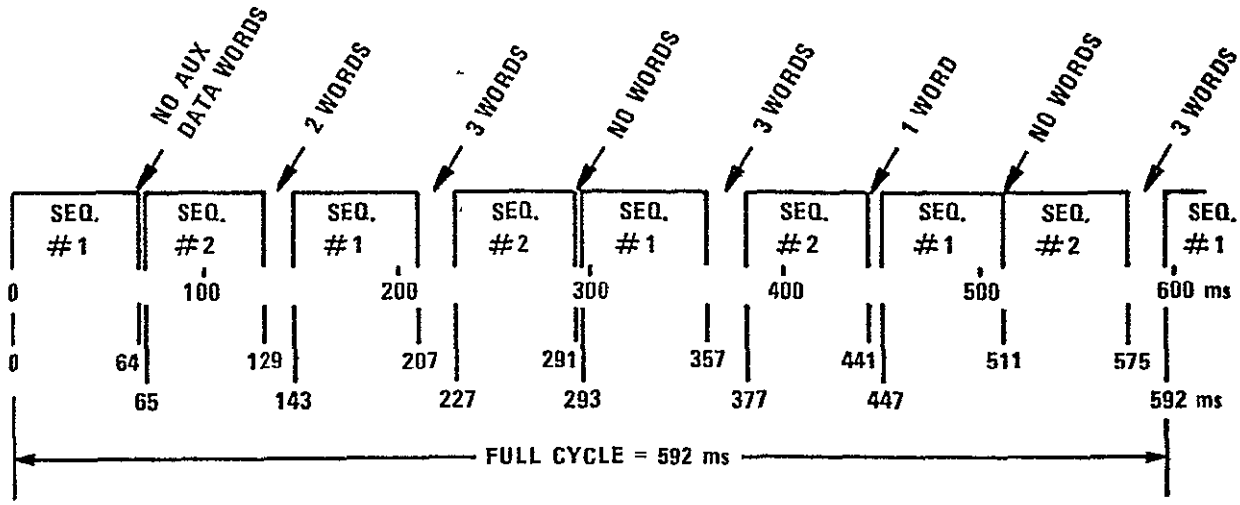

(a) Full Cycle of Functions

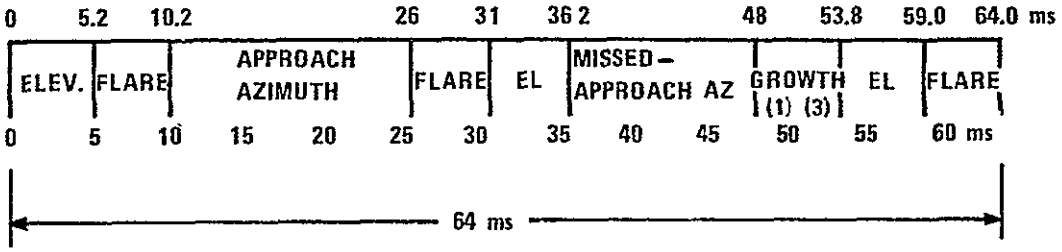

(b) Subsequence #1

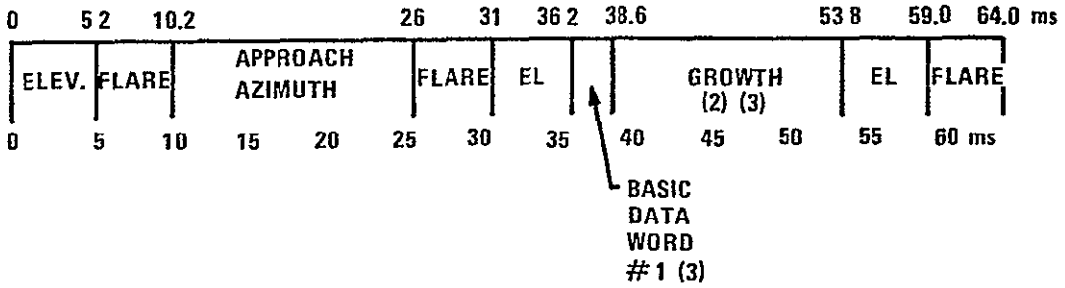

(c) Subsequence #2

NOTES: (1) AUXILIARY DATA (1 WORD) OR MISSED APPROACH ELEVATION
(2) 360° AZIMUTH OR AUXILIARY DATA (2 WORDS)
(3) BASIC DATA WORD #2 TRANSMITTED EITHER IN GROWTH OR BETWEEN SEQUENCES

FIGURE II-3 TRSB TIME MULTIPLEX FORMAT

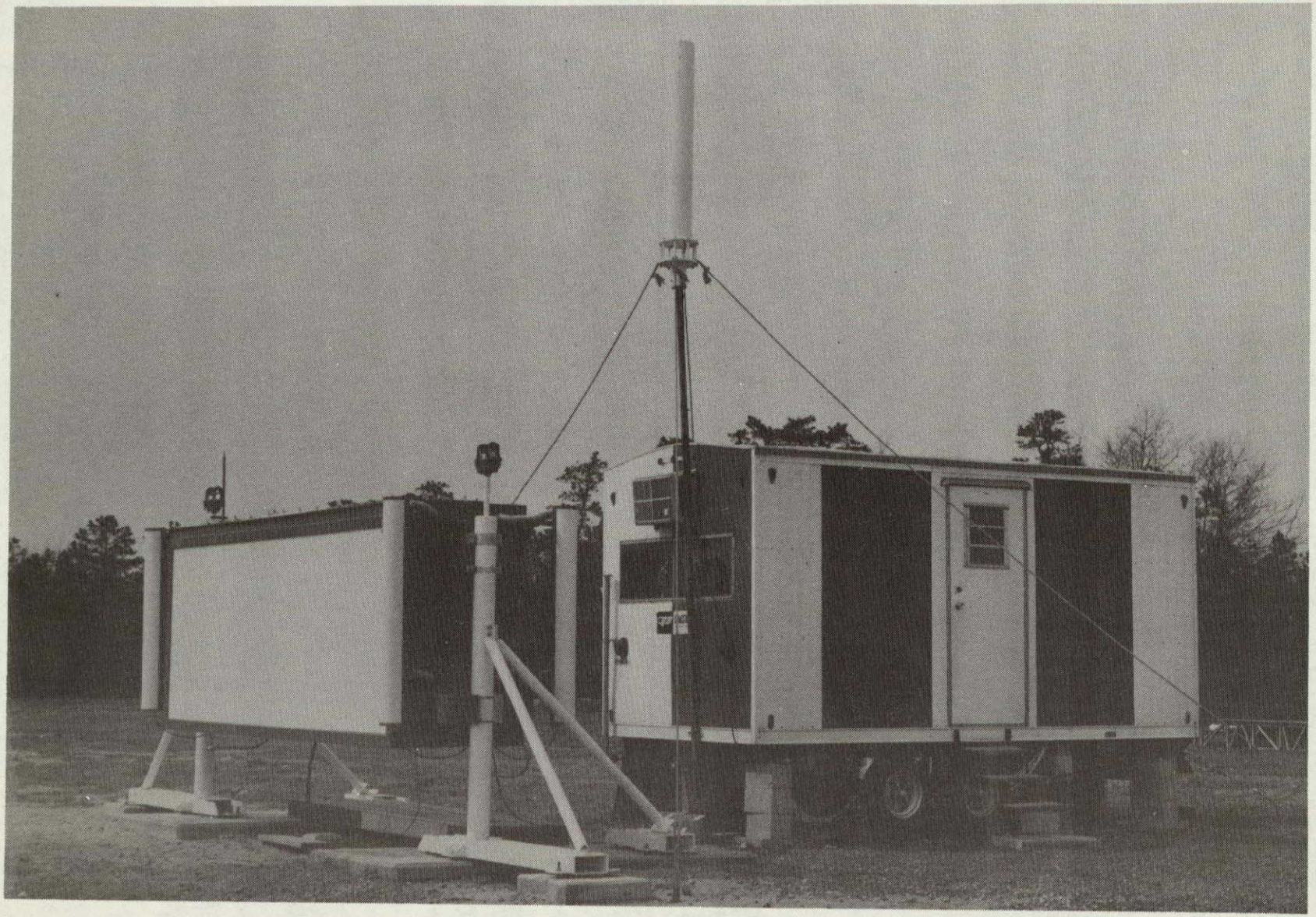

FIGURE II-4 AZIMUTH/DME INSTALLATION

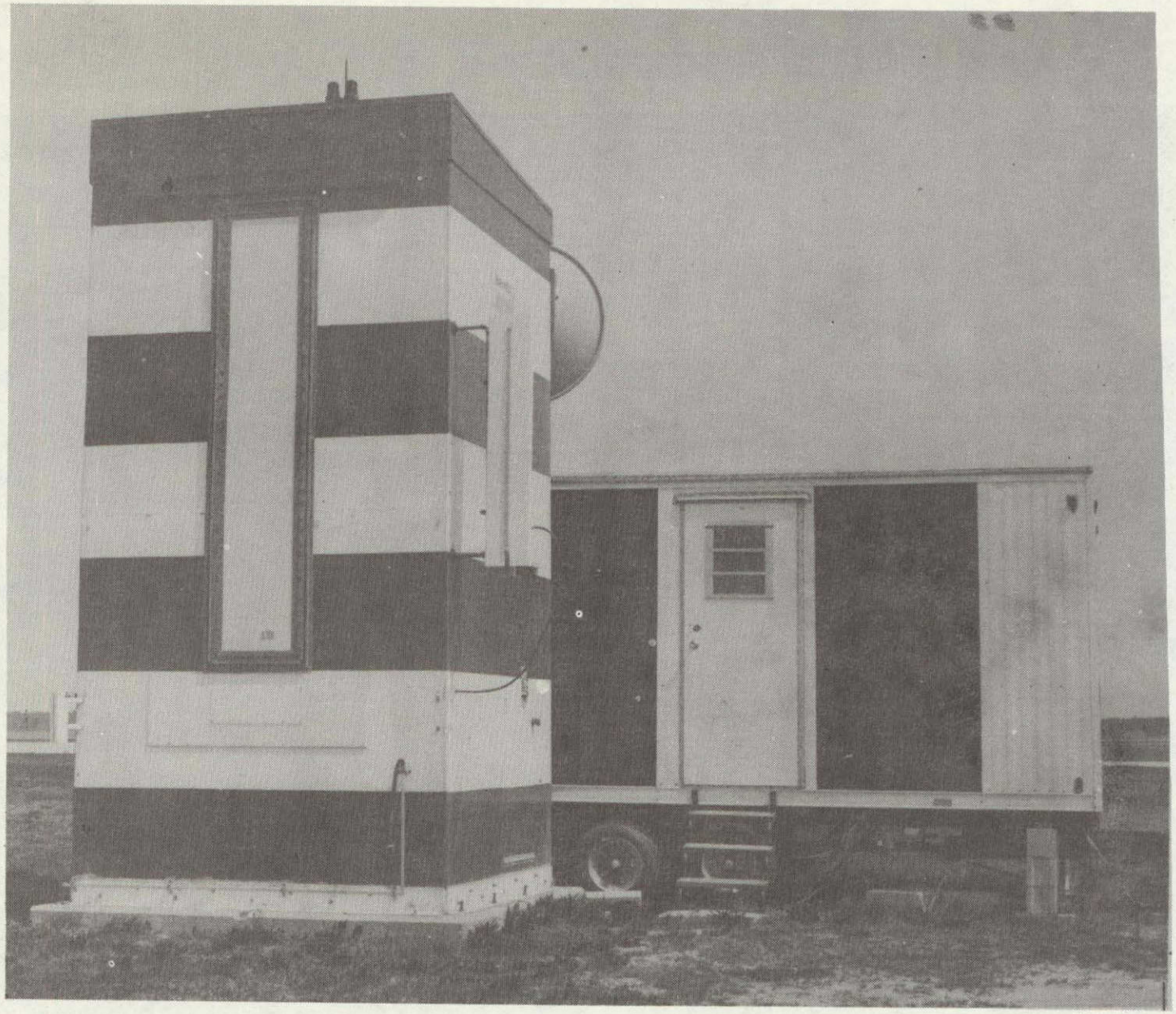

FIGURE II-5 ELEVATION INSTALLATION

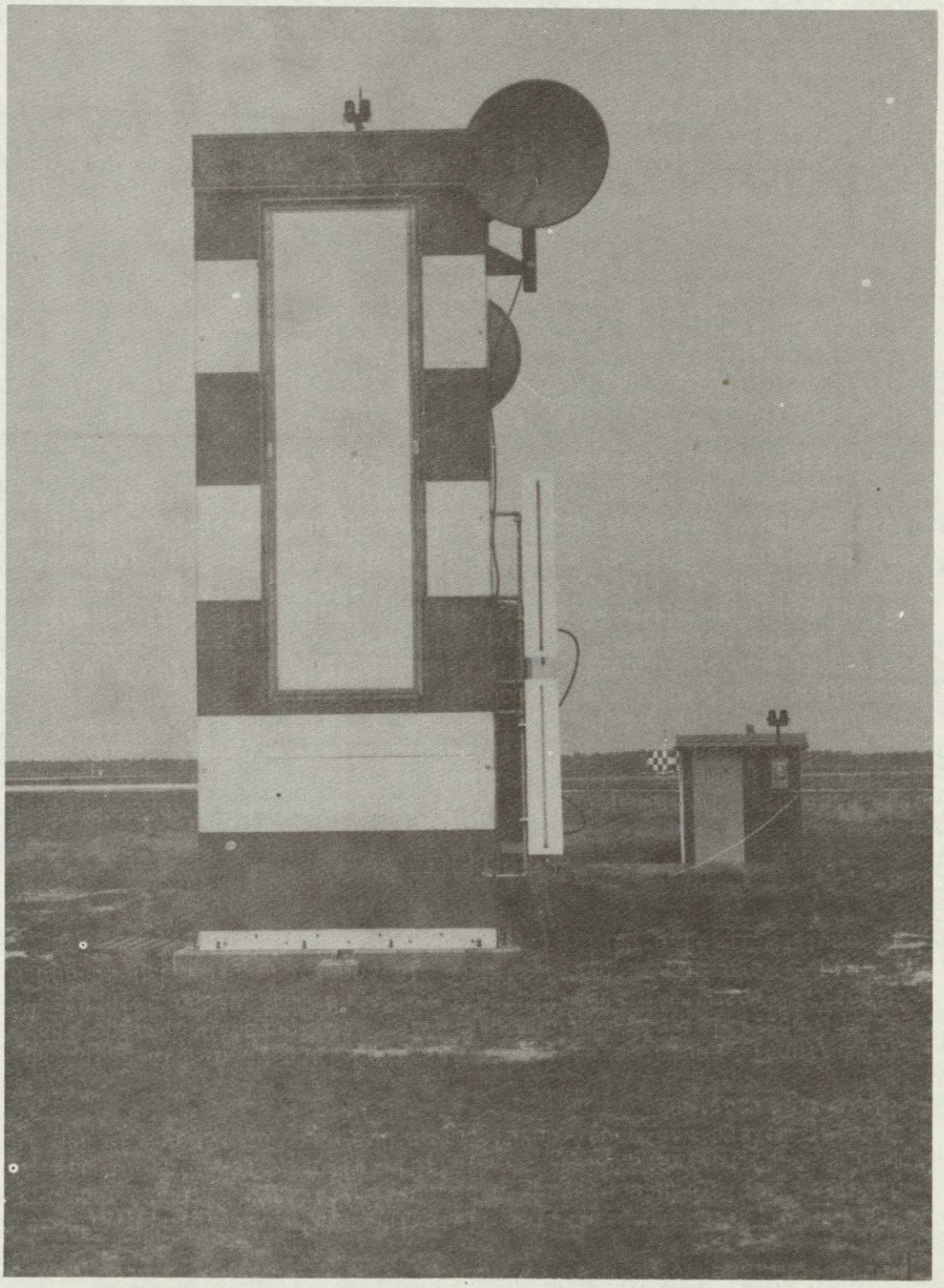

FIGURE II-6 FLARE INSTALLATION

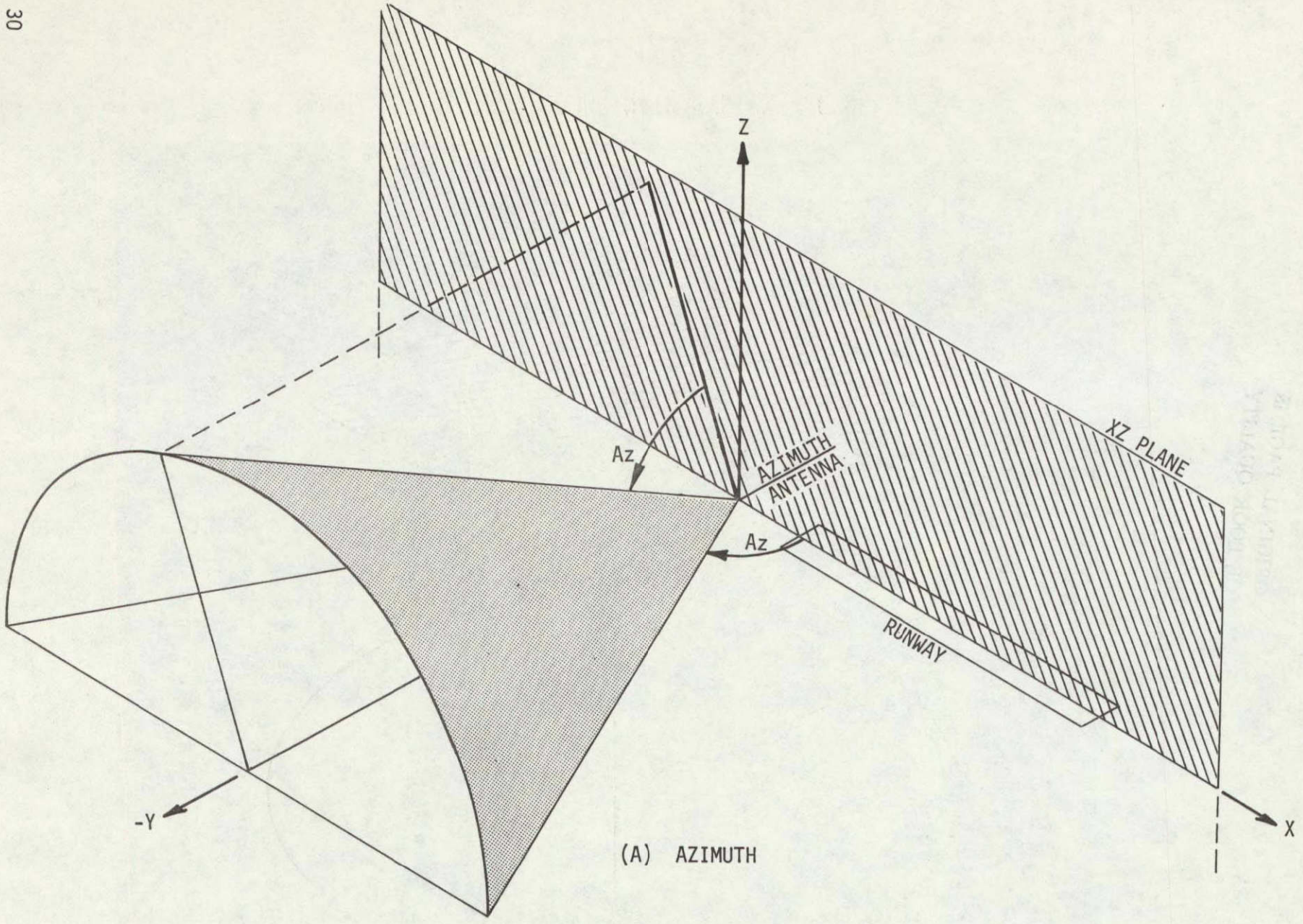

FIGURE II-7 TRSB COORDINATE SYSTEM

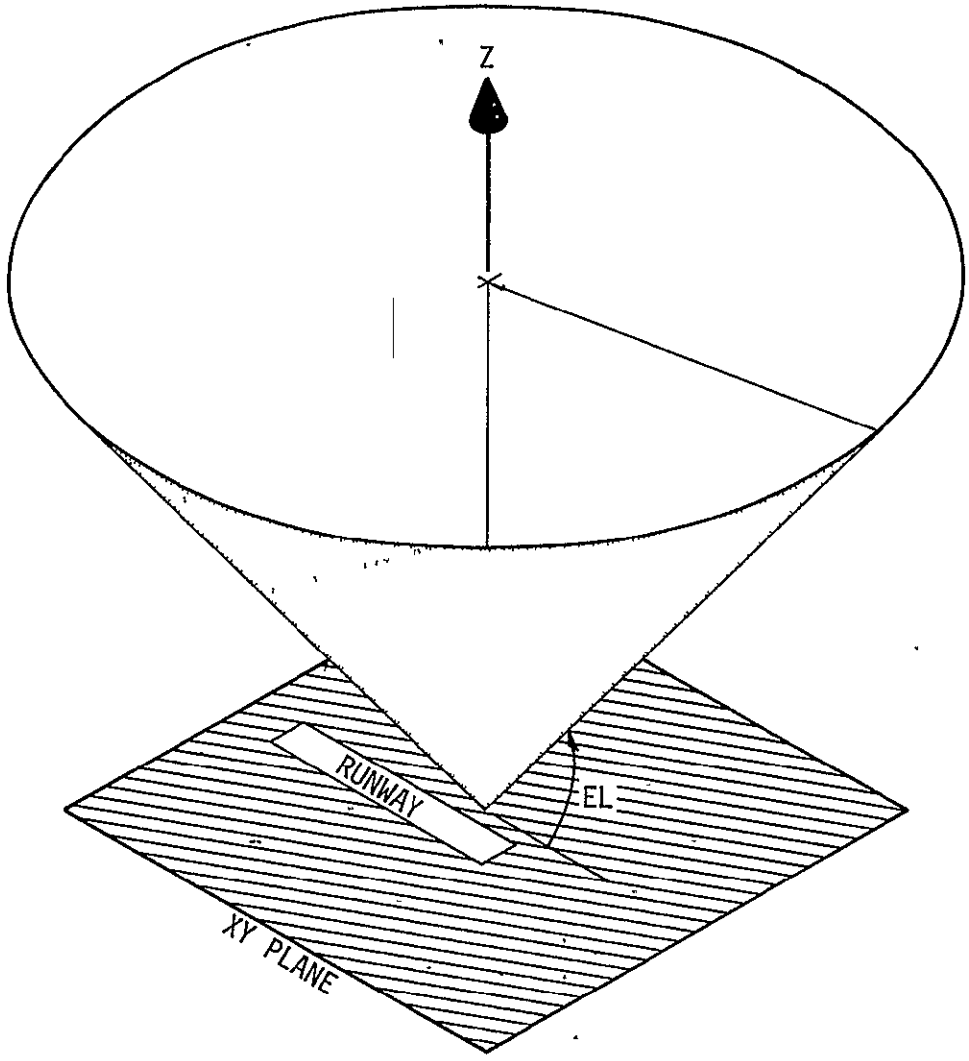

(B) ELEVATION

FIGURE II-7 TRSB COORDINATE SYSTEM - CONCLUDED

Az ANTENNA: 39 28' 13.21" N
74 34' 16.89" W

RUNWAY 04 HEADING: 28 00' 01"

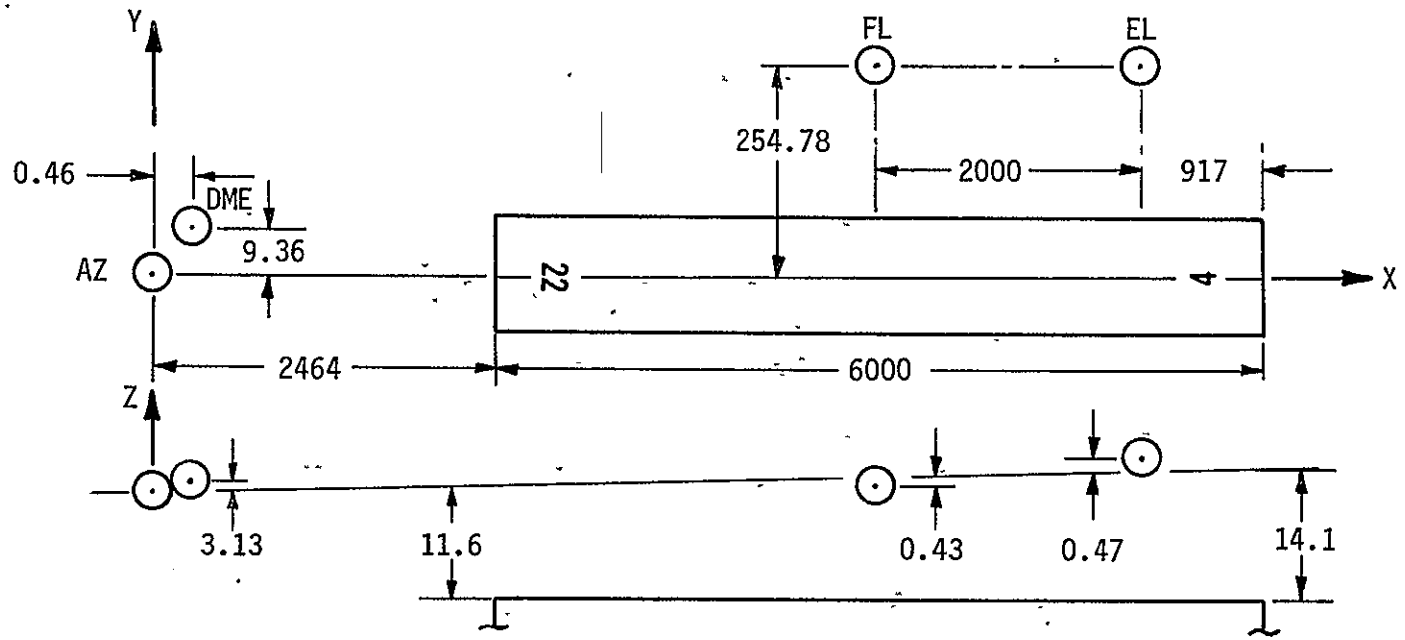

DIMENSIONS IN FEET
(NOT TO SCALE)

FIGURE II-8 MLS INSTALLATION GEOMETRY AT NAFEC

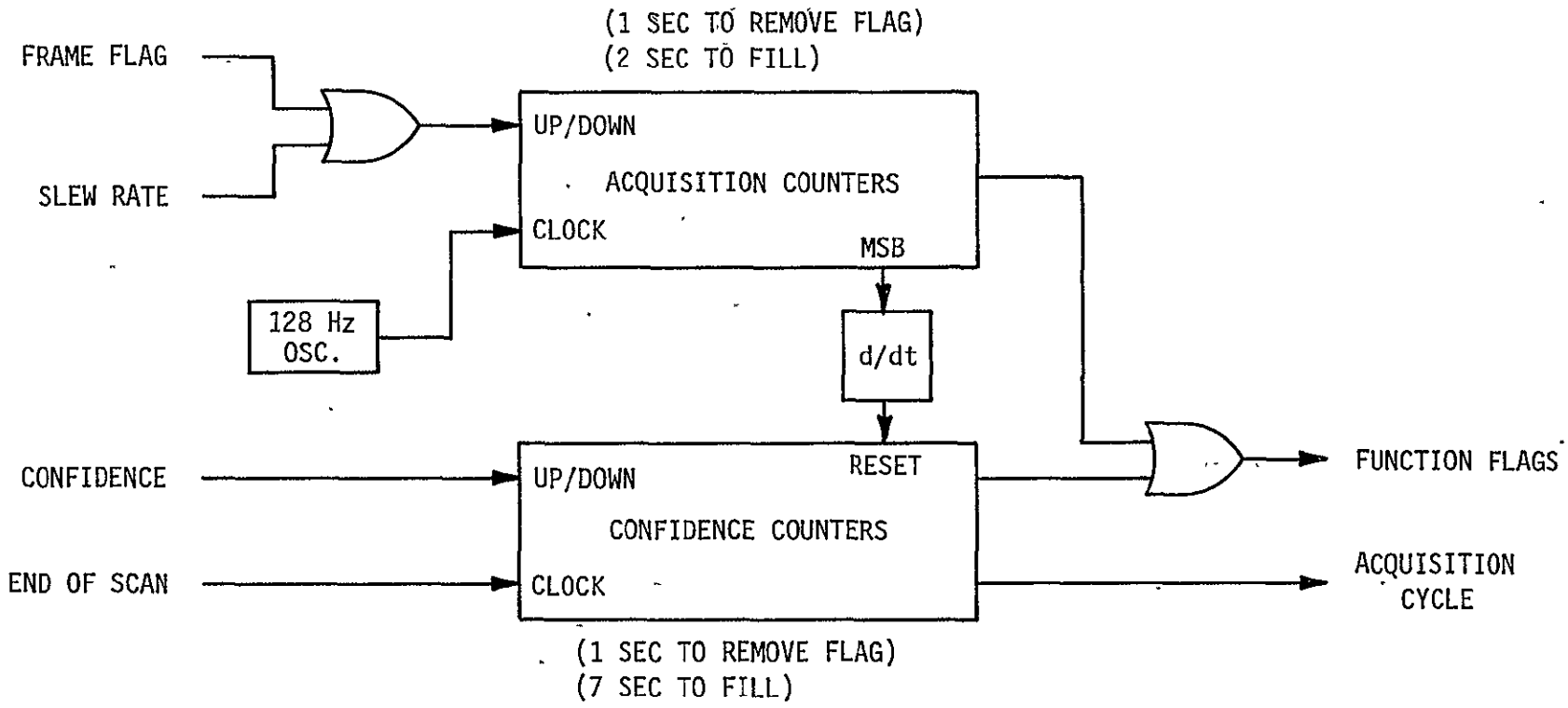

FIGURE II-9 ANGLE RECEIVER FLAG LOGIC

PRECEDING PAGE BLANK NOT FILMED

III. GOALS AND FLIGHT PLANS

By William F. White

INTRODUCTION

The FAA request for a Time Reference Scanning Beam (TRSB) demonstration placed highest priority on automatic landing. The original request listed four methods of guidance for flare and touchdown and expressed a desire that two of them be implemented for comparison if possible. In the specified order of priority, the methods were:

1. TRSB approach guidance, switching to radar altimeter elevation guidance for flare and touchdown.
2. TRSB approach guidance, switching to Inertial Navigation Systems (INS) and radar altimeter elevation guidance for flare and touchdown. This was the flare method in use on the B-737.
3. TRSB-only guidance throughout approach, flare, and touchdown. Originally, this was specified to mean the use of primary elevation and Distance Measuring Equipment (DME) only. Later it was requested that Ku band flare guidance system be utilized.
4. TRSB guidance throughout approach, flare and touchdown with vertical accelerometer augmentation during flare and touchdown.

The system implemented for the demonstration essentially provided options 1 and 4, since flare guidance could be obtained by either the flare guidance function of the TRSB or by radar altitude. In both cases accelerometers were used for complementary filtering.

In addition to the automatic landings, the request also included the use of the aircraft as a test bed to evaluate curved path capability using TRSB guidance.

DEMONSTRATION GROUND RULES

Implicit in the FAA request was the assumption that the B-737 was already capable of making automatic approaches and landings using its DME and ILS updated INS navigation system. The approach followed was, therefore, to adapt the aircraft systems to utilize TRSB guidance in place of the normal systems. Insufficient time was available to allow development of new control laws optimized for TRSB characteristics. The following guidelines were agreed to with FAA:

1. The demonstration would take place at the National Aviation Facilities Experimental Center (NAFEC) using the modified Phase II microwave landing system. Figure III-1 is a diagram of the airport and shows the landing system antenna sites. Landings were made on runway 4.

2. The existing guidance systems and control laws would be retained and modified as necessary to allow curved, descending approaches and automatic landings through rollout on TRSB guidance. Approaches would involve only 3^{0} glidepaths and 3 nautical mile final legs since aircraft performance on shorter or steeper approaches was an unknown quantity.

3. The INS would not be used for navigation and guidance purposes within the TRSB coverage area. Rather, TRSB-derived positions and velocities would be substituted. Signals from the INS platform which were an integral part of aircraft stability and control loops would continue to be used as such.

4. The use of accelerometers for filtering would be avoided if possible. However, performance proved to be unsatisfactory without accelerometers and they were used. A digital filter which did not use accelerometers was under development but was not ready for use in the demonstration.

5. TRSB signals would be used to drive the aircraft displays to the extent possible. In the demonstration configuration, since TRSB signals were merely substituted for the normal guidance inputs, all displays were driven by the TRSB. In addition, groundspeed and wind readouts were also derived from TRSB.

FLIGHT PROFILES

Approach Paths. Two flight paths were considered which were representative of ICAO requirements. The first was an S turn consisting of a 90^{0} right turn to a base leg and a 90^{0} left turn to final approach. The second was a 180^{0} turn from downwind leg to final approach. Initial studies indicated that antenna switching would probably be necessary to fly the 180^{0} pattern. Even though subsequent flight tests indicated the single antenna used would allow the pattern to be flown, it was still rejected because the path passed directly over the Atlantic City racetrack. The pattern was changed to a 130^{0} turn to final in order to put the approach leg over unpopulated territory. This gave a profile similar to the Expressway Approach to LaGuardia's runway 31 shown in Figure II-2, which is also used for noise abatement. However, the latter approach can only be used in good weather since it requires visual reference to the surface.

Coordinate and Waypoint Calculations. A right-handed rectangular coordinate system was used with the origin at the phase center of the azimuth antenna. The positive X axis was in the direction of the runway 22 heading, 208° 00' 01" true. The positive Z azis was upward along the local vertical.

Two glidepath intercept points were calculated. The first represented the intercept of the transmitted 3° beam with the runway and was located 214 feet beyond the elevation antenna. It was designated TDZ04. The second, GPI04, was the intercept of a computed glidepath with the runway and was located immediately opposite the elevation antenna, analogously to ILS. The latter location also provided a little more useable runway length. This was of interest since all available data showed that touchdown on the long side of the 2-sigma dispersion footprint would result in landings with the aircraft heavy, probably experiencing a tail wind, and with only 3700 feet of runway remaining. With repeated approaches this could have caused a problem with brake cooling.

Waypoint altitudes were found as follows: the final approach fix was located in the runway coordinate system to provide a 3° planar descent with respect to the glidepath intercept point. The altitude above mean sea level was then calculated from the equation

$$h = Z + (X^2 + Y^2)^{1/2}/2R_L + h_0$$

where X, Y, and Z are the runway coordinates, h_0 is the MSL altitude of the reference point (66 feet in this case), and $1/R_L$ is the mean local curvature given by

$$1/R_L = (1 - h_0/R_0 + e(1 - 2 \sin^2 \phi_0))/R_0,$$

$$R_0 = 2.09257539 \times 10^7 \text{ feet},$$

$$e = .0033901.$$

After finding the altitude of the final approach waypoint, the other altitudes were found in sequence by adding a delta altitude to the altitude of the preceding point. The delta was obtained by multiplying the alongtrack distance between waypoints by the tangent of 3°, in order to keep the descent angle at approximately 3° with respect to the local vertical all along the track.

Waypoint locations in latitude and longitude were required. As was the case for altitudes, curvature had to be considered even for these relatively short distances for the purposes of automatic control using accurate guidance. The following method was used to calculate waypoint locations: The desired track in the runway coordinate system was defined and the coordinates of the waypoints found. A correction for the local vertical was then applied to find the coordinates of the point on the surface directly under X, Y, Z:

$$X' = (X - x_r)(1 - Z/R_L)$$

$$Y' = (Y - y_r)(1 - Z/R_L),$$

where x_r, y_r are the coordinates of the reference point. In general, the waypoint TDZ04 was used as a reference, but spot checks were made by calculating locations using different references. The adjusted runway coordinates were then rotated to get the north and east distances from the reference:

$$\Delta N = X'\cos\Psi_r + Y'\sin\Psi_r$$

$$\Delta E = -X'\sin\Psi_r + Y'\cos\Psi_r,$$

where Ψ_r is the true heading of the X axis. The north and east distances were converted to delta latitude and delta longitude from the reference point:

$$\Delta\phi = \Delta N\ (1 - h_o/R_o + e\ (2 - 3\sin^2\phi_o))R_o$$

$$\Delta\lambda = \Delta E\ (1 - h_o/R_o - e\ \sin^2\phi_o)/R_o\ \cos\phi_o$$

The deltas were then converted from radians to degrees and added to the latitude and longitude of the reference point.

The values used for the latitude and longitude for TDZ04 were:

$$\phi_o = 39.45256111^o$$

$$\lambda_o = 74.58354722^o.$$

The values were derived independently by calculations from three survey points at NAFEC: a runway 22 benchmark and the locations of phototheodolite towers P13 and P36. The three calculations agreed within 0.01" of latitude and longitude.

The entire path was checked by computing the true great circle bearing and distance from waypoint to waypoint by use of the equations given in Appendix J of Reference III-1.

STAR AC041. The 130^o approach was designated as STAR AC041, and is illustrated in figure III-3. Waypoint AC131 was located at the entry to the nominal TRSB coverage area based on 120^o coverage in azimuth of the elevation antenna, since elevation was the last function to be received on this path.

A common path definition method is to place a waypoint at the intersection of the two straight legs, and the turn is then a circular arc tangent to the two straight portions. For the demonstration a feature of the B-737 navigation system known as "DME arc turns" was used. This resulted in the on-board map display showing a waypoint at the beginning of the turn. The profiles were, therefore, designed with waypoints at the beginning of each turn to correspond to the display the observers would see on the aircraft. This method had the advantage that all waypoints were actually points on the flight path and they could be used by the pilots as checkpoints for establishment of aircraft configuration and power or for performing other operations in preparation for the landing. In addition, the desired altitude was displayed beside each waypoint, which aided observers in verifying that the aircraft was following the programmed profile.

STAR ACO43. Figure III-4 illustrates the S-turn approach, designated STAR ACO43. Most of the discussion of the STAR ACO41 applies here, except that this pattern was executed entirely within TRSB coverage so the initial waypoint was arbitrarily selected. After passing waypoint ACS25 the path was identical to that of ACO41.

Departure or Transition Paths. The flight paths stored in the navigation computer included not just the STARs, but additional waypoints defining a path beginning after takeoff and leading to the entry point of the STARrs. Figure III-5 is a photograph of a topographical chart of the area with the complete flight paths superimposed. These paths include the transition shown from waypoint DD135 in figure III-3 and DDSO5 in figure III-4. These paths allowed sufficient time to get the aircraft stabilized at 4000 feet altitude and a speed of 210 knots in automatic flight, and for the observers to rotate seats before beginning an approach. A dogleg was added to the outbound leg of the S-turn pattern to avoid overflying the town of Mays Landing.

DEMONSTRATION PROCEDURES

Observer Flights. Observers attended a preflight briefing and were given information handouts. These included, among other things, figures III-4 and a page-size version of figure III-5. Ten observers were carried on each flight. Figure III-6 shows the location of observers seats on the aircraft and the rotation scheme. Observers in the forward cockpit moved to the two rearmost seats, and all others moved forward one place. Five approaches were made on each flight so that observers could see one approach from the aft flight deck, where the displays and automatic controls were located, and one approach through the forward cockpit windows. Several of the seats provided a view of repeaters from the aft cockpit displays, and seat allowed monitoring of the TRSB video signals on an oscilloscope as well as oscillographic recordings of receiving and processed TRSB data.

The crew member seated beside each observer briefed him on the function of the particular station and alerted him to significant events during the flight.

Each flight consisted of one S-turn approach and four 130^{o} approaches in order to save time. Takeoffs were made from the forward flight deck by the safety pilots, and control was transferred to the aft deck after the aircraft was established on climbout. The aft pilots flew the aircraft into position to couple the autopilot to one of the two paths shown in figure III-5. From that point the approach was completed in 3D automatic mode. Autothrottles were controlled by dialing in the desired airspeed at the mode control panel. Flaps and landing gear were operated by the pilots and the switch to TRSB guidance was initiated by the pilots after an indicator showed valid signals were being received. The first four approaches of each flight were touch and go landings, with the forward pilots taking control after touchdown for the go-around. The last landing was planned as a full stop landing for each flight. Reverse thrust was applied by the aft pilots but braking was automatic and rollout guidance was provided by the TRSB azimuth signals controlling nosewheel steering.

Range Control Visits. While one observer group was participating in a flight, the others were being given tours of the ground sites. One stop was the phototheodolite tracking control room, where observers could follow the aircraft on closed-circuit television and observe the accuracy of the aircraft's flight path on a large plotting board. In addition telemetry on board the aircraft was transmitting the received TRSB data back to range control where it was fed to a minicomputer. The phototheodolite tracking signals were also fed to the computer and a real-time plot of TRSB errors was generated as the approach progressed. After each approach, hard copies of the plot were generated along with prints of several other types of error plots related to TRSB and aircraft performance.

Video tape recorders were also available at range control to play back video tapes of the display on earlier flights for those observers who had not yet flown or who had questions about the displays.

REFERENCES

III-1. "Approval of Area Navigation Systems for use in the U.S. National Airspace System," Federal Aviation Administration Advisory Circular AC 90-45A, February 1975.

ATLANTIC CITY, N.J. (18-7) APR 30-76 *NASA Langley Research Center*

NAFEC ATLANTIC CITY APT.

Elev 76' N 39 27.4 W 074 34.7

ACY

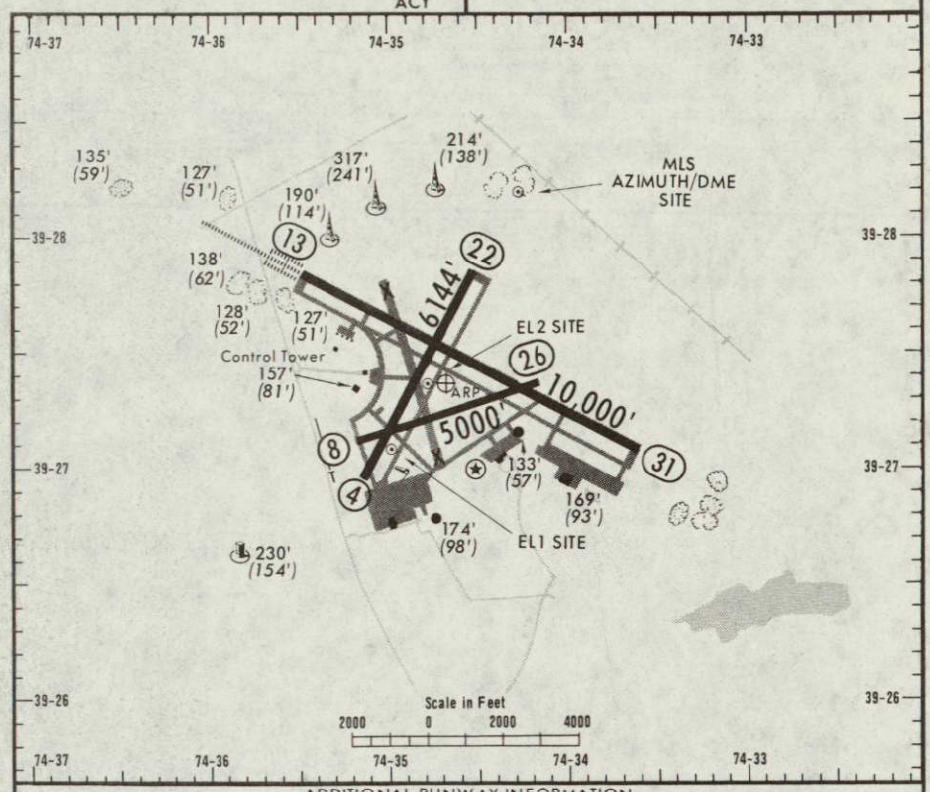

ADDITIONAL RUNWAY INFORMATION

RWY	LIGHTING	USEABLE LENGTHS LANDING BEYOND Threshold	Glide Slope	TAKE-OFF	WIDTH
4 ❶ 22	HIRL				150'
8 26	MIRL				150'
13	HIRL CL HIALS SFL TDZ RVR		8890'		200'
31	HIRL CL TDZ		8950'		

❶ Closed to acft over 100,000 lbs. except with prior permission.

	AIR CARRIER TAKE-OFF				ALTERNATE CEILING-VISIBILITY	
	TAKE-OFF ALTN FILED WITHIN: 15 Min Piston-30 Min Turbine	TAKE-OFF ALTN FILED WITHIN: 1 Hr 2 Eng-2 Hr 3 & 4 Eng		TAKE-OFF ALTN NOT FILED	ILS Approach	Other Approach
	SCHEDULED		Altn Apt & Non-Skd	All Carriers		
2 Eng Tailwheel	❶ RVR 18 or 1/2	RVR 50 or 1	❷ RVR 50 or 1	Landing Weather Minima	600-2	800-2
2 Eng Tricycle	RVR 16 or 1/4				Non-skd 3 & 4 Eng Jet 700-2	
3 & 4 Eng		RVR 16 or 1/4				

AMEND 1

❶ RVR 24 CL out.

❷ FAR Part 135 Operators: Rwy 13 RVR 18.

CHANGES: New chart.

FIGURE III-1 NAFEC AIRPORT DIAGRAM

AL-289

EXPRESSWAY APPROACH (VISUAL) RWY 31

LA GUARDIA

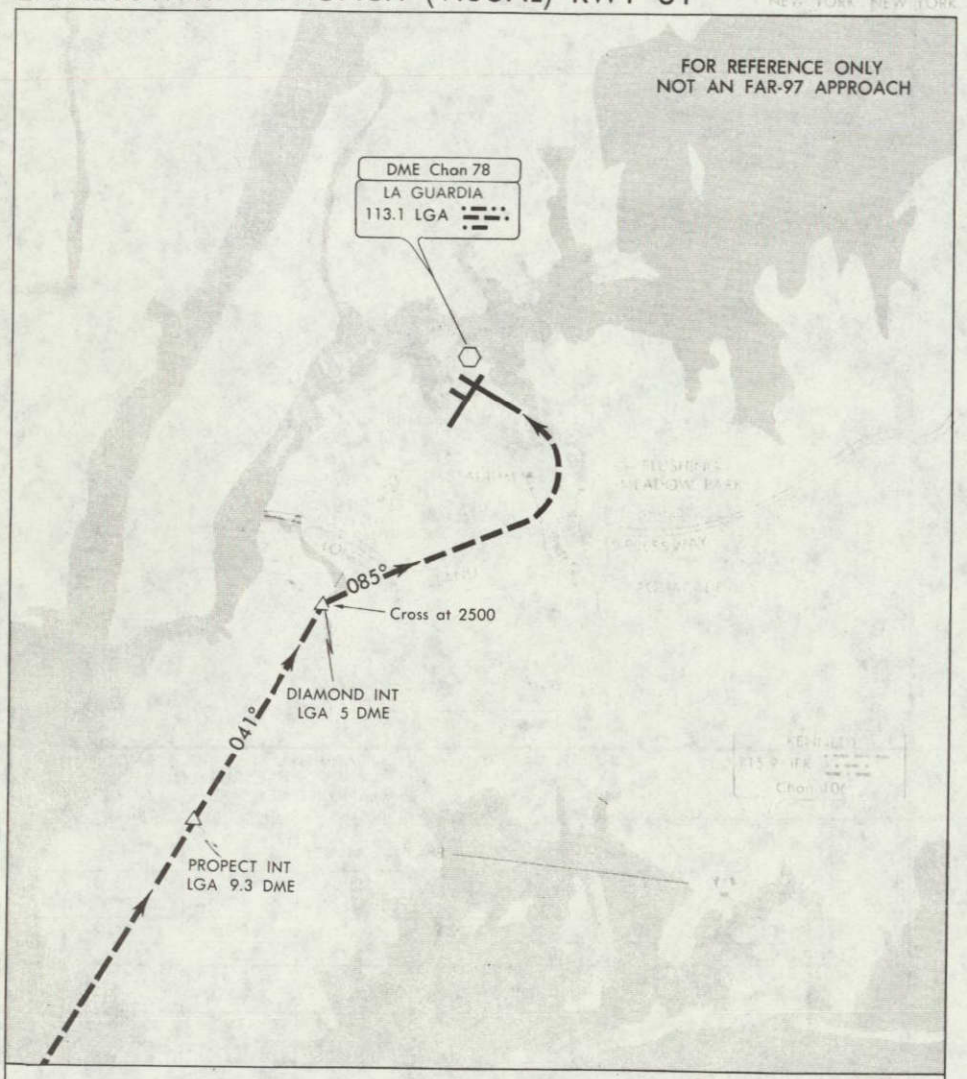

EXPRESSWAY APPROACH (VISUAL) RWY 31

This approach will be utilized when ceiling is 3000 feet and visibility 5 NM or better.

When cleared for an Expressway Approach to Runway 31 (while on La Guardia VOR/DME R-221), cross Diamond Int or 5 DME at 2500 feet. Turn right at Diamond Int heading 085° and descend to Runway 31 via Long Island Expressway and Flushing Meadow Park.

EXPRESSWAY APPROACH (VISUAL) RWY 31

10 APRIL 1

40°46'N – 73°52'W

PUBL NOS, NOAA AT THE DIRECTION FAA

GUARDIA

FIGURE III-2 EXAMPLE OF CURVED NOISE-ABATEMENT APPROACH PROCEDURE

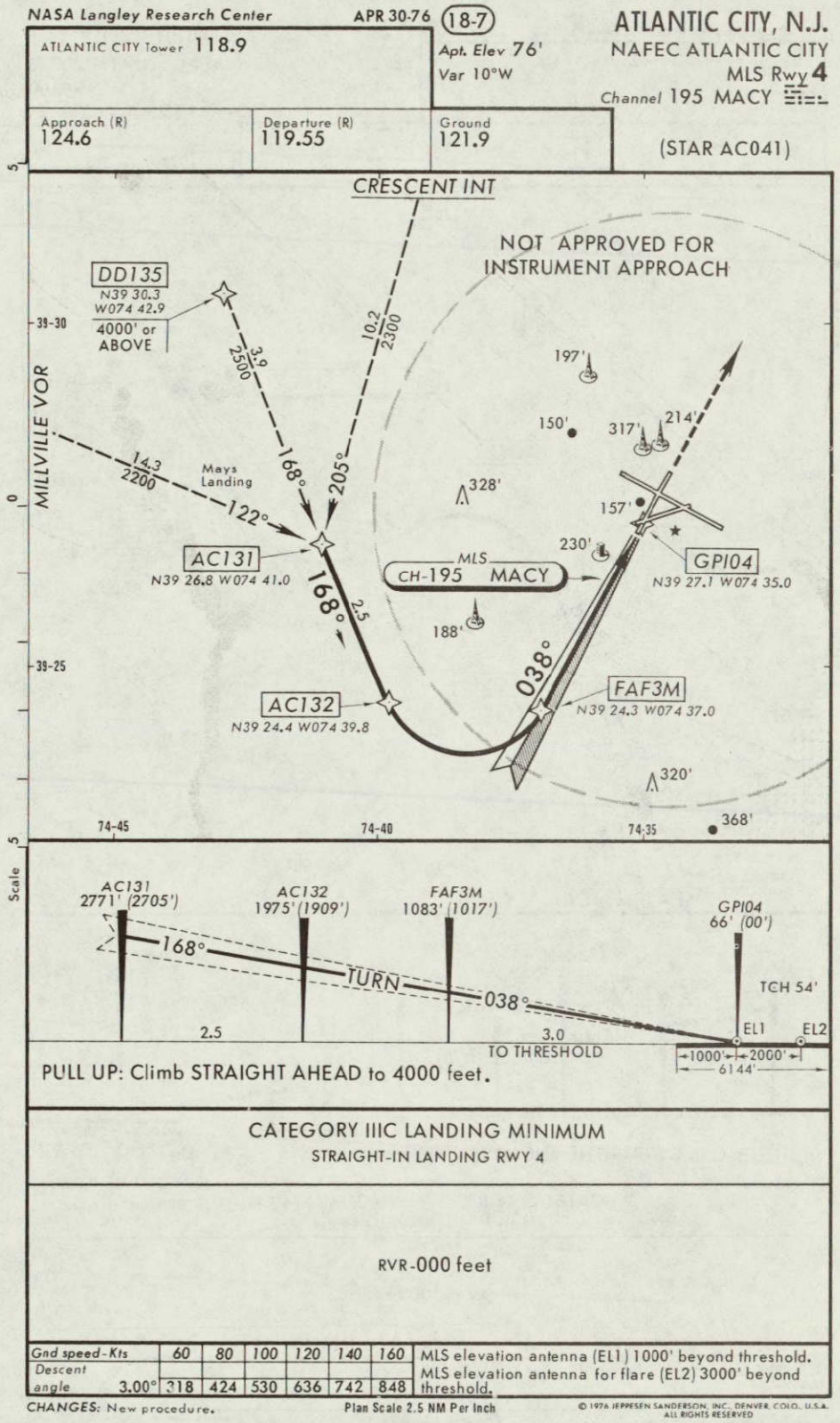

FIGURE III-3 ICAO DEMONSTRATION STAR AC041

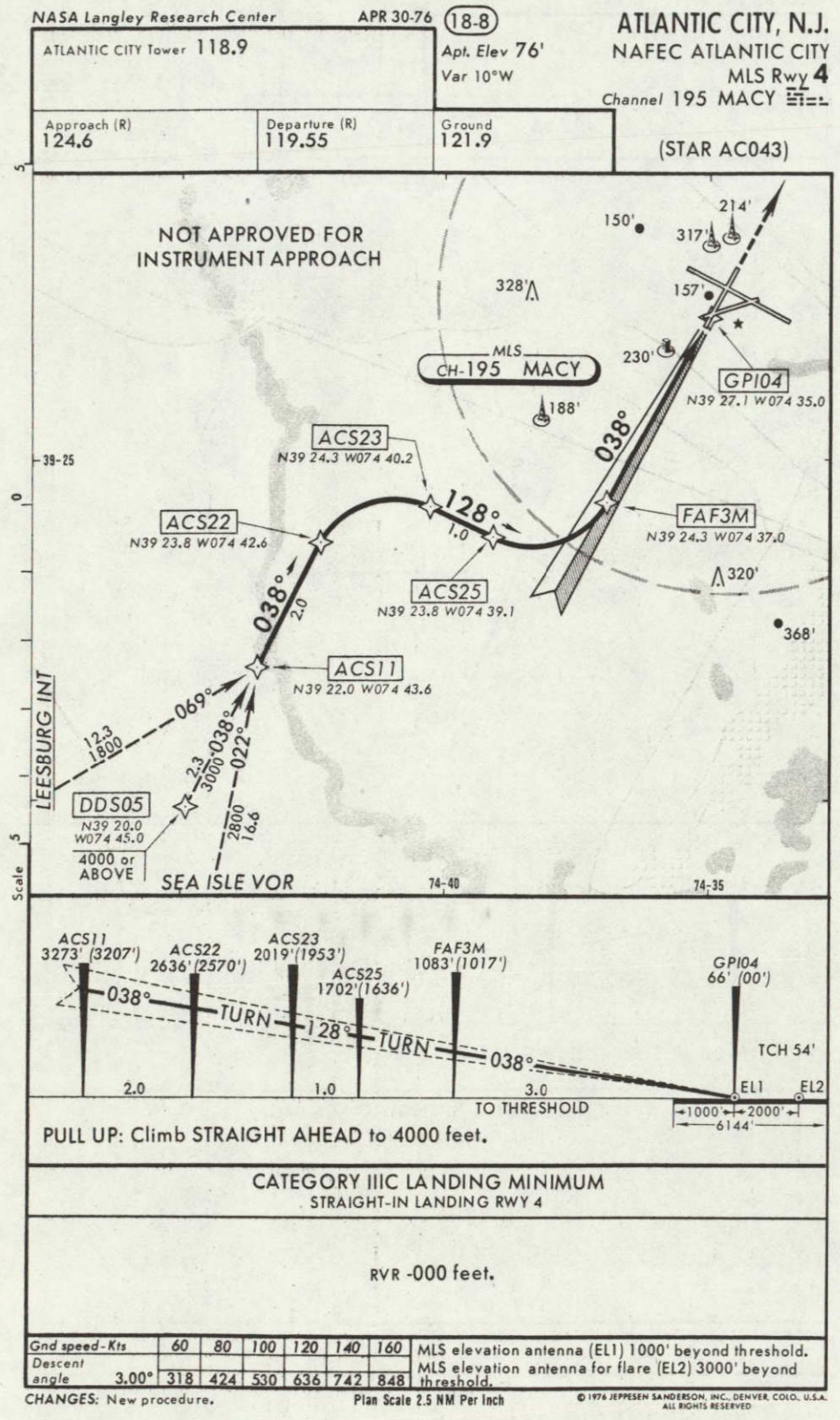

FIGURE III-4 ICAO DEMONSTRATION STAR AC043

FIGURE III-5 COMPLETE FLIGHT PATHS FOR ICAO DEMONSTRATION

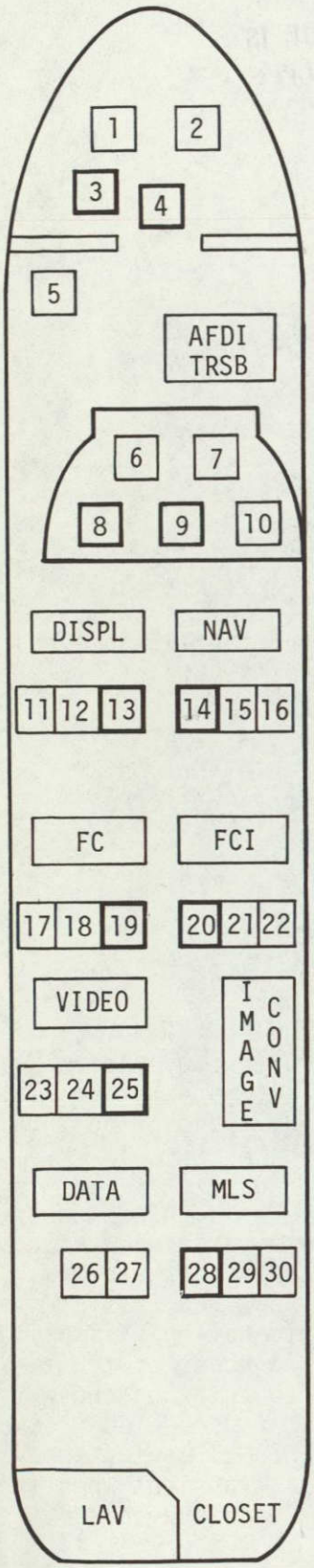

SEAT FUNCTION

1. PILOT
2. PILOT
3. OBSERVER
4. OBSERVER
5. TRSB ENGINEER
6. PILOT
7. PILOT
8. OBSERVER
9. OBSERVER
10. TEST ENGINEER
11. EXP. AVION.-DISPLAY ENGR.
12. TEST DIRECTOR
13. OBSERVER
14. OBSERVER
15. TRSB PROJECT ENGINEER
16. NAV ENGINEER
17. CONTROLS ENGINEER
18. CONTROLS ENGINEER
19. OBSERVER
20. OBSERVER
21. TRSB ENGINEER
22. CREW CHIEF
23. VIDEO ENGINEER
24. TRSB ENGINEER
25. OBSERVER
26. INSTR. ENGINEER
27. NAFEC TRSB ENGINEER
28. OBSERVER
29. TRSB ENGINEER
30. EXP. AVIONICS

NOTE: AFTER EACH CIRCUIT, OBSERVERS MOVE WHEN PILOT GIVES CLEARANCE.

ROTATION SEQUENCE:

SEAT	
3	4
25	28
19	20
13	14
8	9

FIGURE III-6. DEMONSTRATION SEATING ARRANGEMENTS

IV. SYSTEM DESCRIPTION

By Charles W. Meissner, Jr.

INTRODUCTION

The existing experimental avionics system on NASA 515 is a complex, integrated electronic package, capable of accurately controlling the airplane in the present ILS terminal area environment as well as enroute. In order to do this same automatic flight control in the MLS environment, some means was required to introduce the MLS position information without having to seriously disturb the present set of control laws. In addition, a significant departure from the normal operating scheme was required in that body mounted accelerometers were to be used for acceleration in place of the INS accelerometer. To minimize the impact of these changes, the interface point between the MLS equipment and the aircraft guidance equipment was chosen to be the estimates of position, velocity and acceleration required by the navigation and flight control computers. This approach made it possible to interface the MLS to the TCV B-737 without making changes to the existing airplane control laws and to accomodate a variety of filtering techniques and operating modes.

MLS PROCESSING EQUIPMENT

The demonstration configuration is illustrated in Figure IV-1. The MLS receivers provided position information in conical coordinates to the preprocessor. The preprocessor complementary-filtered this with body motion information from airplane sensors to result in MLS-based estimates of position, velocity and acceleration. These estimates were then transformed into the coordinate systems required by the B-737 computers.

Using the additional computer to make MLS-based estimates required only little change of the existing software in the aircraft computers in order to accomodate the MLS navigation function. The display computer software was unchanged, and minor modifications were required to the input routines of the navigation computer and the flight control computers. This not only simplified the interface with the existing system, but also provided a means of transitioning from conventional navigation to MLS navigation when entering the MLS coverage volume. A software switch in the aircraft computers selected MLS-based information when the MLS information became valid and MLS navigation was selected by the "MLS enable" switch. There could be a transient when the switch was activated because of differences in the information provided by the conventional and MLS system.

Equipment Location. Figure IV-2 shows the location of the equipment added to the B-737. The locations were chosen to give the shortest antenna

cable runs to the antennas used for the demonstration. These were the M1 (C-band) antenna and the M5 (Ku-band) antenna. The other antennas were tested but were not used for the demonstration. Adequate coverage for the patterns flown was obtained by using M1. Omnidirectional coverage was not required of the Ku-band flare antenna. The MLS receivers, preprocessor, digital recorder and telemetry encoder were located in a forward rack as shown in Figure IV-3.

In Figure IV-3a the angle receiver is the left-hand ATR case located in the far bay of the double rack. The DME is next to it. The DME power supply is next to the DME and partially visible in Figure IV-3a. The RF components of Figure IV-4 can be seen mounted on a plate under the MLS receivers. A manual data entry unit (MDEU) for the MLS preprocessor is the top panel in the rack. The MLS preprocessor computer is shown mounted on the top left of the rack and the I/O box is on the right. Figure IV-3b shows the digital tape recorder mounted below the MLS receivers. Below that is the data formatter for the tape recorder which also contains a Course Deviation Indicator (CDI) and Azimuth and Elevation Angle selector. A remote CDI was located in the forward flight deck for manual flying during the initial phases of the demonstration development. Below the formatter the IRIG-B time code generator may be seen. This time code was used on all the instrumentation recordings. The second panel from the bottom is the right-hand bay which is the power control panel for the MLS equipment. All the other panels are associated with the existing B-737 experimental equipment. The telemetry encoder is not visible in the photograph.

Three oscillographs located in the after section of the cabin were used for in-flight display of quantities computed in the preprocessor. An oscilloscope was used to display the angle receiver video output from the forward receiver and from a test receiver connected to the fin (M2) antenna. The test receiver was initially for antenna test purposes but proved useful during the development flights for fault diagnosis. This hardware configuration stayed essentially the same throughout the development flights and the demonstration. Changes were made in the system's software to do the development work.

MLS Receivers. Figure IV-4 illustrates the setup for the MLS receivers. The modified Phase II equipment which was used for the demonstration consisted of an angle receiver and a DME interrogator, both operating on C-band between 5 and 5.2 GHz. The same antenna was used for both the DME and the angle receiver. A 3-port circulator separated the transmit and receive signals. On the receiver side, the chain of components began with a limiter to prevent damage to the tunnel diode amplifier. The amplifier was required to obtain sufficient range from the DME. The amplified signal was attenuated 10 db to prevent overload of the angle receiver. The poorer sensitivity of the DME was a result of its 6 MHz bandwidth versus 150 kHz bandwidth for the angle receiver. A separate Ku-band antenna and RF section were used for the flare

elevation function. The flare signal was mixed with the other angle receiver signals at the IF and all the signals were then processed by the angle processor. Angle and distance measurements appeared on separate serial digital data buses from the DME and angle receiver. The range and resolution of each measurement is indicated in Figure IV-4. It was impractical to locate the RF components and the front ends of the equipment at the antenna, therefore the equipment had to be located as near as possible to the antenna. Once that choice was made, locating the remaining equipment at the same place was necessitated by the desire to avoid potential noise problems associated with transmitting high speed digital signals at TTL levels in a noisy aircraft environment.

MLS Preprocessor. In order to permit the development to be done without hardware changes, the MLS preprocessor was chosen to be the most powerful airborne computer which was immediately available. It was provided with a variety of inputs from airplane systems and dedicated transducers so that the systems engineers would have the capability of rapidly reconfiguring the estimation process as development progressed.

Table IV-1 is a listing of the major MLS preprocessor functions. The conversion of parallel digital computer information into the various electrical signals that appear on the airplane was done in the specially designed I/O box. Both the computer and the I/O box appear at the top of figures IV-3a and IV-3b.

The MDEU was used for changing MLS preprocessor parameters and operating modes and observing computed quantities in flight. It provided a means to shorten flight test time and to provide recovery in the face of equipment failures. The I/O box was required to translate the parallel digital input/output of the computer to the multitude of electrical formats used in avionic equipment. The DC Analog, DC Discrete, Synchro and ARINC 561 serial digital are standard avionic interface methods. The Split Phase Bipolar (SPBP) serial digital is similar to the ARINC 575 characteristic digital transmission, but is faster. The MLS serial digital is peculiar to the Phase II MLS equipment and consists of an NRZ-L data bus accompanied by a synchronized group of clock pulses on another bus, and function identification signals that become active in synchronism with the function being transmitted on the data bus. The DC Analog outputs were used to monitor preprocessor variables in flight on oscillographs. The outputs to the aircraft computers were over a SPBP bus.

Another major function of the preprocessor was the transformation of information between the coordinate systems used by the avionic equipment. The MLS receivers provided position information in conical coordinates. Airplane body accelerations and rates were referenced to the airframe. The Intertial Navigation System (INS) output information was referenced to geographic coordinates and to the track of the airplane. All input information was transformed into MLS coordinates which is a Cartesian system with the

MLS runway on the x-axis. Estimation of position, velocity and acceleration was done in MLS coordinates and transformed into the coordinate systems required by the aircraft computers. The estimates were provided to the navigation computer in geographic coordinates and to the flight control computer in a coordinate system referenced to the runway ILS glidepath.

Within the preprocessor computer the input variables were mixed in a complementary filter. The complementary filter utilized techniques which combine the best characteristics of the input variables in a complementary fashion, to obtain estimates of output variables that are more accurate than any individual input variable.

The input variables complementary-filtered in the MLS coordinate system are indicated in Table IV-1. The complementary filtering resulted in estimates of position, velocity and acceleration for the translational degrees of freedom. Rotational quantities were not estimated in the MLS preprocessor although they were used to derive the translational estimates. Several options were selectable in flight. Option 3, body mounted accelerometers, and option 4, INS accelerometers, were flight tested as were radio altitude flares and MLS-EL2 flares. Data used for only one option, for initial conditions or for smoothing over data dropouts is indicated by parentheses.

The flag logic function listed in Table IV-1 was one of the most complex tasks required of the preprocessor. The preprocessor was required to determine what actions to take in the case of equipment failure indications (flags) and in some cases to monitor input variables for reasonableness and generate flags if unreasonable values were input.

The support functions shown in Table IV-1 required a significant portion of preprocessor memory. In addition to controlling a teletype, tape punch and the manual data entry unit, several hardware test conditions were preprorgrammed in the preprocessor. These preprogrammed conditions provided known outputs from the preprocessor which were used to check the transmission of the SPBP bus and to calibrate the oscillograph data recorders. Detailed descriptions of the five major functions listed in Table IV-1 may be found in other sections of this paper.

TABLE IV-1. - PREPROCESSOR FUNCTIONS

o DATA FORMATTING	
Inputs	- DC Analog - 3 Wire Synchro - Serial Digital (MLS) - Serial Digital (ARINC 561)

-continued-

TABLE VI-1. - PREPROCESSOR FUNCTIONS (cont.)

	- Serial Digital (SPBP) - DC Discrete
Outputs	- DC Analog - Serial Digital (SPBP) - DC Discrete

o COORDINATE TRANSFORMATIONS

- Conical
- MLS
- Airplane Body
- Airplane Track
- Geographic (INS)
- ILS

o COMPLEMENTARY FILTERING

Position	- MLS - Radio Altitude (Flare Option)
Velocity	- INS (Track Angle - Option 4) - Airspeed (Initial Conditions) - Baro. Alt. and Rate (Initial Conditions)
Acceleration	- 3 Axis Body Accelerometers (Option 3) - INS (Option 4)
Attitude	- INS
Heading	- INS
Body Rates	- 3 Axis Rate Gyros (Attitude/Heading Coast Mode)

o FLAG LOGIC

Discrete Flags
Reasonableness Tests

O SUPPORT FUNCTIONS

Teletype
Tape Punch
Manual Data Entry Unit
Hardware Test

INSTRUMENTATION

An extensive data recording capability is a part of the TCV B-737. For the demonstration development this was augmented by a parallel digital tape recorder and three oscillographs. A block diagram of the data recording capability is shown in Figure IV-5. The Piloted Aircraft Data System (PADS) is a serial PCM data system and is the main data system on the airplane. Other data systems use other tracks on the PADS tape recorder. Normally, time synchronization is provided from the PADS NASA 36-bit time code generator. This capability was augmented by an IRIG-B time code generator which was recorded on all recorders and synchronized to range time at the test range. This was required to correlate on-board data with radar and phototheodolite tracking data from the test range. Two other serial digital data streams are recorded. These are from the Navigation Computer Unit (NCU) and the Flight Control Computers (FCC). Significant parameters of the data streams are indicated in Figure IV-5.

There is some capability for transferring data between computers when it is desired to record MLS preprocessor data with the precision of the NCU Digital Bus, or NCU data with the quick-look capability of the oscillographs. The parallel digital tape recorder was used to record the MLS receiver output of Figure IV-4 and there was a telemetry link which transmitted MLS receiver output to the ground, where real time plots were made of the errors between phototheodolite tracking and onboard MLS position data. The four oscillographs were used to assess in flight the results of system changes. Pilot displays were recorded on video tape. The displays were an electronic attitude director indicator (EADI) and a multifunction display (MFD) which is an advanced form of electronic horizontal situation indicator. MLS receiver video output was recorded on one track of the PADS tape recorder and used for fault diagnosis.

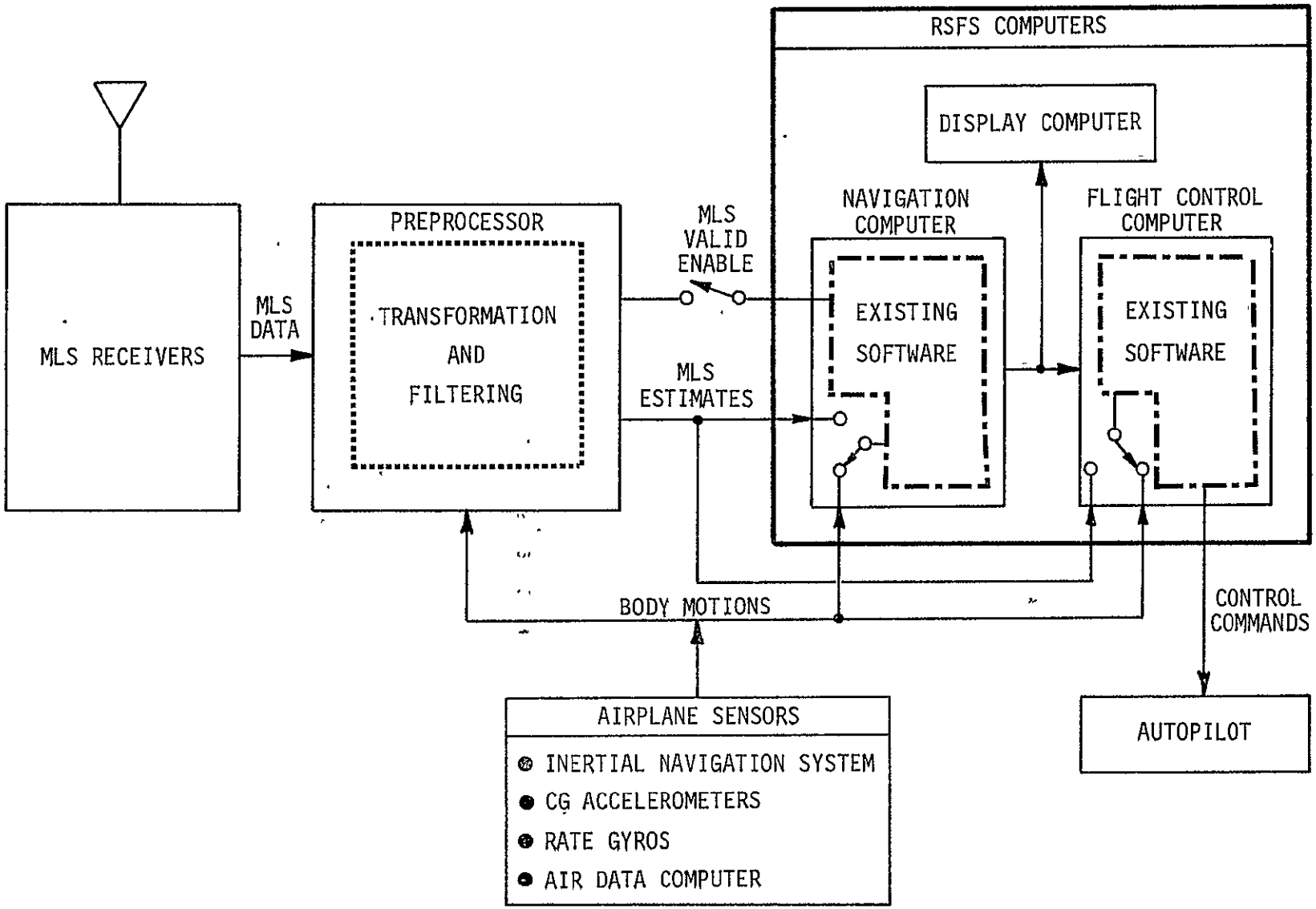

FIGURE IV-1. DEMONSTRATION EQUIPMENT CONFIGURATION

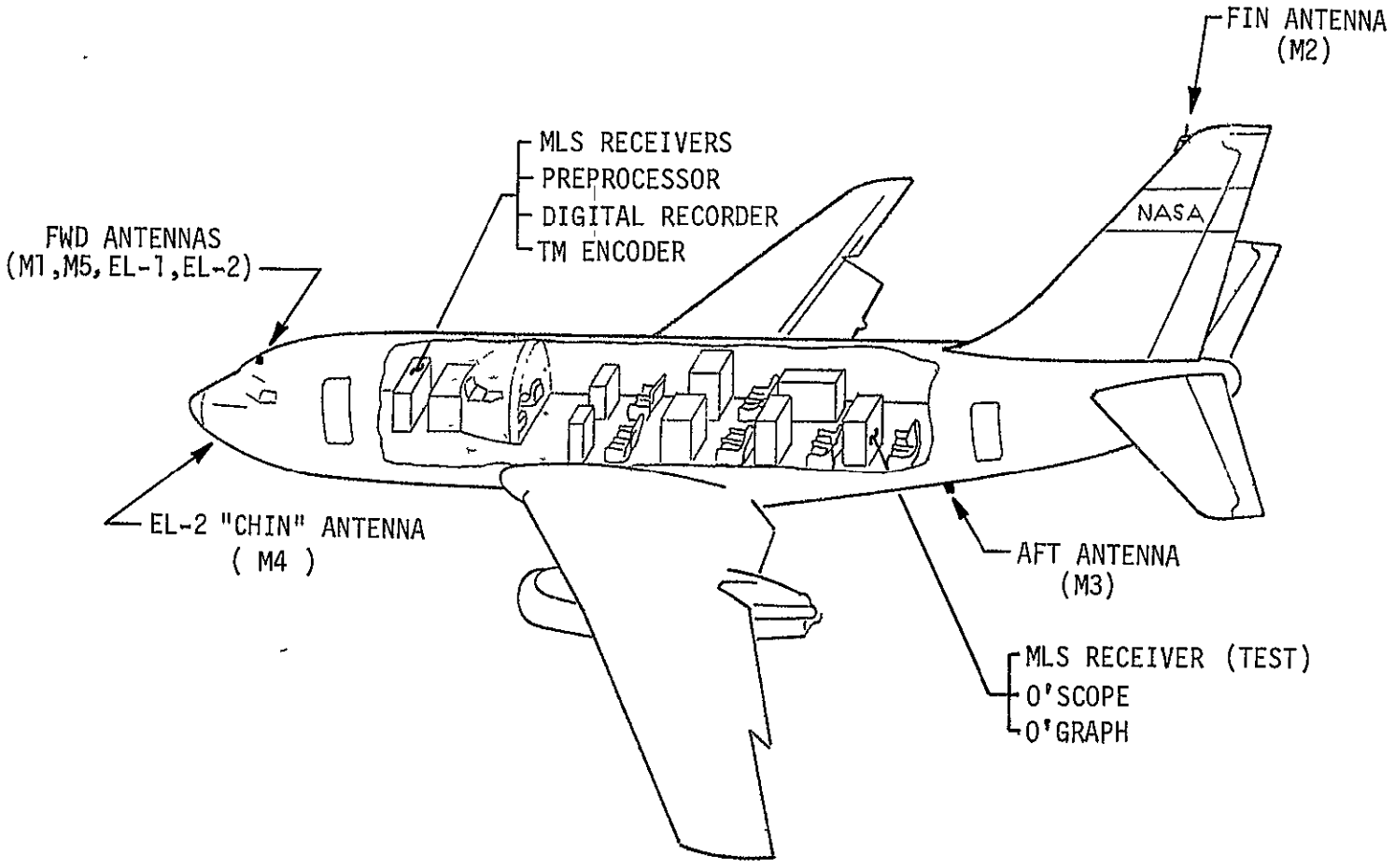

FIGURE IV-2 TRSB EQUIPMENT LOCATION

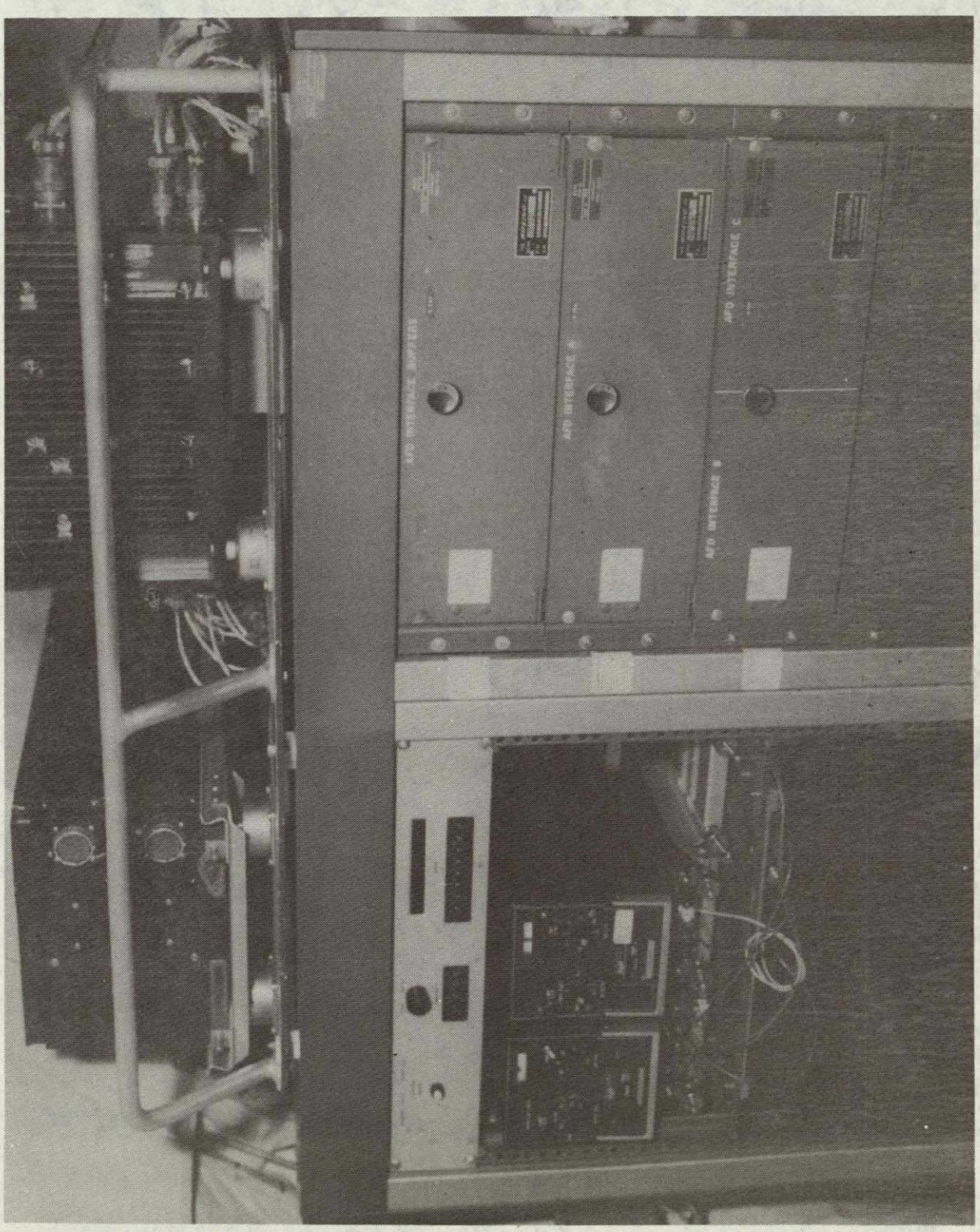

FIGURE IV-3A TRSB RECEIVING EQUIPMENT AND PREPROCESSOR

FIGURE IV-3B TRSB RECEIVING, PROCESSING AND DATA RECORDING EQUIPMENT

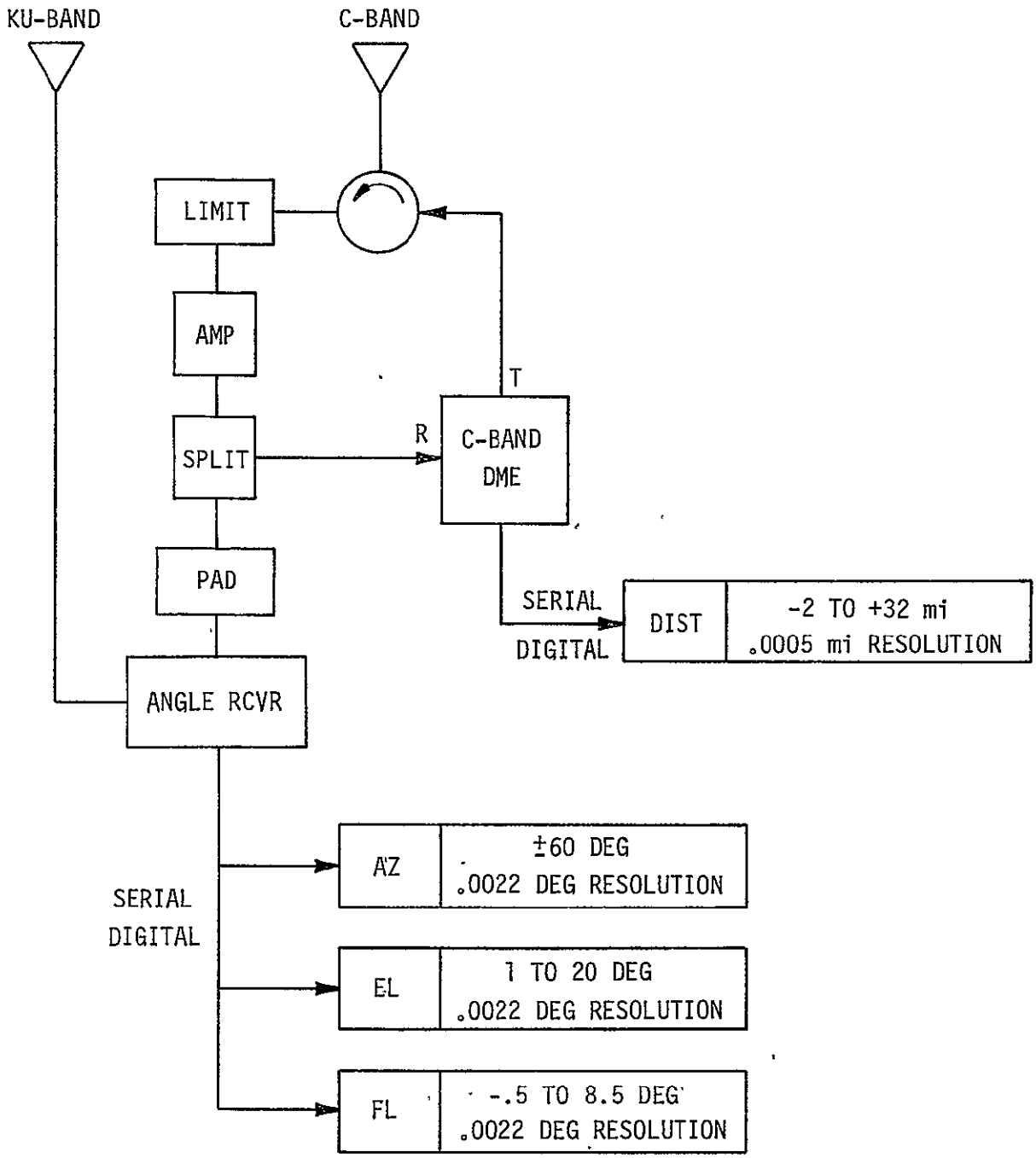

FIGURE IV-4 TRSB RECEIVERS

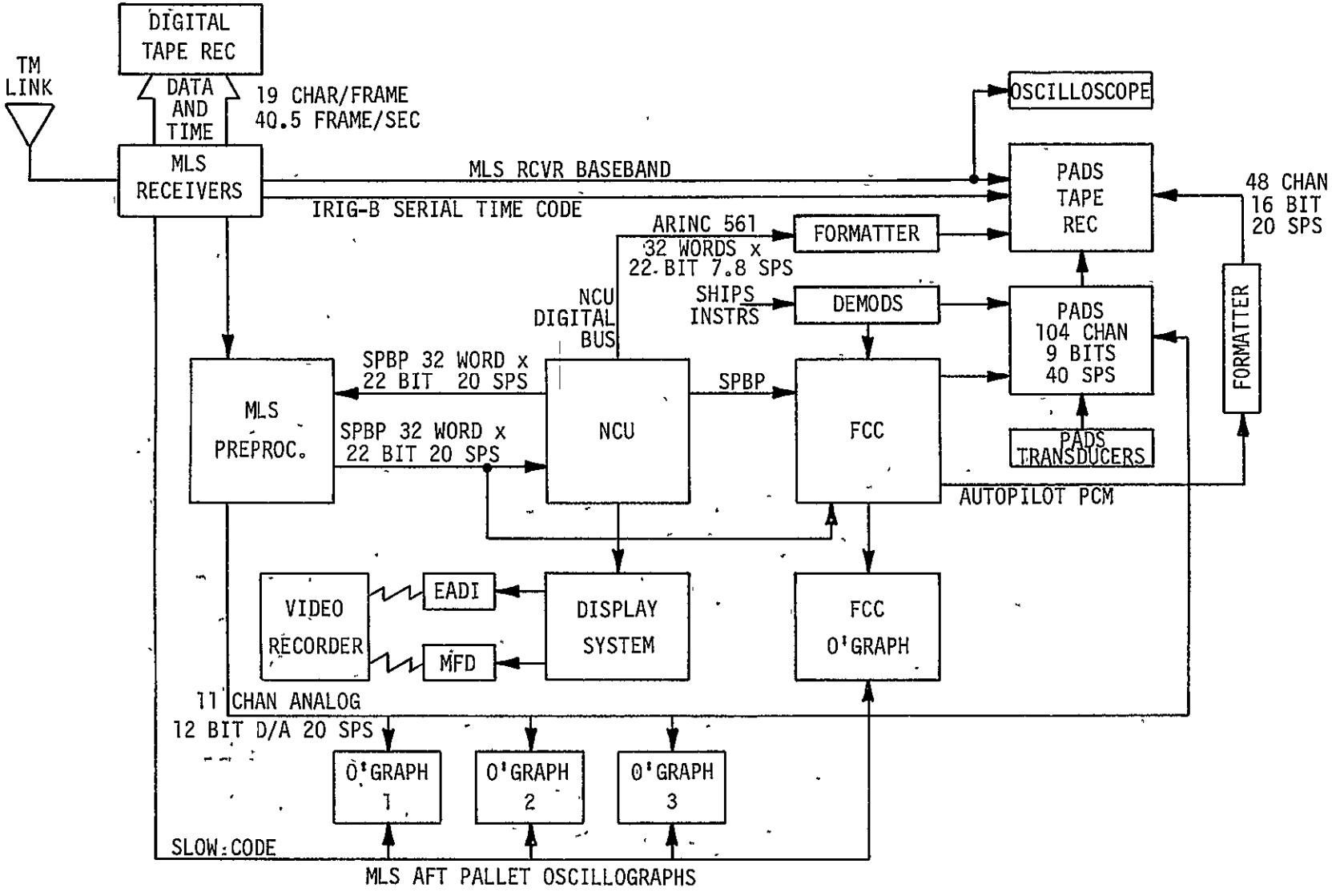

FIGURE IV-5 TCV B-737 DATA RECORDING

V. AIRCRAFT ANTENNA SUBSYSTEM

By Thomas G. Campbell

ANTENNA DESIGN AND DEVELOPMENT PROGRAM

Prior to the ICAO demonstration, a development program was conducted to adapt the TCV B-737 to use MLS guidance. An important step in establishing the MLS airborne configuration for this effort was to determine an antenna and RF subsystem design that would provide adequate signal levels for the various RF links involved. Since multipath effects and antenna radiation pattern effects of the airborne antennas were not known exactly, it was necessary to conduct an antenna test and evaluation program to resolve these points. This program included scale modeling techniques as well as analytical methods to resolve the airframe effects for specific antenna locations. After the scale model tests were concluded, the results were used to select an antenna configuration for the ICAO demonstration. A full-scale flight test was then conducted to verify the antenna design and location on the aircraft.

For the flight test, the B-737 was equipped with several antennas which were tested simultaneously. The various antenna locations are shown in Figure V-1. The flight evaluation consisted of measuring the signal strength and all pertinent MLS data during a straight-in approach, racetrack pattern approaches, and the proposed ICAO demonstration approach profiles. Two independent antenna/receiver combinations were used simultaneously to compare C-band monopole antennas. The two main antennas tested were located at body stations 239.5 (on top of the fuselage) and 1169 (on top of the vertical fin). In addition, two racetrack approach patterns were flown with a third antenna, at station 946.5 (on the bottom of the fuselage), substituted for the fin antenna. This was done to test for better coverage below and behind the aircraft.

By nature of the aircraft installation used, the cable losses associated with the vertical fin (M2) antenna were about 8 dB greater than those for the station 239 (M1) antenna. Consequently, the ranges obtained with those antennas were about 30 and 11 nautical miles, respectively. Signal dropouts were experienced during the various approach profiles but only a small percentage could be attributed to antenna pattern effects. Some in-beam and out-of-beam multipath signals were observed. The out-of-beam multipath had no detectable effect on the receiver output.

A complete description of the antenna development program is given in reference V-1. Based on the result of that program, the M1 antenna was selected for the C-band functions of the MLS (azimuth, EL-1, EL-2 omni ID signal, and DME). Later flight testing resulted in the use of the Ku-band omni antenna (see Figure V-1) for flare guidance during the demonstration.

A photograph of these antennas mounted on the B-737 fuselage is shown in Figure V-2. The physical configuration and electrical performance characteristics of these antennas are given in reference V-1.

RF SUBSYSTEM DESCRIPTION

A block diagram of the radio frequency components that fed the two MLS antennas is shown in Figure V-3. These components were located at the AFDI pallet in the cabin of the B-737 so that cable losses could be minimized. A low-loss semi-rigid coaxial cable was used to feed the C-band antenna, and elliptical waveguide fed the Ku-band omni antenna. As shown in the block diagram of Figure V-3, a tunnel diode amplifier was used ahead of the power splitter to insure adequate signal levels for the DME receiver. The sensitivity of the angle receiver was measured to be about -100 dBm, but the flight evaluation test demonstrated that at least -90 dBm would be required for an adequate video signal. The system margen calculations for the C-band and Ku-band functions are presented in Tables V-1 and V-2. The actual signal results for the C-band link are also presented in Table V-2.

CONCLUSIONS

The aircraft antennas selected to be used during the ICAO MLS demonstration performed well. The only time that the M1 antenna would not meet the coverage requirements would be for the back-course azimuth conditions. This case was not tested for the demonstration. Otherwise the M1 C-band and Ku-band omni antenna locations performed satisfactorily during the MLS flight tests and ICAO demonstration.

REFERENCES

V-1. Campbell, T. G.; White, W. F.; and Gilreath, M. C.: The Design, Development, and Flight Test Results of the Boeing 737 Aircraft Antennas for the ICAO Demonstration of the TRSB Microwave Landing System. NASA TMX-73943, August, 1976.

TABLE V-1. - MLS C-B AND SIGNAL STRENGTH PREDICTIONS AND RESULTS (RANGE 30 NM)

PARAMETER	AZIMUTH (5189.4 MHz) OMNI SIGNAL		AZIMUTH (5189.4 MHz) SCANNING BEAM		DME (5092 MHz) UPLINK SIGNAL		DME (5027 MHz) DOWN-LINK SIGNAL	
	FIN ANT.	STA. 250 ANT.	FIN ANT.	STA. 250 ANT.	FIN ANT.	STA. 250 ANT.	FIN ANT.	STA. 250 ANT
Ground Trans. Power	44 dB	44	44	44	53 dB	53 dB	54 dB	54
Ground Antenna Gain	15	15	30	30	15	15	15	15
Cable Loss	-3.0	-3.0	-3.0	-3.0	-3.0	-3.0	-3.0	-3.0
Space Loss	141.9	149.9	141.9	141.9	141.9	141.9	141.9	141.9
Aircraft Antenna Gain	-5.50	+2.0	-5.5	+2	-5.5	+2.0	-5.5	+2.0
Aircraft Cable Loss	-6.83	-1.43	-6.83	-1.43	-6.83	-1.43	-6.83	-1.43
Aircraft Component Loss	-1.00	-18.3	-1.00	-18.3	-1.00	-5.0	-1.00	-1.0
Polarization Loss	0	0	0	0	0	0	0	0
Aircraft Component Gain	0	+12.0**	0	+12.0	0	+12.0	0	0
Multipath Loss	0	0	0	0	0	0	0	0
Receiver Sensitivity	-103 dBm*	-103 dBm	-103 dBm	-103 dBm	-84 dBm	-84 dBm	-81 dBm	-81 dBm
Predicted Signal Level	-100	-90.2	-85	-75	-89.0	-79.0	-88	-76.0
Measured Signal Level	-98	-88.0	-93 dBm	-81.0	Not Meas.	Not Meas.	Not Meas.	Not Meas.
S/N Required for Lock (Experimentally Determined)	10 dB	10 dB	10 dB	10 dB	------	------	------	------
Actual Signal Margin	-5 dB	+5 dB	0	+12 dB	-1.3	+9.0	0	+8.57

TABLE V-2. - MLS KU-BAND SIGNAL STRENGTH

FREQUENCY = 15,468.4 MHZ

PARAMETER	OMNI ANTENNA
Ground transmitter power	43 dBm
Ground antenna gain	29 dB
Cable loss	Included
Space loss	-135.6 dB
Aircraft antenna gain	0 dB
Aircraft waveguide loss	-3.0 dB
Polarization loss	0 dB
Aircraft component gain	0 dB
Multipath loss	0 dB
Receiver sensitivity	-96 dBm
Predicted signal level	-67 dBm
S/N required for lock	10 dB
Actual margin	20.0 dB

Antenna	Body Station	Water Line	Buttock Line
Ku-band horn	180.5	173.0	R 3.3
Ku-band omni	239.0	283.5	L6
C-band omni	239.0	283.5	R6
C-band omni	946.5	169.0	
C-band omni (Vertical fin)	1169.75	542.5	

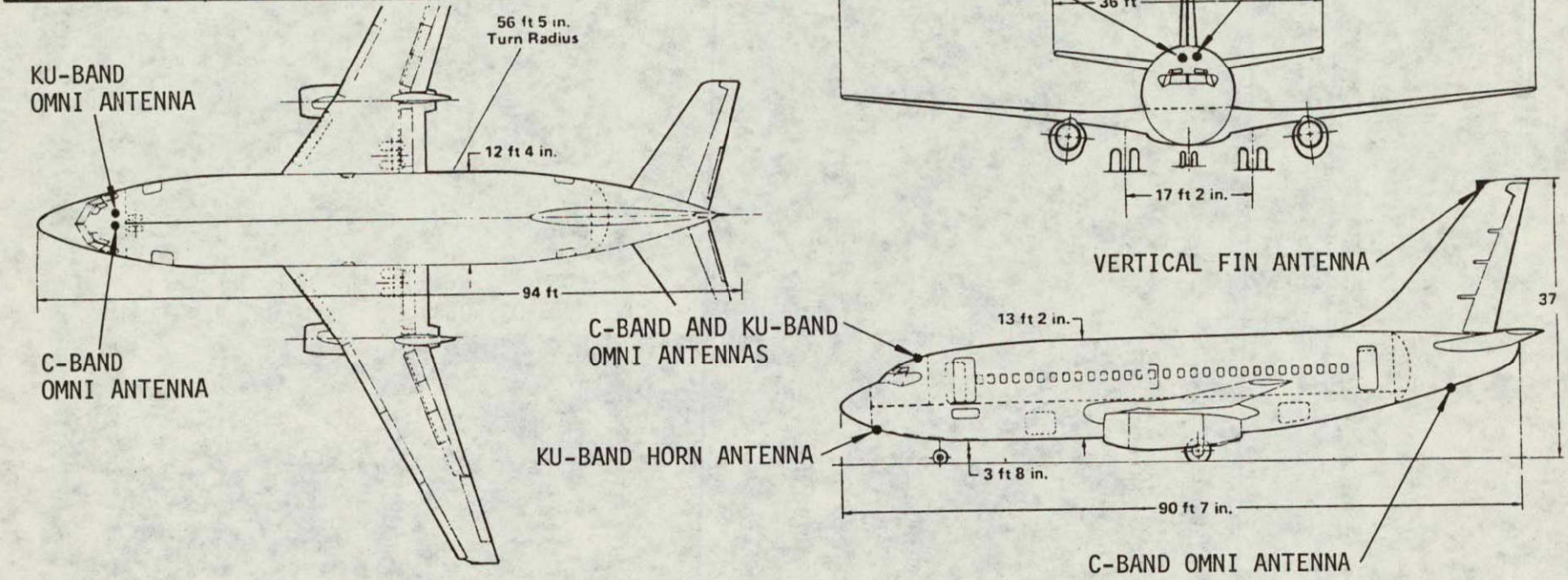

FIGURE V-1 MLS ANTENNA LOCATIONS

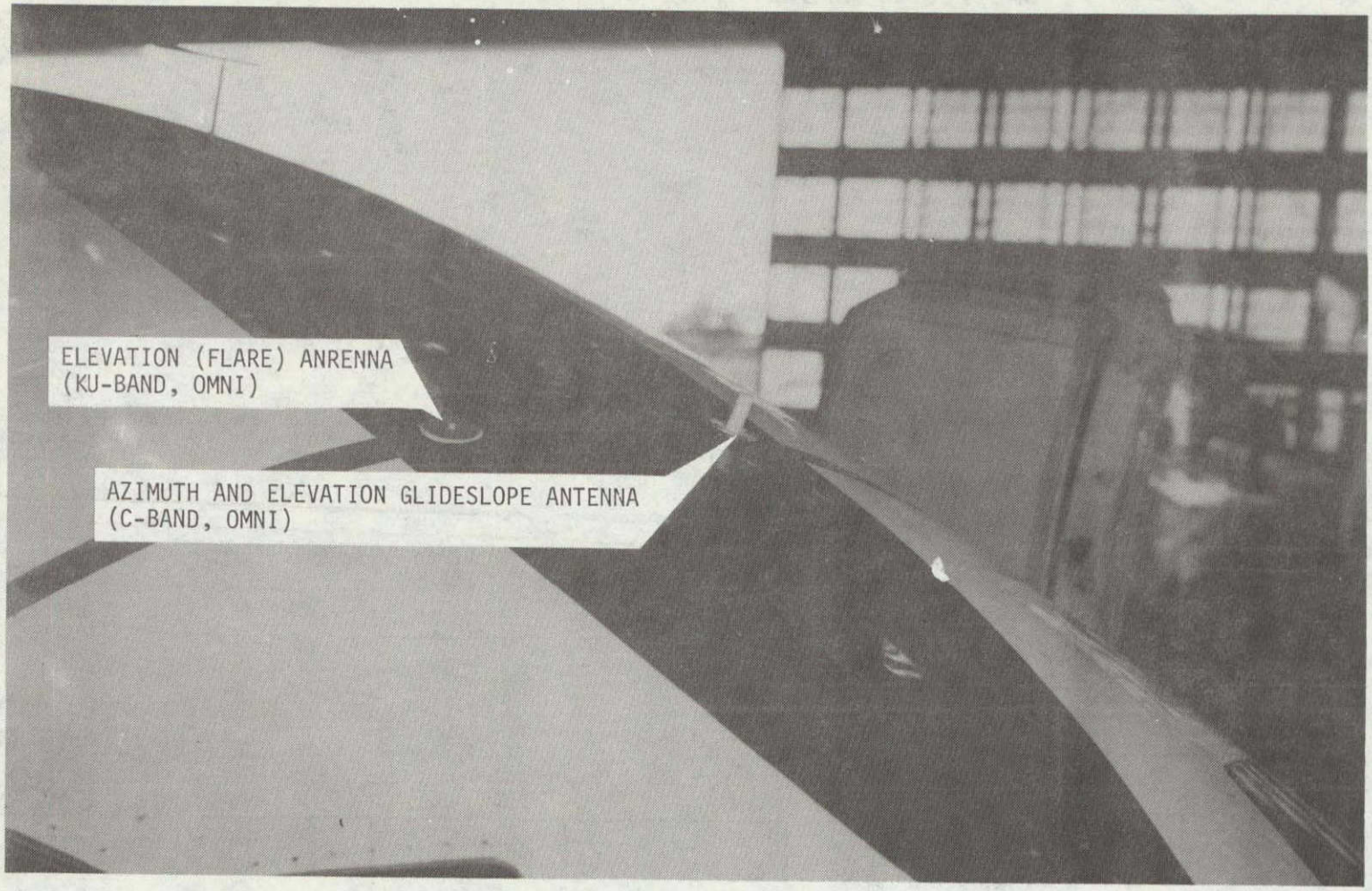

FIGURE V-2 PHOTOGRAPH OF OMNI MLS ANTENNAS AT STATION 239

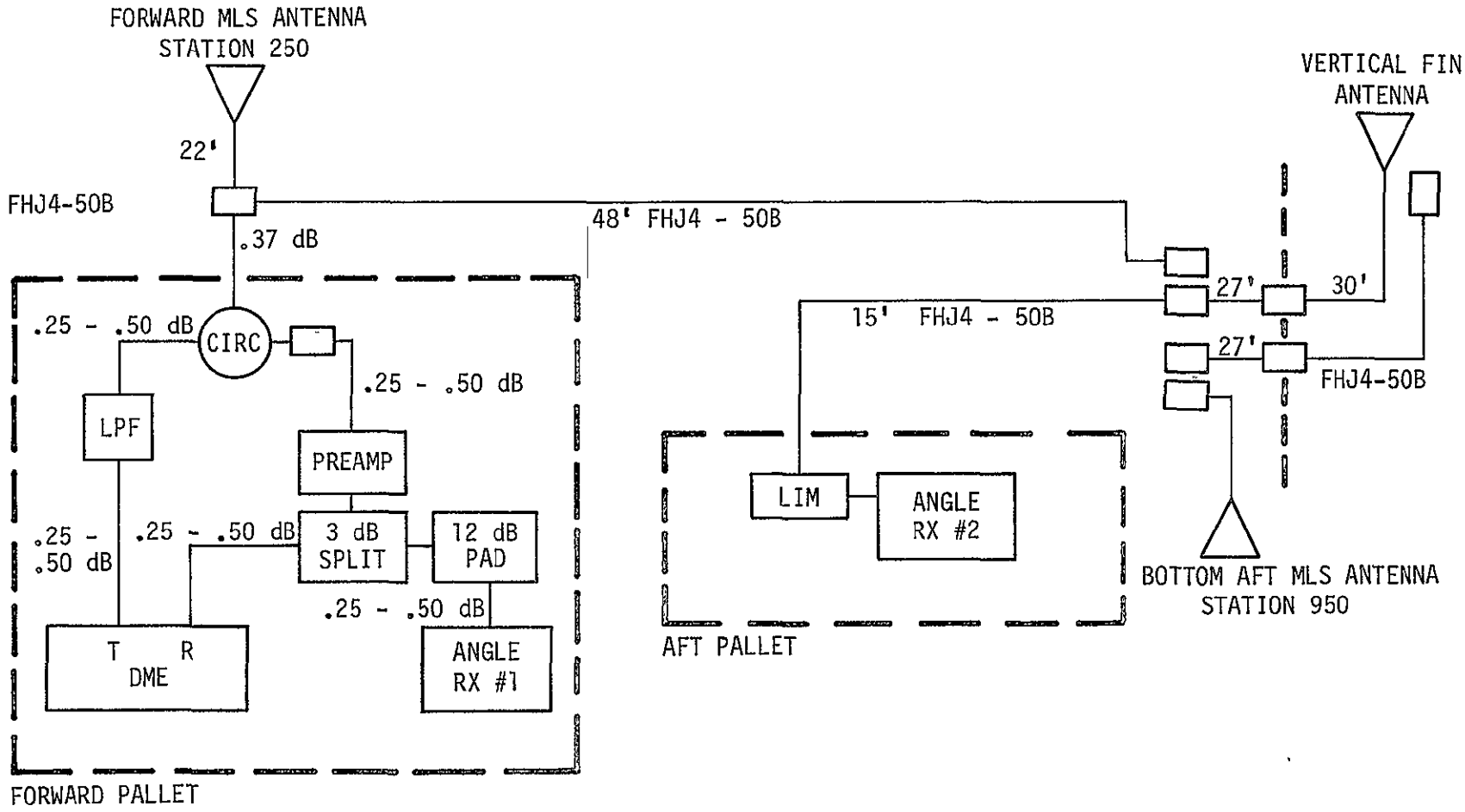

FIGURE V-3 RF EXPERIMENT CONFIGURATION FOR AIRCRAFT ANTENNA TESTS

PRECEDING PAGE BLANK NOT FILMED

VI. MLS PREPROCESSOR AND INTERFACE UNIT

By J. Larry Spencer

INTRODUCTION

The preprocessor consisted of a general purpose digital computer, an input/output (I/O) unit, and a manual data entry unit (MDEU). The function of the preprocessor was to receive data from the existing aircraft sensors, body mounted accelerometers and TRSB/MLS receivers; process the data; and transmit the results to the onboard flight control, navigation, display and recording systems. Figure VI-1 is a photograph of the preprocessor as installed in the NASA 515 aircraft. The unit at the upper left is the general purpose digital computer, a Singer Kearfott SKC-2000. The unit to the right of the computer is the I/O box and the rack-mounted unit below the computer is the MDEU.

PREPROCESSOR INPUT/OUTPUT

A block diagram of the preprocessor is shown in Figure VI-2. The transfer of data into and out of the computer was by the parallel channels of the computer. The transfer of data from the computer to the I/O unit utilized the 16-bit computer output channel and the 4-bit output device address channel. The computer output data and output device address were simultaneously transmitted from the computer to the I/O unit by control of the stored program. The output device address was decoded in the I/O unit and used to route the output data to the selected output device in the I/O unit. The transferring of data from the I/O unit to the computer utilized the computer input data channel, the input device address channel, and the computer interrupts. The digital computer executed an instruction to transfer the input device address to the I/O unit. The I/O unit decoded the address and enabled the selected input device on the computer input data bus. The computer executed a second instruction to read the data from the computer input data channel. The computer data read initiation was either from an external interrupt or stored program control. The MDEU interfaced directly with the computer for display and through the I/O unit for address selection and data entry. The MDEU was used for changing and displaying the contents of a selected memory location for either fixed point or floating point numbers.

Preprocessor Input/Output Unit. The preprocessor I/O unit block diagram is shown in Figure VI-3. The portion of the I/O unit above the broken line in the diagram was to transfer data from the TRSB/MLS receivers, body mounted accelerometers, and existing aircraft sensors into the computer via the computer input data channel. The input quantity, data format, and transmitting

system from which the preprocessor received data is listed in Table VI-1. The portion of the I/O unit below the broken line in Figure VI-3 was used to transfer computer output data to the navigation, flight control, display and recording systems aboard the NASA 515 aircraft. The output quantities, data format, and receiving system to which the preprocessor transmitted data is listed in Table VI-2.

The output from the computer to the I/O unit consisted of 16 parallel bits of data and four parallel bits of output device address which were transmitted simultaneously. The four bits of output device address were decoded and used to strobe the computer output data into the selected output device holding registers. There were 16 output device holding registers consisting of two for the Split Phase Bipolar (SPBP) transmitter, one for the output discretes and one for each of the 13 digital-to-analog converters (DACs). The output devices automatically tranformed the digital word in the holding register to their respective formats once the holding register was updated. The SPBP output bus was a transformer-coupled self-clocking digital data bus similar to the ARINC 575 digital data bus. The data format of the SPBP bus consisted of 32 bits of data, of which 8 were for word identification, one for data sign, one for redundant sign, one for odd parity and 21 for digital data. The 32 bits of SPBP output word were loaded into a 32 bit holding register in two 16 bit bytes. When the final byte was loaded, the SPBP transmitter was initiated and the word was transmitted.

The input portion of the I/O unit was used to transform preprocessor input data to a digital format and send the digital data to the computer. The input portion is shown above the broken line in Figure VI-3. For the computer to receive data from the I/O unit, the computer first had to send an input device address to the I/O unit. The input device address was transmitted to the I/O unit over the 8 bit input device address bus. The input device address decoded decoded the address and sent a signal to the selected input device to start the data conversion process and to enable the selected input device holding register on the input data bus. Digital tri-state drives were used on the output of each holding register so that the select register could be enabled on the 16 bit computer input data bus and the digital data could be transmitted to the computer. Once an input holding register was enabled on the computer input data bus, the computer had to execute a read instruction to store this input data in an accumulator or memory location. The initiation of data retrieval by the computer was either under computer program control or external interruption from the I/O unit. The external interruption was used so the computer would read incoming data to the I/O unit before the data was destroyed by more incoming data. The preprocessor input data which were read under interrupt control were as follows:

TRSB/MLS
SPBP receiver
ARINC 561 receiver
Entry data from the MDEU

The data which was read at periodic intervals under program control was as follows:

DC analog
3 wire synchro
Input discretes
MDEU address selection

Each of the 9 analog inputs were converted into a 12 bit digital word and each of the 5 synchro inputs were converted into a 14 bit digital word. The 8 input discretes were transformed directly to an 8 bit input word for the computers. Both the SPBP receiver and ARINC 561 receiver had the same data format as the SPBP transmitter word except the ARINC 561 format had an error bit instead of a redundant sign bit. The 32 bits of ARINC 561 word and SPBP word had to be read into the computer in 16 bit bytes. The ARINC 561 and SPBP receiver generated an odd parity on the received data and compared this parity bit against the transmitted parity bit. If the received parity and transmitted parity agreed, an interrupt was sent to the computer to initiate the reading of data. On receiving the interrupt, the computer would read the selected holding register and decode the input word into the 21 bits of data plus a sign bit. The TRSB/MLS digital-to-digital (D-to-D) interface sent a 16 bit word to the computer for each azimuth, elevation-1 or elevation-2 quantity received from the TRSB/MLS angle receiver. A 16 bit data word representing slant range was also sent to the computer by the D-to-D interface. The slant range information came from the TRSB/MLS DME receiver. The TRSB/MLS D-to-D interface also sent a flag word to the computer concerning the status of the data received by the TRSB/MLS receivers and the polarity of the slant range data received.

The I/O unit was constructed and designed at Langley Research Center. A closeup picture of the I/O unit is shown in Figure VI-4. Power supplies were mounted internally to the heat sink. All electronic components were mounted on printed circuit boards which have a card connector on one edge. A picture of a typical card is shown in Figure VI-5. Interconnection between cards and connection to the external connectors were made through the card edge connectors. The I/O unit operated approximately 1000 hours during checkout and flight without a failure.

Manual Data Entry Unit. The manual data entry unit (MDEU) was a software-controlled device used for displaying or changing the contents of selected memory locations either in a fixed-point or a floating-point number system. A photograph of the MDEU is shown in Figure VI-7. To display a memory location content, the address of the location was selected by use of the hexadecimal thumbwheel switches marked "address". The contents of the location were displayed on the eight hexadecimal readout lights. To change the contents, the desired contents had to be selected on the eight hexadecimal data switches, and the red "data entry" button had to be pushed. The data on the thumbwheel

data switches would appear on the readout lights when the data was entered into memory. The address and data from the MDEU was read into the computer via the I/O unit in 8 bit bytes. The hexadecimal display lights on the MDEU were driven directly from the computer with two 16 bit parallel output channels. The contents of any memory location could be changed except in certain areas of hardware-protected core memory. To change the contents of a memory location in protected memory, the Computer Control Unit (CCU) had to be used to override hardware memory protect. The computer error light which was on the front of the MDEU was connected directly to the built-in test in the digital computer. If the computer failed the light would be illuminated. The MDEU was designed and built at Langley Research Center and operated approximately 1000 hours without a failure.

DIGITAL COMPUTER

The digital computer used in the preprocessor was a Singer-Kearfott SKC-2000. A photograph of the computer is shown in Figure VI-6. The computer used 900 watts of 3-phase 115-vac 400 Hz input power. The computer required 3 pounds per minute of forced air for cooling. A list of the basic characteristics of the computer is shown in Table VI-3.

GROUND SUPPORT EQUIPMENT

The ground support equipment for the preprocessor consisted of an I/O checkout unit and a computer programming facility. A photograph of the I/O checkout unit is shown in Figure VI-8. The checkout unit was a carry-on piece of equipment used to verify the operation of the I/O unit. The checkout unit could transmit data in the required format to drive each preprocessor input port. The format of the data transmitted was selected by the mode switch which was located on the front panel. The data transmitted was manually selected by the eight thumbwheel switches also located on the front panel of the checkout unit. The checkout unit was used to verify that the I/O unit was transmitting correctly by receiving the I/O unit outputs and displaying the received values. The DC analog outputs from the I/O unit were displayed on the analog meter, the SPBP outputs on the hexadecimal readout lights and the output discretes on the eight individual lamps on the front panel. The I/O checkout unit was used in conjunction with special hardware test software, which was resident in the computer at all times. The I/O checkout unit and hardware test software were used in performing a complete preflight check on the preprocessor.

A photograph of the programming facility for the preprocessor's digital computer is shown in Figure VI-9. In the photograph from left to right is a card reader, line printer, teletype unit and paper tape reader/punch which were all connected to the minicomputer. The minicomputer formatted data to and from

the peripherals for communication with the digital computer via the CCU. The teletype unit and paper tape reader/punch could be used directly with the CCU without the minicomputer. In addition to the CCU being used as a communication link between the digital computer in the preprocessor and the minicomputer, it also was used as a software programming/debugging aid. The CCU could be manually used to single step, monitor and change software in the digital computer. Below the CCU in the photograph is a laboratory power panel which controlled the input power to the preprocessor's computer and also the power for the cooling blowers. The power panel had an interlock so the power could not be applied to the computer unless the cooling unit was operating. To the extreme right in the photograph, the preprocessor's digital computer is shown with the plumbing connected for laboratory cooling.

TABLE VI-1. - PREPROCESSOR INPUT QUANTITIES

INPUT QUANTITIES	FORMAT	TRANSMITTING SYSTEM
Normal acceleration	DC analog	Body mounted accelerometer
Lateral acceleration	DC analog	Body mounted accelerometer
Longitudinal acceleration	DC analog	Body mounted accelerometer
Radio altitude	DC analog	Radio altimeter #1
Pitch rate	DC analog	Pitch rate gyro
Roll rate	DC analog	Roll rate gyro
Yaw rate	DC analog	Yaw rate gyro
Vertical acceleration	DC analog	Inertial Nav. System (INS) #2
Vertical velocity	DC analog	Central Air Data Comp. (CADC)
Calibrated airspeed	3 wire synchro	CADC #2
Pitch attitude	3 wire synchro	INS #2
Roll attitude	3 wire synchro	INS #2
True heading	ARINC 561	INS #2
Velocity north	ARINC 561	INS #2
Velocity east	ARINC 561	INS #2
Crosstrack acceleration	ARINC 561	INS #2
Alongtrack acceleration	ARINC 561	INS #2
Azimuth	MLS (Bendix)	MLS angle receiver
Elevation 1	MLS (Bendix)	MLS angle receiver
Elevation 2	MLS (Bendix)	MLS angle receiver
Slant range	MLS (Bendix)	MLS DME receiver
Ground speed	SPBP	Navigation computer

-continued-

TABLE VI-1. - PREPROCESSOR INPUT QUANTITIES (continued)

INPUT QUANTITIES	FORMAT	TRANSMITTING SYSTEM
Radar altimeter #1 flag	28 volt discrete P	Radio altimeter #1
CADC air speed flag	28 volt discrete P	CADC #2
INS attitude flag	28 volt discrete P	INS #2
INS navigation flag	28 volt discrete P	INS #2
Azimuth function flag	5 volt discrete Y	MLS angle receiver
Elevation 1 function flag	5 volt discrete Y	MLS angle receiver
Elevation 2 function flag	5 volt discrete Y	MLS angle receiver
Slant range flag	5 volt discrete Y	MLS DME receiver

TABLE VI-2. - PREPROCESSOR OUTPUT QUANTITIES

OUTPUT QUANTITIES	FORMAT	RECEIVING SYSTEM
Glide slope deviation	DC analog	Display system
Localizer deviation	DC analog	Display system
Velocity east	DC analog	Recording
Alongtrack acceleration	DC analog	Recording
Altitude	DC analog	Recording
Altitude rate	DC analog	Recording
MLS vertical acceleration	DC analog	Recording
Cross runway velocity	DC analog	Recording
Cross runway error	DC analog	Recording
Altitude error	DC analog	Recording
MLS X acceleration	DC analog	Recording

-continued-

TABLE VI-2. - PREPROCESSOR OUTPUT QUANTITIES (continued)

OUTPUT QUANTITIES	FORMAT	RECEIVING SYSTEM
MLS Y acceleration	DC analog	Recording
Velocity north	DC analog	Recording
Vertical velocity	SPBP	Control computer system
Vertical acceleration	SPBP	Control computer system
Altitude	SPBP	Control computer system
Glide slope deviation	SPBP	Control computer system
Localizer deviation	SPBP	Control computer system
Cross runway velocity	SPBP	Control computer system
Ground speed	SPBP	Control computer system
Lateral error	SPBP	Control computer system
Altitude error	SPBP	Control computer system
EL-1 valid	SPBP	Cont. and nav. comp. systems
AZ valid	SPBP	Cont. and nav. comp. systems
Crosstrack acceleration	SPBP	Navigation computer system
Alongtrack acceleration	SPBP	Navigation computer system
Velocity north	SPBP	Navigation computer system
Velocity east	SPBP	Navigation computer system
Altitude (mean sea level)	SPBP	Navigation computer system
Change in longitude	SPBP	Navigation computer system
Change in latitude	SPBP	Navigation computer system
Estimated MLS X position	SPBP	Navigation computer system
Estimated MLS Y position	SPBP	Navigation computer system

-continued-

TABLE VI-2. - PREPROCESSOR OUTPUT QUANTITIES (continued)

OUTPUT QUANTITIES	FORMAT	RECEIVING SYSTEM
Estimated MLS Z position	SPBP	Navigation computer system
MLS valid	Switch closure	Display system
MLS valid	Switch closure	Navigation system

TABLE VI-3. - SKC-2000 CHARACTERISTICS

Whole word
General purpose
Stored program
Parallel
Binary
Fractional
Two's complement
Hardware - fixed and floating point arithmetic

32 bit word length, ½ word capability
Double precision capability

8k core memory (32 bit words) for addressing 131k

Read only memory

Sine, cosine, square root, matrix (add, subtract, multiply and transpose)

Hardware memory
64 index register
One microsecond memory cycle time
32 external interrupts

FIGURE VI-1 PREPROCESSOR INSTALLED ABOARD THE NASA 515 AIRCRAFT

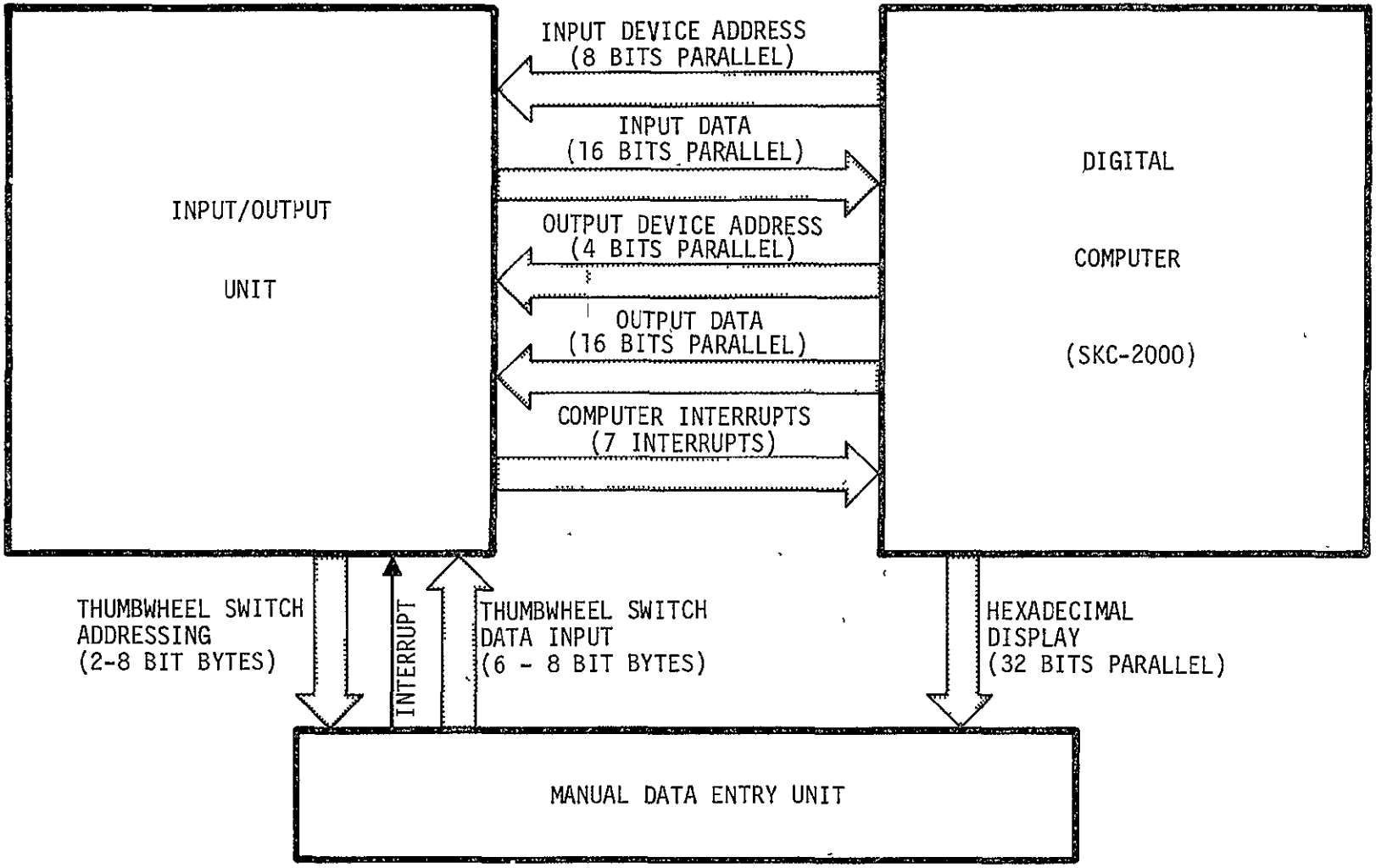

FIGURE VI-2. PREPROCESSOR BLOCK DIAGRAM

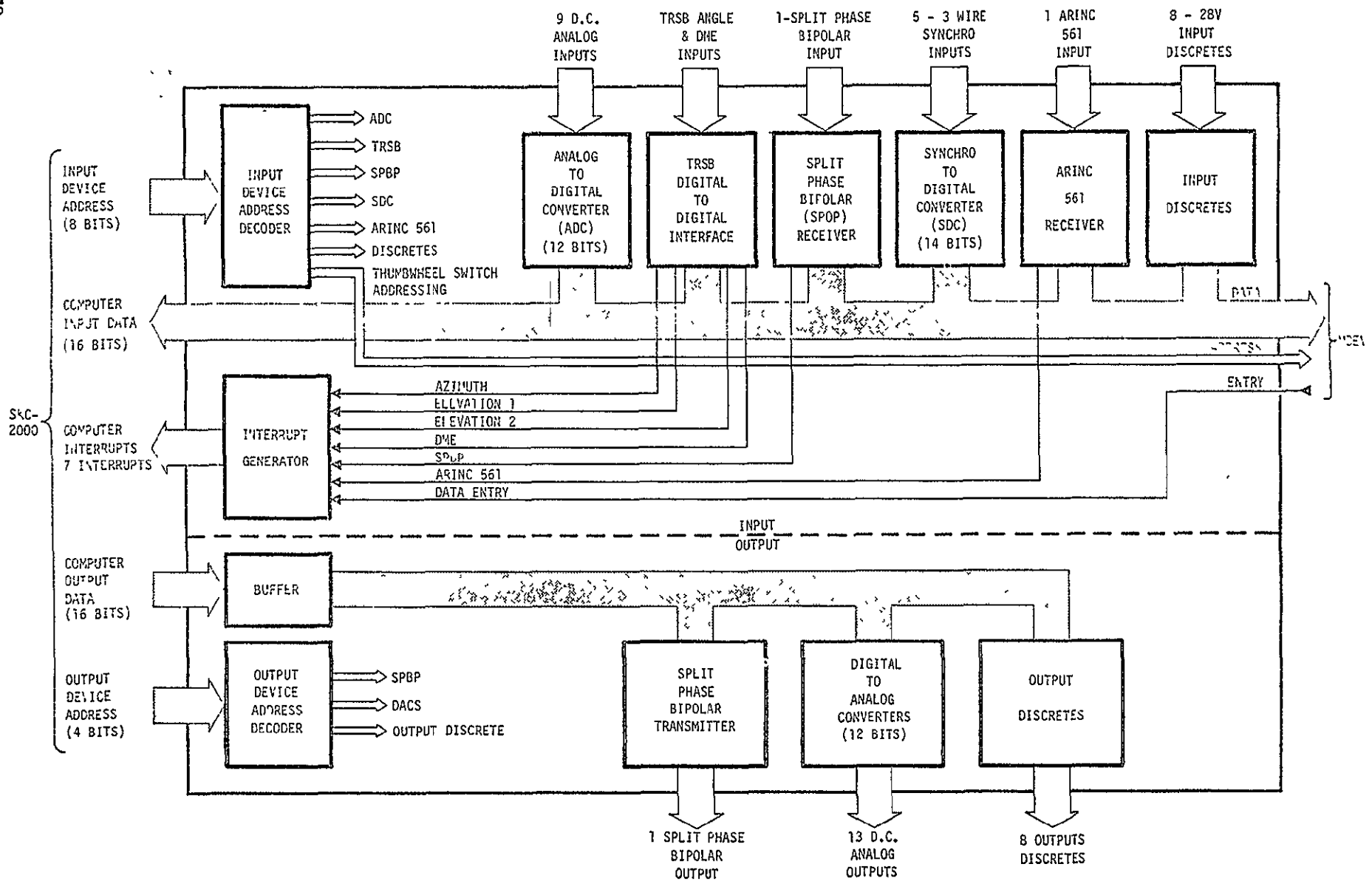

FIGURE VI-3 PREPROCESSOR INPUT/OUTPUT UNIT BLOCK DIAGRAM

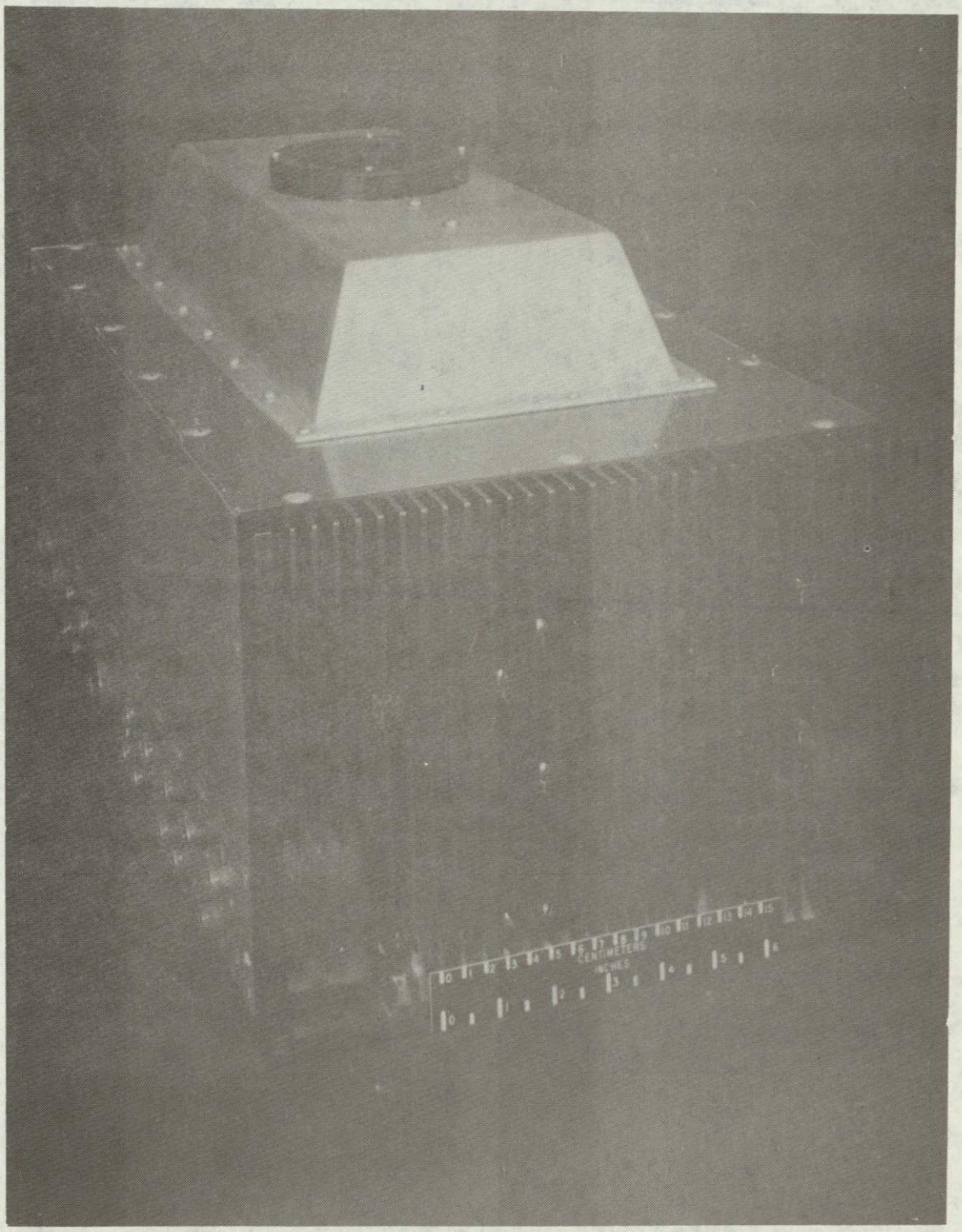

FIGURE VI-4 INPUT/OUTPUT UNIT

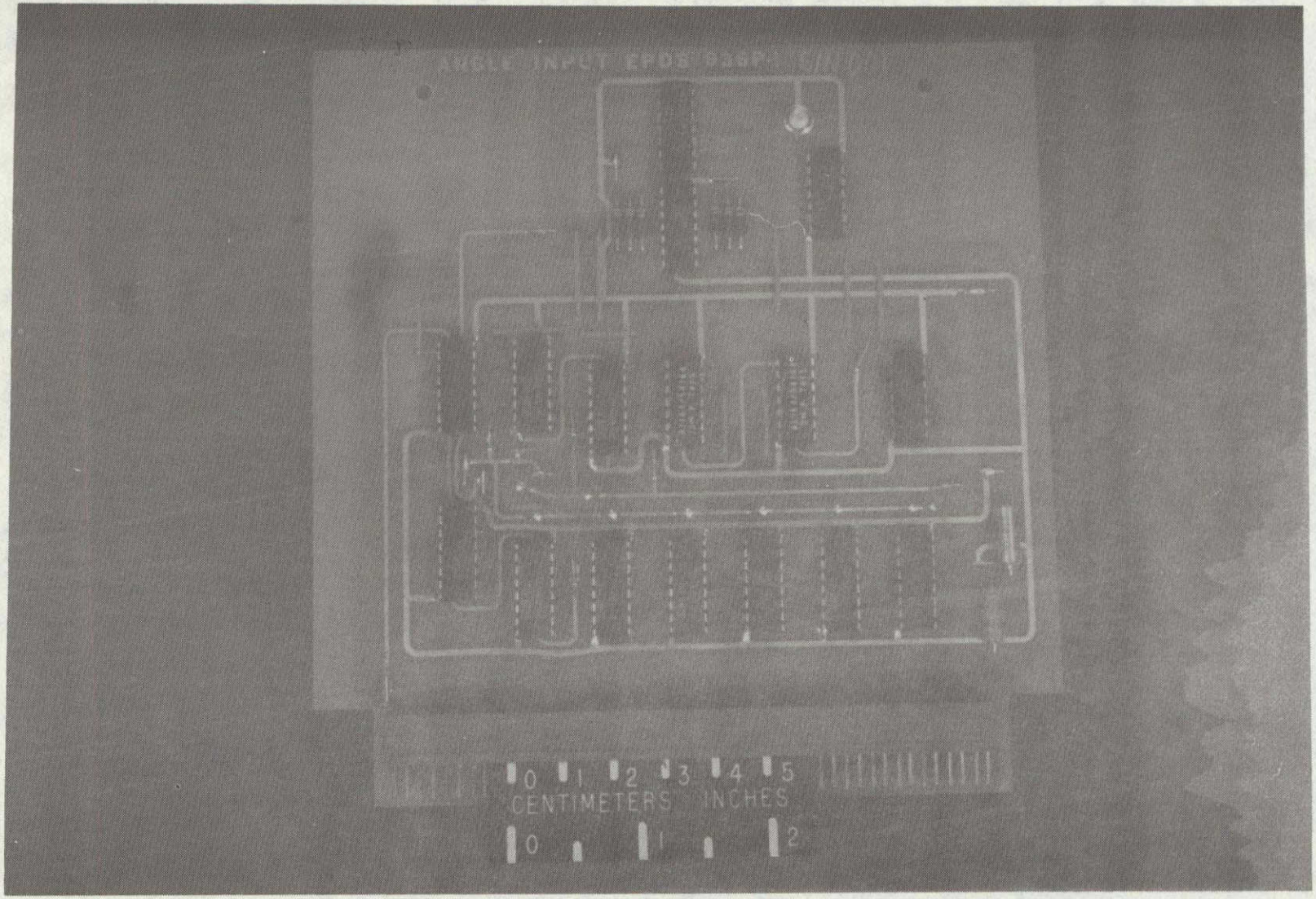

FIGURE VI-5 TYPICAL I/O UNIT CARD

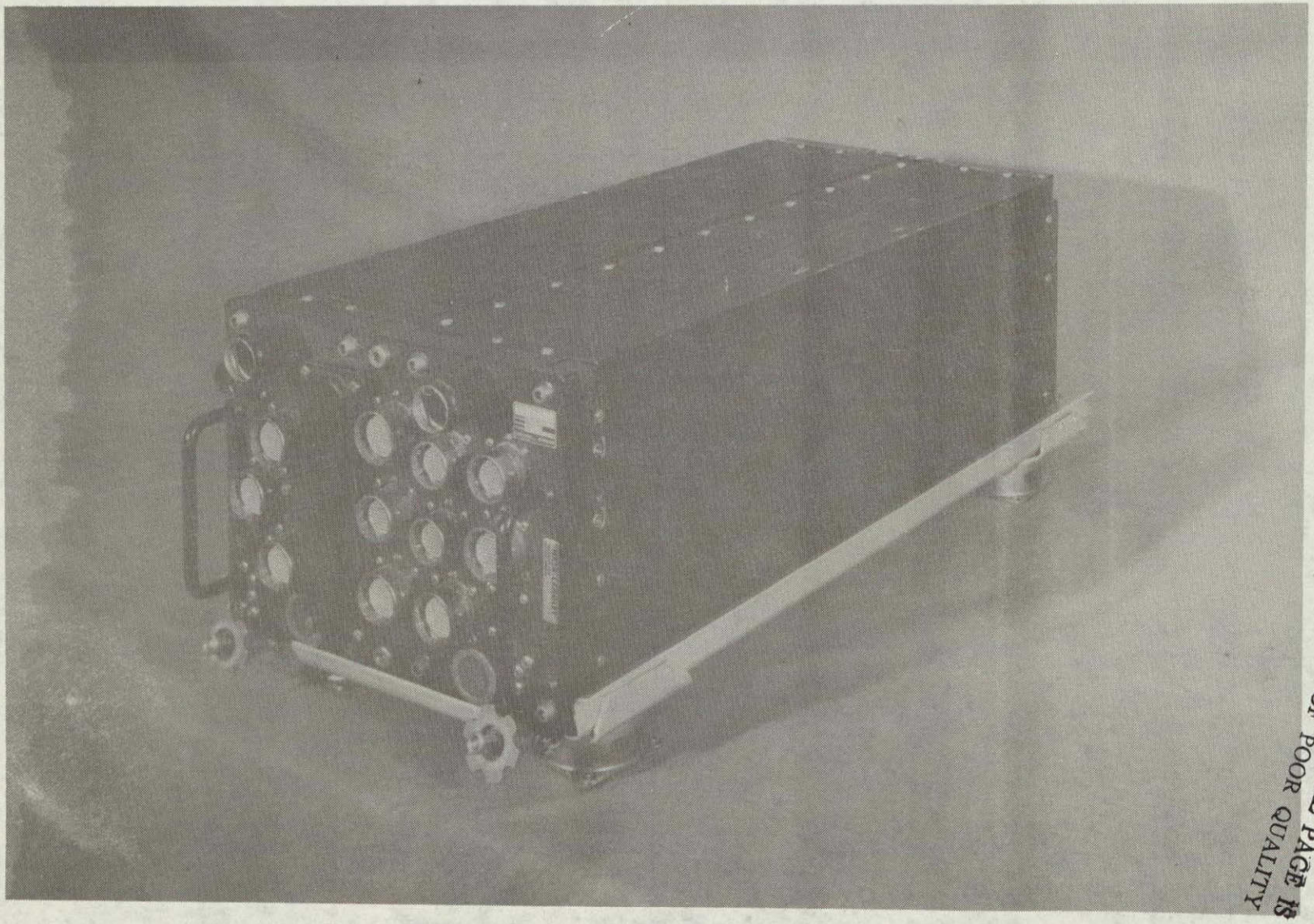

FIGURE VI-6 GENERAL PURPOSE DIGITAL COMPUTER (SKC-2000)

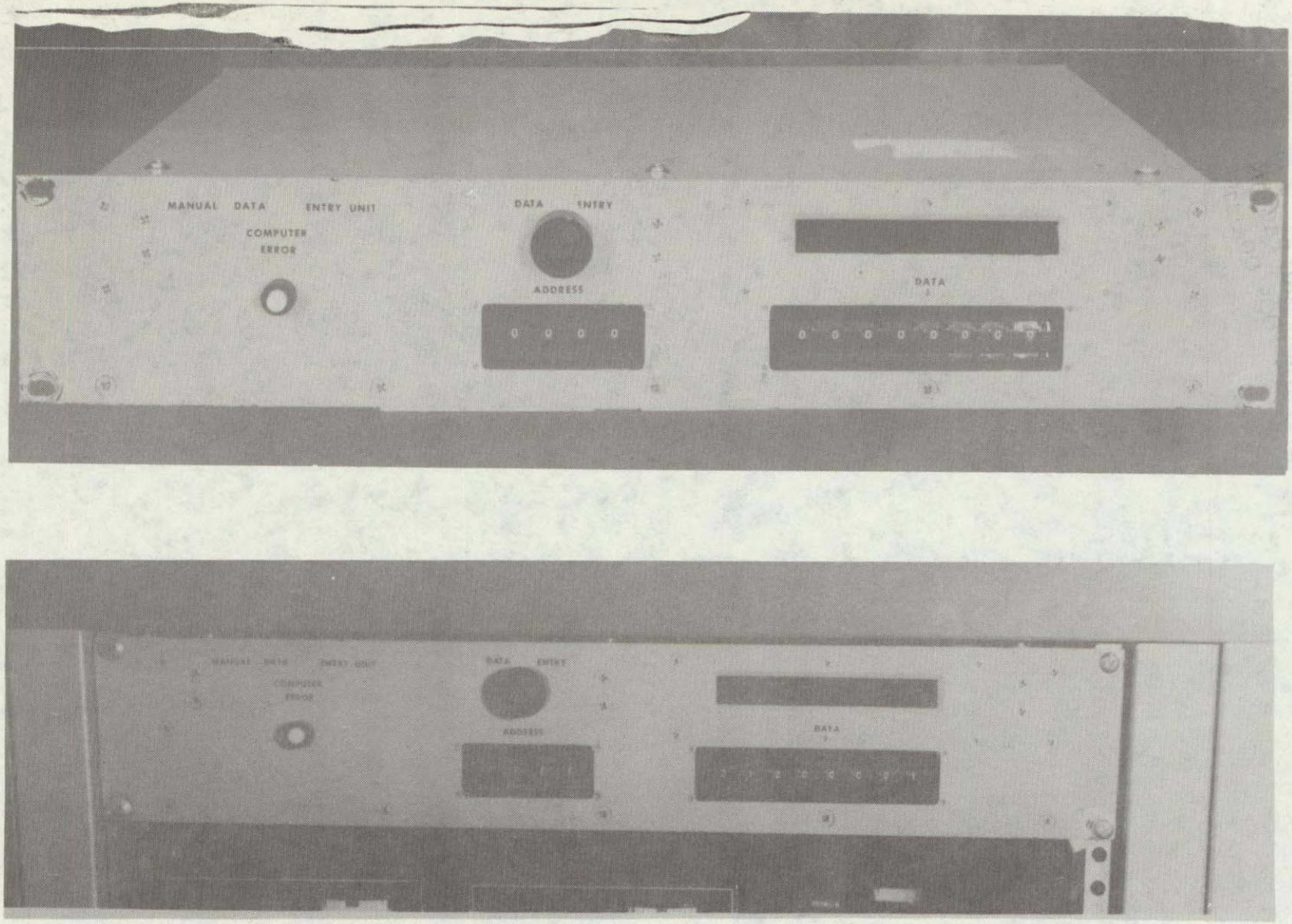

FIGURE VI-7 MANUAL DATA ENTRY UNIT

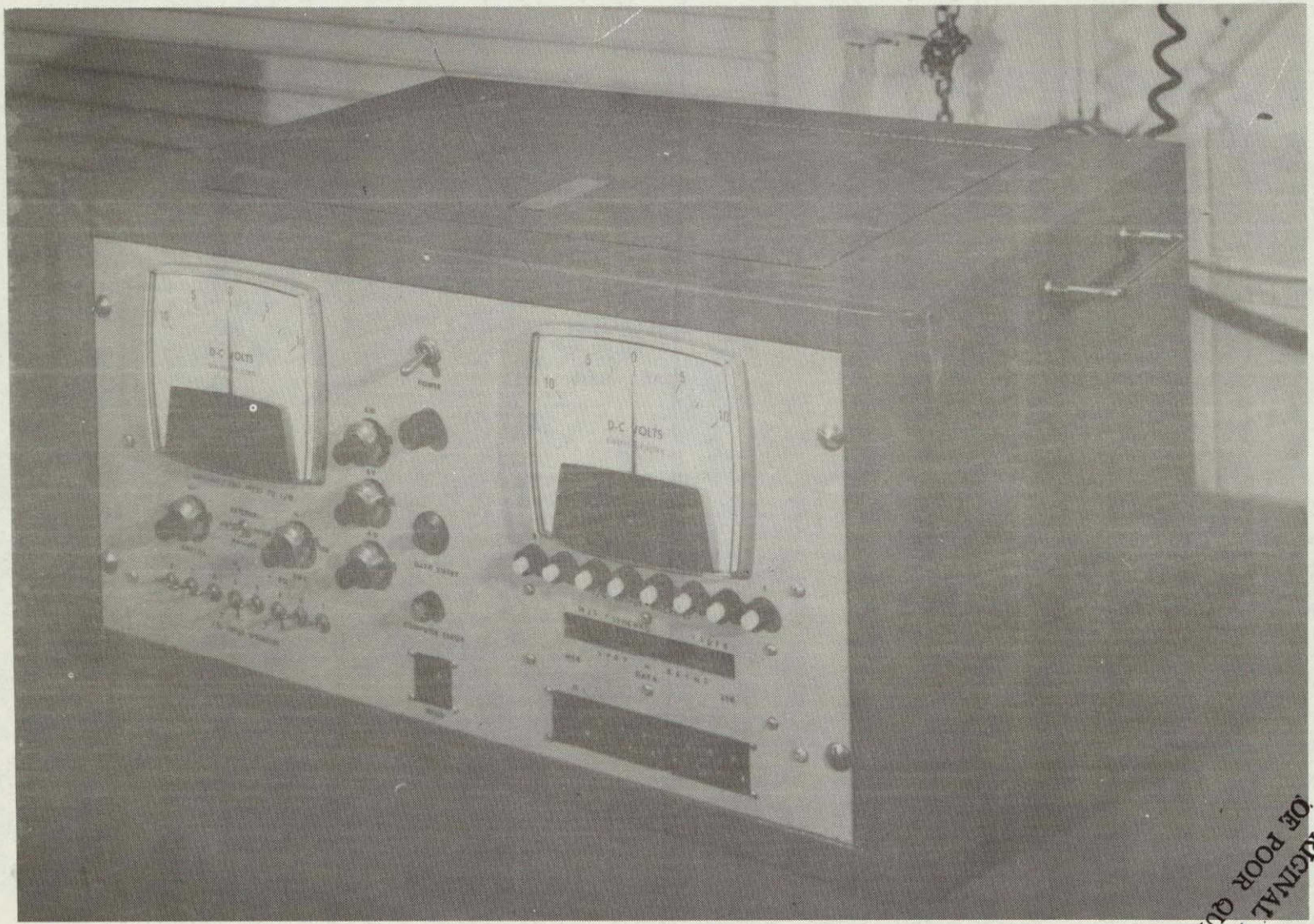

FIGURE VI-8 INPUT/OUTPUT CHECKOUT UNIT

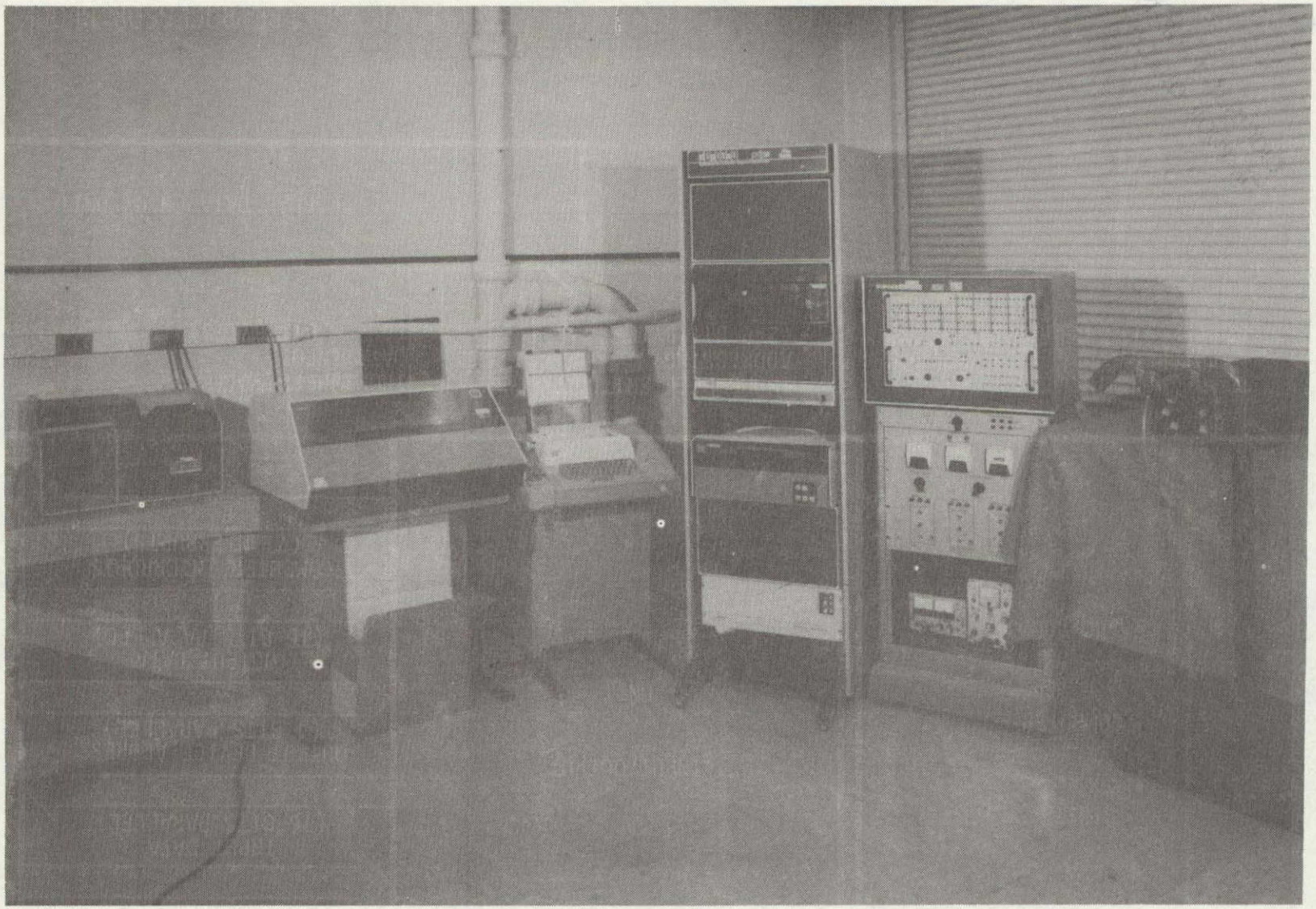

FIGURE VI-9 COMPUTER PROGRAMING FACILITY

CHAPTER VII. SIGNAL PROCESSING TECHNIQUES

By William T. Bundick

INTRODUCTION

This chapter will discuss (1) the analysis of various types of filters undertaken to select a pre-filter for the MLS data, (2) the choice of pre-filter bandwidth, (3) the technique used to remove outliers from the MLS data, and (4) the transformation from MLS conical coordinates to MLS cartesian coordinates.

PRE-FILTERS

The functions performed in the pre-processor for the MLS/ICAO Demonstration flights are shown in figure VII-1. The angle and range data from the MLS receivers were filtered prior to the transformation from MLS to Cartesian coordinates. The reason for pre-filtering the MLS data were: (1) to reduce the bias introduced into the x, y, z coordinates by the non-linear transformation of noisy MLS data and (2) to provide estimates of the MLS data for inputs into the coordinate transformation in the case of data dropouts.

Three types of pre-filters were analyzed: (1) α-β filters, (2) low-pass filters, and (3) upgraded moving window filters. The low-pass filter was the type already existing in the MLS angle receiver (filtered output), and the upgraded moving window filter was the type that was in the MLS DME receiver. The filters were evaluated on the basis of noise smoothing performance, tracking accuracy with noiseless inputs, tracking accuracy during data dropouts, and ease of implementation.

α-β filter. The α-β filter is described by the following difference equations:

$$\hat{x}_n = (1 - \alpha)\, x_{pn} + \alpha x_n \tag{1a}$$

$$\hat{\dot{x}}_n = \hat{\dot{x}}_{n-1} + \frac{\beta}{T}\,(x_n - x_{pn}) \tag{1b}$$

$$x_{pn+1} = \hat{x}_n + T\hat{\dot{x}}_n \tag{1c}$$

where $\hat{x}_n$ = estimate of x at time index n

$\hat{\dot{x}}_n$ = estimate of $\dot{x}$ (= dx/dt) at time index n

x_{pn+1} = prediction at time index n of the value of x at time index n + 1

x_n = measured value of x at time index n

T = sample interval

α,β = filter constants

It has been shown that optimum filter performance is obtained when $\beta = \alpha^2/(2 - \alpha)$.

Low-pass filter. - The low-pass (LP) filter is described by the following difference equation:

$$\hat{x}_n = (1 - a)\hat{x}_{n-1} + ax_n \tag{2}$$

In the existing low-pass filter in the angle receiver a = 0.5 in the azimuth filter, and a = 0.25 in the elevation and flare filters.

Moving Window Filter. - An ordinary moving window (MW) filter is described by the equation

$$\hat{x}_n = \frac{1}{N} \sum_{i=1}^{N} x_{n+1-i} \tag{3}$$

The filter analyzed has been called an upgraded moving window because a velocity correction term has been added to equation (3). Since the filter output is an average of present time and past values, the output is an estimate of the value of x at a time past. The velocity correction is used to predict this estimate for the present time. The upgraded moving window filter is described by

$$\hat{x}_n = \frac{1}{N} \sum_{i=1}^{N} x_{n+1-} + \hat{\dot{x}}_n \Delta t \tag{4}$$

where Δt = elapsed time between the mean time of the averaged samples $x_{n + 1 - i}$ and the present.

$$\Delta t = \frac{(N - 1)}{2} T$$

$\hat{\dot{x}}_n$ = velocity estimate.

The velocity estimate is determined by

$$\hat{\dot{x}}_n = \frac{1}{K_1} \sum_{i=1}^{K_1} x_{n + 1 - i} - \sum_{i=K_2+1}^{K_2 + K_1} x_{n + 1 - i} \qquad (5)$$

For the filter in the DME receiver, N = 8, K_1 = 8, K_2 = 56, and T = 1/40 sec.

ANALYSIS

Tracking Accuracy. - Tracking accuracy was evaluated using as filter inputs noiseless MLS data generated during simulated flight following the path pictured in figure VII - 2. The aircraft velocity was 120 kts. The turn radius in this path was the same as the turns in the ICAO flight paths. The estimates of position and velocity were initialized at the start point by setting all estimates equal to zero. This procedure produced a start-up transient in many cases.

Range and azimuth tracking accuracies were studied. Elevation tracking performance was not studied because of the similarity to the azimuth case. In fact, elevation tracking accuracy should have been better than azimuth because the rates of change were lower and the elevation sample rate was higher.

Although the DME data rate was 40 samples/sec, the range tracking analysis was performed at the azimuth sample rate of 13 1/3 Hz to conserve computer time and memory. With the change in sample rate, the values of N and k_2 were adjusted to 3 and 18 respectively, but the tracking accuracy should have been nearly the same for the two cases. Note that the azimuth tracking error for the straight-in portion of the path was not computed, since the tracking error (but not noise error) for that segment was zero for all three filters.

Typical results for the noise free tracking errors in the range filter outputs for the three types of filters are plotted in figure VII-3. The spikes in the center of the plots are for data drop-outs, and will be discussed later. The results in figure VII-3 are for the aircraft flying the circular portion of the path in figure VII-2. The filter constants are:

for the α-β filter: $\alpha = 0.474$, $\beta = 0.147$

for the low-pass filter: $a = 0.5$

for the moving window filter: $N = K_1 = 3$, $K_2 = 18$

The 3-dB bandwidth of all three filters was approximately 2.2 Hz. As would be expected, the α-β and moving window filters have smaller errors than the low-pass because the former two have an inherent velocity correction term while the low-pass does not. The low-pass filter error goes through zero at about 49 sec. because the range rate goes to zero at about that point.

The errors for the azimuth filters are similarly plotted in figure VII-4 for the aircraft flying the circular arc, and the errors for the range filters are shown in figure VII-5 for the aircraft on the straight-in approach. Since the range rate is constant on the straight-in segment and the input data is noiseless, the α-β and moving window filters have zero error in this case.

Data Drop-out Performance. - The filters were tested to determine what happens to the tracking errors during periods when no MLS data is being received. Data dropout periods of 1 sec and 6.4 sec were simulated. The 1 sec period corresponds to the time required by the angle receiver to generate a function flag, and 6.4 sec in the time required by the DME receiver to generate a DME flag, as discussed in Chapter II. In analyzing the dropout performance it was assumed that the occurrence of data dropouts was flagged by the MLS receivers such that the filters could be adapted. The adaptation procedure is discussed below.

For the α-β when the receiver indicated a bad data point, the coefficients α and β were set equal to zero in the appropriate filter. With $\alpha = \beta = 0$, the algorithms (from eqs. (1)) become

$$\hat{x}_n = \hat{x}_{pn}$$

$$\hat{\dot{x}}_n = \hat{\dot{x}}_{n-1}$$

$$x_{pn+1} = \hat{x}_n + T\hat{\dot{x}}_{n-1} \qquad (6)$$

$$\therefore \hat{x}_n = \hat{x}_{n-1} + T\hat{\dot{x}}_{n-1}$$

Thus, the filter output (position estimate) becomes the last good estimate of position updated by the last good estimate of velocity.

For the low-pass filter when the data flag is present, the filter constant a is set equal to zero, and the low-pass algorithm becomes (from eq. 2).

$$\hat{x}_n = \hat{x}_{n-1} \qquad (7)$$

In this case the last good estimate of position is maintained for the length of the dropout. Obviously the estimate error increases with time for a non-zero velocity.

For the moving window filter when the data flag is present, the algorithms for the moving window filter become (from eqs. (3) through (5)).

$$\hat{x}_n = \hat{x}_{n-1} + \overline{\hat{\dot{x}}_n T}$$

$$\hat{\dot{x}}_n = \hat{\dot{x}}_{n-1}$$

$$x_n = \hat{x}_n \qquad (8)$$

Thus, the current estimate of position becomes the last good estimate of position updated by the last good estimate of velocity.

Dropout performance was tested by indroducing a period of no MLS input data and adapting the filters to operate as described above. The resulting errors are shown in figures VII-3 through VII-5. The range error on the circular flight path is smallest for the low-pass filter because the range rate is small and passes through zero, while the range acceleration is relatively large at the point of dropout. Note in figure VII-5 that for the straight-in approach the range error is zero even during the dropout for the α-β and moving window filters because the range rate is constant.

During actual operation this error would, of course, not be precisely zero because the previous filter estimate of range rate would have some error because of noise on the data. The results for the moving window type range filter indicate how the existing filter in the DME receiver performs.

Noise Smoothing. - The noise smoothing performance of the three filters was calculated for the following cases: the α-β filter with $\alpha = 0.474$, the low-pass filter with a = 0.5, and the moving window filter with N = 3 and $K_2 = 18$. Note that the LP filter constant and the MW constants were equivalent to the existing receiver filters in terms of bandwidth. The analysis assumes that the input data errors are statistically independent from sample to sample. This assumption is valid for receiver noise, but it is not valid for multipath errors. Thus, the noise smoothing results may not be valid for multipath errors.

It has been shown that the ratio K_x of the variance of the filter output to the variance of the input is given by (for $E\{x_n\} = 0$)

$$K_x = \frac{E\{\hat{x}_n^{-2}\}}{E\{x_n^2\}} = \frac{\sigma_{\hat{x}}^2}{\sigma_x^2} = \sum_{K=0}^{\infty} g_k^2 \qquad (9)$$

where g_k is the filter impulse response. The impulse response g_k was computed numerically by applying an impulse at the filter input and calculating the response (output $\hat{x}_n$). The results for K_x, which are listed in Table VII-1, show that the three filters have approxmiately the same noise smoothing performance, as would be expected from their similar bandwidths. It should be noted that the noise smoothing performance of the MW filter with N = 8, $K_2 = 56$, as in the DME receiver, is better than with N = 3, $K_2 = 18$. This is because the N = 8 filter is averaging over more noise samples.

Results of Analysis. - Results are summarized in Table VII-1. In terms of noise smoothing there is little difference in three filters. The tracking accuracy of the α-β and MW filters are clearly superior to the LP filter accuracy. The tracking accuracy of the α-β is slightly better than the MW for the filter constants examined. This difference is probably negligible.

TABLE VII-1. - SUMMARY OF RESULTS OF PREFILTER ANALYSIS

Filter Type	Filter Constants	3 dB Freq., Hz	Noise Reduct. dB	Tracking Error (no noise)							
				Range, feet				Azimuth, degrees			
				Turn		Straight		Turn		Straight	
				(1)	(2)	(1)	(2)	(1)	(2)	(1)	(2)
α-β	α = 0.1	0.33	-12.8	4.09	127.9	0	0	-0.011	-0.011	0	0
	α = 0.474	2.2	-5.0	0.085	91.92	0	0	-0.0002	0.0047	0	0
Lowpass	a = 0.5	2.1	-4.8	15.15	-35.48	15.15	1303	0.0253	2.172	0	0
Moving Window	N = 3, K_2 = 18	2.1	-4.3	0.22 1.86*	106.7	0	0	-0.0006	0.0065	0	0
	N = 8, K_2 = 56**	2.3	-8.5							0	0

(1) With no data dropouts
(2) With 6.4 second data loss
* Error with 3 out of 4 data points missing
** Sample rate = 40 Hz; 13 1/3 Hz for all other filters

In terms of complexity the α-β and LP are recursive filters. For these reasons the α-β filter was selected as the MLS data prefilter. This analysis showed that the response of the moving-window filter in the DME receiver was adequate. Additional prefiltering was used to provide additional noise smoothing.

PREFILTER BANDWIDTHS

An expression for the frequency response of the α-β filter can be obtained by first taking the z - transform of the difference equations (eqs. (1)) and combining to get an expression for the filter output (the estimate $\hat{x}_n$) in terms of the input (x_n).

$$H(z) = \frac{X_n\ (z)}{X_n\ (z)} = \frac{\alpha + (\beta - \alpha)z^{-1}}{1 + (\alpha + \beta - 2)z^{-1} + (1 - \alpha)z^{-2}} \qquad (10)$$

In H (z) substitute $z = e^{sT}$, and make the approximations

$$e^{-sT} \approx 1 - j\,\omega\,T \qquad (11a)$$

$$e^{-2sT} \approx (1 - j\omega T)^2 \qquad (11b)$$

The transfer function then becomes

$$H(j\omega) \qquad \frac{\alpha + (\beta-\alpha)(1 - j\omega T)}{1 + (\alpha + \beta - 2)\ (1 - j\omega T) + (1 - \alpha)(1 + j\omega T)^2} \qquad \omega << \frac{1}{T} \qquad (12a)$$

$$\left|H(j\omega)\right| \qquad \frac{\beta^2 + (\alpha - \beta)^2\ T^2\ \omega^2}{[\beta - (1 - \alpha)\ T^2\ \omega^2]^2 + (\alpha - \beta)^2\ T^2\ \omega^2} \qquad \omega << \frac{1}{T} \qquad (12b)$$

The filter bandwidths should be chosen such that the desired information on the MLS dat is passed essentially unaltered while the higher frequency noise components are filtered out. In order to properly choose these bandwidths, the spectra of the information must be determined. To this end, eighteen runs of the digital simulation of the 737 aircraft were made using the approach and landing profiles and wind conditions specified in table VII-2. The landing profiles were a 120^0 turn and an S-turn similar to the paths flown in the ICAO Demonstration. The wind conditions used in the simulation covered the variety of conditions which it was anticipated may have

been encountered during the demonstration flights.

TABLE VII-2 - MLS DATA CUT-OFF FREQUENCIES
FROM DIGITAL SIMULATION OF 737 FLIGHT

RUN #	FLIGHT PROFILE	WIND SPEED (KT) /DIRECTION	TURBULENCE	20 dB CUT-OFF FREQUENCY, Hz		
				AZ	EL-1	DME
1	120° turn	None	None	.057	.10	.063
2	"	15/head	4	.057	.12	.061
3	"	12/tail	2	.058	.11	.064
4	"	12/R.C.	2	.057	.095	.062
5	"	15/L.C.	4	.059	.090	.062
6	"	Shear	4	.058	.11	.064
7	"	None	None	.057	.096	.062
8	"	12/R.C.	2	.057	.080	.061
9	"	15/L.C.	4	.058	.083	.062
10	S-turn	None	None	.058	.24	.058
11	"	15/head	4	.049	.23	.057
12	"	12/tail	2	.049	.25	.060
13	"	12/R.C.	2	.048	.23	.058
14	"	15/L.C.	4	.048	.22	.058
15	"	Shear	4	.049	.23	.061
16	"	None	None	.048	.24	.058
17	"	12/R.C.	2	.048	.24	.059
18	"	15/L.C.	4	.049	.23	.059

The outputs of the simulation were a time history of the aircraft position in MLS coordinates (AZ, EL1, and DME range). These time histories of the MLS data (coordinates) were further analyzed to determine the autocovariance function and the power spectral density (PSD) for each data type for each run. A sample azimuth time history and the associated power spectral density are shown in figures VII-6 and VII-7 respectively. In this case the aircraft flew the S-turn flight path, and the simulated winds included both shear and turbulence.

The plots of PSD were examined, and the frequency at which the PSD had fallen to 20 dB below its peak value was determined. These results, or cut-off frequencies, are listed in table VII-2. In all cases the peak value was the lowest frequency data point (0.004 Hz). From the table VII-2 the maximum

cut-off frequencies were 0.059 Hz, 0.25 Hz, and 0.064 Hz for AZ, EL1, and DME respectively. Allowing a factor of 2, the pre-filter 3 dB frequencies were chosen initially to be 0.12 Hz and 0.50 Hz for AZ and EL1, respectively. A factor of 2 would produce a 0.13 Hz 3 dB-frequency for the DME channel, but since the DME data was already filtered in the DME receiver by a moving window filter with a 3 dB frequency of 2.3 Hz, the bandwidth of the DME α - β pre-filter was set at 0.20 Hz.

The tracking error for the AZ and DME pre-filter was re-evaluated using the above bandwidths, and the maximum noise free tracking errors were found to be about 0.04 deg and 11 ft. for AZ and DME, respectively. Since these errors were of the same order of magnitude as the anticipated MLS noise and bias errors, the filter bandwidths for AZ and DME were increased to 0.35 Hz and 0.30 Hz, respectively, with a corresponding reduction in tracking error to 0.009 deg and 5 ft.

Equation (12) was solved iteratively to obtain the values for the coefficients and which would produce the desired bandwidths. A sample rate of 20 Hz (T = 0.05 sec) was used in these calculations because the pre-filter computations are accomplished in the SKC-2000 at a 20 Hz rate even though the basic MLS data rates are 13.5, 40.5, and 40 samples/sec for AZ, EL1, and DME, respectively.

The final values of bandwidth, α, β and noiseless tracking error are listed in Table VII-3. The noise smoothing was re-evaluated for these filter parameters, and the results are also in Table VII-3. The phase response of the three pre-filters was calculated using equation (12a), and the results are plotted in figure 8 along with the amplitude response computed using equation (12b).

OUTLIER REMOVAL

An examination of MLS data recorded during an early NAFEC test flight revealed that the data contained a number of outliers, that is data points which far exceeded the expected noise errors. An analysis of the effect of outliers on the pre-filter outputs and of an outlier removal technique was subsequently conducted. In figure VII-9 the DME filter output error is shown for the case where one outlier has been inserted in the input data (data point #5). This data point had a value of 200K ft., which is close to the maximum value of the DME data word. The actual range at this time was approximately 20K ft. All other input data points were noise free. The filter output error jumps immediately to a value in excess of 11K ft. and then decays. After 10 sec., the error is still around 20 ft. Such performance obviously could not be tolerated, and some form of outlier protection was required.

C-2

TABLE VII-3. - FINAL VALUES FOR PREFILTER PARAMETERS

Function	α	β	CUTOFF FREQ. (3 dB), Hz	NOISE REDUCT. FACTOR dB	MAXIMUM NOISEFREE TRACKING ERROR*
AZ	0.075	0.00292	0.36	-14	0.009 deg.
EL1	0.10	0.00526	0.50	-13	N/A
DME	0.063	0.00205	0.30	-15	5 feet

* Racetrack flight path with no turbulence

N/A - Not available

The following test for data anomalies was inserted into the filter algorithm:

$$\left| \text{if } x_n - x_{pn} \right| > \text{errmax},$$

$$\text{then } x_n = x_{pn}$$

where errmax = maximum allowable error and x_n, x_{pn} are defined in eqs. (1).

Instead of using the prefiltered-predicted value x_{pn} when the outlier test is failed, x_n could be set equal to the predicted value computed from the complementary filter outputs. Since the complementary filter outputs were the most accurate estimate of position available to the system, this latter technique was actually implemented, as discussed in Chapter VIII. The values of errmax were determined as follows: Since the filter computations and MLS measurements are asynchronous, the MLS measurement can be as much as 1/20 second (1 compute cycle) old when it is tested for outliers. In this time the aircraft position has changed. The maximum change in azimuth for the ICAO flight paths occured at the point where the aircraft velocity vector was perpendicular to the radius vector from the AZ antenna. Assuming a maximum ground speed of 235 kts, the maximum rate error, that is, the maximum change in azimuth due to azimuth rate in one computer cycle was 0.038 deg.

The test limit, errmax, should be large to avoid false alarms due to inherent noise on the data, but small to avoid missed detections of small outliers. A reasonable compromise appeared to be setting the limit equal to the linear sum of the MLS bias error, six times the MLS noise error and the maximum rate error. The azimuth outlier limit then became

$$\begin{aligned} AZMAX &= (\bar{e}_{AZ} + 6\sigma_{AZ})_{max} + \varepsilon_t \\ &= .025 + (6)\ (.02) + .038 \\ &= 0.183 \Rightarrow 0.2^{o} \end{aligned}$$

where $\bar{e}_{AZ}$ = bias error, that is, mean AZ error (max.)

σ_{AZ} = noise error, that is, std. dev. of AZ error (max.)

ε_t = maximum azimuth rate error

Outlier limits for E1-1 and DME are computed similarly. The resulting limits are tabulated in Table VII-4.

TABLE VII-4. - MLS OUTLIER TEST LIMITS

Function	Bias error	Noise error	Rate error	ERRMAX
AZ	.025°	.02°	.038°	0.2°
EL1	.057°	.10°	*	0.7°
DME	15 ft.	40 ft.	9.8 ft.	265 ft.

*negligible

COORDINATE TRANSFORMATION

As discussed in Chapter II, the MLS TRSB System at NAFEC measured aircraft position in conical coordinates. On the other hand, the complementary filter operated in rectangular coordinates. Thus a coordinate transformation was required.

Assume that the AZ and DME antennas are colocated. Define a right handed MLS rectangular (x-y-z) coordinate system with the origin located at the phase center of the AZ antenna with the xy-plane orthogonal to the local vertical, and with the x-axis parallel to the runway centerline. Assume that the phase center of the EL1 antenna is located at $x = x_0$, $y = y_0$ and $z = 0$, as in figure VII-10.

It can be shown that the transformation from MLS conical coordinates to MLS rectangular coordinates is given by the following equations:

$$x = g + (g^2 - h)^{\frac{1}{2}} \tag{14a}$$

$$y = -R \sin A \tag{14b}$$

$$z = (R^2 - x^2 - y^2)^{\frac{1}{2}} \tag{14c}$$

$$= (R^2 - 2(xx_0 + yy_0) + x_0^2 + y_0^2)^{\frac{1}{2}} \sin \varepsilon$$

where

$$g = x_0 \sin^2 \varepsilon \tag{15a}$$

$$h = (x_0^2 + y_0^2) \sin^2 \varepsilon + y^2 - R^2 \cos^2 \varepsilon - 2yy_0 \sin^2 \varepsilon \tag{15b}$$

A = azimuth

ε = elevation

R = slant range from DME antenna

$\simeq$ DME measurement + 7546.8 ft.

x_0 = 7546.8 ft.

y_0 = 254.78 ft.

From Chapter II, figure II-5, it can be seen that the assumptions of colocated AZ and DME and of the ELI antenna being in the xy-plane were not precisely justified by the NAFEC MLS geometry. However, the errors introduced by the assumptions were negligible. It should be noted that the error caused by the DME offset (9.36 ft.) in the y-direction was smaller on the final approach portion of the flight paths where greater accuracy was desired.

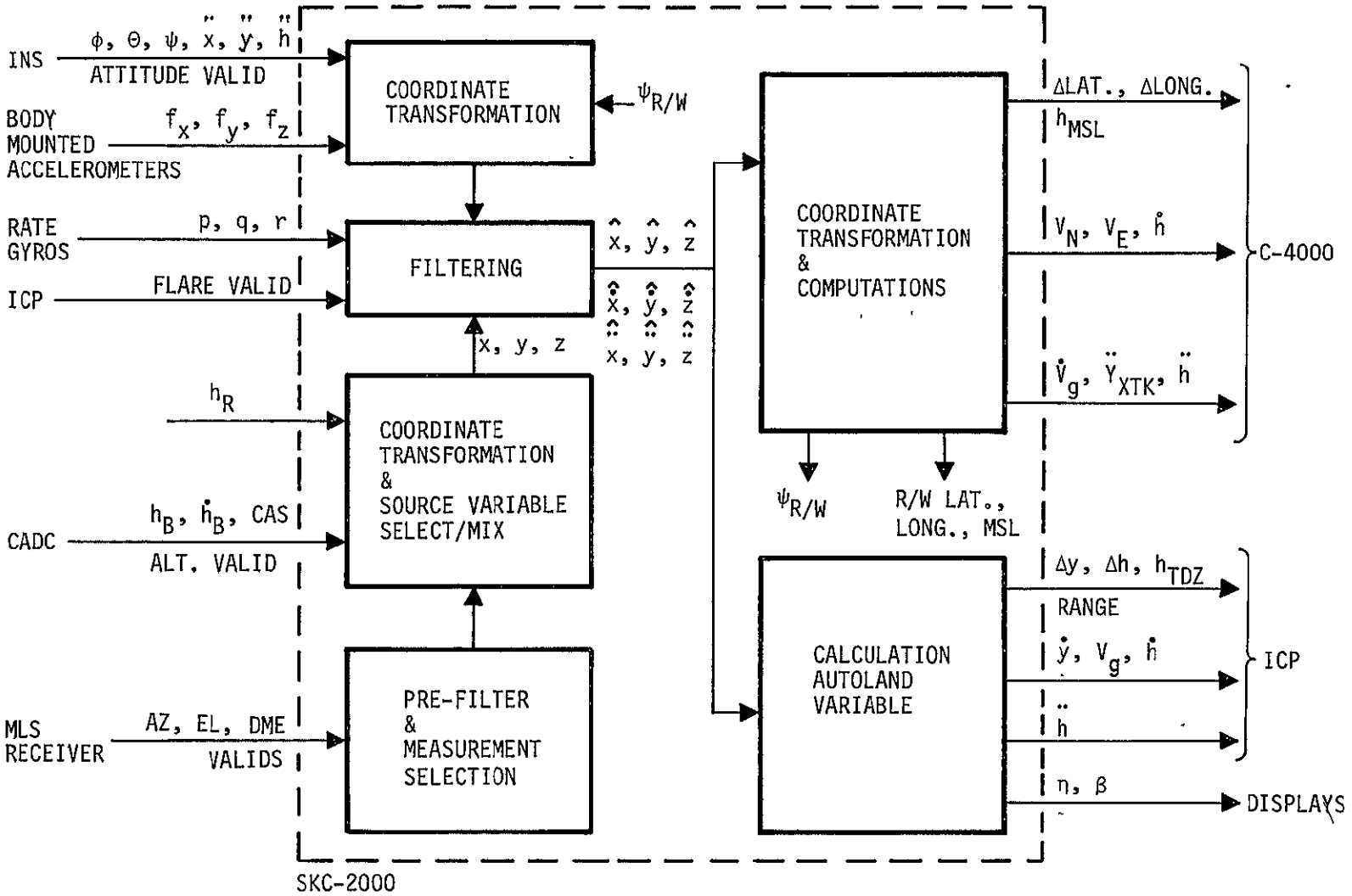

FIGURE VII-1 SKC-2000 INPUT/OUTPUT AND FUNCTIONAL DIAGRAM

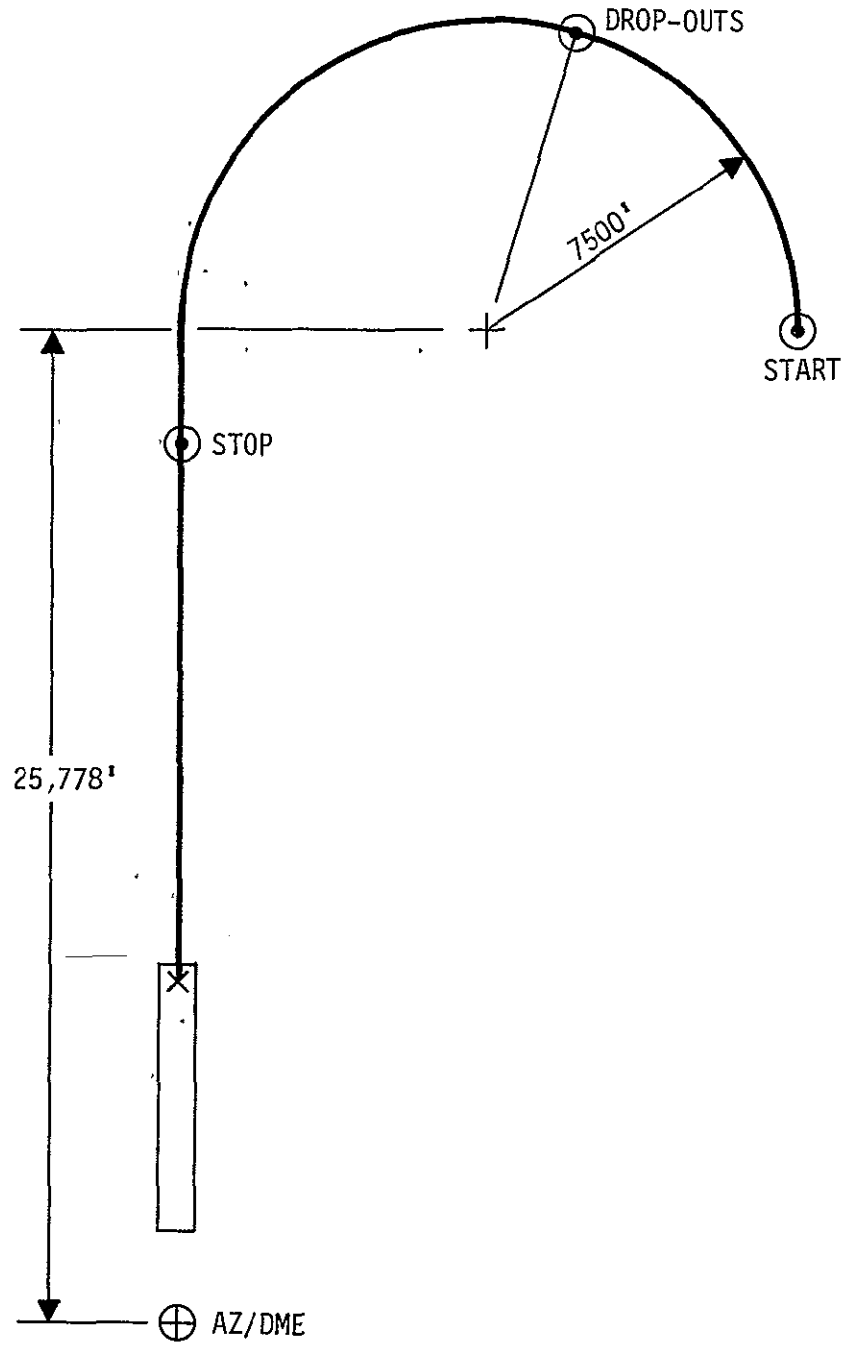

FIGURE VII-2 SIMULATED FLIGHT PATH FOR FILTER EVALUATION

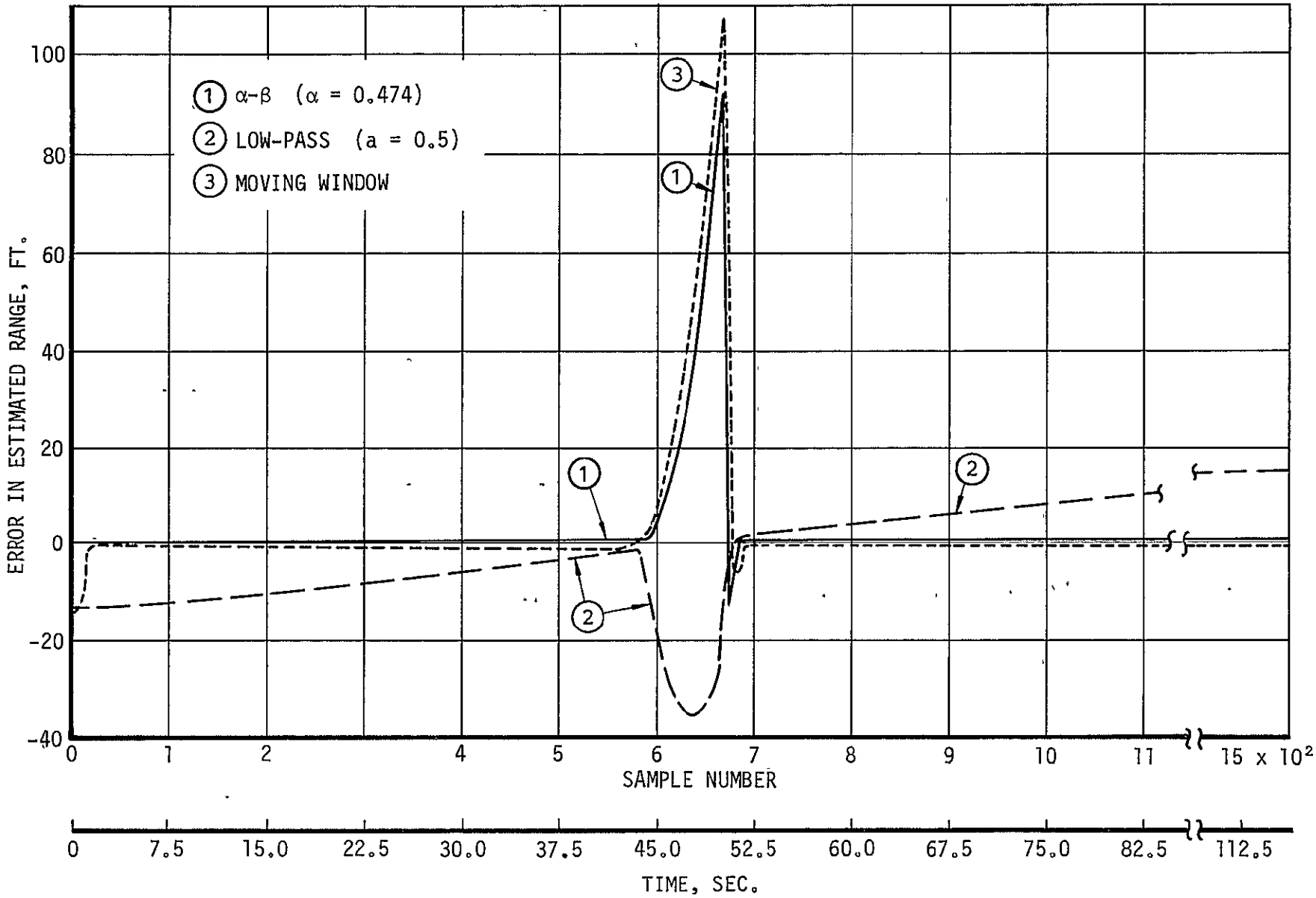

FIGURE VII-3 COMPARISON OF FILTER RANGE ERRORS, A/C ON CIRCULAR ARC

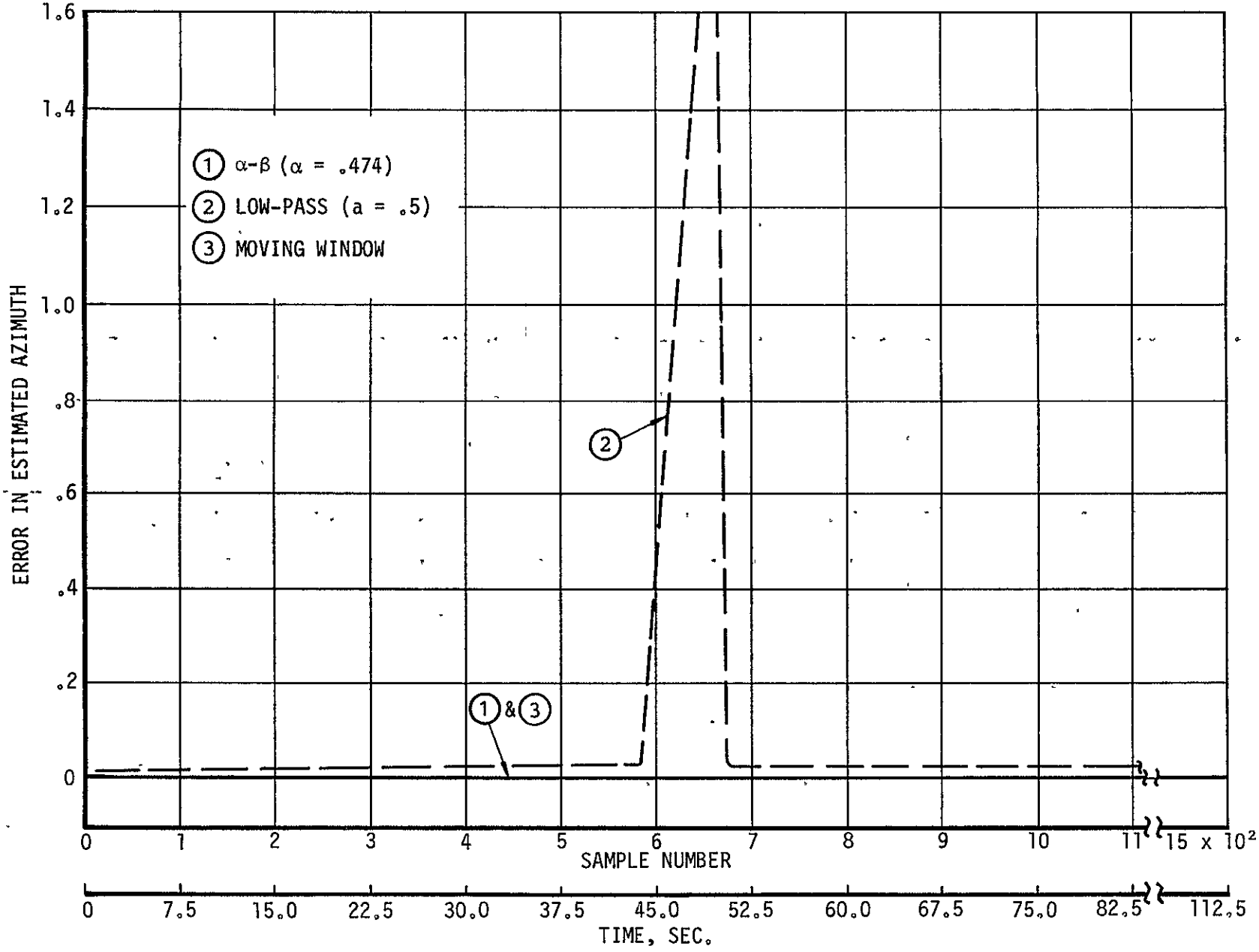

FIGURE VII-4 COMPARISON OF FILTER AZIMUTH ERRORS, A/C ON CIRCULAR ARC

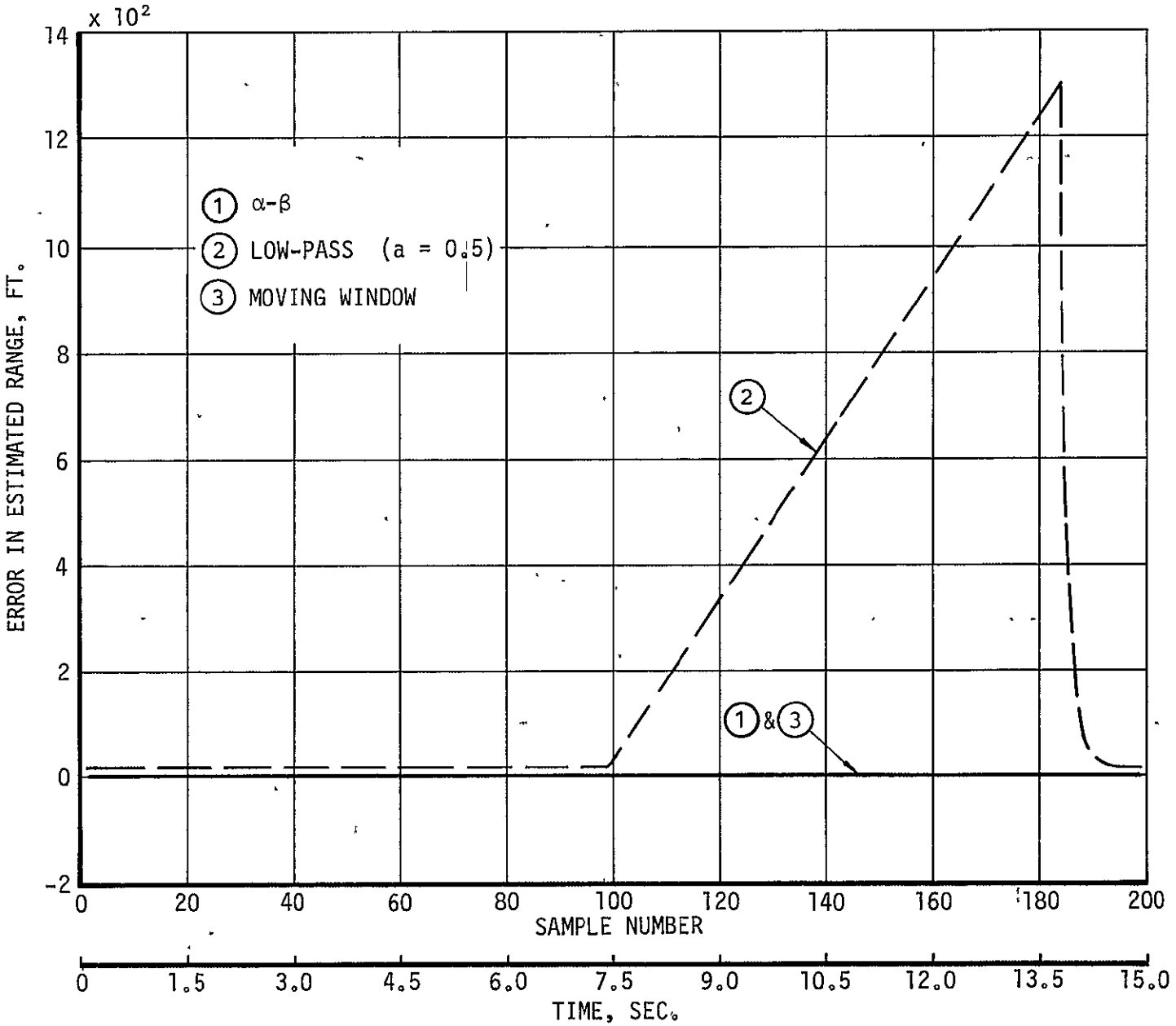

FIGURE VII-5 COMPARISON OF FILTER RANGE ERRORS, A/C ON STRAIGHT APPROACH

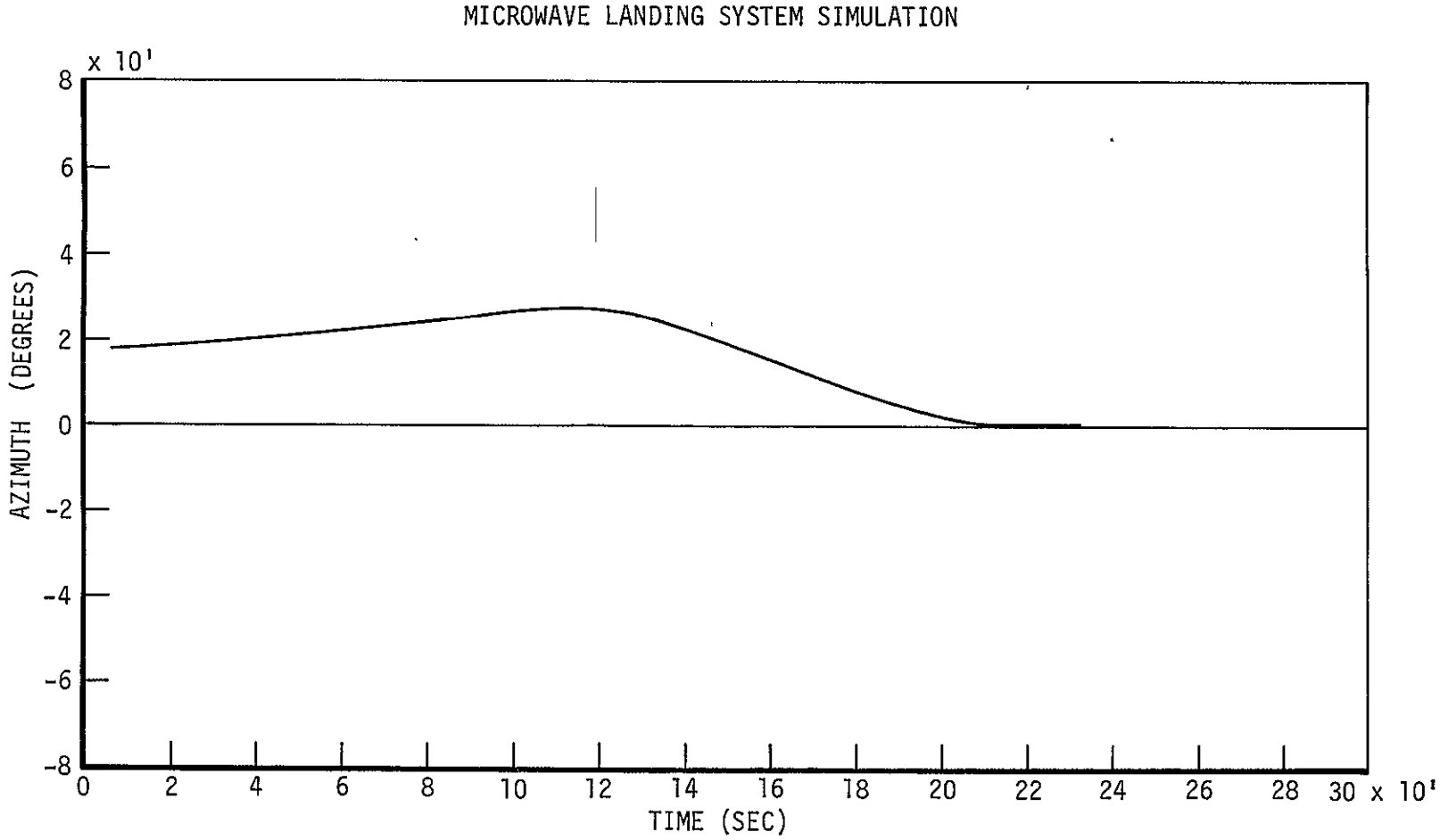

FIGURE VII-6 AZ TIME HISTORY

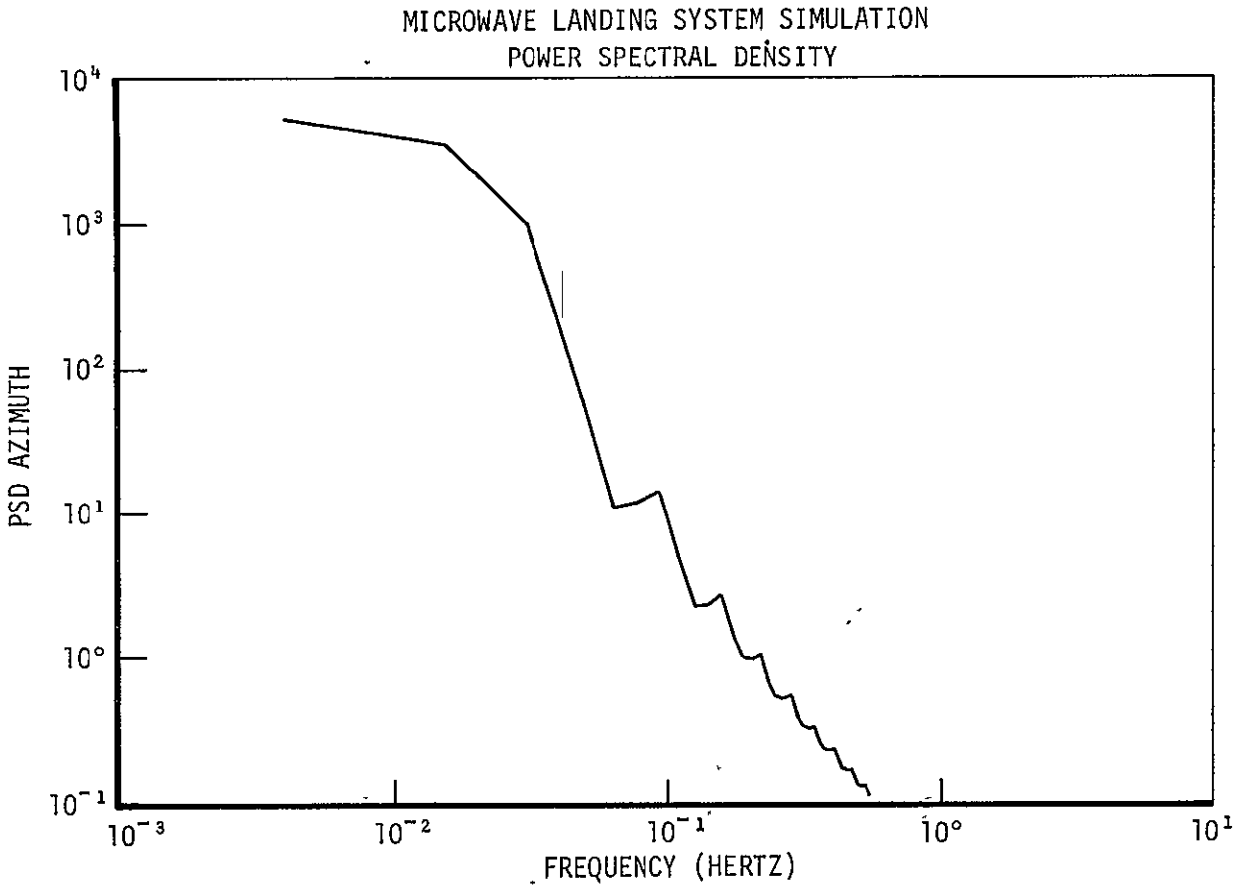

FRAME 45 REEL 1414017
SERIAL NUMBER = 15
DELTA T = .12500
DELTA F = 15625 x 10^{-6}
2372 INPUT DATA POINTS
257 POWER POINTS PLOTTED

ALGORITHM:
FREQUENCY DOMAIN BLACKMAN-TUKEY
WITH PARZEN AUTOCORRELATION WINDOW OVER 257 LAGS

FIGURE VII-7 POWER SPECTRAL DENSITY FOR Az

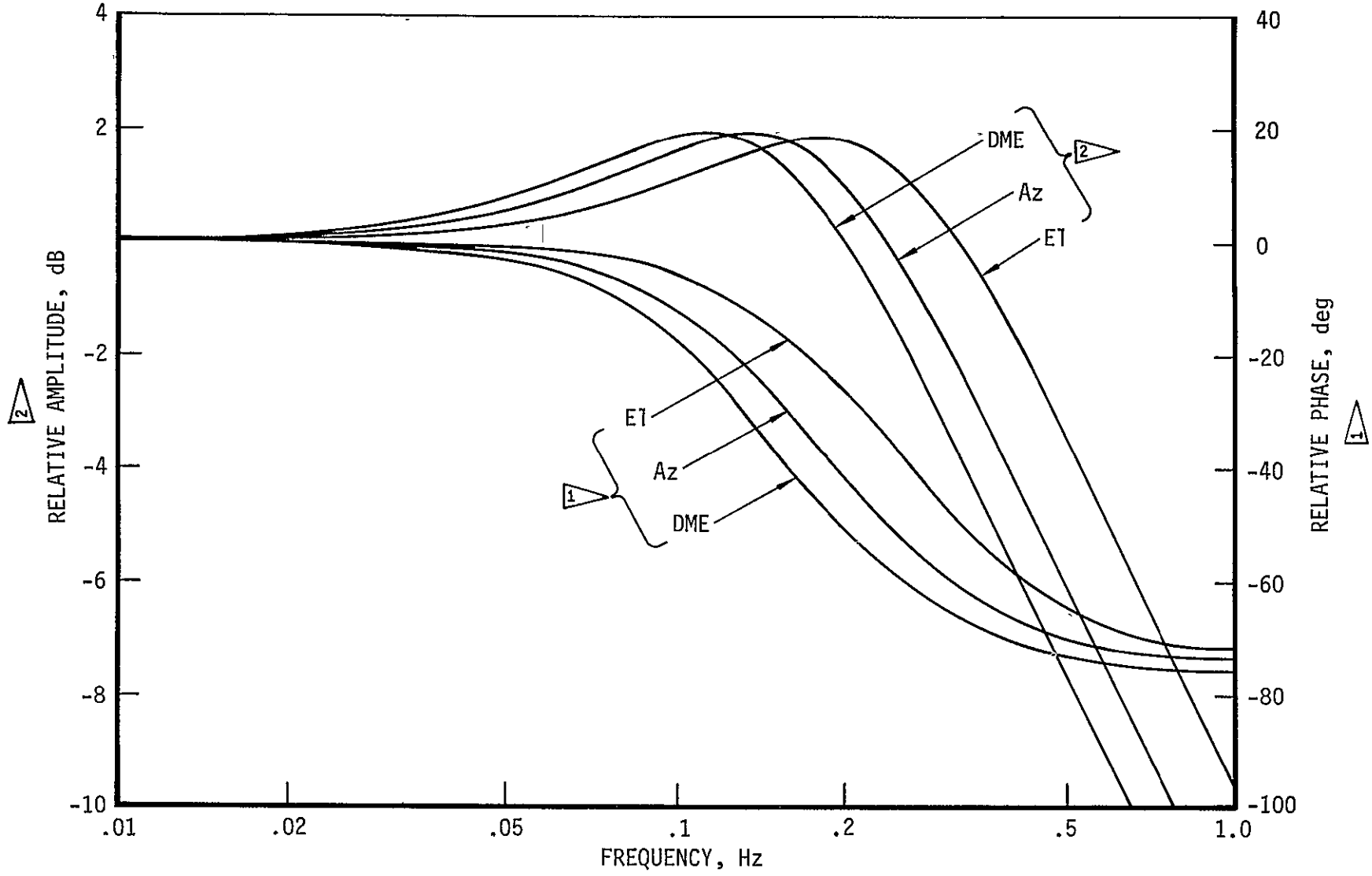

FIGURE VII-8 PRE-FILTER RESPONSE

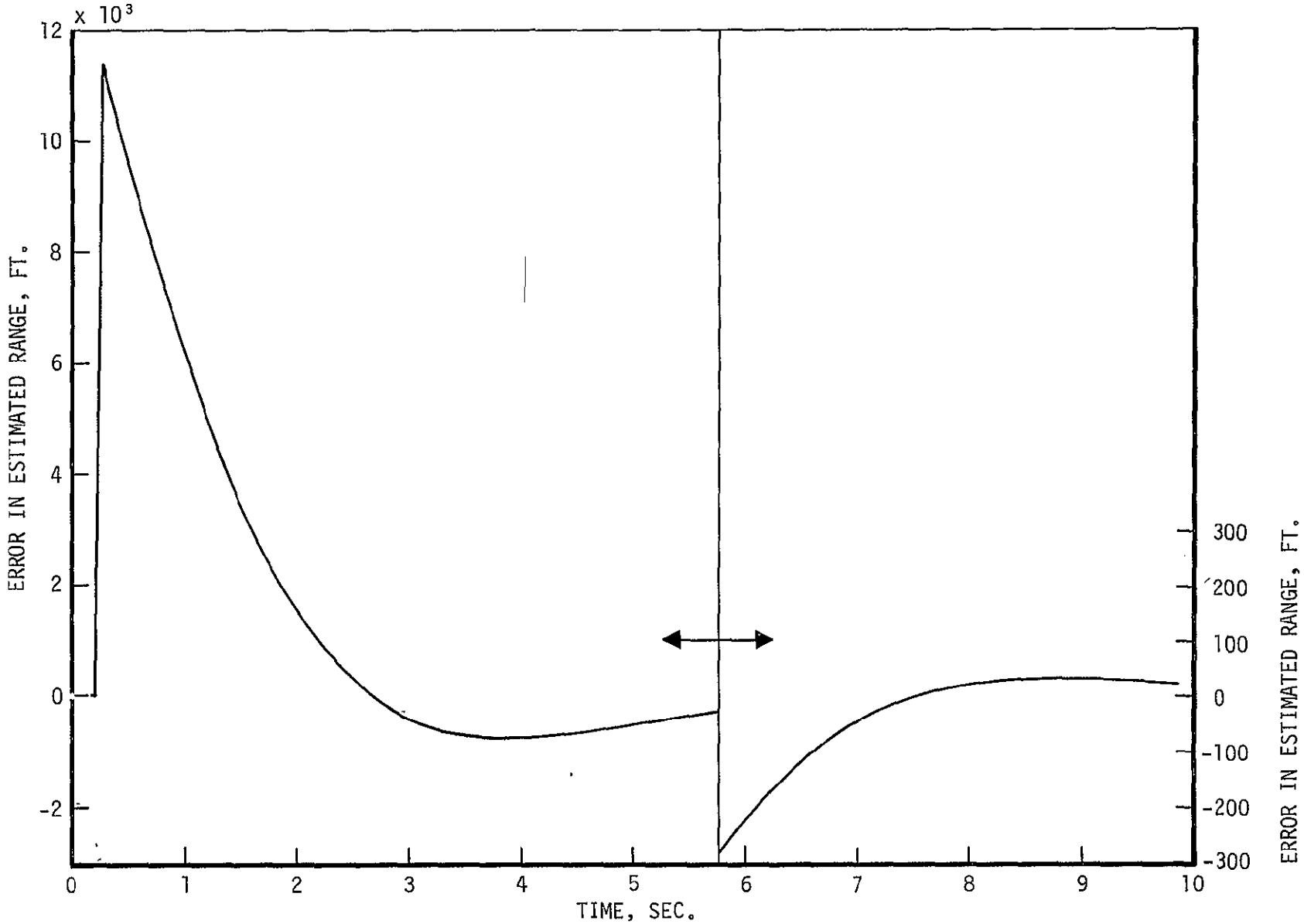

FIGURE VII-9 FILTER RANGE ERROR WITH INPUT OUTLIER (200K FT.) AT T=0.2 SEC., α =0.063

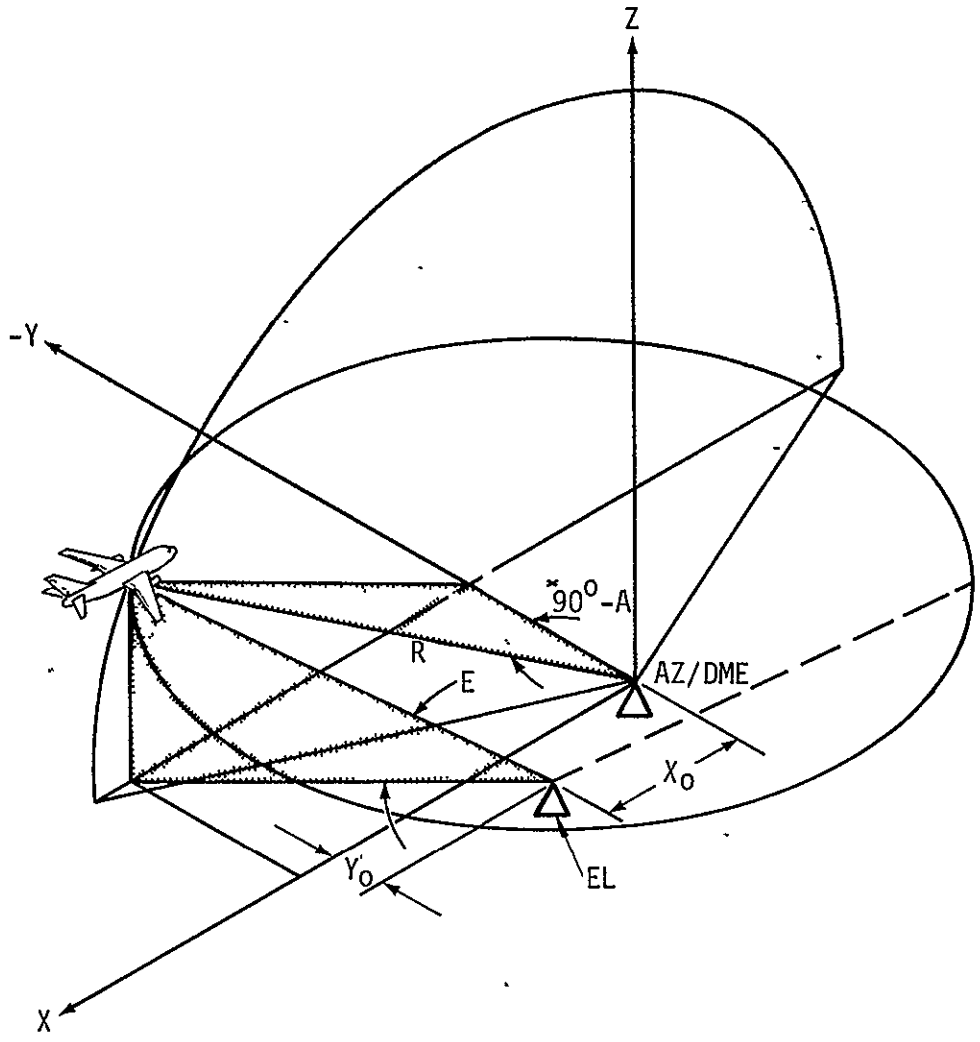

FIGURE VII-10 MLS COORDINATE TRANSFORMATION GEOMETRY

VIII. MLS DATA PROCESSOR AND FORMATTER

by

Richard M. Hueschen

INTRODUCTION

Three factors played a role in the selection of the filtering and processing techniques developed for the MLS demonstration. These factors were (1) the objectives of the demonstration, (2) the time available for the design, development, and flight testing of the system (9) months), and (3) the complexity of the NASA 515 research aircraft and systems to be used for the demonstration.

One of the objectives of the demonstration was to demonstrate the full capability of the MLS system. In other words, develop a system that would provide high quality guidance and control signals through the use of the MLS signals combined with conventional or inexpensive on-board sensors. The intent was to demonstrate the MLS capability without using expensive on-board systems such as a stabilized inertial platform.

About 2 1/2-3 months were available to develop and test a filtering technique such that decisions about on-board computer software and hardware requirements could be made.

The TCV B-737 contains advanced and sophisticated guidance, control and display systems involving a large amount of software in three different computer systems. Since the implementation, checkout and verification of changes made to the software and hardware system can require a significant amount of time, it was decided that changes to existing systems should be minimized. Also, the time constraint would not allow for the development of new guidance and control laws specifically designed for MLS utilization (existing guidance and control laws were designed to utilize VOR, DME, ILS, and a stabilized INS platform).

Deriving position, velocity and acceleration information from the MLS alone was most desirable from the point of view of demonstrating the MLS accuracy and capabilities. However, to obtain acceleration and velocity information from MLS only would require differentiation of the position signals. Based on past history it was felt that satisfactory velocity information might be derived from the MLS (at least for the RNAV guidance and control), but that suitable acceleration signals would be much more difficult to obtain. Obtaining autoland-quality velocity and acceleration signals would most likely be even more difficult.

Thus, in considering the above factors, it was decided that a third order complementary filter would be developed to provide estimates of position, velocity and acceleration. A Kalman filter was also considered, but it was decided that software checkout and debugging would be more difficult and that sufficient manpower and time were not available. In addition, the use of complementary filtering techniques had been demonstrated to provide good estimates (References VIII-1 and VIII-2). The complementary filter's relationship to Kalman filtering had also been described in the literature (Reference VIII-3.)

SIGNAL PROCESSING AND FILTERING

Complementary Filter. The general form of third order complementary filter is shown in figure VIII-1. Three of these filters were used to provide estimates of position, velocity and acceleration in the MLS coordinate frame.

Three variations of the filter were tested through digital simulation. The variations involved only the acceleration measurement source in figure VIII-1. One variation was to set the acceleration measurement to zero. This filter was referred to as the "MLS only" or "A" filter. A second variation was to calculate psuedo acceleration measurements from equations based on the coordinated turn aircraft equations of motion. This filter was referred to as the "pseudo acceleration" or "B" filter. The third variation which used acceleration inputs transformed from body-mounted accelerometer outputs was referred to as the "C" filter. A fourth variation, implemented in flight software but not in the digital simulation, used transformed INS acceleration signals as inputs and was called the "D" filter. The "A" filter was most dependent of the MLS signals, the "B" less dependent and so forth. The approach taken was that if the "A" filter could not provide satisfactory performance, then demonstrate the "B" filter and so on. The "D" filter was to be implemented as a baseline performance filter and as a backup in case problems arose in using the "C" filter.

The acceleration calculations for the "B" filter are given as follows:

$$\ddot{x} = - g \tan \phi \sin (\psi - \psi_R)$$

$$\ddot{y} = g \tan \phi \cos (\psi - \psi_R)$$

$$\ddot{z} = 0$$

where x, y, and z are respectively the input accelerations in the MLS coordinate frame, ϕ is the bank angle, ψ is the aircraft heading, ψ_R is the heading of the x axis of the MLS coordinate frame, and g is the gravitational constant. The acceleration input for the "C" filter is given by

$$\begin{bmatrix} \ddot{x} \\ \ddot{y} \\ \ddot{z} \end{bmatrix} = \begin{bmatrix} 0 \\ 0 \\ g \end{bmatrix} + T_3(\sigma)\, T_2(-\theta)\, T_1(-\phi) \begin{bmatrix} f_y \\ f_y \\ f_y \end{bmatrix}$$

where

$$\sigma = \psi - \psi_R$$

$$T_1(\phi) = \begin{bmatrix} 1 & 0 & 0 \\ 0 & \cos\phi & \sin\phi \\ 0 & -\sin\phi & \cos\phi \end{bmatrix}$$

$$T_2(\theta) = \begin{bmatrix} \cos\theta & 0 & -\sin\theta \\ 0 & 1 & 0 \\ \sin\theta & 0 & \cos\theta \end{bmatrix}$$

$$T_3(\sigma) = \begin{bmatrix} \cos\sigma & \sin\sigma & 0 \\ -\sin\sigma & \cos\sigma & 0 \\ 0 & 0 & 1 \end{bmatrix}$$

and f_x, f_y, and f_z are respectively the specific force measurements from the body-mounted accelerometers. These measurements were made in the aircraft body axes frame (see reference VIII-4 for the body axes definition).

The acceleration calculations for the "D" filter (see figure VIII-2) are given as:

$$\ddot{x} = \dot{V}_g \cos \Delta\psi - \ddot{y}_{XTK} \sin \Delta\psi$$

$$\ddot{y} = -\dot{V}_g \sin \Delta\psi - \ddot{y}_{XTK} \cos \Delta\psi$$

$$\ddot{z} = \ddot{h}$$

where

$$\Delta\phi = \tan^{-1} \frac{V_E}{V_N} - \psi_R$$

and $\dot{V}_g$, $\ddot{y}_{XTK}$, V_N, and $\ddot{h}$ are respectively the INS along-track acceleration cross-track acceleration, east velocity, north velocity and vertical acceleration.

Coordinate Transformations. The x, y, and z coordinate inputs to the filter were calculated from one of three different combinations of signals depending on the altitude, mode selection and valid flags. These combinations were (1) MLS azimuth, elevation-1 and DME signals, (2) MLS azimuth, elevation-2 and DME, or (3) MLS azimuth and DME plus radar altimeter signals. The transformation of the first two combinations to x, y, and z coordinates is given in chapter VII of this report. For the third combination of signals, the coordinate transformation is given as follows:

$$x = \sqrt{R^2 (1-\sin^2 \hat{Az}) - z^2}$$

$$z = \hat{h}_R - h_{R1}$$

$$y = - R \sin Az$$

$$R = \hat{R}_{DME} + R_o$$

and $\hat{Az}$, $\hat{R}_{DME}$ and $\hat{h}_R$ are respectively the prefiltered azimuth, DME and radio altimeter signals. R_o and h_{R1} are constants.

Estimated Guidance Parameters. The complementary filter shown in figure VIII-1 provided estimates of postion, velocity and acceleration of the aircraft's C-band antenna in the MLS coordinate frame. The complementary filter provides these estimates by integrating the acceleration measurements and by adjusting the integrations through feedback signals which are functions of the position error term. In addition, the filter makes an estimate of the negative of the acceleration bias error to correct the acceleration signal being integrated. The limiter as shown in figure VIII-1 is used to detect erroneous acceleration data. The complementary filter estimates are processed as follows to provide the input variables needed in the guidance and control laws of the RNAV and Autoland Computers.

The deviation in latitude and longitude from the origin of the MLS coordinate frame is approximated by:

$$\Delta \text{ lat} = (K_L \cos \psi_R)\ \hat{x} + (K_L \sin \psi_R)\ \hat{y}$$

$$\Delta \text{ long} = (-K_\lambda \sin \psi_R)\ \hat{x} + (K_\lambda \cos \psi_R)\ \hat{y}$$

where $\hat{x}$ and $\hat{y}$ are, respectively, the estimates of x and y position from the complementary filter and K_L and K_λ are geodetic latitude and longitude constants. The values used for constants were:

$$K_L \cos \psi_R = -2.423996218 \times 10^{-6}$$

$$K_L \sin \psi_R = -1.288876726 \times 10^{-6}$$

$$K_\lambda \sin \psi_R = -1.66290132 \times 10^{-6}$$

$$K_\lambda \cos \psi_R = -3.127425943 \times 10^{-6}$$

$$\psi_R = 208^0\ 00'\ 01"$$

At 10 nautical miles the equations give approximately .02% errors.

The mean sea level altitude is given by

$$h_{MLS} = \hat{z} + z_o + \hat{x}^2 + \hat{y}^2 \quad \left(\frac{1}{2R_L}\right)$$

where $\hat{z}$ is the z position estimate and z_o and $(1/2R_L)$ are constants.

The values used for the constants were

$$z_o = 78.76 \text{ ft.}$$

$$1/2R_L = .23090 \times 10^{-7}$$

The north, east, and vertical velocities were given by the following approximate equations:

$$V_N = \hat{x} \cos \psi_R + \hat{y} \sin \psi_R$$

$$\dot{V}_E = \hat{\dot{x}} \sin \psi_R - \hat{\dot{y}} \cos \psi_R$$

$$\dot{h} = \hat{\dot{z}}$$

where $\hat{x}$, $\hat{y}$, and $\hat{z}$ are the estimates of velocities from the filter. The approximate equations for along-track and cross-track accelerations are given by (see figure VIII-2):

$$\hat{\dot{V}}_g = \hat{\ddot{x}} \cos (\psi_T - \psi_R) - \hat{\ddot{y}} \sin (\psi_T - \psi_R)$$

Since $\cos (\psi_T - \psi_R) = \dfrac{\hat{\dot{x}}}{\hat{V}_g}$ and $\sin (\psi_T - \psi_R) = \dfrac{-\hat{\dot{y}}}{\hat{V}_g}$,

then $$\dot{V}_g = \frac{\hat{\ddot{x}}\hat{\dot{x}} + \hat{\ddot{y}}\hat{\dot{y}}}{\hat{V}_g}$$

where $$\hat{V}_g = \sqrt{\hat{\dot{x}}^2 + \hat{\dot{y}}^2}$$

The cross-track acceleration is

$$\hat{\ddot{y}}_{XTK} = -\hat{\ddot{x}} \sin (\psi_T - \psi_R) - \hat{\ddot{y}} \cos (\psi_T - \psi_R)$$

or $$\hat{\ddot{y}}_{XTK} = \frac{\hat{\ddot{x}}\hat{\dot{y}} - \hat{\ddot{y}}\hat{\dot{x}}}{\hat{V}_g}$$

The vertical acceleration was approximated as

$$\ddot{h} = \hat{\ddot{z}}$$

Altitude to touchdown, h_{TD}, was calculated by the equation

$$h_{TD} = \hat{z} + h_{TDC} + x_A \sin \theta .$$

where h_{TDC} and x_A are constants whose values were

$$h_{TDC} = -6.12$$

$$x_A = -38.25$$

and θ is the pitch angle.

The localizer and glideslope angular deviations were calculated according to the following equations:

$$\eta = \tan^{-1} \frac{-\hat{y}}{\hat{x}}$$

$$\beta = \tan^{-1}\left(\frac{\hat{z} + h_o}{\hat{x} - x_G}\right) - \theta_G$$

where h_o, x_G, and θ_G are constants whose values were

$h_o = 11.76$

$x_G = 7546.8$

$\theta_G = (\pi/180)\ (3^o)$

The position deviations from the localizer and glideslope were calculated as follows:

$$\Delta y = \begin{cases} -\hat{y} & \text{for } |-\hat{y}| \leq L_{\Delta y} \\ L_{\Delta y}\ \text{sgn}\ (-\hat{y}) & \text{for } |-\hat{y}| > L_{\Delta y} \end{cases}$$

Let $d = z + h_o - (x - x_G) \tan \theta_G$, then

$$\Delta h = \begin{cases} d & \text{for } |d| \leq L_{\Delta h} \\ L_{\Delta h}\ \text{sgn}\ (d) & \text{for } |d| > L_{\Delta h} \end{cases}$$

The limits, $L_{\Delta y}$ and $L_{\Delta h}$, are defined as

$$L_{\Delta h} = .07 h_{TD}$$

$$L_{\Delta y} = \begin{cases} e_1 + f_1 h_{TD} & \text{if } h_{TD} < h_1 \\ e_2 + f_2 h_{TD} & \text{if } h_1 \leq h_{TD} < h_2 \\ e_3 + f_3 h_{TD} & \text{if } h_2 \leq h_{TD} < h_3 \\ e_4 + f_4 h_{TD} & \text{otherwise} \end{cases}$$

where $h_1 = 500$, $h_2 = 750$, $h_3 = 1000$

$$e_1 = 34.375,\ e_2 = 68.75,\ e_3 = 205.4,\ e_4 = 392.2$$

$$f_1 = .06875,\ f_2 = .5506,\ f_3 = .7432\quad f_4 = .2602$$

The cross-runway velocity, $\dot{y}_{XRW}$, was defined as

$$\dot{y}_{XRW} = \dot{\hat{y}}$$

Switching Logic and Flag Processing. Switching logic and the processing of input data and internal function flags was conducted to (1) assure the use of valid input data, (2) reject the invalid input data and (3) provide flags or valids which indicated the validity of the data or variables being used by the RNAV and Autoland system.

As discussed earlier, the position information was derived from different combinations of input signals depending on system input position data modes selected and input signal validity. Two input position data modes were available. They were the elevation-1/elevation-2 (EL1/EL2) mode and the elevation-1/radio altimeter (EL1/h_R) mode. In each mode the system would initialize on EL1 information and at a specified altitude switch to the other input providing it was valid. It was necessary to switch to the other signal at some point in the final approach since the EL1 signal was lost during flare because of the EL1 antenna location with respect to the glidepath. The switch point for the EL1/EL2 mode was at 900 ft altitude and for the EL1/h_R mode at 36.12 ft.

The system contained reversion modes which were used when the logic indicated that the EL1, EL2 or h_R signals were invalid. The reversion switching depended on whether the aircraft was climbing or descending through altitude switch points. If we let h_1 be the altitude at which the normal switching occurs from EL1 to EL2 or h_R and h_2 be an altitude above h_1, then the switching between these signals is summarized below. The switch is from h_R when in the EL1/h_R mode and between EL1 and EL2 in the EL1/EL2 mode.

- If climbing from below h_1 through h_2:
  - From h_R (or EL2) to EL1 at h_2 if EL1 is valid
    From h_R (or EL2) to EL1 if h_R (or EL2) goes invalid and EL1 is valid
    Set output flag if h_R goes invalid and EL1 is invalid

If descending from above h_2 through h_1:

Set output flag if EL1 goes invalid above h_1

Switch to h_R (or EL2) at h_1 if h_R (or EL2) is valid

Switch to EL1 (if valid) when h_R (or EL2) goes invalid below h_1

If h_R (or EL2) and EL1 are both invalid set output flag.

The validity of a number of input data channels and internal parameters were determined by means of "window" counters. A window counter here is defined as a counter which determines the number m, out of the last n measurements which either had bad data flags or values lying outside of bounds specified around a predicted value (outlier removal). Counters were used for pitch, roll, yaw, pitch rate, roll rate, yaw rate, EL1, EL2, AZ, DME and radio altimeter input data and the position error terms computed in the complementary filter (see figure VIII-1).

Outlier removal was not used for the pitch, roll and yaw inputs and so only the bad data flags were counted. For each attitude measurement, if 5 out of the last 10 measurements were bad the counter flag was set.

For pitch rate, roll rate and yaw rate the counters were incremented if the attitude rate measurements exceeded specified limits. If 3 out of the last 10 measurements exceeded the limit, the counter flag for the particular measurement was set.

The counters for AZ, EL1, EL2, DME and h_R incremented whenever bad input flags were present or when the measured value exceeded the bounds specified around the predicted value. If 75 out of the last 138 measurements were bad or exceeded the bounds the counter flag was set.

The position error counters were incremented when the error exceeded a specified limit. The counter flag was set when 75 out of the last 138 comparisons exceeded the limit. The position error counter provided a validity check of the acceleration inputs to the complementary filter.

Although outlier removal was not used for attitude measurements, predicted attitudes were used whenever bad attitude data flags were detected. The predicted value was obtained by adding a computed increment to the last measurement. The increment was determined by multiplying the attitude rate measurement by the update interval.

The predicted values for AZ, EL1, EL2, DME and h_R used for outlier removal were determined from the complementary filter variables and prefilter values. A predicted value was used in place of the measurement whenever

the measurement was a detected outlier or flagged as bad data. When the data was flagged as bad and the predicted values were not available, then the prefiltered value was updated by setting the α gain to zero in the α-β filter.

The predicted measurements were determined as follows:

1. Determine the predicted MLS position coordinates, x_p, y_p, and z_p, by updating the complementary filters one update interval with the position error set to zero.

2. Find the predicted range R_c:

   $$R_c = R_p,$$

   Where R_p is the predicted range from the prefilter

3. Update DME prefilter channel to get range estimate $\hat{R}$.

4. Find the predicted azimuth value AZ_c

   $$AZ_c = \sin^{-1} \frac{y_p}{\hat{R}}$$

5. Update azimuth prefilter channel to get estimated azimuth angle $\hat{AZ}$.

6. Determine predicted elevation value EL_c:

   $$y_c = -\hat{R} \sin \hat{AZ}$$

   $$EL_c = \sin^{-1} \frac{z_p}{\sqrt{\hat{R}^2 + (x_o^2 + y_o^2) - 2x_o xp - 2y_o y_c}},$$

   where x_o and y_o are the elevation antenna coordinates in the MLS frame.

7. Determine the predicted radio altimeter value h_{Rc}:

   $$h_{Rc} = z_p - h_{RI},$$

   where h_{RI} is a constant referred to previously.

Three data output valids, V_{MLS}, V_{LONG}, and V_{LAT} were computed as a function of the counter flags and other logic variables. V_{MLS} was valid if both V_{LONG} and V_{LAT} were valid. It was used by the navigation and guidance computer. V_{LONG} and V_{LAT} were used by the Autoland computer. V_{LONG} indicated the validity of the computed longitudinal variables and V_{LAT} the validity of the lateral variables. V_{LONG} was set true when the counter flags and variable flags associated with the longitudinal variables and the initialization counter flag were valid. V_{LAT} was set true when the counter flags and variable flags associated with the lateral variables and the initialization counter were valid. The initialization counter flag was set true or valid when all flags from the window counters remained valid for a specified period of time after the complementary filter integrators were initialized.

Initialization of the integrators occured when all the needed window counters (those associated with variables being used in the selected filter mode and input data mode) provided a valid flag. Before initialization or immediately after an output flag was set invalid, the complementary filter ran open loop. In other words, the position error signal was set to zero and the acceleration data was integrated to get position and velocity. The integrators of the complementary filter were initialized according to the following equations:

For position

$$x(0) = x_{measured}$$

$$y(0) = y_{measured}$$

$$z(0) = z_{measured}$$

For velocity

$$\dot{x}(0) = V_{CAS} \cos(\psi_R - \psi)$$

$$\dot{y}(0) = V_{CAS} \sin(\psi_R - \psi)$$

$$\dot{z}(0) = K_{CAS} V_{CAS} \sin(\theta - \alpha_o) + K_{zb} \dot{z}_b + K_o$$

where V_{CAS} is the calibrated airspeed, and K_{CAS}, K_{zb}, K_o, and α_o are constants whose values were taken as

$$K_{CAS} = .1$$

$$K_{zb} = .9$$

$$K_o = 0$$

$$\alpha_o = \pi/180$$

For the acceleration bias

$$\ddot{x}_b = 0$$

$$\ddot{y}_b = 0$$

$$\ddot{z}_b = 0$$

SIMULATION TESTING DESCRIPTION

The performance of the complementary filter with the different acceleration sources discussed earlier was assessed using a digital simulation program. An overall block diagram of the simulation is shown in figure VIII-3. The program, coded to run on the CDC-6600 computer at LRC's computer facilities, contained a dynamic model of the NASA 515 aircraft, models of the guidance and control and autothrottle laws, a model of the MLS, first order actuator models, a first order engine response model, models for steady state, shear and turbulent winds, and sensor error models.

Aircraft Model. The dynamic model of the aircraft consisted of six-degree-of-freedom nonlinear equations of motion with constant stability derivatives which were specified in the input data. Ground effects were included in the model as increments to the lift, drag and pitching moment coefficients. The increments were computed as a function of angle of attack, flap setting and wheel height. Details of the aircraft model and equations used to calculate aerodynamic forces and moments are found in reference VIII-5.

The Vertical Path Command (VPC) and Horizontal Path Command (HPC) modes of the AGCS were modeled for the automatic RNAV portion of flight to be demonstrated. The block diagrams for the VPC and HPC guidance laws are given respectively in figures VIII-4 and VIII-5.

Block diagrams of the Autoland guidance and control laws modeled are shown in figures VIII-6, VIII-7, VIII-8 and VIII-9. These were the laws used for the demonstration and were modified versions of the existing Autoland laws. The modifications will be discussed later.

Block diagrams of the first order elevator and aileron servo models and engine response model are shown in figure VIII-10. The block diagram for the autothrottle control law is shown in figure VIII-11.

The standard yaw rate damper was also modeled and the block diagram of the modeled version is shown in figure VIII-12.

MLS Model. The MLS was modeled to include the "jitter" in the signal as defined in reference VIII-6. Signals were generated for the EL1, AZ and DME but not for EL2. The antenna locations were as defined in reference VIII-7 except it was assumed that the DME was co-located with the azimuth (this was the assumption used in deriving the MLS coordinate transformation equations).

Wind Model. The shear wind was modeled by linearly varying wind velocity with altitude. Turbulent winds were generated according to the Dryden spectrum as defined in reference VIII-8. The effects of both the linear velocity turbulent components and rotation effects due to non-uniform distribution of turbulent wind on the aircraft were included in the simulation.

Sensor Error Models. The simulation included measurement error models for the various sensor measurements simulated. The MLS error model consisted of biases and random errors. The random errors were modeled as first order exponentially correlated noise as follows:

$$\eta_{EL}(n) = \sigma_{EL}(1-A_{EL}^2)^{\frac{1}{2}} u(n) + A_{EL}\eta_{EL}(n-1)$$

$$\eta_{AZ}(n) = \sigma_{AZ}(1-A_{AZ}^2)^{\frac{1}{2}} u(n) + A_{AZ}\eta_{AZ}(n-1)$$

$$\eta_{R}(n) = \sigma_{R}(1-A_{R}^2)^{\frac{1}{2}} u(n) + A_{R}\eta_{R}(n-1)$$

where

$$A_{EL} = e^{-\alpha_{EL}T}$$

$$A_{AZ} = e^{-\alpha_{AZ}T}$$

$$A_{R} = e^{-\alpha_{R}T}$$

and α_{EL}, α_{AZ} and α_{R} are correlation time constants, T is the update

interval, u(n) is a random number from a Gaussian sequence with zero mean and standard deviation of 1, and σ_{EL}, σ_{AZ} and α_R are respectively the standard deviation of the errors for elevation, azimuth and range. For the MLS as well as the other sensors the bias errors were specified through input data.

For the airspeed measurement, the sensor error was modeled as multiplicative noise as follows:

$$\eta(n) = V_a \sigma_{air} u(n)$$

where V_a is the errorless airspeed, σ_{air} is the standard deviation of the percentage of airspeed error, and u(n) is a random number from a Gaussian sequence with zero mean and standard deviation of 1.

The sensor errors for attitude and attitude rate measurements were modeled as Gaussian white noise with a specified standard deviation. In addition, the attitude measurements included bias errors specified through input data.

For the acceleration measurements, the sensor errors were modeled as Gaussian white noise plus a bias. In addition, scale factor errors and misalignment errors were included in the acceleration measurements.

The standard deviations, biases, time constants, and scale factor and alignment errors for the error models are given in Table VIII-1.

Flight Profile. The flight path flown in the simulation was a portion of the 130^0 ICAO flight profile. The portion flown was the circular arc and the final 3 n.m. segment to touchdown.

The aircraft was initialized in a wings level and minus 3 degree descent attitude at a 120 knot airspeed and 130 degree heading relative to the runway heading on the flight path.

The wind conditions were specified for a given run including both speed and direction. Steady winds varied from 0 to 20 ft/sec while the values used for the standard deviation of the turbulence were 2, 3, and 4 ft/sec. Shear wind was introduced at an altitude of 200 feet with a rate of change of 8 kt/100 ft.

Test Procedure. After the initialization of variables, the simulation began with the RNAV portion of the flight. The aircraft began tracking the desired path using the VPC and HPC automatic RNAV modes and the

calibrated airspeed hold mode for the autothrottle. When the aircraft heading was within 5 degrees of the runway heading or the position within 100 ft of the runway extended line, the system switched to the Autoland tracking modes. The capture modes were not used because of the circular 3 degree descent RNAV path being matched up with the final straight line segment (normal capture of the localizer and glideslope is to fly to them straight and level at some intercept angle). At 150 feet the system began the decrab maneuver followed by flare and touchdown. The flare nominally occurred around 50 feet of altitude, being triggered by a combination of the altitude-to-touchdown and vertical sink rate inputs.

The iteration rate for the simulation was 20 times per second. Output data was printed once per second and plots of 12 selected variables were made with data also stored once per second for the plots.

Simulation Results. The simulation results showed that the performance of the complementary filter without acceleration inputs ("A" filter) and the filter with psuedo acceleration inputs ("B" filter) were unacceptable. Acceptable performance was possible with sensor errors set to zero and mild winds. However, with sensor errors and moderate winds, the RNAV and Autoland tracking performance was poor. For many cases, the aircraft was near the edge or off of the runway at touchdown.

The "D" filter was not simulated since it was the same as the "C" filter except that it used inertial platform acceleration inputs rather than body-mounted accelerometer inputs.

The "C" filter did provide satisfactory performance. Different filter gains were evaluated for various wind conditions and the typical measurement errors as shown in Table VIII-1. After evaluation of the output data (printout and plots), the filter gains were chosen the same for each filter channel (x, y, and z). The gains chosen were as follows:

$$k_1 = 0.2$$

$$k_2 = 0.015$$

$$k_3 = 0.0005$$

Figures VIII-13 and VIII-14 show plots of the performance for control variables for two wind conditions using the complementary filter gains specified above.

Category II decision height deviations (100 feet altitude) and touchdown conditions for the two runs are shown in Table VIII-2.

TABLE VIII-1. - ERROR MODEL PARAMETERS

MEASUREMENT	STANDARD DEV.	BIAS	CORRELATION TIME CONSTANT	SCALING ERROR	ALIGNMENT ERROR
Pitch	0.23^{o}	0.23^{o}	N. A.	N. A.	N. A.
Roll	0.23^{o}	0.23^{o}	N. A.	N. A.	N. A.
Yaw	0.23^{o}	0.23^{o}	N. A.	N. A.	N. A.
Pitch rate	0.02^{o}/sec	N. A.	N. A.	N. A.	N. A.
Roll rate	0.02^{o}/sec	N. A.	N. A.	N. A.	N. A.
Yaw rate	0.02^{o}/sec	N. A.	N. A.	N. A.	N. A.
Specific force (Acceleration) for x, y, & z	0.32 ft/sec^2	0.32 ft/sec^2	N. A.	0.25% all axes	0.23^{o} all axes
Azimuth	0.01^{o}	0.0125^{o}	3 sec	N. A.	N. A.
Elevation	0.01^{o}	0.0125^{o}	4 sec	N. A.	N. A.
Range	7.5 ft	7.5 ft	3 sec	N. A.	N. A.
Airspeed	2%	N. A.	N. A.	N. A.	N. A.

TABLE VIII-2. - PERFORMANCE DATA FOR "C" COMPLEMENTARY FILTER

WIND				CATEGORY II DECISION HEIGHT			TOUCHDOWN CONDITIONS				
Steady Wind (knots)	Turbulence (1-σ, ft/sec)	Shear	Wind Direction with Respect to Runway (degrees)	Airspeed Deviation (knots)	Altitude Deviation (feet)	Lateral Deviation (feet)	Distance from Threshold (feet)	Vertical Velocity (ft/sec)	Lateral Deviation (feet)	Roll (degrees)	Heading with Respect to Runway (degrees)
6	2	yes	30	5.58	-1.21	-0.01	1406	-4.04	0.04	-1.81	-0.64
15	2	yes	150	-5.05	-3.91	-1.97	927	-4.65	-2.76	-2.18	-1.96

REFERENCES

VIII-1. F. R. Niessen, "A Complementary Filtering Technique for Deriving Aircraft Velocity and Position Information." Presented at AGARD Meeting on "Methods for Aircraft State and Parameter Identification", Hampton, VA, November 5-8, 1974.

VIII-2. R. I. Bleeg, H. F. Tisdale, R. M. Vircks, INERTIALLY AUGMENTED AUTOMATIC LANDING SYSTEM: Autopilot Performance with Imperfect ILS Beams, DOT Report No. FAA-RD-72-22, April 1972.

VIII-3. Higgins, W. T. Jr., "A Comparison of Complementary and Kalman Filtering", IEEE Trans. Aerospace and Electronics System Vol. AES-11, No. 3, May 1975.

VIII-4. Bernard Etkin, Dynamics of Atmospheric Flight, John Wiley and Sons, Inc., 1972.

VIII-5. S. Pines, S. F. Schmidt, and F. Mann, "Simulation, Guidance and Navigation of the B-737 for Rollout and Turnoff Using MLS Measurements", NASA CR-144959, December, 1975.

VIII-6. W. T. Bundick, "MLS Characteristics," NASA Memorandum, Langley Research Center, September 13, 1975.

VIII-7. W. T. Bundick, "MLS Characteristics," NASA Memorandum, Langley Research Center, November 19, 1975.

VIII-8. Roskam, J., Flight Dynamics of Rigid and Elastic Airplanes, Roskam Aviation and Engineering Corp., 519 Boulder, Lawrence Kansas, 1972.

VIII-9. Bundick, W. T., "MLS Error Model", NASA Memorandum, Langley Research Center, January 22, 1976.

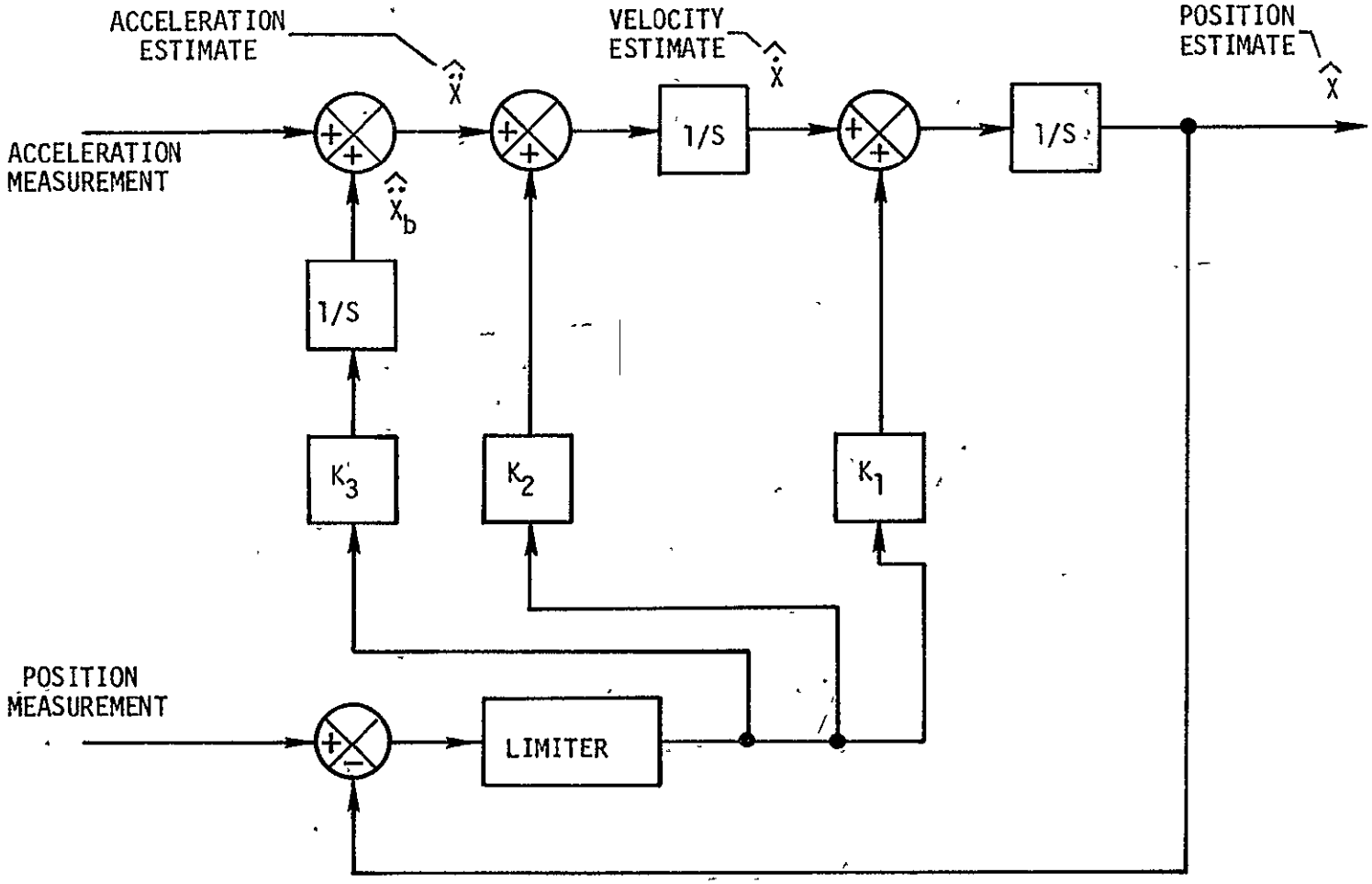

FIGURE VIII-1. THIRD ORDER COMPLEMENTARY FILTER

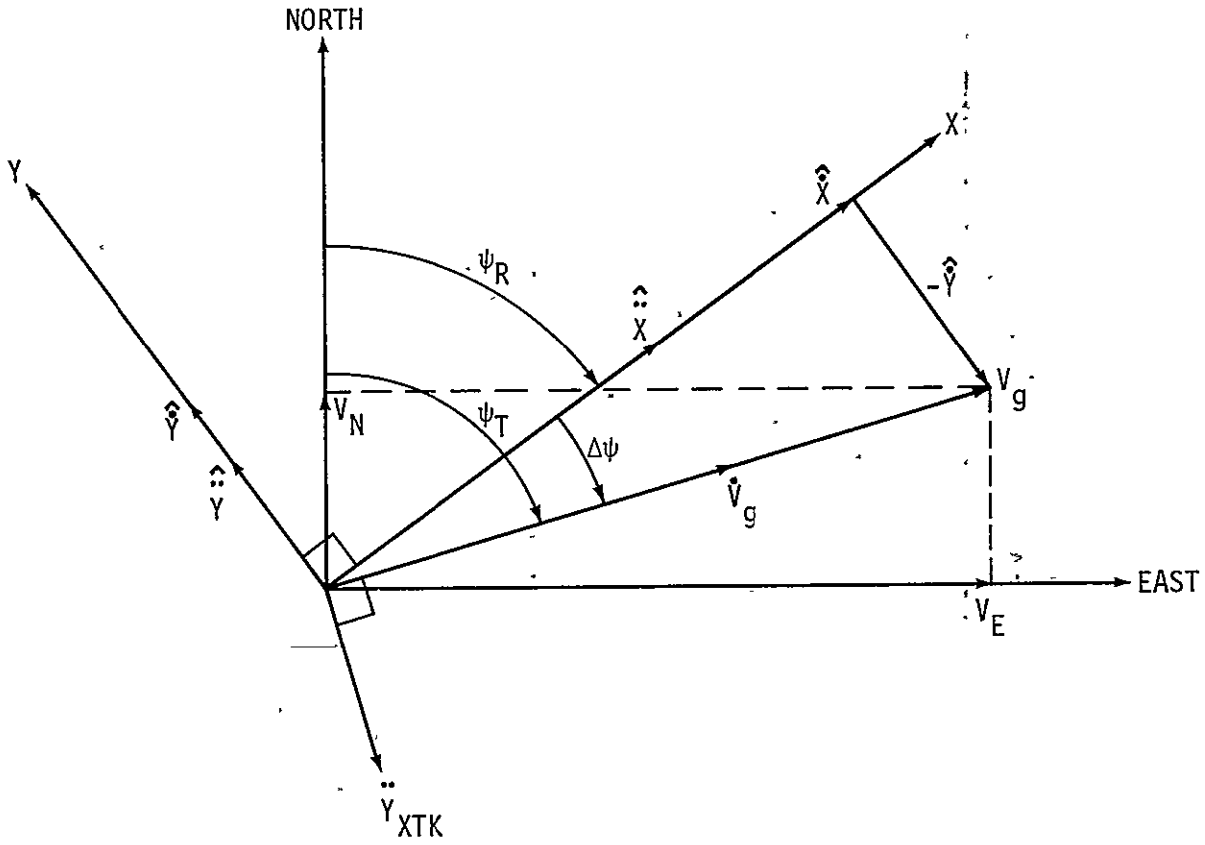

FIGURE VIII-2 ALONG-TRACK AND CROSS-TRACK ACCELERATION VECTOR DIAGRAM

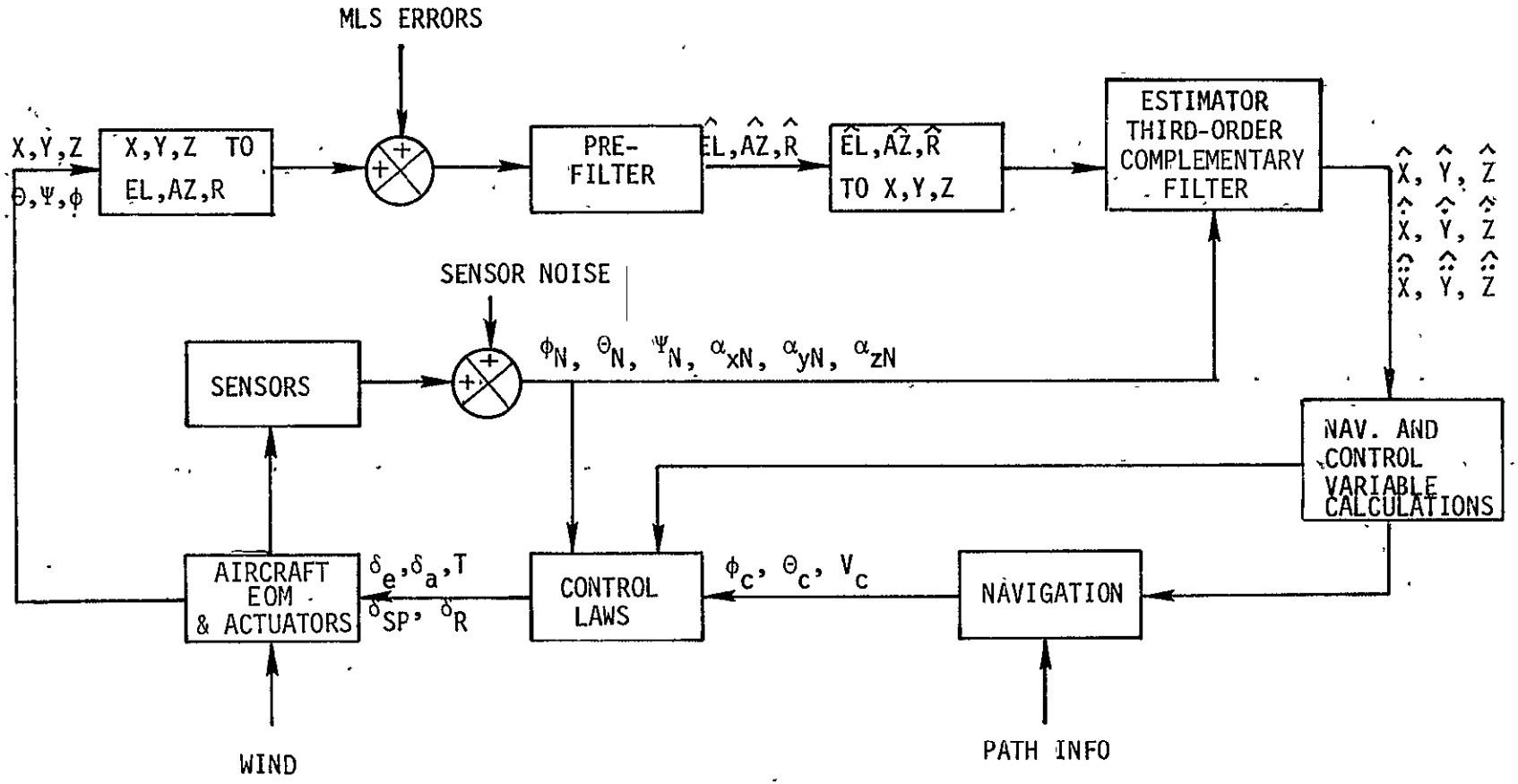

FIGURE VIII-3 BLOCK DIAGRAM OF DIGITAL SIMULATION

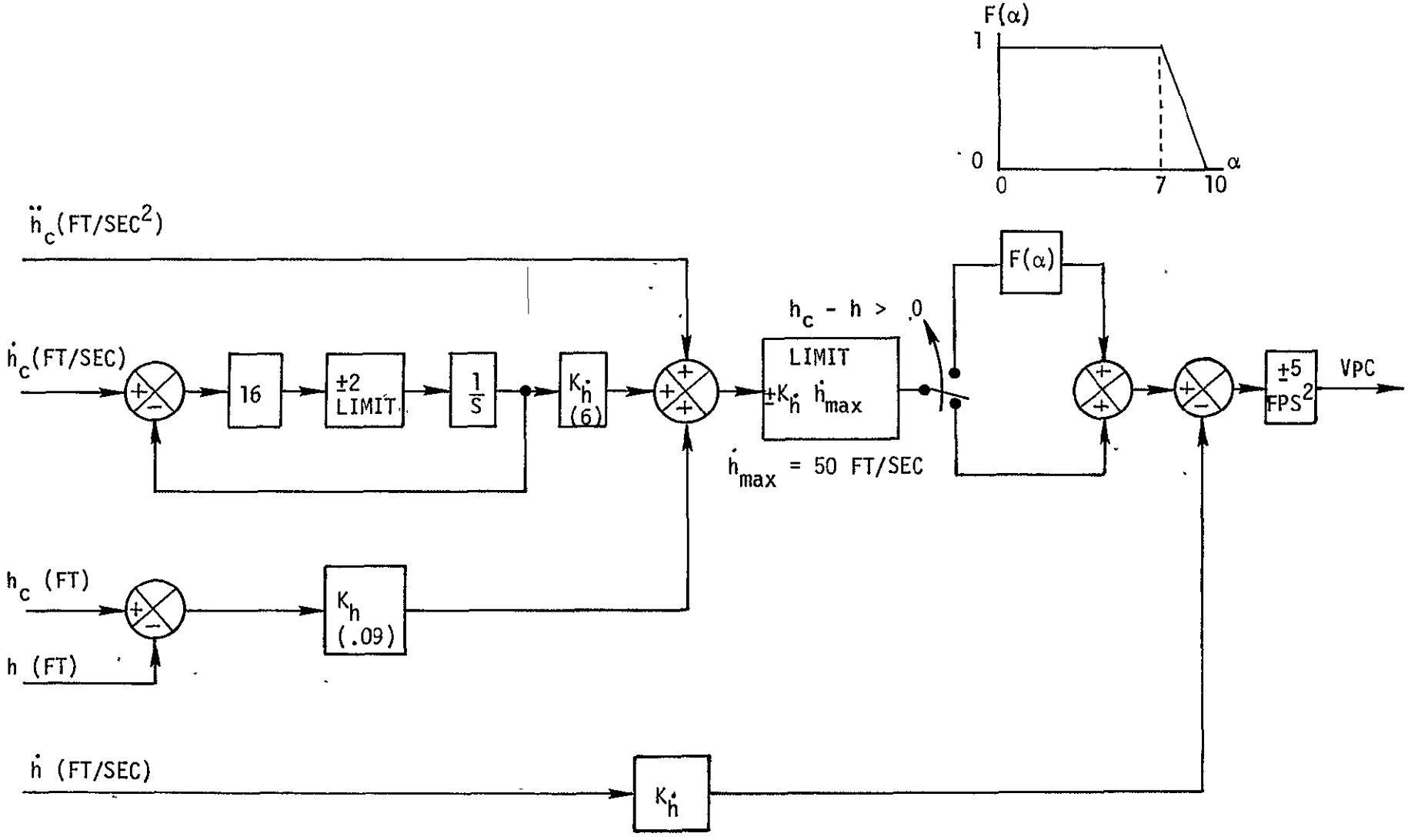

FIGURE VIII-4 VERTICAL PATH GUIDANCE

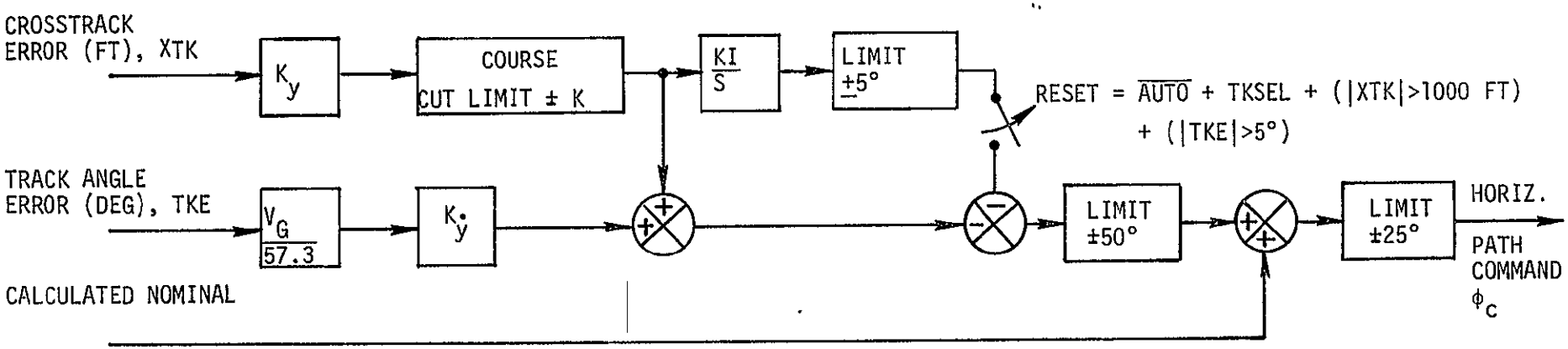

$$K_y = \frac{K_{\dot{y}}^2}{7.12}, \quad KI = .01254$$

$$\phi_{NOM} = \frac{V_g^2}{gR} \quad 57.3$$

$$K_{\dot{y}} = \begin{cases} .5 \text{ for CAS} < 100 \text{ KTS} \\ .68 - .0018 \text{ CAS FOR } 100 < \text{CAS} < 500 \text{ KTS} \\ .14 \text{ FOR CAS} < 300 \text{ KTS} \end{cases}$$

$$L = \frac{V_G K_{\dot{y}}}{57.3} \psi_I$$

$$\psi_I = \begin{cases} 30° \text{ FOR } x < 30° \\ 90° \text{ FOR } x > 90° \\ x \text{ OTHERWISE} \end{cases}$$

$$x = \frac{470|XTK|}{V_g^2} - 30°$$

FIGURE VIII-5 HORIZONTAL PATH GUIDANCE

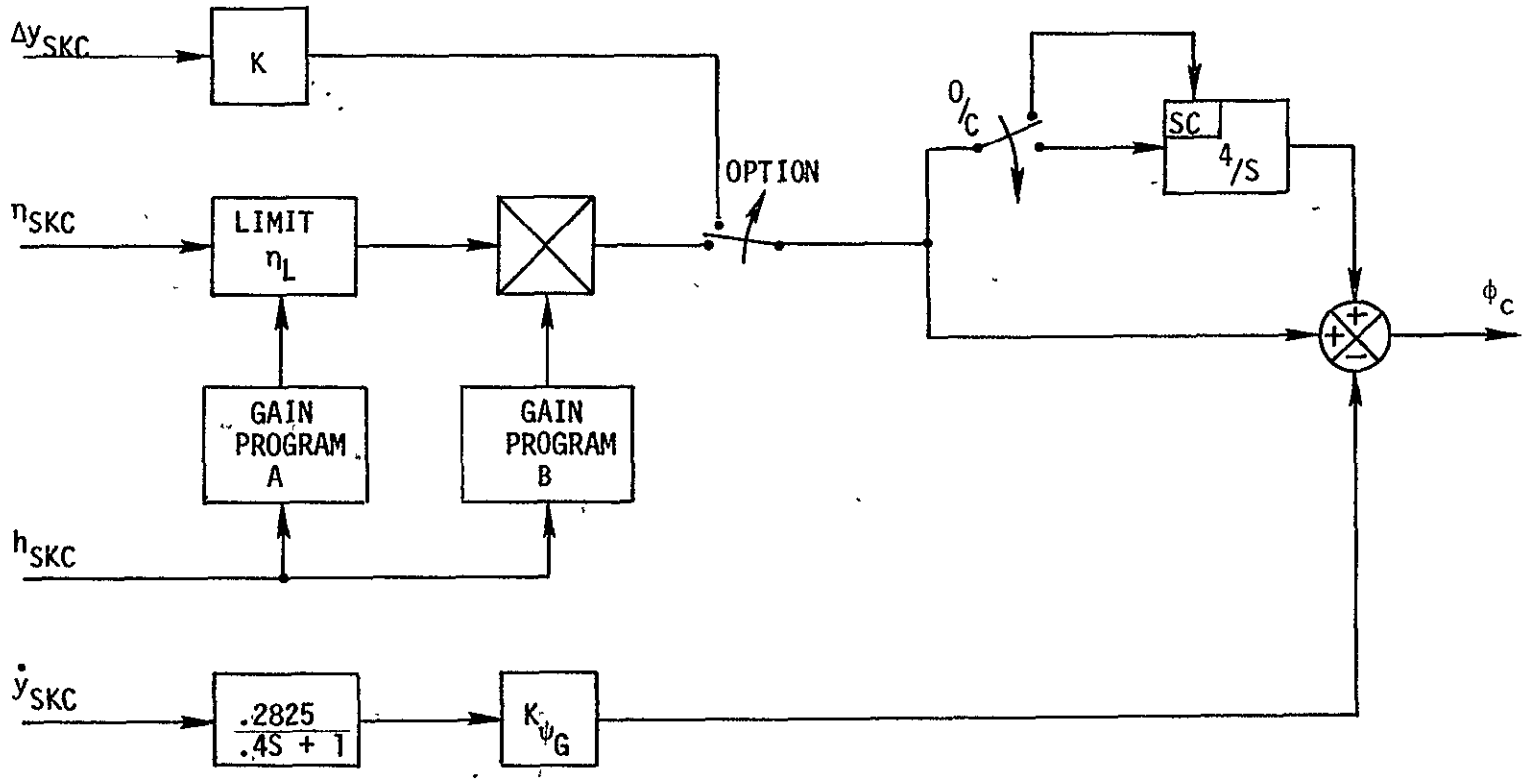

FIGURE VIII-6 ICAO LONGITUDINAL AUTOLAND

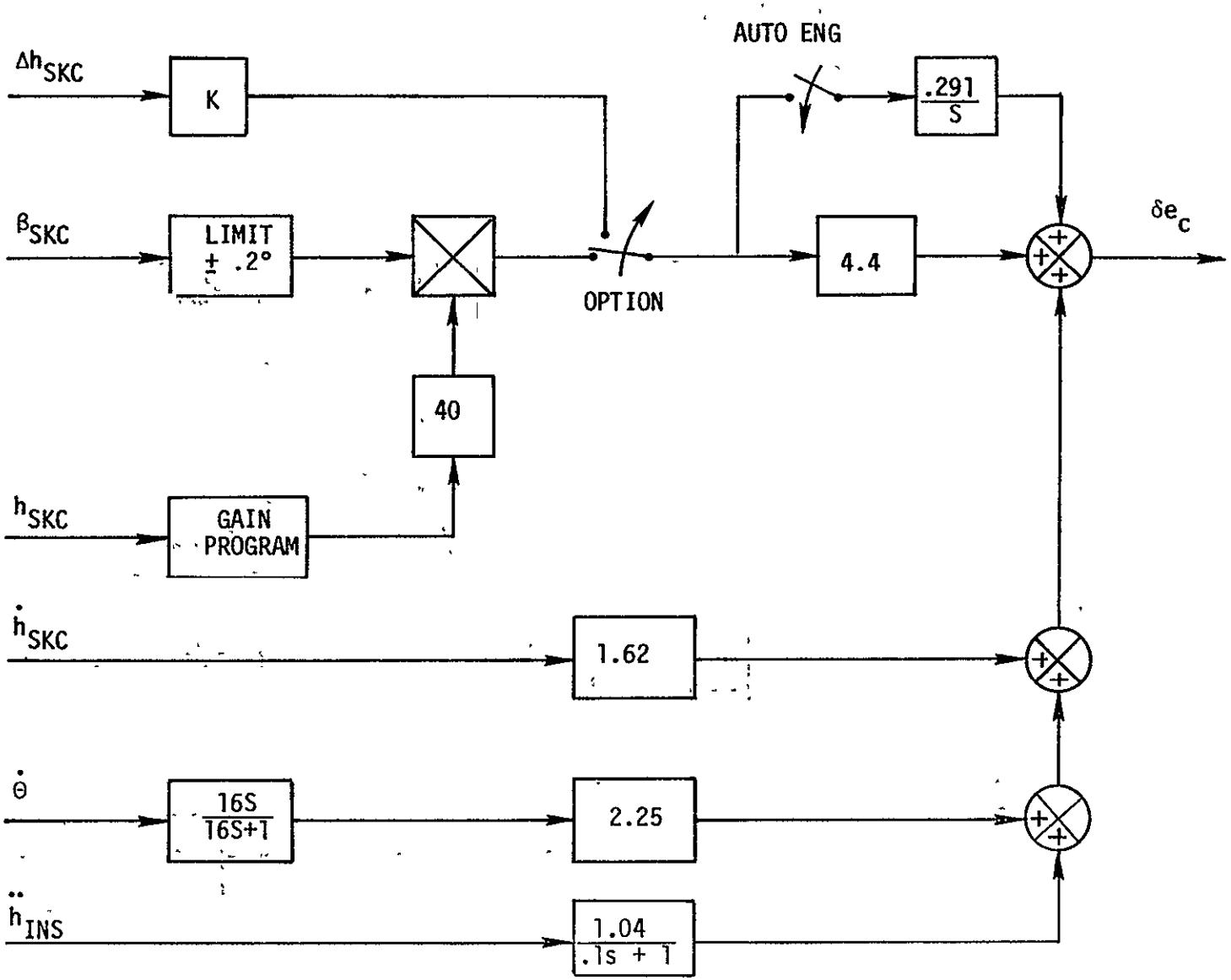

FIGURE VIII-7 ICAO LATERAL AUTOLAND

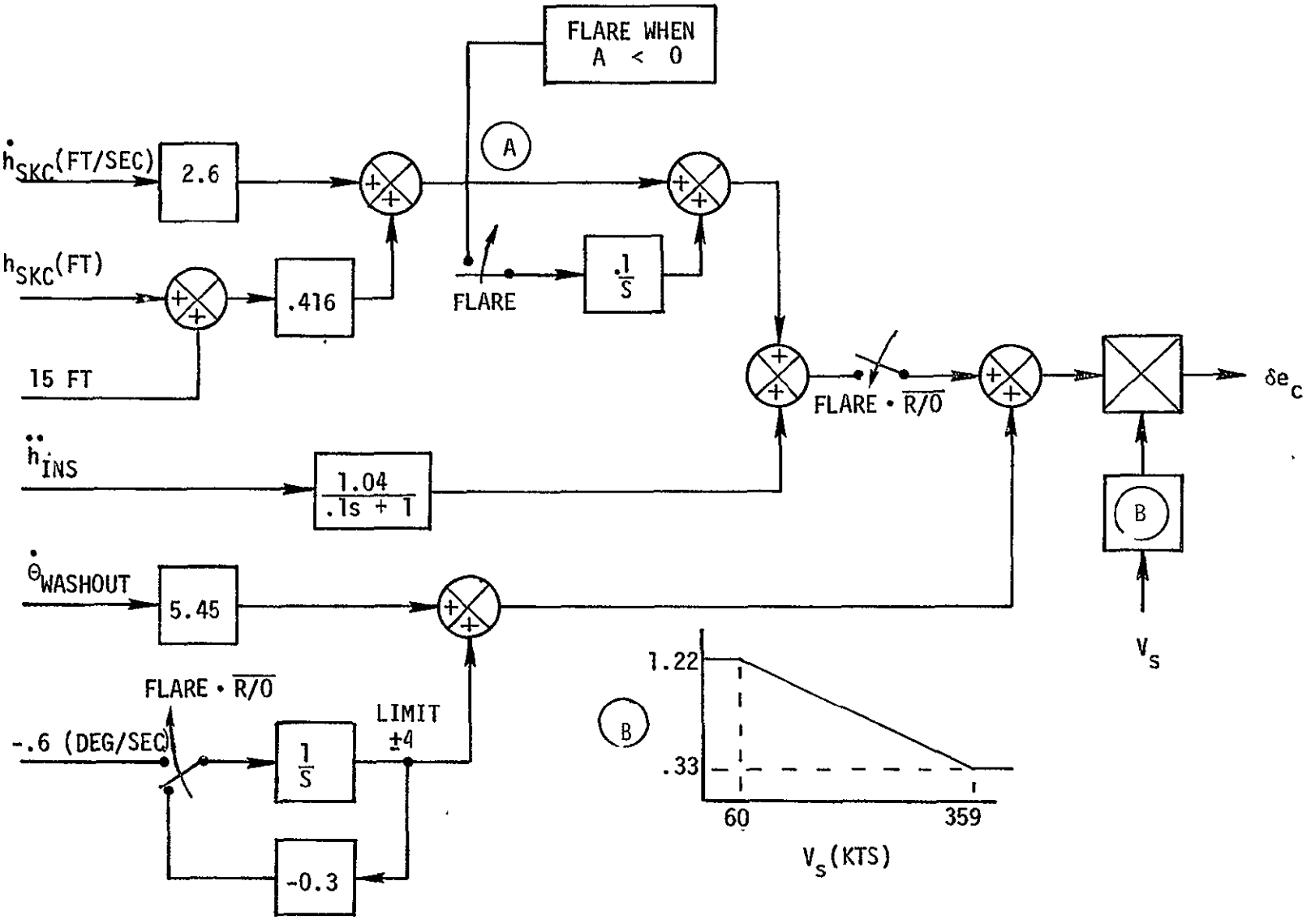

FIGURE VIII-8 ICAO FLARE AND ROLLOUT CONTROL LAW

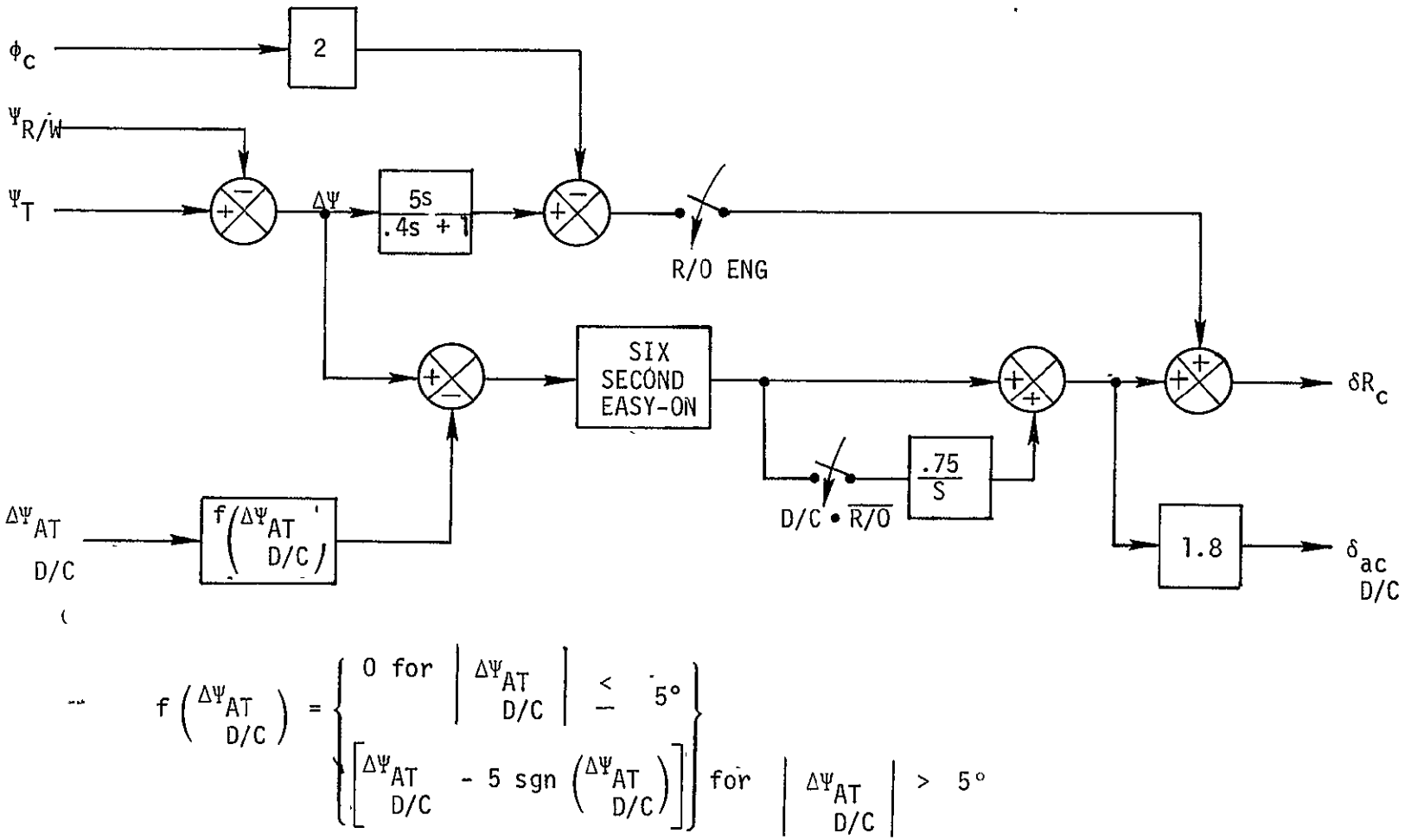

$$f\left(\Delta\Psi_{AT}\right)_{D/C} = \begin{cases} 0 \text{ for } \left|\Delta\Psi_{AT}\right|_{D/C} \leq 5^\circ \\ \left[\Delta\Psi_{AT} - 5\ \mathrm{sgn}\left(\Delta\Psi_{AT}\right)\right]_{D/C} \text{ for } \left|\Delta\Psi_{AT}\right|_{D/C} > 5^\circ \end{cases}$$

FIGURE VIII-9 ICAO DECRAB AND ROLLOUT CONTROL LAW

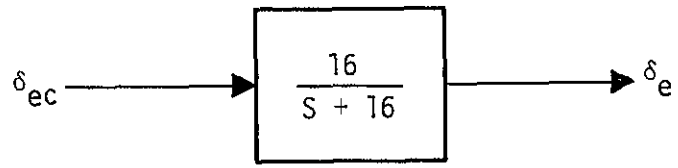

a) ELEVATOR SERVO MODEL

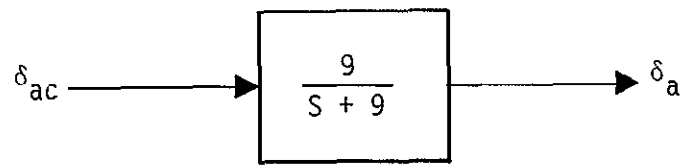

b) AILERON SERVO MODEL

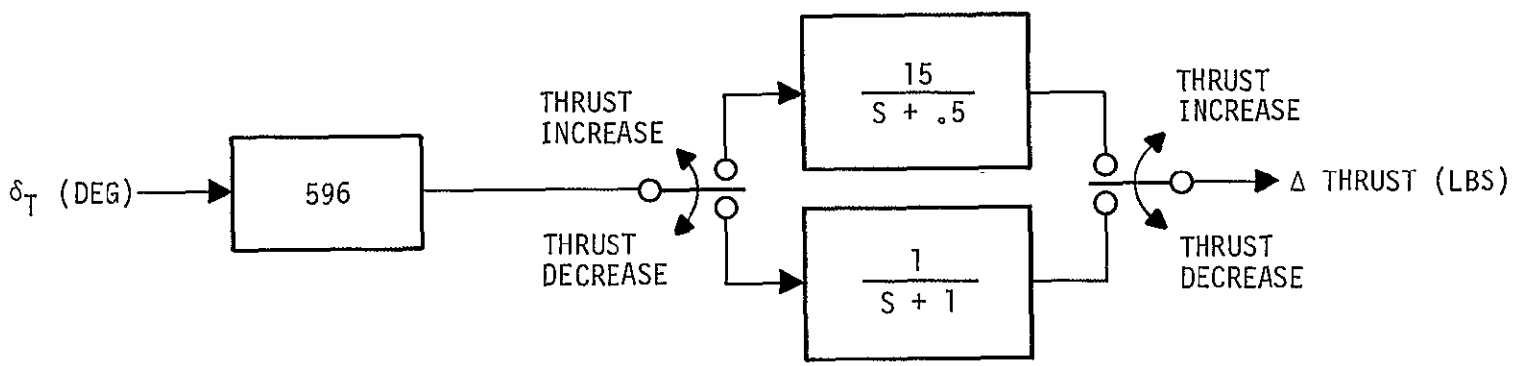

c) ENGINE THRUST RESPONSE MODEL

FIGURE VIII-10 SIMULATION SERVO AND ENGINE RESPONSE MODELS

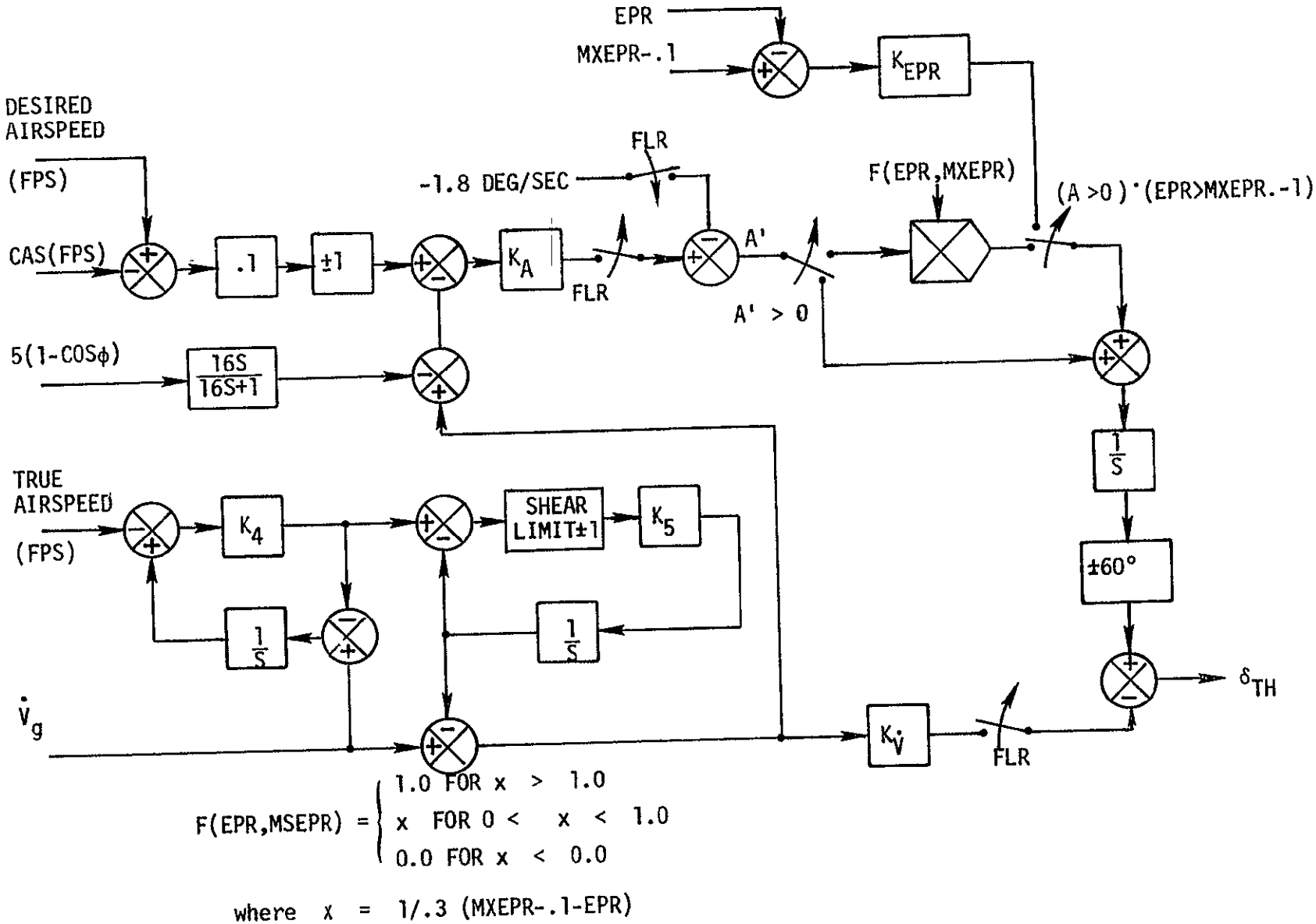

$$F(EPR,MSEPR) = \begin{cases} 1.0 \text{ FOR } x > 1.0 \\ x \text{ FOR } 0 < x < 1.0 \\ 0.0 \text{ FOR } x < 0.0 \end{cases}$$

where $x = 1/.3\ (MXEPR-.1-EPR)$

FIGURE VIII-11 ICAO AUTOTHROTTLE CONTROL LAW

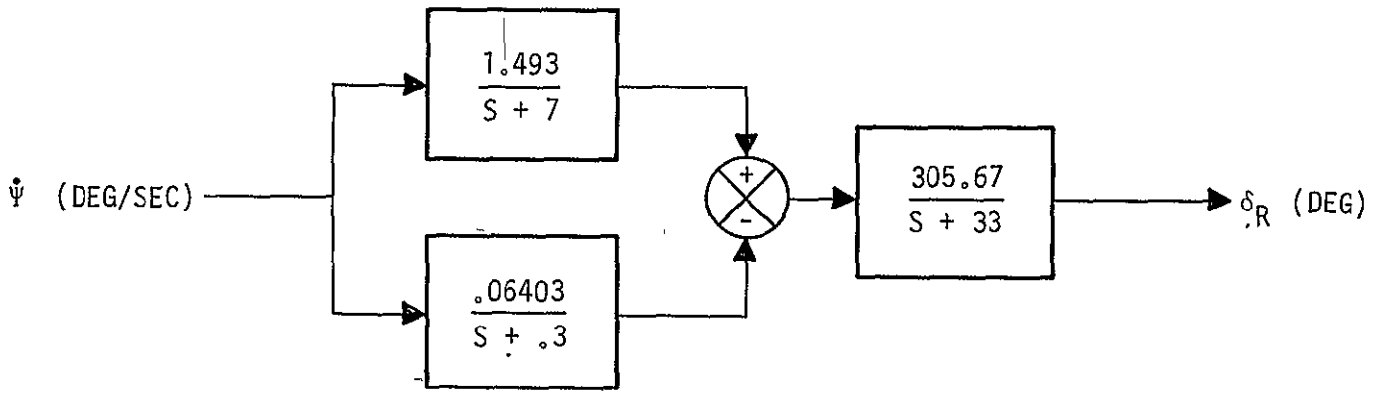

FIGURE VIII-12 B-737 YAW RATE DAMPER MODEL

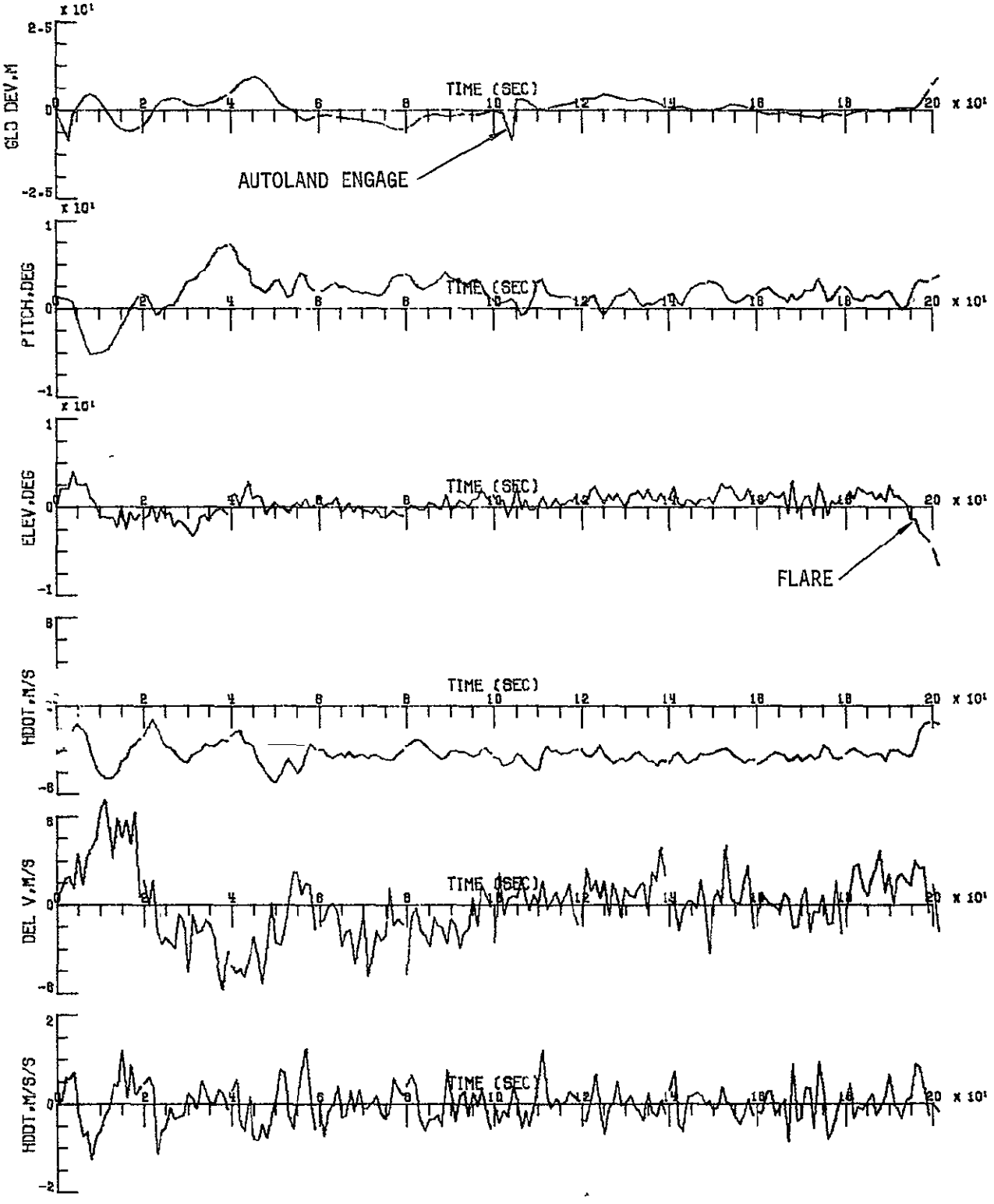

FIGURE VIII-13A LONGITUDINAL PERFORMANCE "C" FILTER (TAILWINDS)

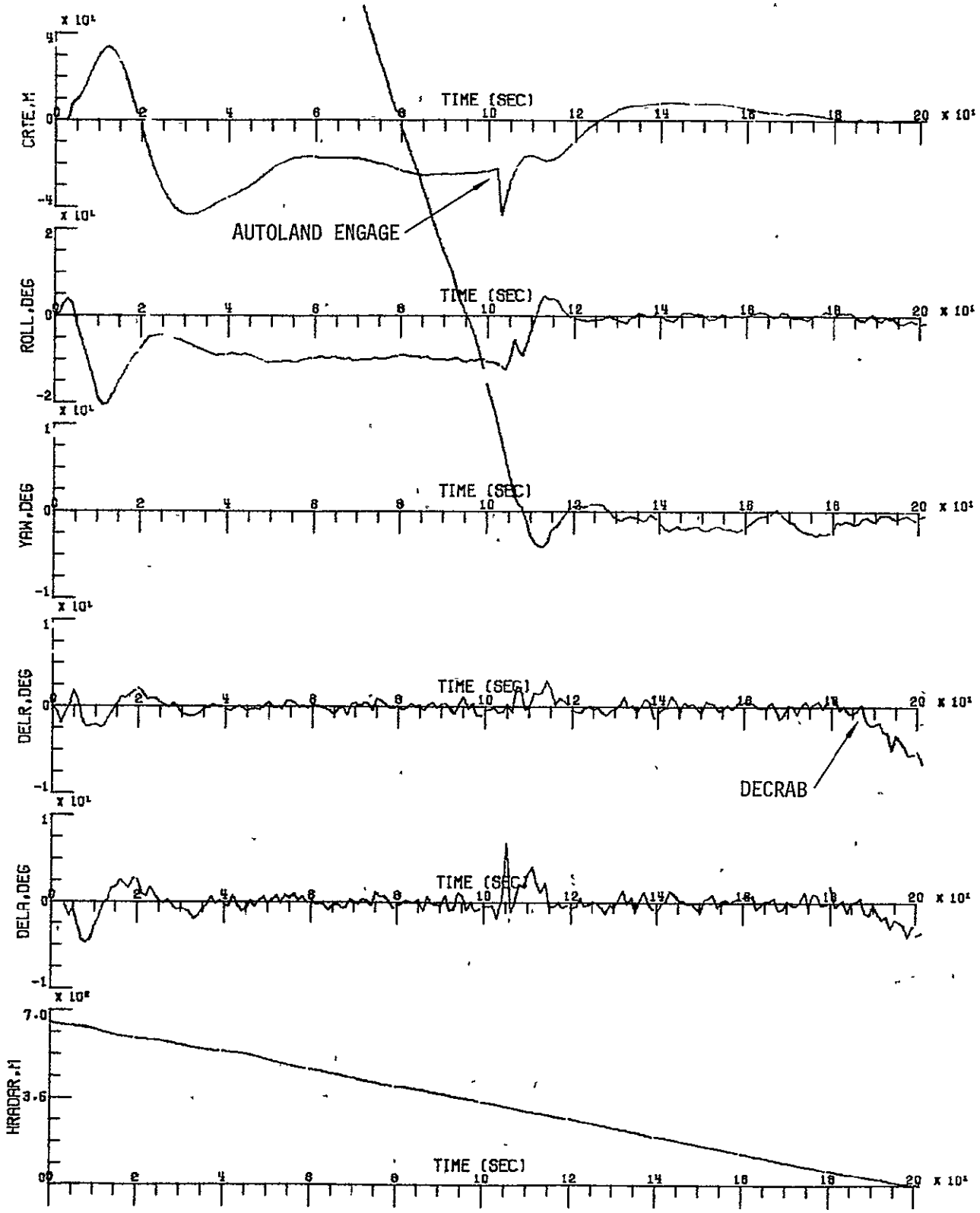

FIGURE VIII-13B LATERAL PERFORMANCE "C" FILTER (TAILWINDS)

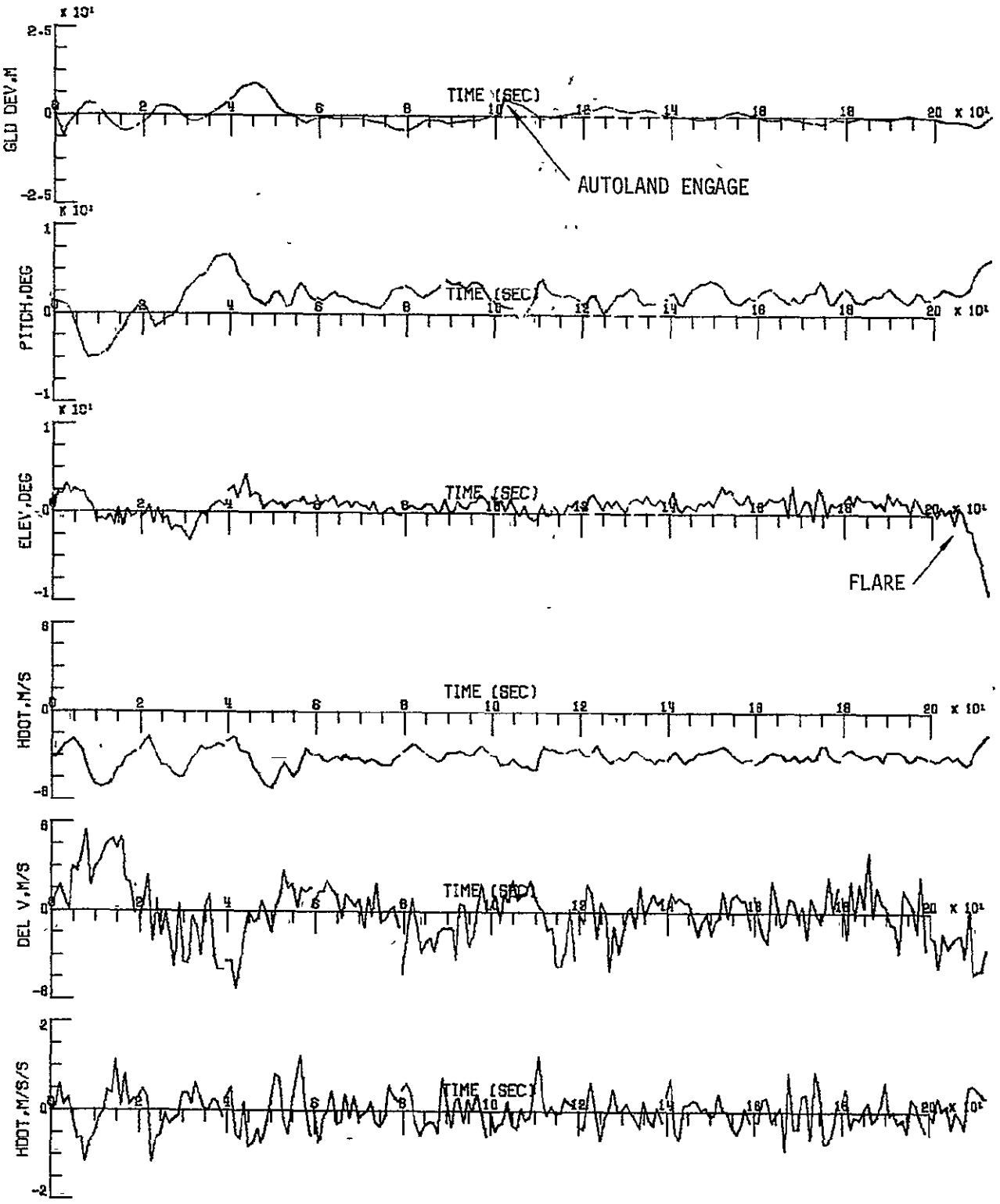

FIGURE VIII-14A LONGITUDINAL PERFORMANCE "C" FILTER (HEADWIND)

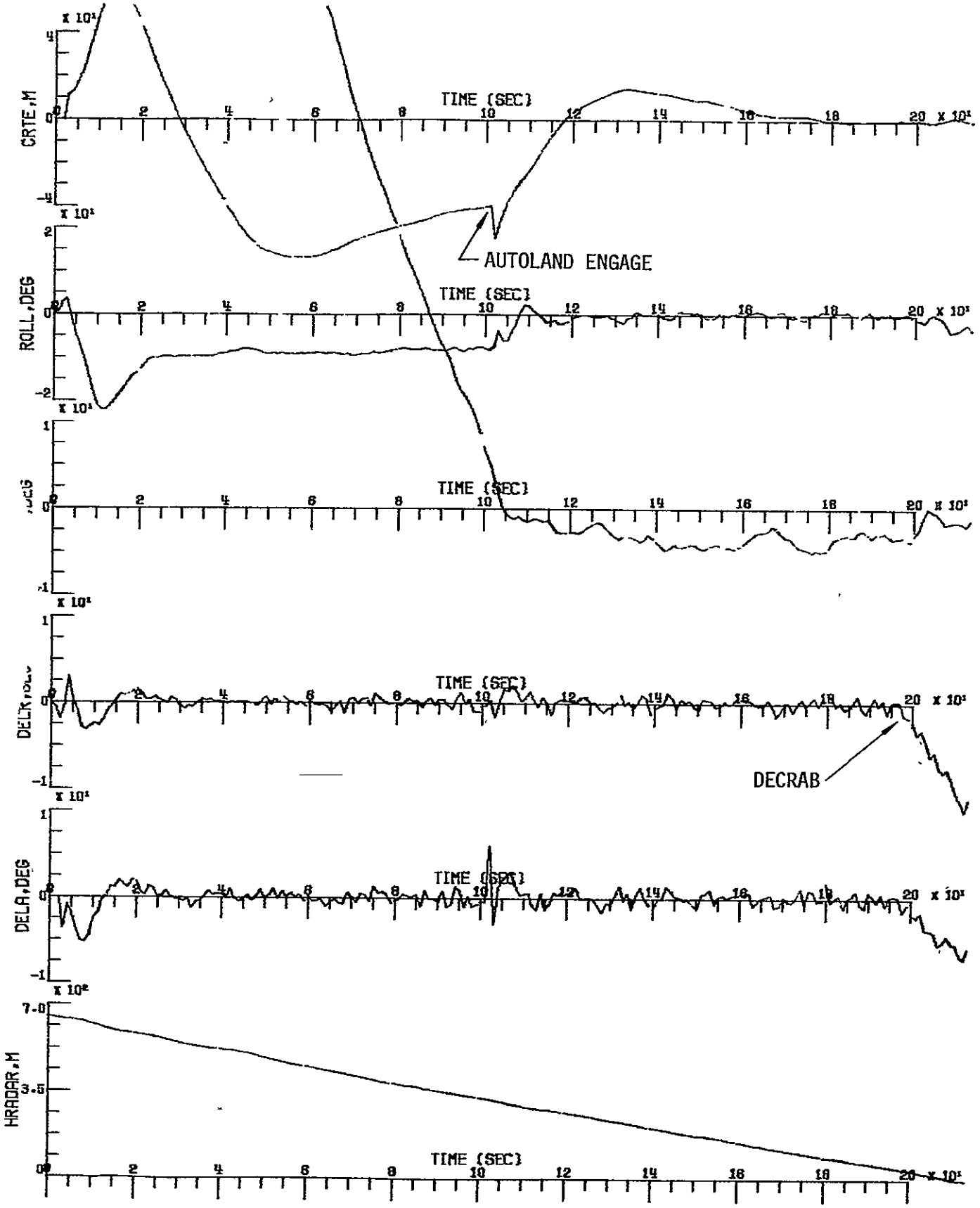

FIGURE VIII-14B LATERAL PERFORMANCE "C" FILTER (HEADWINDS)

IX. NAVIGATION, GUIDANCE AND CONTROL LAW MODIFICATIONS

By Richard M. Hueschen

INTRODUCTION

The guidance and control laws of the TCV B-737 as delivered to the NASA were not designed to utilize the MLS either in the RNAV or autoland automatic modes. These systems were designed to utilize conventional navigation aids. The RNAV systems made use of VOR, DME and the inertial platforms for navigation and guidance. The autoland system was designed to use the Instrument Landing System (ILS) and inputs from the inertial platforms and Central Air Data Computers (CADC). Thus the RNAV and autoland systems contained filtering and signal processing tailored for these navigation aids.

The approach taken in providing guidance and control laws to demonstrate the MLS used the following guidelines: first, the changes to the basic form of the existing guidance and control laws were to be minimized. Minimal changes were necessary in order to design, build and check out a system in time for the demonstration. In addition, guidance and control laws designed specifically for MLS needed more development before implementation was possible. Changes to the basic form of the laws would have resulted in a large effort for re-programming, debugging and verification. Second, the modified system was to make full use of the estimates provided in the MLS processing and complementary filtering discussed in an earlier chapter.

CONTROL LAW MODIFICATIONS

Two changes were made to the navigation system to satisfy the above guidelines. First, filtered signals from the MLS preprocessor were fed directly to the RNAV guidance laws, bypassing all filtering and signal processing in the navigation computer. Second, the navigation computer was programmed to provide its normal DME-updated inertial solution in parallel with the MLS RNAV solution to allow a comparison of the two navigation solutions. Functionally, the navigation computer operation was as shown in figure IX-1.

Similar changes were made to the autoland guidance laws. Existing first and second order complementary filters were bypassed as shown by the MLS switch and heavy lines in figures IX-2 and IX-3, the longitudinal and lateral autoland block diagrams. In addition, an option switch was provided to utilize Δy and Δh directly from the MLS preprocessor instead of the Δy and Δh determined in the flight computers through gain programming and the use of η, β and h.

Figure IX-2 and IX-3 also show where the processed MLS signals (subscripted SKC) replaced existing signals (shown in parentheses). Software and hardware modifications were made to have all existing inputs and those being provided by the MLS processor available at the input section of the flight control computers. This provided the capacity to replace existing input signals by software selection with the processed MLS signals on a step by step approach. For example, existing position signals could be replaced by the MLS position signals while the existing velocity and acceleration signals were retained. This capability was used during flight development and checkout of the system to simplify the tasks of (1) evaluating the effects of the MLS signals in the existing autoland control laws, and (2) isolating problems that may have arisen in using the MLS signals.

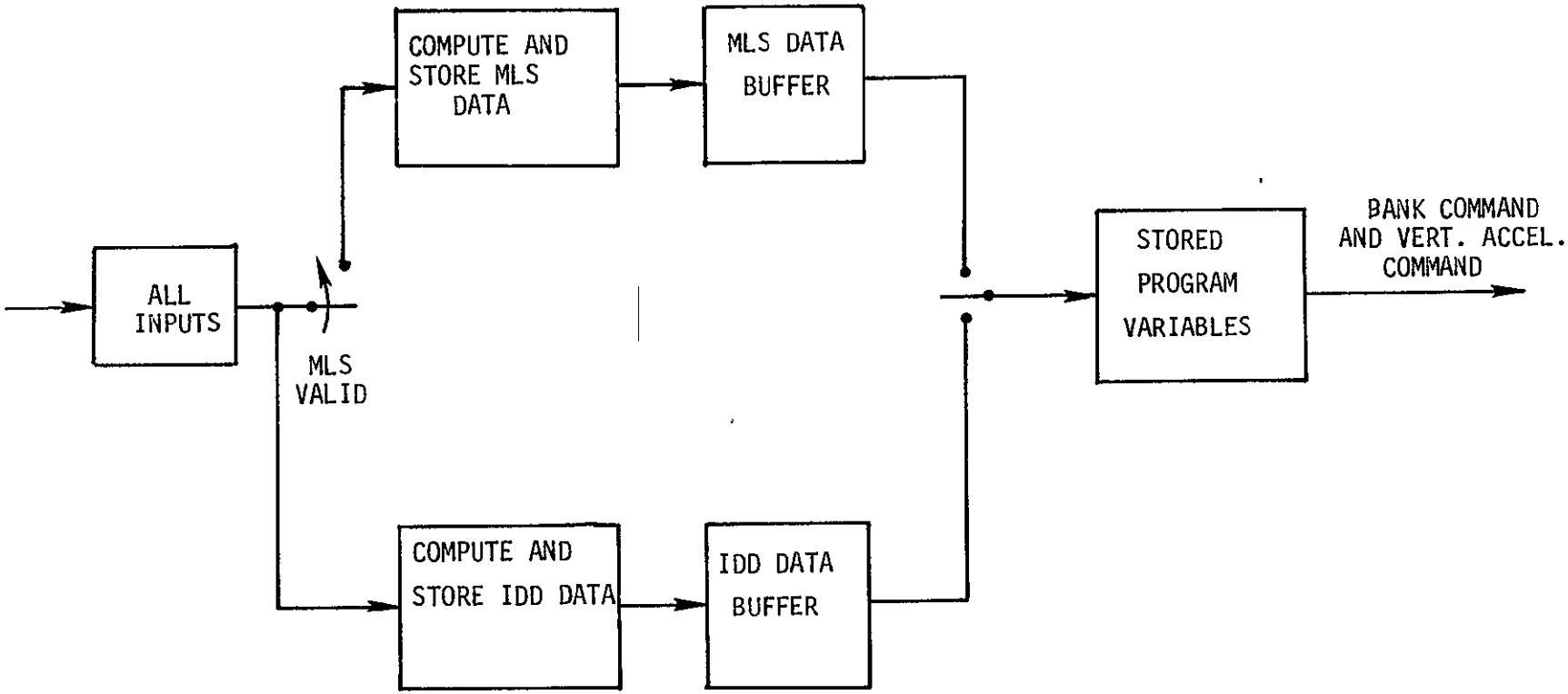

FIGURE IX-1 NAVIGATION AND GUIDANCE - FUNCTIONAL OPERATION

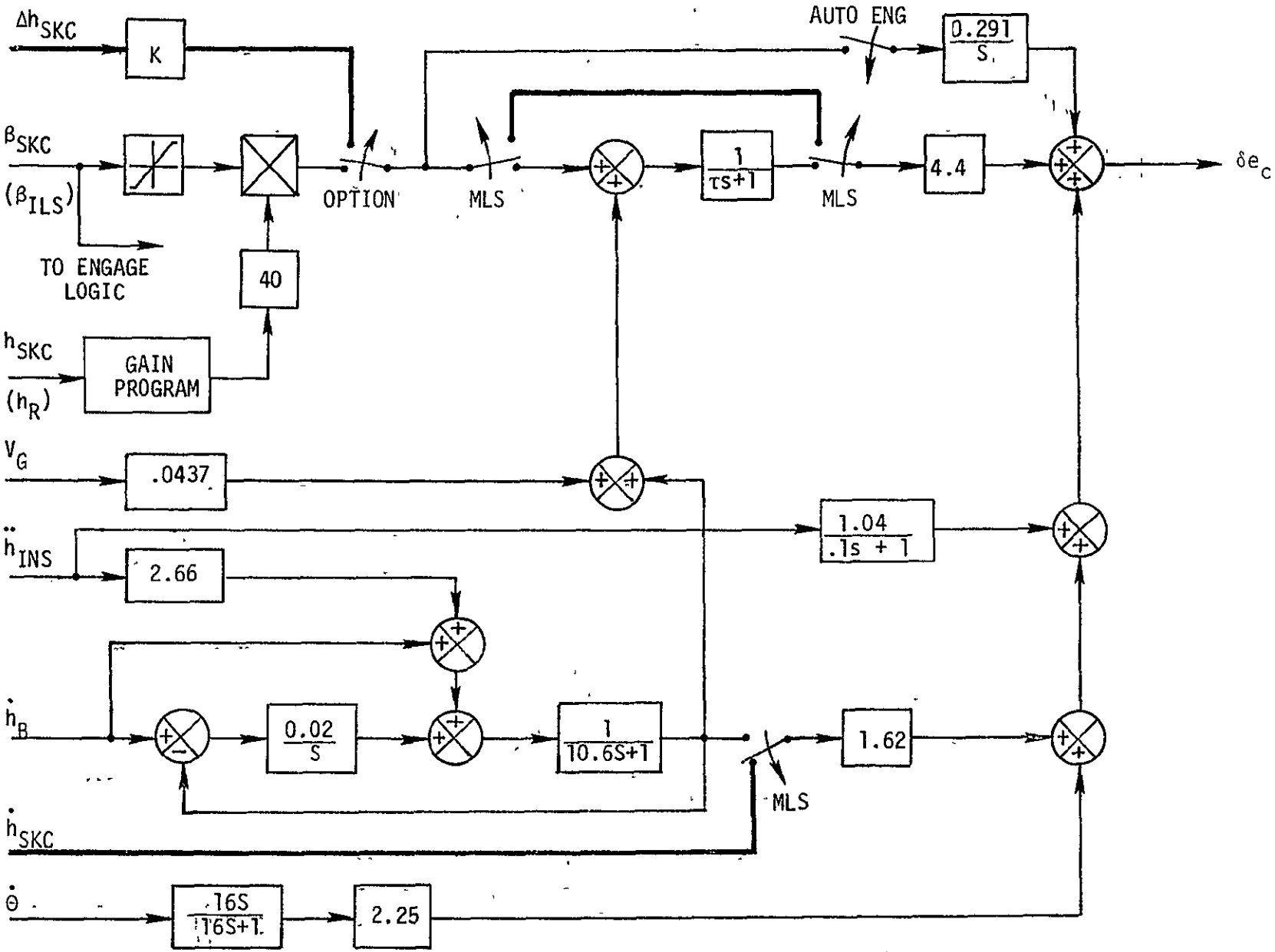

FIGURE IX-2 LONGITUDINAL AUTOLAND

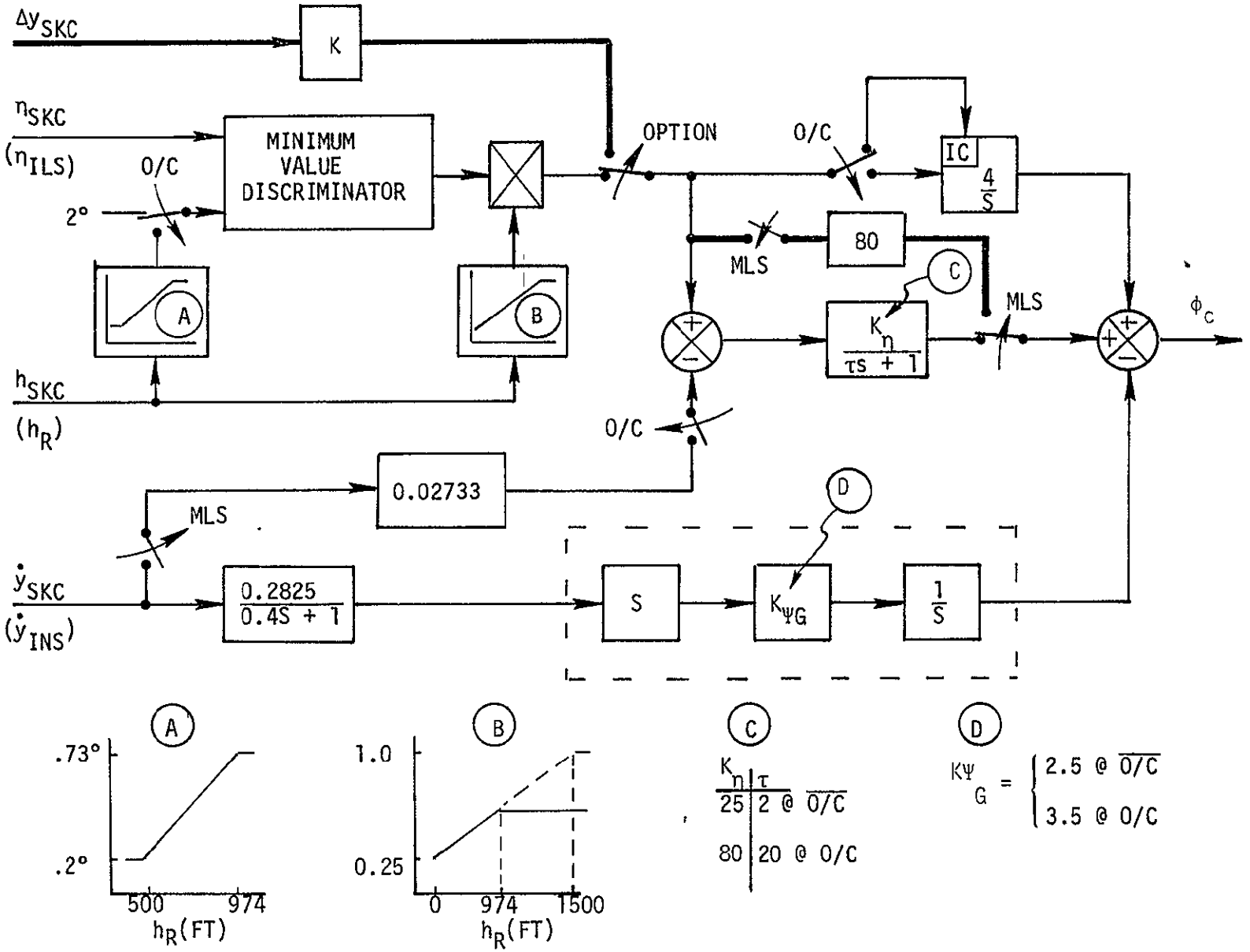

FIGURE IX-3 LATERAL AUTOLAND

X. PREPROCESSOR SOFTWARE

By Gerard E. Migneault

INTRODUCTION

This chapter describes software implemented for the SKC-2000 computer described in Chapter VI. The required flight function algorithms were inferred from the functional requirements, characteristics of the system external to the SKC computer, and the resources available for development. A second type of algorithmic requirements supported auxiliary functions which were not active during flight but were used in developing the flight system. Software required to assist in checking interface hardware before flight, and software to communicate with display devices available in the laboratory but not in the aircraft are examples of the second type.

Flight Function Algorithms. The data transformation and transmission control algorithms were derived from knowledge of the coordinate systems, data formats and transmission rates at the hardware interfaces. Uncertainty about quality of the position data available from the MLS receiver, and about the quality required in the position, velocity and acceleration estimates, led to the specification of alternative sets of estimation and transformation algorithms. These sets of algorithms required various supplementary data, e.g., attitude data, thus expanding the interface hardware and transmission control requirements (Figure X-1). Validity algorithms were specified which determined the validity of each instance of each variable. A requirement to monitor and alter gave rise to additional hardware and data transmission control algorithmic requirements. Finally, the irregular occurence of interrupts from external sources, requesting the performance of specific algorithms out of sequence, resulted in a set of system control and self-status-checking algorithmic requirements.

Auxiliary Function Algorithms. Hardware testing algorithmic requirements arose from a need to verify, prior to flight, that interconnections between the SKC computer and systems external to it were functioning properly. The hardware test function was a specially selectable member of the set of alternate estimation, transformation and validity algorithms. In this option, the data entry device was used to insert known values into the system. The hardware test function simultaneously verified proper functioning of the interface hardware and data transmission control algorithms to be used during flight.

The characteristics of the entry and display devices available in the laboratory during the development phase of the software, and the need for a testing tool able to excite and observe elements of an incomplete software (and external hardware) system resulted in a set of data transmission control algorithms to allow data and/or instructions to be inserted into or displayed from

any desired locations in the SKC computer. Although these algorithms had no function in flight, they resided in the SKC simultaneously with the flight algorithms since they were of use in a total aircraft systems simulation test. The auxiliary algorithms were used then for convenient system testing, monitoring and modifying.

Software System Structure. The design goal for the software system structure was characterized by unidirectional data flow, nonbifurcating control flow, and absence of feedback control paths around modules. The consequence was that data file interfaces between software modules which were simple, single and fixed sufficed. The objective of this design technique was that testing of the total software system would be reduced almost entirely to separate testing of component modules since there was almost no control interaction among modules. The difficulty of isolating causes of system failures during system testing also proved considerable lessened. The price extracted by this design technique, namely software using more memory space than otherwise necessary, was not a contraint since the SKC memory was larger than needed.

SYSTEM CONTROL

General Requirements. The principal function of the system control algorithms was to manage a hierarchical interleaving of algorithms in order to ensure successful completion of planned algorithmic sequences, while accomodating other algorithmic sequences unpredictably and instantly required for processing input/output data and emergency status data. The control algorithms, upon receiving an interrupt signal, acted as switches which uncoupled operating algorithms, coupled in requested algorithmic sequences to completion, then recoupled the interrupted algorithms. In addition, the interrupt handling algorithms could interrupt themselves.

The control algorithms were designed on the assumption that in normal operation all sequences belonging to one iteration time interval would be completed in less than that time interval, so that the control algorithm "idled" during the latter portion of each iteration interval until the interval time had elapsed. Then the sequence of required functions started anew. Had an abnormality caused any sequence to not be completed at the end of an iteration time interval, the control algorithms would cause an automatic restart of the SKC to occur.

System Startup. When the SKC computer was turned on, a hardware feature passed control to subprogram CTL00 which set system control words, initialized table XIFLG (flight input section) and calculated a checksum of the entire software to verify that the code in the computer had not been altered since its last use. CTL00 used subprogram INIT to operate other subprograms (ATTSUP, PRESUP and FLTSUP; their functions are described elsewhere) which initialized

tables within the set of estimation, transformation and validity algorithms. Next CTL00 reset the SKC's real time clock, reset indicators for the two buffers used to output to the split-phase bipolar (SPBP) electrical bus, enabled SKC interrupt hardware and set external interrupt masks to identify permitted interrupt lines. Control of the SKC was then handed over to subprogram CTL01, the preplanned sequence controller.

Algorithmic Sequence Control. Subprogram CTL01 controlled the preplanned sequence of algorithms and maintained the constant iteration time. CTL01 began by setting the iteration time interval (nominally fifty milliseconds) into a hardware countdown timer which caused an interrupt to occur, signalling the time to start the next iteration, when the timer had counted to zero. CTL01 then caused an input data set to be generated by sequentially operating subprograms ASIN, XLCN and DEBE (described in the flight input section). Next CTL01 operated subprogram FCNT which controlled the sequential operation of the subprograms of the estimation, transformation and validity algorithms. When FCNT finished, CTL01 caused the output data set to be transmitted by sequentially operating subprograms LXCN, AOUT, XSCN, DOUT and MNIN, which are described in the flight output section. CTL01 then set an indicator to indicate that all computations for this iteration were completed, and then continually tested an indicator word (T2FLG) until the word took on a zero value, at which time CTL01 restarted itself. With the following exceptions and interruptions, this process was repeated until power to the SKC was turned off.

Hardware Test. After having operated input subprograms ASIN and XLCN but before operating DEBE, CTL01 tested the option number contained in the word OPT. An option number equal to zero indicated that a hardware test was to be performed. CTL01 then operated subprogram HWTST, which is described in the hardware test section. When HWTST finished, CTL01 needed only to operate the last two output subprograms DOUT and MNIN, bypassing all other algorithms, then set the "computation complete" indicator and continue its idling phase.

Auxiliary Data Entry and Display. Immediately after having set the indication that all computations for the iteration time interval had been completed, CTL01 tested flag word TTYFLG for a non-zero value which indicated a pending request to enter data from a teletype input device. Subprogram CTL03 was used to interpret the teletype input command and control the use of auxiliary algorithms. When CTL03 finished, CTL01 reset TTYFLG and continued into its idle phase.

Teletype inputs interfered with the cycling of CTL01 since they stopped the system until all teletype input/output was completed and a termination character entered. No non-teletype interrupts were enable until then. This cycle interruption could not occur in flight since there was no teletype on the aircraft.

Suprogram CTL03 examined the teletype character which caused a TTY interrupt. Only four characters were legitimate: A, C, D, and L. If the character

was an "A", the subprogram DCIO2 was used to input floating point data from the teletype into the SKC memory; if the character was a "C", subprogram CHM was used to enter hexadecimal characters into the SKC memory. If the character was a "D", subprogram HMD was used to print selected memory locations in hexadecimal format on the teleprinter; if the character was an "L", selected memory locations were printed out in floating point format by use of subprogram FLD. For any other character, subprogram IER was used to print an error comment on the teleprinter. Subprograms DCIO2, CHM, HMD, FLD and IER are described in the auxiliary data entry and display section.

Interrupts. When any of a number of sources, either internal or external to the SKC, presented a signal to the SKC interrupt hardware, the event was recorded in an interrupt source register. The SKC hardware then examined an "enable" mask to see whether or not the signal was to be allowed to interrupt any currently processing algorithm (allowing the current instruction to complete) and activated an associated subprogram to service the source requesting the interruption. The various sources had a priority assigned within the hardware.

If power levels fell below a minimum level, SKC hardware caused a power failure interrupt subprogram PFI to be activated. PFI recorded the occurrence of the power failure. If, after approximately 300 microseconds, the SKC had not completely stopped but the power level was still below the minimum, PFI halted the computer. If the power level had returned to a normal level, PFI reactivated the interrupted routine.

When the iteration-interval timer had counted down to a zero value, an interrupt handling algorithm within subprogram CTLO1 was activated. The CTLO1 interrupt handler saved SKC registers and examined the "computation complete" indicator. If the indicator was set, CTLO1 reset the timer to start counting off another interval, and reset indicator word T2FLG. It then reset SKC registers and reactivated the interrupted algorithm. If the "computation complete" indicator was not set, the interrupt handler recorded the fact and caused subprogram CTLOO to be activated. The system then restarted as if power had just been turned on. Some memory of past activity, such as the recording of the occurence of the time out failure, remained in the system for historical and diagnostic purposes.

When the virtual automatic data channel timer had counted to zero and an interrupt was enabled, subprogram SINT (described in the flight output section) was activated.

When either an SPBP or ARINC request for service was received and was enabled, subprogram EG1I (described in the flight input section) was activated.

Either an MLS or MDEU request for service, when enabled, caused subprogram CTLO2 (described in the flight input section) to be activated.

When a teletype key was depressed, it caused subprogram TTI to be activated, if enabled. TTI first verified that the signal was an input request. If so, the character was input and stored in word TICHAR. TTI then set an indicator word TTYFLG to indicate that a teletype character had been input and was available in TICHAR. If TTI recognized neither an output nor an input request, it recorded the occurrence of a console control unit erroneous input. The interrupted algorithm was then reactivated.

FLIGHT INPUT

General Requirements. The estimation, transformation and validity algorithms assumed simultaneous measurements. However, the data were not sampled simultaneously; indeed, some of the data were not direct measurements but were the results of computations. A "nearly simultaneous" set of input data was assumed to suffice, i.e., all the data were sampled during the same iteration time interval and as immediately prior to processing as equipment allowed. One type of input was composed of data whose sampling was initiated by the algorithms in the SKC at preselected points in the algorithmic sequences. The other type of input was of those data whose sampling was asynchronous and unpredictable relative to the algorithmic sequence.

Data Sampled By Command. Data sampled by the interface hardware upon SKC command readily conformed to the assumption of "near simultaneity". These consisted of data transmitted via analog to digital converters, synchro to digital converters, and discrete signal links merged into a discrete bit word. The interface hardware permitted up to fourteen such variables (nine analog and five synchro) and one discrete bit word.

The subprogram ASIN controlled input of data into the SKC by sequentially commanding the devices whose address codes were contained in a table (ICDAW) along with corresponding device delay times. Device register lengths were in a companion table (ICSFT). For each entry in table ICDAW, a fixed point number was input into the SKC and placed into a table (XIDAT) of integers. Immediately after each individual variable was input, the subprogram DSIN was used to input the discrete bit word and place it into a companion table (XIFLG) of sampled discrete bit words. After an interrupt ASIN restarted the sampling of the variable it had been commanding or inputting at the time of interruption.

Immediately after a variable and status word had been inserted into tables XIDAT and XIFLG, subprogram XLCN was used to convert each integer in table XIDAT into floating point format and to place it into table LITAB. In addition to "floating" the integer values, XLCN multiplied each value by an appropriate scale factor and added a bias (obtained from tables XISCL and XIBIA, respectively). All variable values in table LITAB were thus constructed to be unscaled floating point values with dimensions of radians for angular, and feet for linear, measurements.

The subprogram DEBE was next used to transform the discrete bit words in table XIFLG into a table (LIFLG) of floating point numbers. For each discrete bit word in table XIFLG, a mask obtained from a table (ICFMK) of mask words was used to extract the appropriate variable value in table LITAB. Otherwise the value set into table LIFLG was zero.

Tables LITAB and LIFLG contained the "nearly simultaneous" set of input data for subsequent processing during one iteration. Data of the asynchronous type was included, since the last arriving value of each such variable and an associated status word were present in tables XIDAT and XIFLG. Such data were placed there the last time the variable was unpredictably available, as explained in the following paragraphs.

Data Sampled by Interrupts. Some asynchronous data originated in the navigation computer or the Inertial Navigation System and was transmitted to the SKC via the SPBP or ARINC 561 interfaces, respectively, and some was data transmitted from the MLS receiver. These data generated requests for service when they were ready for input into the SKC from the interface hardware. If not serviced within a stated interval of time the data were lost. Because of the higher possible rate of data transmission on the SPBP and ARINC buses, compared to MLS data, in the case of conflicting requests for service the SPBP and ARINC data had the higher priority.

An additional asynchronous source of data was the Manual Display and Entry Unit (MDEU). Since the permissible delay time for servicing this device was greater than the iteration time interval, a request for service was merely noted for later servicing at a selected point in the algorithmic sequence.

SPBP and ARINC data are similar in that part of the data is a label which identifies the variable. When a request for service for either SPBP or ARINC data interrupted the SKC, subprogram EG1I was activated to distinguish between them by examining the interrupt source register. If SPBP data was to be serviced, the subprogram CFIN was used to control the data input. The interface hardware was commanded to subprogram CFAR which assembled the data bits and separated the variable label from the value. CFIN determined whether or not the variable was one of interest. If so, the value was placed into table XIDAT. No corresponding status word was placed into table XIFLG since SPBP data transmission out of the navigation computer implied a functioning computer. Subprogram ARIN serviced ARINC data. Subprogram CFAR input the label and value. ARIN compared the label to a table (ICLAB) of legal ARINC labels, and placed legal input values in table XIDAT. Then a discrete bit word was input and placed in table XIFLG. SPBP and ARINC data were assigned the highest priority among input data. Their input process was not interruptable by any other external request for service.

When a request for service for MLS data or from the MDEU appeared, subprogram CTL02 was activated to determine whether an azimuth, elevation,

range or MDEU request was present. The subprogram MLIN was used to command that the appropriate data and a status word be input from the interface hardware, and to place the status word in table XIFLG. As did ASIN, when resuming processing after an interrupt, MLIN restarted the reading of the variable it was inputting at the time of interruption. Subprogram CTL02 further converted the MLS input data into binary format and then placed the value in table XIDAT.

When a MDEU request was present, subprogram MINI was used to note the fact. No further action was taken at this time. When CTL02 had serviced all MLS and MDEU requests the interrupted algorithmic sequence was resumed.

FLIGHT OUTPUT

Requirements and Constraints. The output hardware and data transmission algorithms transmitted the set of estimated variables to the navigation and flight control computers by means of the SPBP interface. Additional estimated data was output to analog cockpit display and recording devices and discrete signal lines, and to the MDEU.

By construction (and definition) the set of estimated variable values generated during each iteration of the estimation, transformation algorithms represented a set of simultaneous data values. Since no further processing was done to the data transmitted to the analog display and recording devices and MDEU, and since the data appeared to be instantaneous at the iteration rates involved, sequential transmission of these data after the complete set of estimated variable values had been converted to appropriate formats was assumed to be sufficient. For convenience the same assumption was made about the data transmitted over the SPBP interface. This assumption permitted the SPBP data transmission, a relatively slow serial bit shifting process operating at approximately 3/4 millisecond per transmitted word, to be programmed such that it appeared to be performed by an autonomous data channel, simultaneously with other algorithms in the SKC and without any interleaving of algorithms or increased complexity apparent. The transmission began before input of data for the next iteration.

Format Conversion. During each iteration a complete set of estimated variable values and their validity indicators was computed and placed into the table (LOTAB) of floating point numbers for output. Subprogram LXCN then began the output process by converting each floating point number into an integer and placing it into a table (XOTAB) of fixed point numbers scaled for output. Scale factors were obtained from another table (SCTAB). LXCN also tested and limited each variable, since floating point numbers had a greater magnitude range possible than fixed point.

Data Output. After the last entry into table XOTAB was made, subprogram AOUT sequentially commanded each of the first thirteen values in the table to be output to the thirteen digital to analog converters. No test was made to verify that the variables were successfully output. Next, subprogram XSCN was used to initiate transmission of data over the SPBP interface by means of a virtual autonomous data channel (VADC). First, the values in table XOTAB to be transmitted were each imbedded into a "nearly SPBP" formatted word by affixing a complemented sign bit and appropriate identification bits obtained from a table (SCTAB) of labels. A parity check bit to complete the SPBP format was generated by the interface hardware. Any operation of the VADC was suspended while XSCN placed the formatted data in one of two buffers, choosing the buffer into which data had not been placed during the previous iteration. Then, if the VADC was idle, i.e., transmission of the alternate buffer loaded during the previous iteration had been completed, the new buffer location and size was set into the status words by subprogram SSUP. SSUP started the VADC into operation by activating subprogram SOUT. If the VADC was not idle, XSCN rather than SSIP activated SOUT; this caused the VADE to resume operation where it had been suspended.

Two subprograms, SOUT and SINT, in conjunction with a countdown timer and the SKC interrupt feature simulated an independent data channel. Given a buffer location and size, this channel output the buffer data at a rate compatible with the SPBP interface, and independently of any other process or algorithm in the SKC. When activated, SOUT examined a pointer to a word in the buffer, commanded that word to be output to the SPBP interface, and advanced the pointer by one. If the pointer still pointed within the buffer, SOUT set a countdown timer to count off the time interval for one word to be transmitted over the SPBP bus. If the pointer was outside the buffer, SOUT examined indicators to see whether or not another buffer was ready to be output. If it was, the pointer was altered to point to that buffer's first data word and the timer was started. The subprogram SINT responded to an interrupt triggered by the countdown timer. SINT activated SOUT unless a lockout indicator set by XSCN was present; in which case SINT merely set an indicator to inform XSCN that more data in the current buffer remained to be output.

After the VADC had been started the subprogram DOUT was used to output the discrete signal lines. The last eight entries in table XOTAB were considered to be discretes and were merged into one or more bits of a discrete bit word by use of a mask from a table (DBTAB) of discrete bit masks. After forming the discrete bit word, DOUT commanded its output to the interface hardware.

The last data output was to the MDEU. Subprogram MNIN was used to input the number manually set into the four hexadecimal address switches. The data in the location addressed was output by MNIN to the MDEU display lights as a signed decimal fraction and exponent. If, however, subprogram MINI (described in the flight input section) had noted a request for MDEU input, MNIN first

input the number contained in the input switches, converted it into a floating point format and inserted it into the addressed location, and then output to the display lights. If the leading bit of the address switches was a "1", it was ignored as an address bit and all data transfer in and out was handled in hexadecimal format.

HARDWARE INTERFACE TESTING

The hardware test feature of the system was necessary to assist the operators in verifying, prior to flight, that the SKC computer was properly connected to the appropriate equipments. This was determined by observing the presence of known values input from external sources into tables in the SKC, and by observing the SKC output at external display devices and other computers in the system.

Sub Options. When the hardware test option was selected, subprogram HWTST was activated. HWTST immediately examined a secondary option indicator HWTOPT. A zero value caused the data in input table XIDAT to be transferred without further processing to output table XOTAB. HWTST then activated subprograms AOUT and, if an indicator word SPENCER had a zero value, XSCN. AOUT and XSCN are described in the flight output section. If SPENCER did not have a zero value, XSCN was not activated and the contents of SPENCER were output on the SPBP bus.

When HWTOPT had a value of "1", subprogram LXCN was activated to convert and transfer the floating point data in table LOTAB into XOTAB as described in the flight output section. Appropriate data was inserted into LOTAB by teletype input; this was done in lieu of inputting data through the flight input algorithms. HWTST then activated AOUT and XSCN (or not) as described above.

ESTIMATION, TRANSFORMATION AND VALIDITY ALGORITHMS

These algorithms were a straightforward implementation of the mathematical equations given in chapters VII and VIII, which transformed the input set of data contained in tables LITAB and LIFLG to the output set contained in table LOTAB.

The algorithmic sequence was controlled by subprogram FCNT, which sequentially activated subprograms ATT, TACC, COPT, PREDICT, PFCONT, TPOS, FILTER and TOUT. Each subprogram transformed a set of input variables into an output set according to a prescribed set of mathematical relationships as described in Chapters VII and VIII. Note that the algorithmic sequence subprogram PFCONT repeatedly activated subprogram PREFILTER.

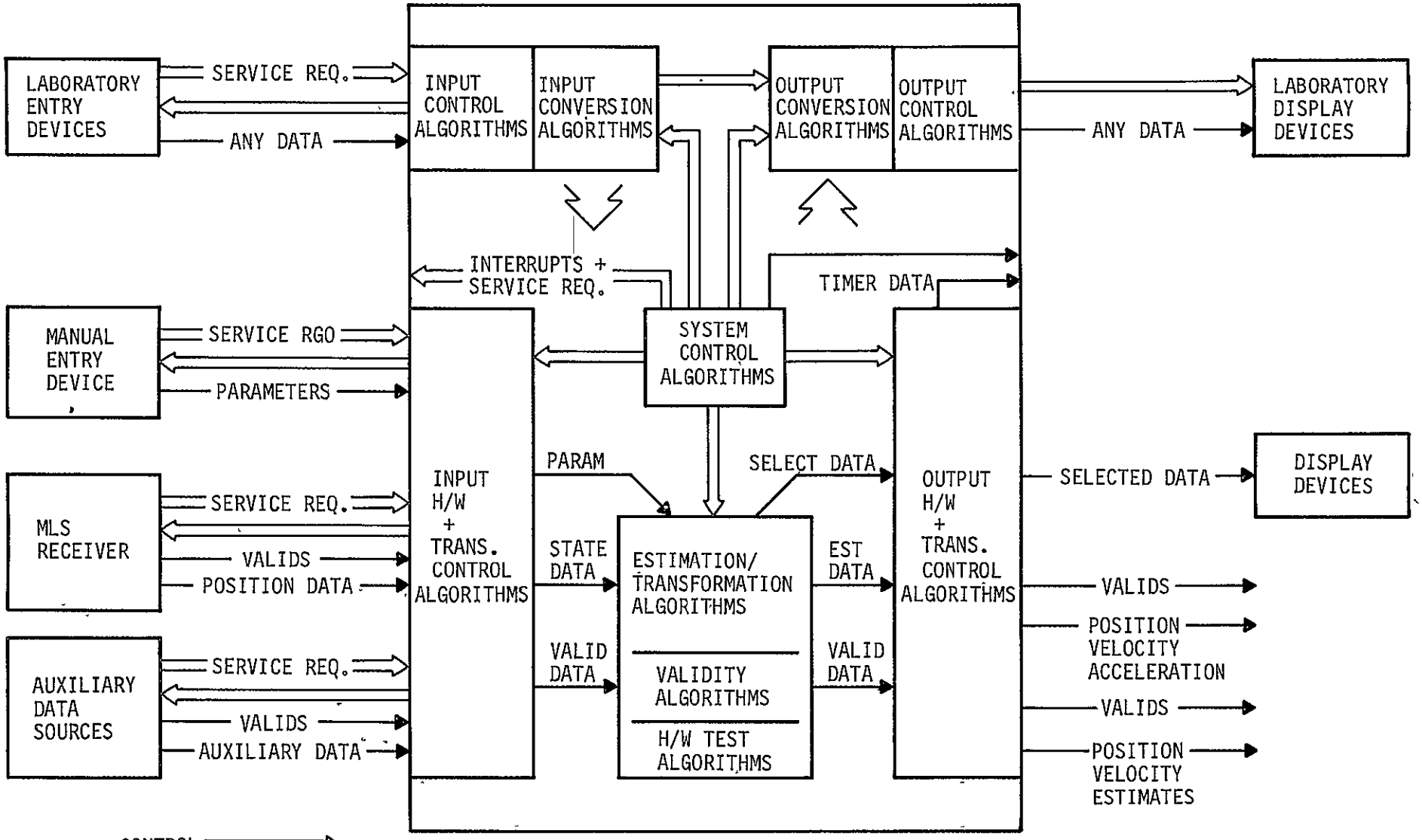

FIGURE X-1 SOFTWARE FUNCTIONAL DIAGRAM

XI. TRSB-MLS RECEIVER SIMULATOR

By Dale G. Holden

INTRODUCTION

The "Hot Bench" Simulation Facility needed a special interface system between the TRSB-MLS Analog Computer Simulator and the TRSB-MLS Preprocessor (SKC-2000 computer). This interface system was to faithfully simulate in real time the TRSB-MLS receiver signal outputs in the laboratory that would normally be presented to the preprocessor while airborne in the MLS environment. The analog computer would generate the TRSB-MLS signals typical of a flight in the MLS environment. The TRSB-MLS receiver simulator interface would receive the analog angle and range signals and reformat them into the proper time-multiplexed serial digital signals as would normally be output by the TRSB-MLS receiver. The receiver simulator would also be responsible for generating bad signal characteristics as could be expected under actual flight conditions.

In particular the TRSB-MLS receiver simulator would be responsive to the following requirements:

1. Receive analog angle and range data representative of a typical autoland flight.
2. Digitize, scale and reformat data for digital serial transmission.
3. Control angle and range signal output timing interrelationships.
4. Command under preprogrammed control the generation of corrupt signals and associated flags.
5. Simulate exactly the TRSB-MLS receiver output signal level and timing interface characteristics to the MLS preprocessor (SCK-2000 computer).

The TRSB-MLS receiver simulator was implemented using an INTEL 8080 microprocessor for timing and control with dedicated and specialized hardware input and output interfaces. Figure XI-1 is a picture of the simulator system.

SYSTEM DESCRIPTION

A general system block diagram is shown in Figure XI-2. The microprocessor under interrupt control of a real time clock and a range transmitter clock commanded the analog-to-digital converter to selectively sample the analog data representing the angle and range information generated by the TRSB-MLS

analog computer simulator. The microprocessor then reformatted the digital input data, generated flags as required and sent the data to the appropriate angle or range transmitter. Once the transmitter received the data it was commanded by the microprocessor to asynchronously transmit the data to the SKC-2000 computer. The diagnostic receivers were used to monitor proper transmitter operation and give a wrap-around check of transmitted data.

Microprocessor Interfaces. The operator interfaced the microprocessor through two means: (1) the teletype with special INTEL-MONITOR support software, and (2) the display control panel that was developed specifically for this application. The teletype could be used to access any location in memory for display or manipulation, initiate a number of diagnostics, or allow an application program to take control. This latter operation was used to start the receiver simulator operation. The control panel allowed the operator to select any number of optional display formats for diagnostic or real time data display purposes.

The microprocessor interfaced the input and display subsystems via a 16-bit-wide bi-directional bus and dedicated control lines. Eight analog inputs were multiplexed under microprocessor control and subsequently digitized by a 12 bit analog-to-digital converter. The digitized data was taken into the microprocessor and scaled, formatted, and then placed on a dedicated 16-bit-wide output data bus at the proper time for subsequent transmission to the MLS preprocessor (SKC-2000 computer). The diagnostic receivers associated with the angle and range transmitters were identical to the data receivers used in the MLS preprocessor and were used to monitor transmitted data and verify proper operation of the data transmitters.

Output Timing. Figure XI-3a shows the peculiar timing relationships of the azimuth and elevation signals as they were transmitted in the actual TRSB-MLS environment. Note that the data rate of the angle signals was not constant, but the data bytes occur at a pseudo-random period repeating every 8 data bytes for the azimuth and every 24 data bytes for the elevation transmissions. This timing phenomena is called "stagger" and has been purposely designed into the TRSB-MLS system to reduce multipath problems associated with propellor-driven aircraft. Actual stagger time intervals and equivalent counts of the real-time clock are tiven in Table XI-1. The average transmission rate for azimuth is 13 Hz and elevation is 40 Hz.

Figure XI-3b illustrates the angle signal level and timing characteristics which had to be exactly simulated. There were a total of 7 data lines required for the angle transmitter, one signal data line, one gated clock line, and two gates (AZ and EL). The angle data was in sign-magnitude form with 15 bits of data and the MSB was always a zero (low level).

Angle and Range Transmitters. Figure XI-4 is a more detailed block diagram of the angle transmitter. Angle and control data were placed on the 16

TABLE XI-1. - STAGGER INTERVALS FOR AZIMUTH AND ELEVATION SIGNALS

Azimuth		Elevation	
Milliseconds	Counts at 0.3 ms/count	Milliseconds	Counts at 0.3 ms/count
65	195	31.0	93
78	234	22.8	68
84	252	11.2	34
66	198	31.0	93
84	252	22.8	68
70	210	24.2	73
64	192	31.0	93
81	243	22.8	68
		30.2	91
		31.0	93
		22.8	68
		12.2	37
		31.0	93
		22.8	68
		16.2	49
		31.0	93
		22.8	68
		10.2	31
		31.0	93
		22.8	68
		27.2	82

bit output data bus by the microprocessor at the appropriate time, and strobed into the appropriate register or control latches. The strobes -1 and -2 were time sequenced by the microprocessor. Strobe-1 loaded the 16-bit data byte and cleared the counter, and then Strobe-2 loaded the 6-bit control latch and commanded the subsystem to transmit the data to the preprocessor. The transmitter operated independently of the microprocessor during its high speed transmission period and shut itself off after the proper number of clock pulses were transmitted. The operation of the range transmitter was similar to that of the angle transmitter with but a few exceptions. The data format and timing were similar to that shown in Figure XI-3b, the exceptions being that the clock rate was 632 kHz and the data word was 16 bits instead of 15. Figure XI-5 is a more detailed block diagram of the range transmitter. The range transmitter ran asynchronously with respect to the angle transmitter to transmit, and then at the end of transmission to interrupt the microprocessor for data and control information update. The microprocessor responded with data and a sequence of control strobes similar to the angle transmitter

operation update. Transmission of this new data did not occur until the next 40 Hz command signal was generated.

Software Implementation. The software for the TRSB-MLS receiver simulator was structured around the use of real-time interrupts. There were two real-time clocks; one operated at 3.33 kHz and the other at 40 Hz. The 3.33 kHz real-time clock was used to develop the relative "stagger" transmission times of the TRSB-MLS azimuth and elevation angle signals as found in the airport MLS environment. However, range transmission was not staggered but was asynchronous to the angle transmissions, which suggested the use of another real-time clock running at 40 Hz. These clocks interrupted a background program that serviced the displays and display controller.

Interrupts. Figure XI-6 is a flow diagram of the interrupt structure which can be thought of as overlaying the background program that was continually running in an endless loop. The flow from top to bottom is suggestive of the interrupt priority structure developed for this system. The reset interrupt was used to bring the system up and make it responsive to user commands through a special software support package *MONITOR* supplied by INTEL. The next interrupt to be recognized was that of commanding the receiver simulator to produce corrupt data and/or bad data flags. Following this interrupt was the DME or range transmitter update interrupt, and finally the real-time clock interrupt to service the azimuth and elevation stagger counters that in turn commanded the pseudo-random angle data transmissions. The end point of servicing any interrupt was to check for other interrupts to be served, and if none, to "return" to the background program at the point of original interrupt.

Initialization. Figure XI-7 is a state diagram illustrating the method of initializing the simulator operation upon first turn-on, and subsequent initialization for various test conditions. Upon power-up the microprocessor reset interrupt vector was entered into memory via the microprocessor front panel switch (Figure XI-1). The reset interrupt caused the microprocessor to enter the INTEL *MONITOR* operating system that serviced the teletype (TTY). Access to application programs MLSIZ, BDON, FLGON, and FLNBD was through the indicated *MONITOR* commands "GO address (carriage return)" entered via the TTY. Return to the *MONITOR* from any application package was via the RESET interrupt.

Background Program. Figure XI-8 is a high level flow diagram of the Background program. The Background program could be entered by one of four entry points. Each of the entry points initialized the RAM to allow certain simulation sequences to be activated under command of interrupt number 5. There were, in effect, four application programs. The first was MLSIZ. MLSIZ (Microwave Landing System Initialize) was a normal simulation operation where all flags and data were constantly good. BDON (Bad Data On) activated the program-controlled insertion of bad data with all flags still showing

Stagger Counter Program. A flow diagram of the Stagger Counter Program is shown in Figure XI-9. This routine was entered every time a real-time interrupt was generated (300 microseconds). When the various counter states reached zero the appropriate service routine was called. At no time through the routine would more than one call be executed because there was a set time relationship between the Azimuth (AZ), Elevation-1 (EL-1), and Elevation-2 (EL-2) transmissions. This routine established the stagger timing for transmitting the Azimuth and Elevation signals.

Angle Service Routines. The Azimuth service routine shown in Figure XI-10 was called by the Stagger Counter Program. This routine updated the Azimuth Stagger Counter with a new count taken from a table stored in PROM. The process continued by enabling the appropriate channel of the analog input multiplexer and commanding the A-to-D converter to digitize the coarse azimuth data. This data was examined to discern in which of four 15-degree segments the information was located. Once the proper segment was determined then that segment's analog data was input for scaling and formatting. The segmentation of the azimuth data was required because of the need for greater information accuracy than could be derived from the coarse azimuth data. The elevation service routines (EL-1 and EL-2) are structured in the same way as the Azimuth service routine described above with the exception that the 15-degree segmentation was not required.

DME Service Routine. The DME service routine shown in Figure XI-11 was entered via an interrupt generated at the end of every range data transmission. This routine got the new DME data, scaled and formatted the data, checked for a bad data and flag generation request, and then subsequently sent the data to the range transmitter. This routine also generated the flags for the angle data if so requested.

Requests for bad data and flags were generated under control of a pseudo-random counter subroutine that created the value of two table-pointers. One pointer pointed to a table of predetermined numbers used to set a counter controlling the number of continuous bad data or flag generation requests, while the other pointed to a table containing codes for selecting the various combinations of bad data and flags to be generated.

CONCLUSION

The TRSB-MLS Receiver Simulator was successfully installed into the "Hot Bench" simulation facility as scheduled and performed its functions well.

that the data was good. FLGON (Flags On) activated the program-controlled operation of bad data flags, and FLNBD (Flag and Bad Data) activated both the BDON and FLGON programs.

After the appropriate RAM initialization had been selected by the operator and was completed (Figure XI-8), the display switches were interrogated and checked for an "all-ones" condition. This allowed the operator the option of selecting normal background operation upon first pass through the program. The normal operation was to service the displays as a function of switch selection as shown in Table XI-2. The diagnostic option allowed the user to display each of the 256_{10} RAM locations under control of the display switches. This allowed the user to observe the dynamic operation of the application program, such as counters counting and intermediate changes of data. This latter function was extremely useful during program debug and operation evaluation.

TABLE XI-2. - DISPLAY SELECTIONS

Switch Number								Selected Display
7	6	5	4	3	2	1	0	
0	0	0	0	0	0	0	0	Test all displays by displaying "ICAO"
0	0	0	0	0	0	0	1	AZ receiver data in engineering units
0	0	0	0	0	0	1	0	EL-1 receiver data in engineering units
0	0	0	0	0	1	0	0	Range receiver data in engineering units
0	0	0	0	1	0	0	0	AZ, EL-1 and range receiver data, engr. units
0	0	0	1	0	0	0	0	Digitized AZ fine input data
0	0	1	0	0	0	0	0	Digitized EL-1 input data
0	1	0	0	0	0	0	0	Digitized range input data
1	0	0	0	0	0	0	0	EL-2 receiver data in engineering units
1	0	0	0	0	0	0	1	AZ binary output data
1	0	0	0	0	0	1	0	EL-1 binary output data
1	0	0	0	0	1	0	0	Range binary output data

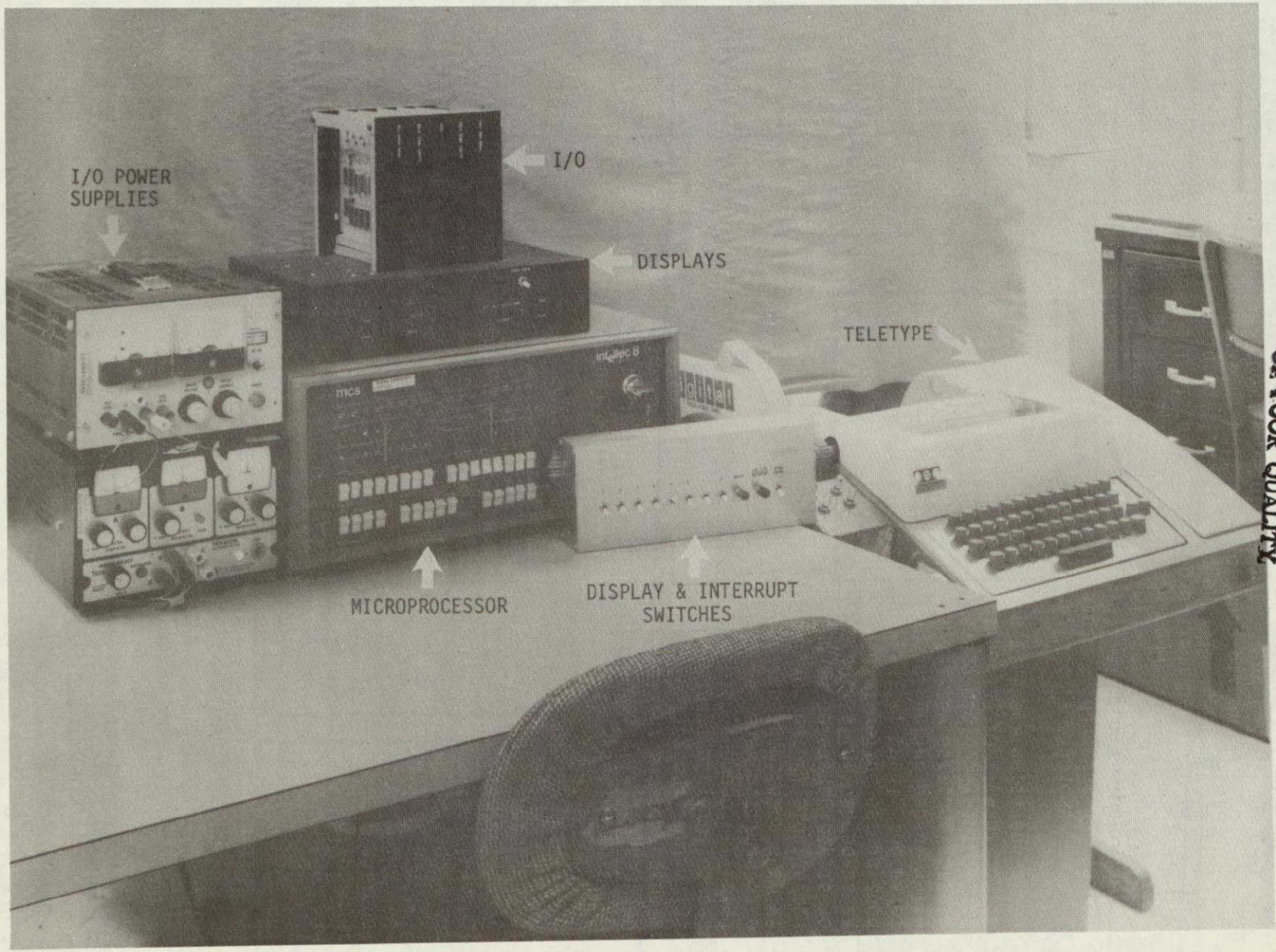

FIGURE XI-1 TRSB-MLS RECEIVER SIMULATOR SYSTEM

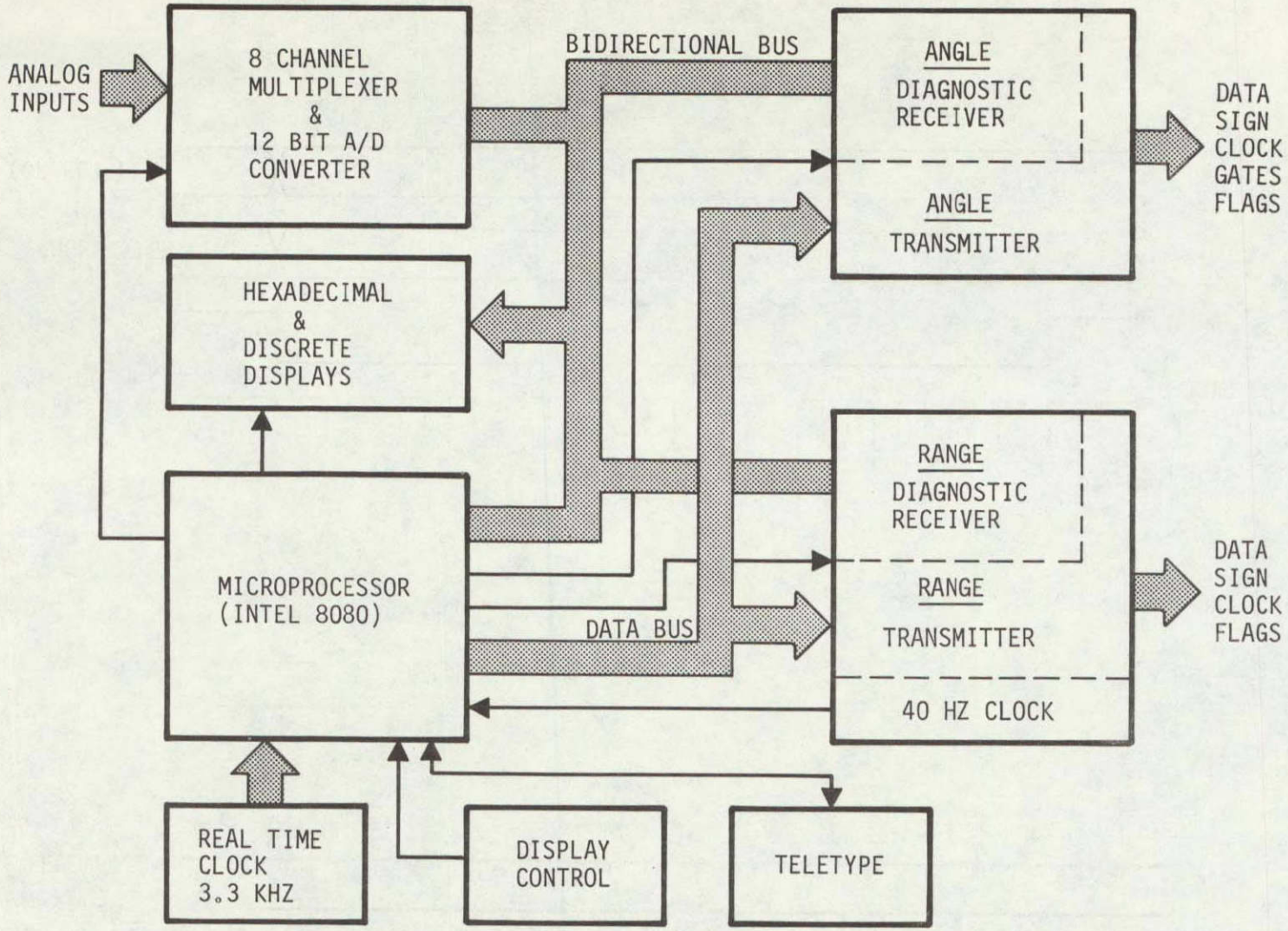

FIGURE XI-2 TRSB-MLS RECEIVER SIMULATOR BLOCK DIAGRAM

a. AZIMUTH & ELEVATION SIGNAL OUTPUT TIMING RELATIONSHIPS SHOWING 'STAGGER'

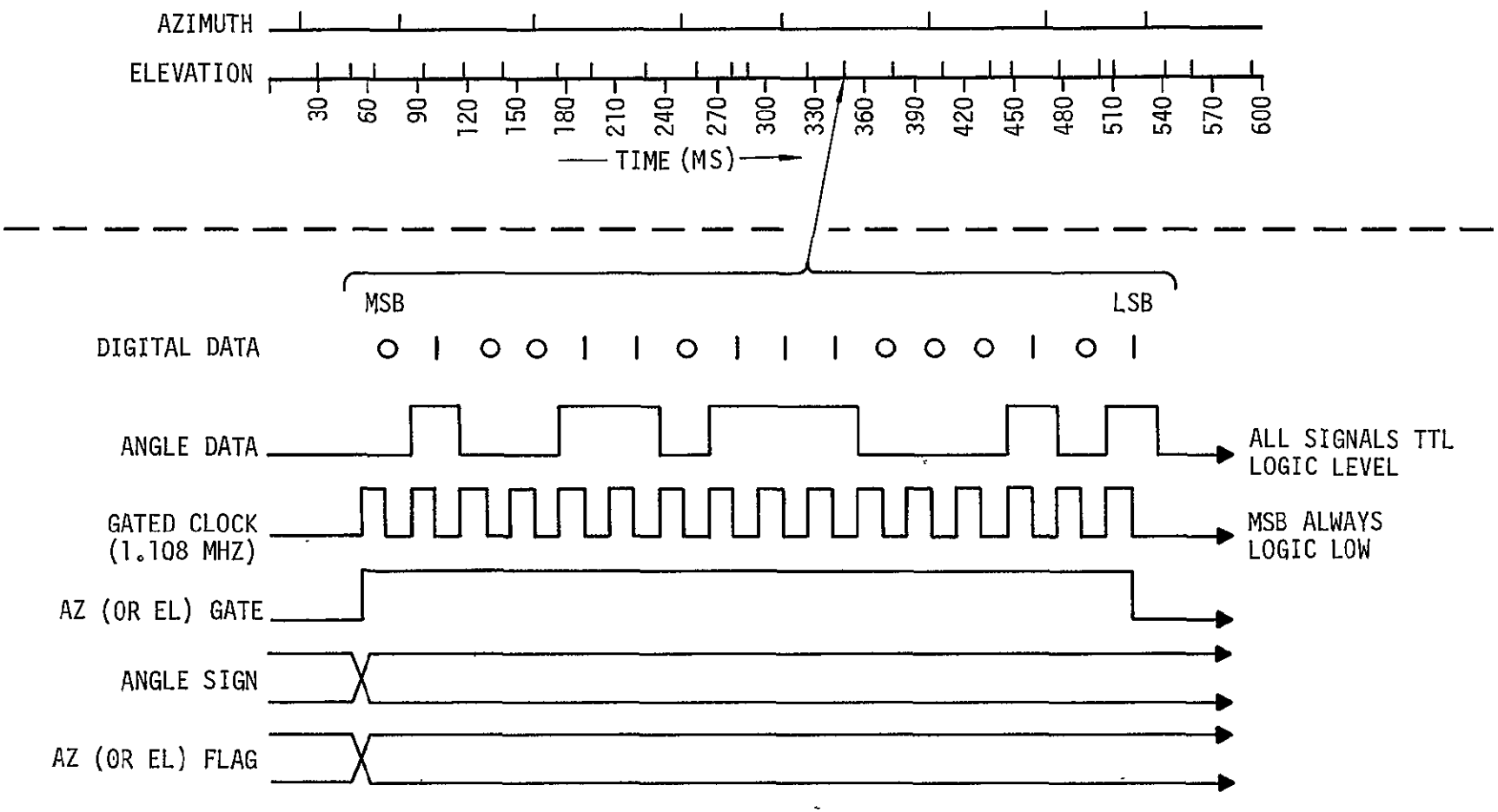

FIGURE XI-3 AZIMUTH (OR ELEVATION) SIGNAL LEVEL AND TIMING

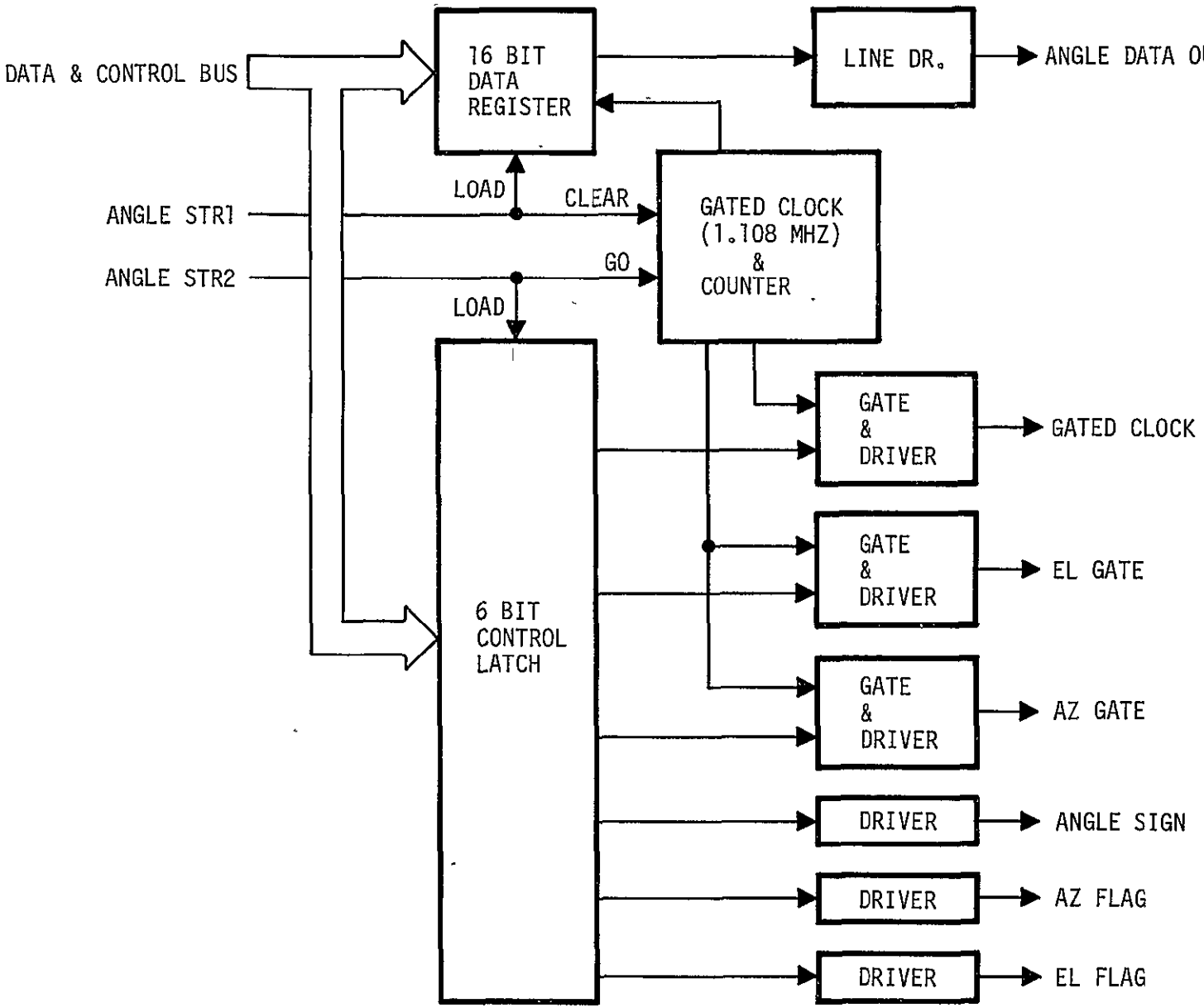

FIGURE XI-4 ANGLE DATA OUTPUT INTERFACE BLOCK DIAGRAM

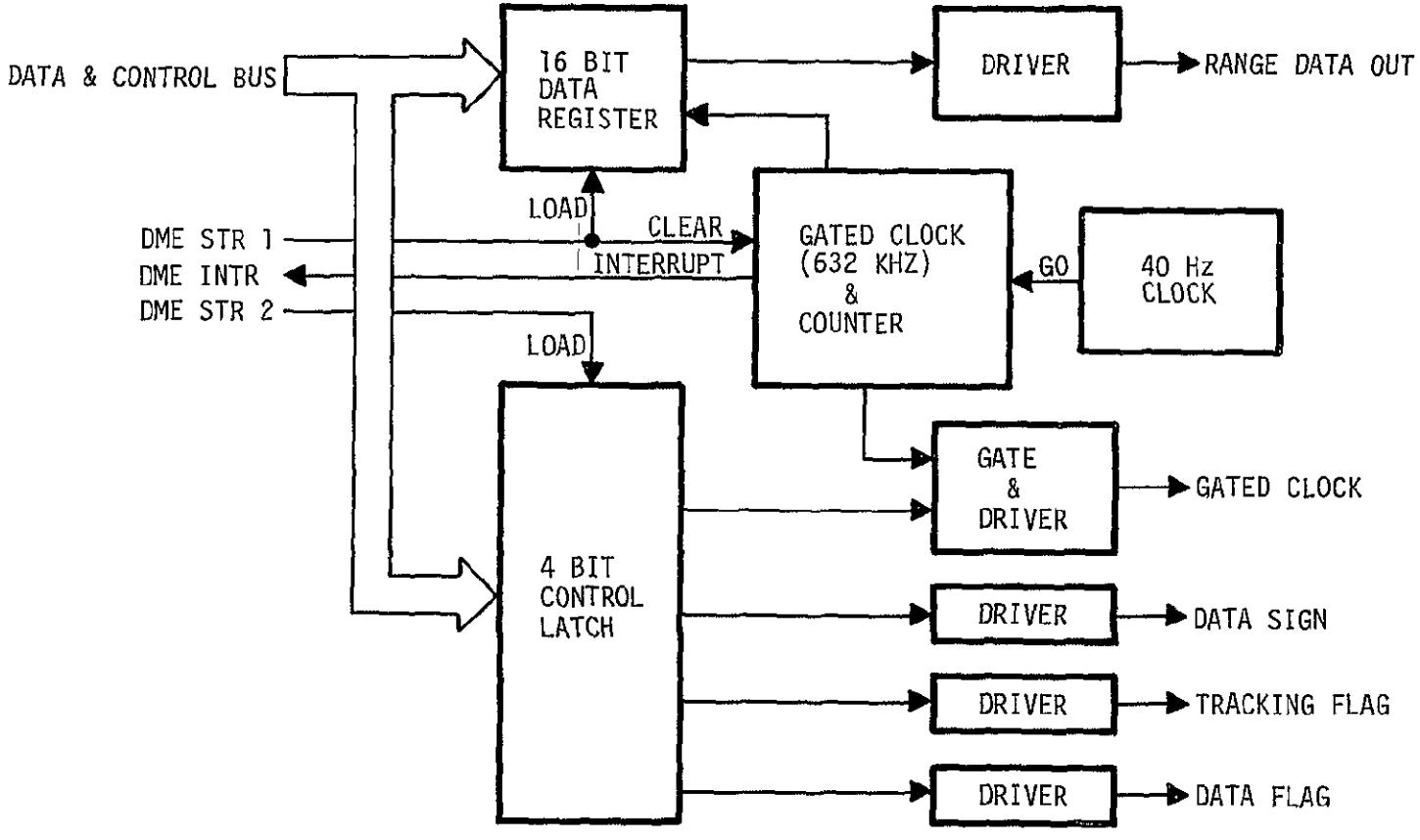

FIGURE XI-5 RANGE DATA OUTPUT INTERFACE BLOCK DIAGRAM

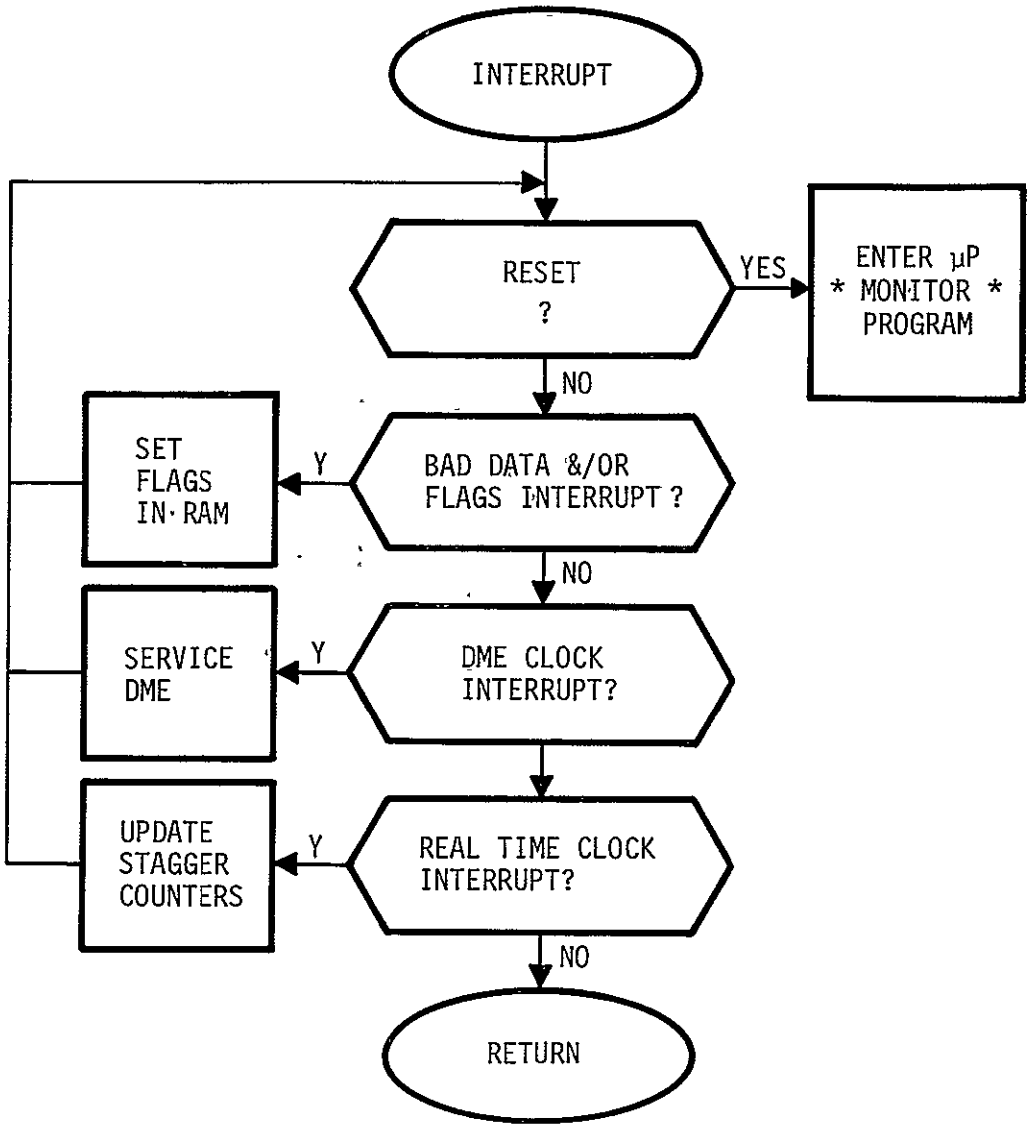

FIGURE XI-6 INTERRUPT STRUCTURE

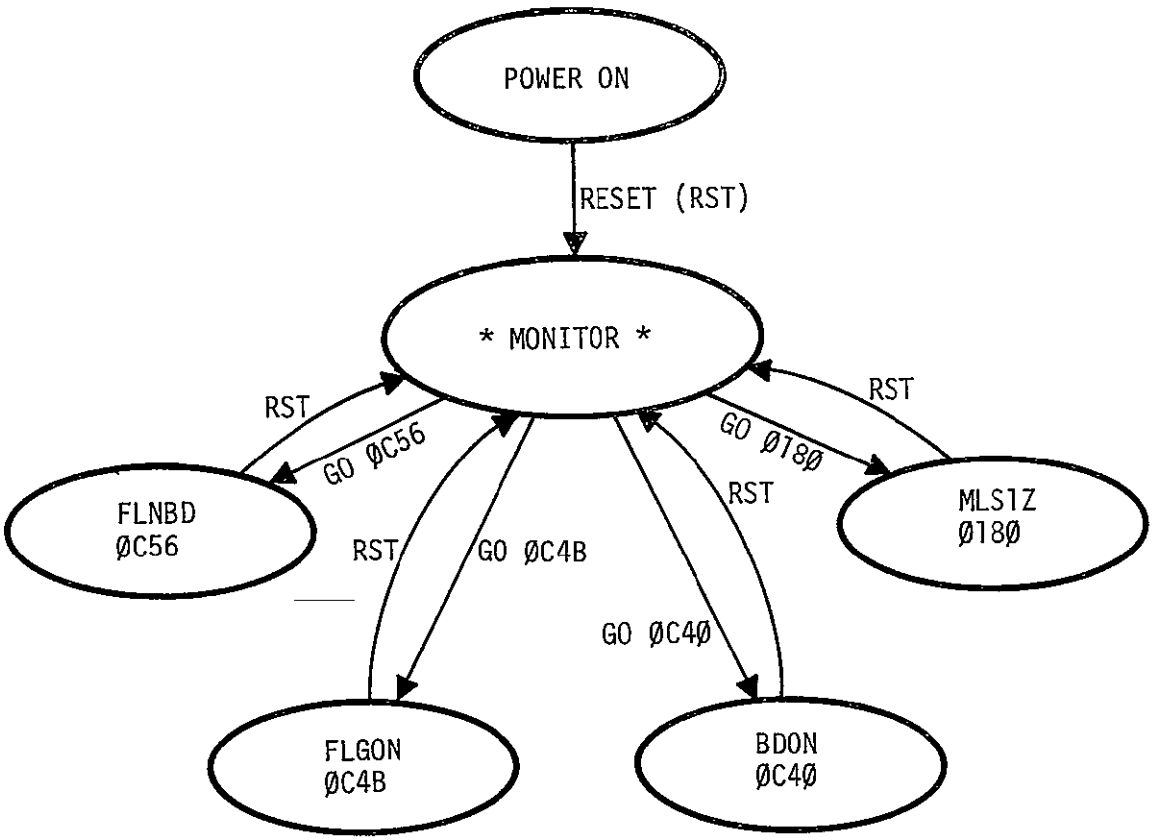

MLSIZ = MLS INITIALIZE AND NORMAL OPERATION
BDON = BAD DATA ON
FLGON = FLAGS ON
FLNBD = FLAG AND BAD DATA ON

FIGURE XI-7 POWER UP SEQUENCE

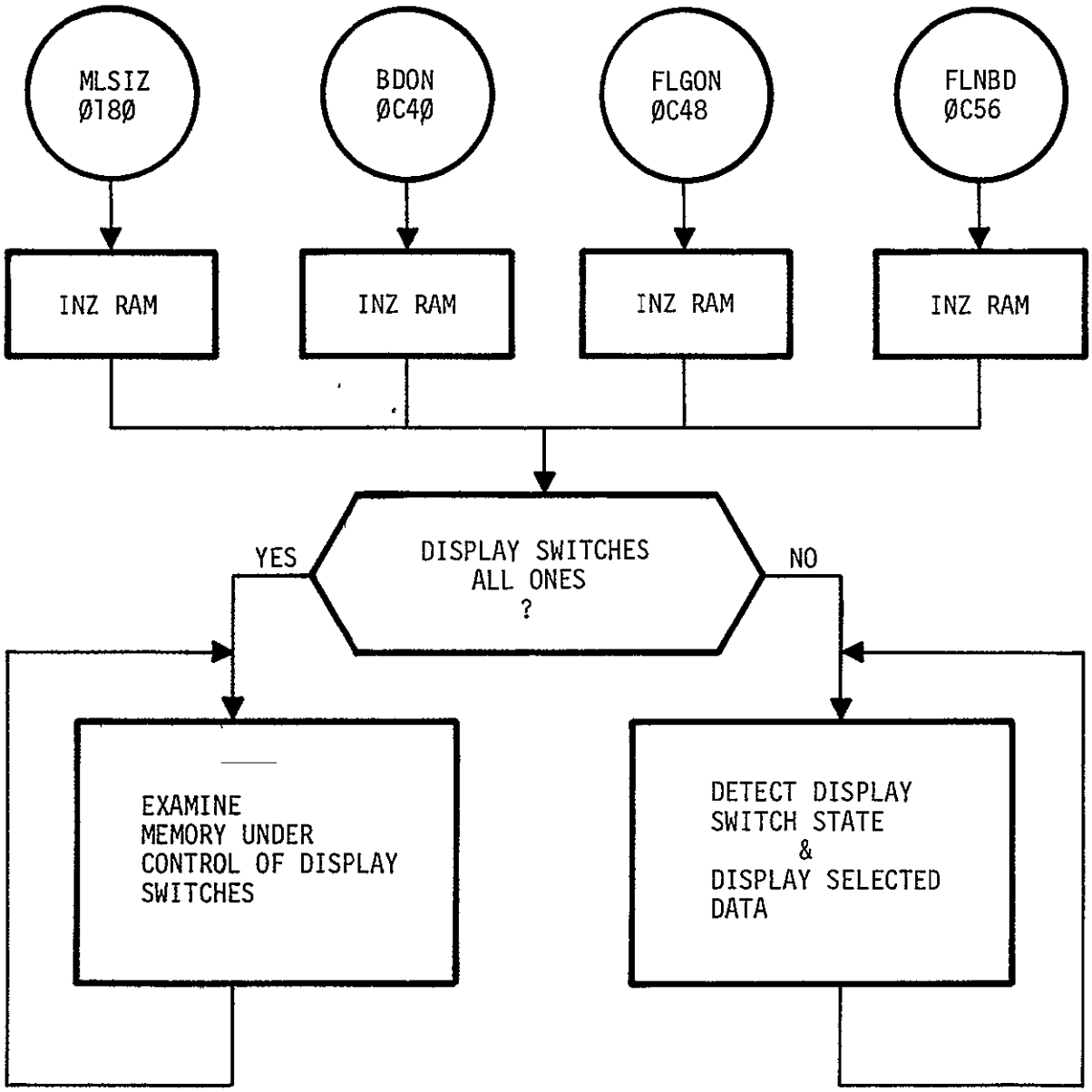

FIGURE XI-8 BACKGROUND PROGRAM

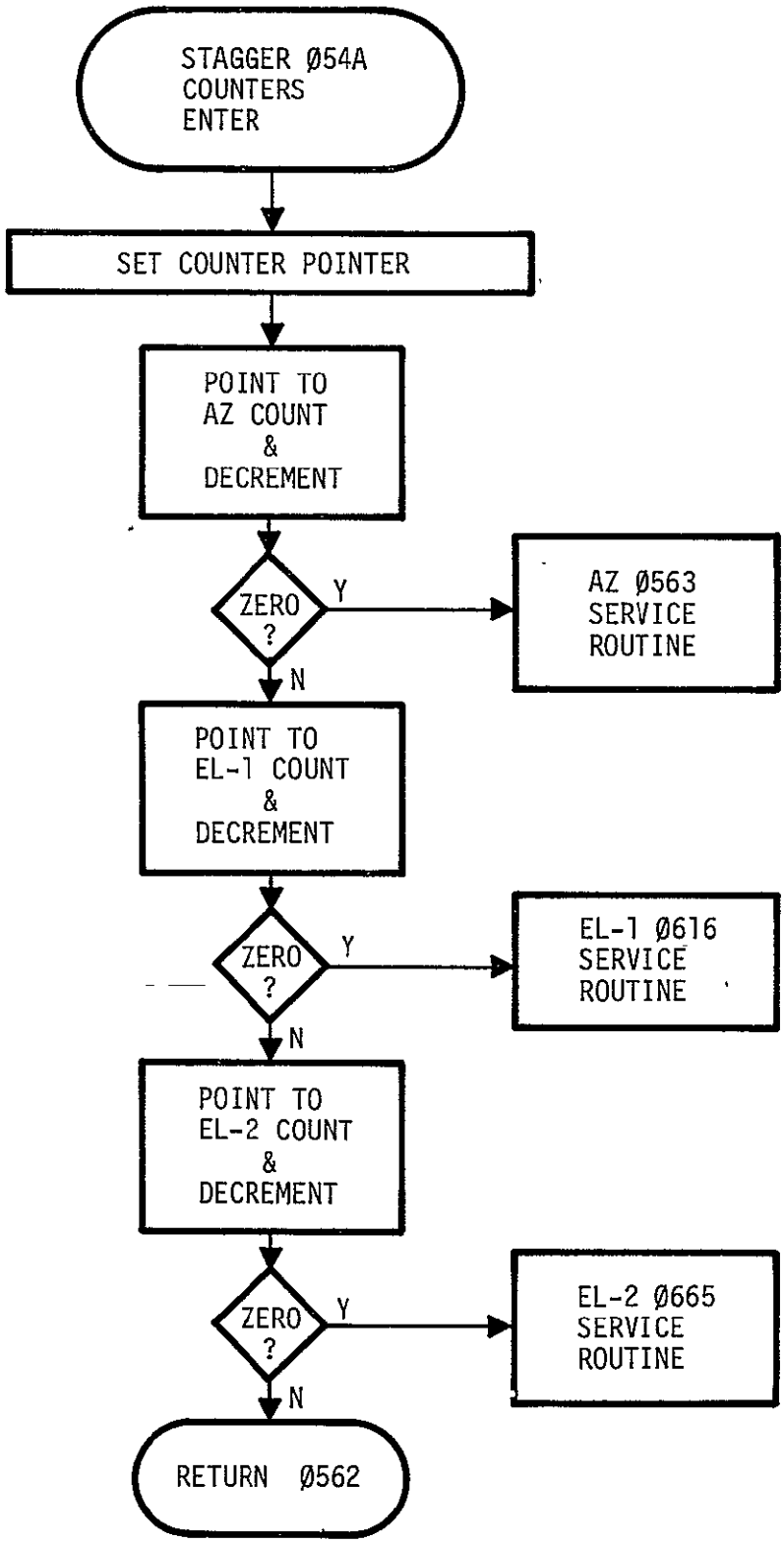

FIGURE XI-9 STAGGER COUNTER PROGRAM

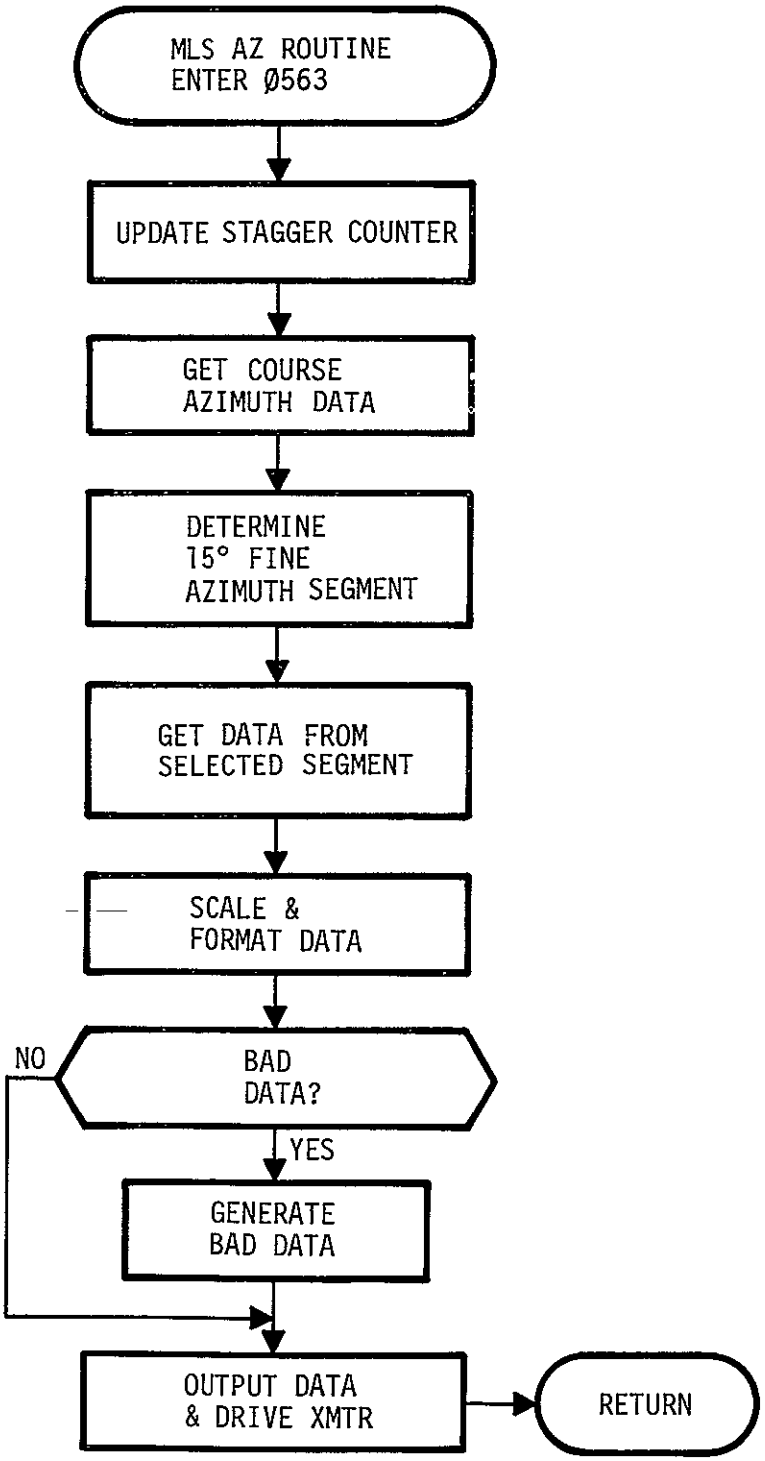

FIGURE XI-10 AZIMUTH SERVICE ROUTINE

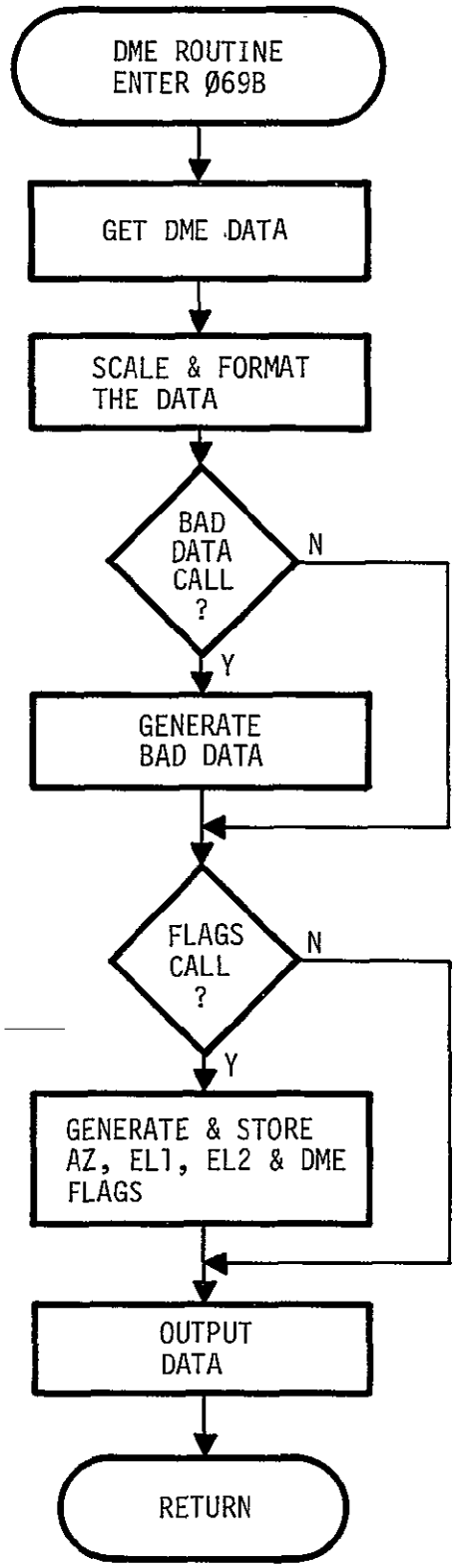

FIGURE XI-11 DME SERVICE ROUTINE

XII. FLIGHT SYSTEM LABORATORY SIMULATION AND TESTS

By Nicholas D. Murray

INTRODUCTION

The ICAO Demonstration flight system had numerous new equipments, new computer software and re-assembled software with modifications. In order to minimize inflight time devoted to the purpose of flight system check-out and performance adjustments, a "hot bench" simulation facility was utilized. The hotbench provided a controlled and repeatable simulated flight environment for (1) system integration, (2) interface check, calibration and test, (3) subsystem check and test and (4) system performance test. The hotbench configuration is illustrated in Figure XII-1 with the flight system equipment distinguished by heavy lines. The flight equipment not actually tested in the hotbench was the TRSB/MLS Receiver and the data instrumentation system.

DESCRIPTION OF SIMULATION

The analog computer simulation contained the (1) aircraft body referenced motions, (2) aircraft earth referenced motions, (3) aircraft autopilot functions, (4) aircraft control surface dynamics, (5) TRSB/MLS receiver signals with runway location reference and (6) aircraft sensor functions such as inertial reference, accelerometers, rate gyros and air data. These functions were provided from the analog computer in analog signal form with proper scaling. The encoder/calibrator (figure XII-2) was a specially designed and constructed equipment which accepted the analog signal data and provided calibrated data in analog, ARINC 561 and synchro formats for interfacing with the flight system. The TRSB/MLS receiver simulator (XII-3) received azimuth, elevation and slant range in analog form and provided this information plus data flags in digital format to the pre-processor. In addition, it simulated the effects on the digital format of MLS signal/receiver disturbance anomalies expected in actual MLS demonstration flights.

The flight system consisted of the pre-processor, flight control computer subsystem, navigation computer subsytem and display computer subsystem. The pre-processor accepted data from the TRSB receiver simulator and the encoder/calibrator, and provided filtered/estimated data to the flight control, navigation and display subsystems. The pre-processor consisted of new equipment and software added to the existing B-737 experimental systems and required the most extensive check-out and testing on the hotbench. The navigation subsytem accepted data from the pre-processor and the encoder/calibrator, and generated deviation from a pre-programmed flight profile from which guidance commands were computed for the flight control system. The navigation subsystem had an added I/O port, software modifica-

tions and re-assembled programs, all of which required check-out and performance tests on the hotbench. The flight control subsystem accepted guidance commands from the navigation subsystem and data from the encoder/calibrator, and generated flight control commands to the autopilot contained within the analog computer simulation. The flight control subsystem was essentially unchanged except for software modifications which required a re-assembled program and then check-out and performance tests on the hotbench. The display subsystem provided a flight profile track display and an attitude display with runway perspective. The display subsytem was unchanged for the MLS demonstration.

SYSTEM TESTS

A significant part of the hotbench effort was devoted to the checking and testing of interfaces to the flight system and between subsytems. This effort consisted of checking for proper scaling, calibrating each signal interface, checking for specified format and testing subsystem functional compatibility. Figure XII-4 illustrates the complexity of the flight system interfaces. Additional interface checking and testing were required for the analog computer simulation, the encoder/calibrator and the TRSB/MLS Receiver simulator.

The hotbench performance tests were conducted with the same pre-programmed flight profiles anticipated for the MLS Demonstration (figure XII-5). This consisted of two test profiles with each profile tested with pre-processor option 3 and option 4 programs. In addition, a special test profile 3 was designed during hotbench testing for diagnostic purposes. Use of TP 3 allowed the elimination of the navigation and display subsystems, and subsequent easier trouble shooting.

Table XII-1 is a listing of the performance test conditions conducted on the hotbench. The initial tests under test profile 1 with open loop control were conducted to facilitate system integration. Succeeding tests with closed loop control were for performance evaluation with most testing conducted under test profile 2. Flight system mode variation tests were conducted with test profile 2 and pre-processor program options 3 and 4. The system mode variations tested with each pre-processor program were listed in Table XII-2 and consisted of using filtered/estimated data from the pre-processor as inputs to the indicated control laws in lieu of analog simulation data inputs. These input changes to the flight control and navigation subsystems resulted in little or no change in system performance for the hotbench tests and succeeding tests were conducted in mode 1.

TABLE XII-1. - PERFORMANCE TESTS

TEST PROFILE	PRE-PROCESSOR PROGRAM	CONTROL LOOP	MODE	TRSB/MLS RECEIVER SIMULATOR
TP1	OPT3	OPEN	1	No Disturbances
TP1	OPT4	OPEN	1	"
TP1	OPT3	CLOSED	1	"
TP1	OPT4	CLOSED	1	"
TP2	OPT3	CLOSED	1-4	"
TP2	OPT4	CLOSED	1-4	"
TP2	OPT3	CLOSED	1	Blunder Point
TP2	OPT4	CLOSED	1	
TP2	OPT3	CLOSED	1	Data Drop Out
TP2	OPT4	CLOSED	1	
TP2	OPT3	CLOSED	1	Combined Blunder Point and Data Drop Out
TP2	OPT4	CLOSED	1	

RESULTS & DISCUSSION

Table XII-3 is a summary of the flight system experience under hotbench testing. The only major hardware correction required was to the added I/O port of navigation computer. The pre-processor required program and parameter adjustments for performance and for compatibility with other flight subsystems. The majority of the adjustments were required for the proper operation of the error windows, error counters and error flag logic, particularly in response to testing with the TRSB/MLS receiver disturbance. Software corrections for the navigation computer were:

(1) change in the way the SINE function was computed and (2) correction of response to error flags from the pre-processor. The flight control computer required opening the glide slope acceptance window.

The flight system performed acceptably under the hotbench tests after the previously noted corrections and adjustments. Good correlation was observed between the hotbench performance and the flight performance of the system.

TABLE XII-2. - SYSTEM MODES

MODE	GLIDE SLOPE LAW	FLIGHT CONTROL FLARE LAW	NAVIGATION VERTICAL PATH COMMAND LAW
1	$\dot{h}_{acs}$ $\dot{y}_{acs}$ $\ddot{h}_{acs}$	h_{acs} $\dot{h}_{acs}$ $\ddot{h}_{acs}$	$\dddot{h}_{acs}$
2	$\dot{h}_{acs} \Rightarrow \dot{h}_{pp}$ $\dot{y}_{acs} \Rightarrow \dot{y}_{pp}$		
3		$h_{acs} \Rightarrow h_{pp}$ $\dot{h}_{acs} \Rightarrow \dot{h}_{pp}$	
4	$\ddot{h}_{acs} \Rightarrow \ddot{h}_{pp}$	$\ddot{h}_{acs} \Rightarrow \ddot{h}_{pp}$	$\ddot{h}_{acs} \Rightarrow \ddot{h}_{acs}$
acs - Analog Computer Simulation pp - Pre-processor			

TABLE XII-3. - FLIGHT SYSTEM EXPERIENCE SUMMARY

HARDWARE o NAVIGATION COMPUTER

- NEW I/O PORT

SOFTWARE o PRE-PROCESSOR

- NEW PROGRAM
- PROGRAM CHANGES
- EXTENSIVE PARAMETER ADJUSTMENTS

o NAVIGATION COMPUTER

- SINE FUNCTION

TABLE XII-3. - FLIGHT SYSTEM EXPERIENCE SUMMARY, (cont.)

	-	ERROR FLAG ROUTINE
	o	FLIGHT CONTROL COMPUTER
	-	GLIDESLOPE WINDOW
SYSTEM	o	HOTBENCH PERFORMANCE ACCEPTABLE
	o	GOOD CORRELATION BETWEEN HOTBENCH PERFORMANCE AND FLIGHT PERFORMANCE

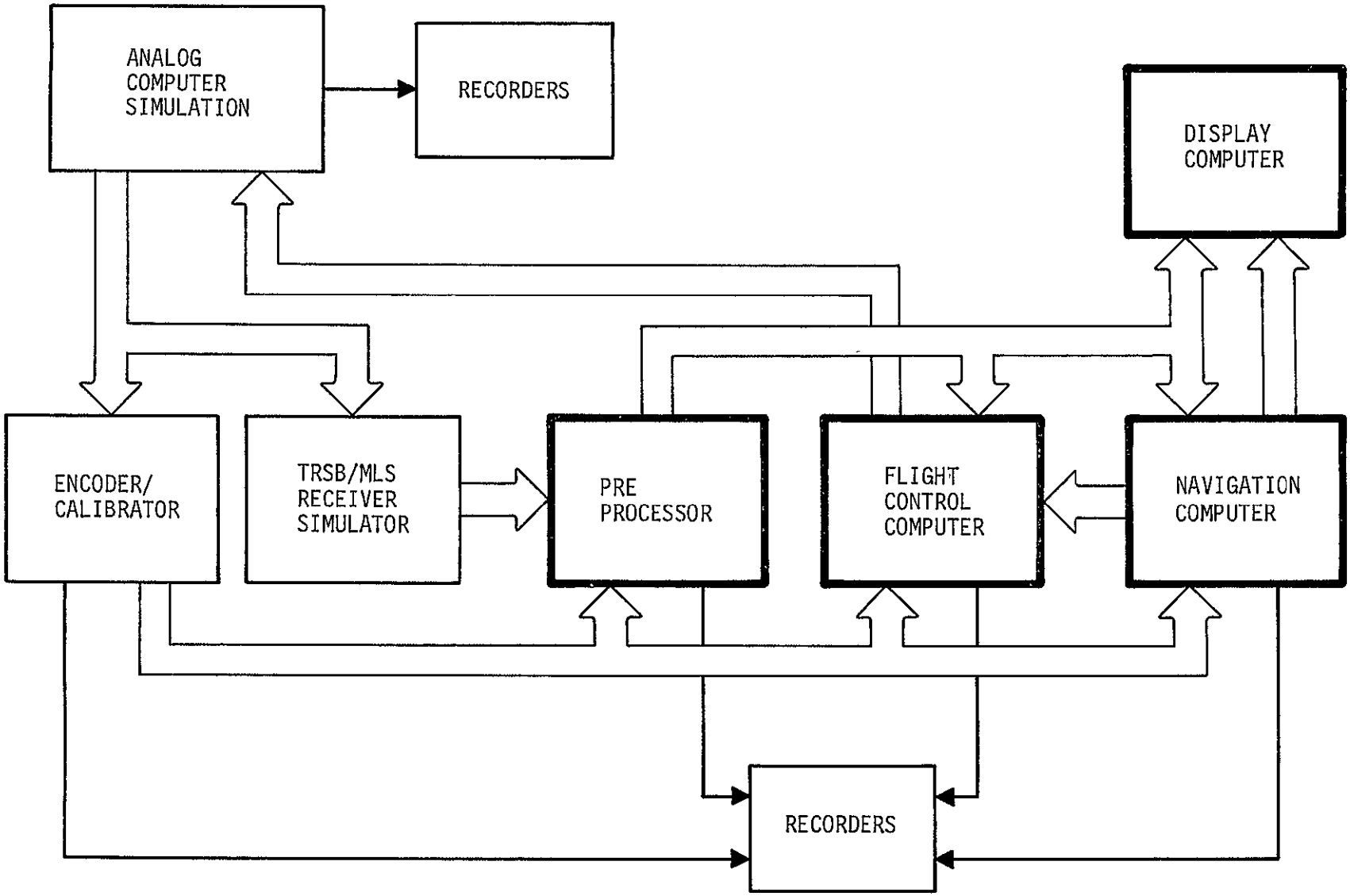

FIGURE XII-1 SIMPLIFIED DIAGRAM OF HOTBENCH

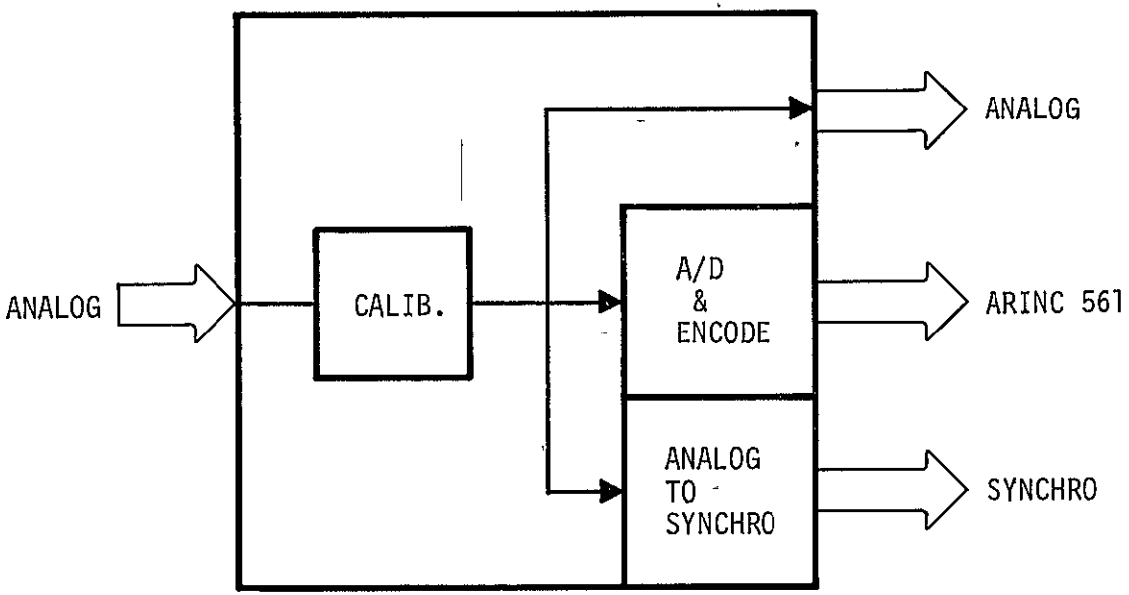

FIGURE XII-2 ENCODER/CALIBRATOR

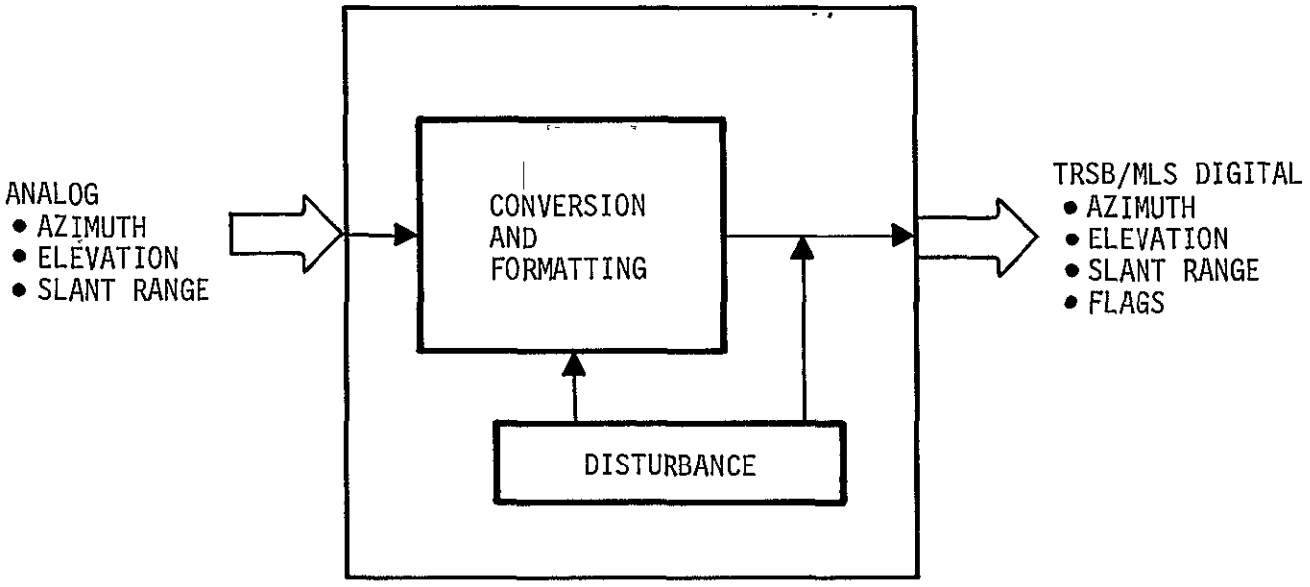

DISTURBANCE - BLUNDER POINTS (RANDOM BAD DATA, GOOD FLAGS)
- DATA DROPOUT (RANDOM BAD FLAGS)

FIGURE XII-3 TRSB/MLS RECEIVER SIMULATOR

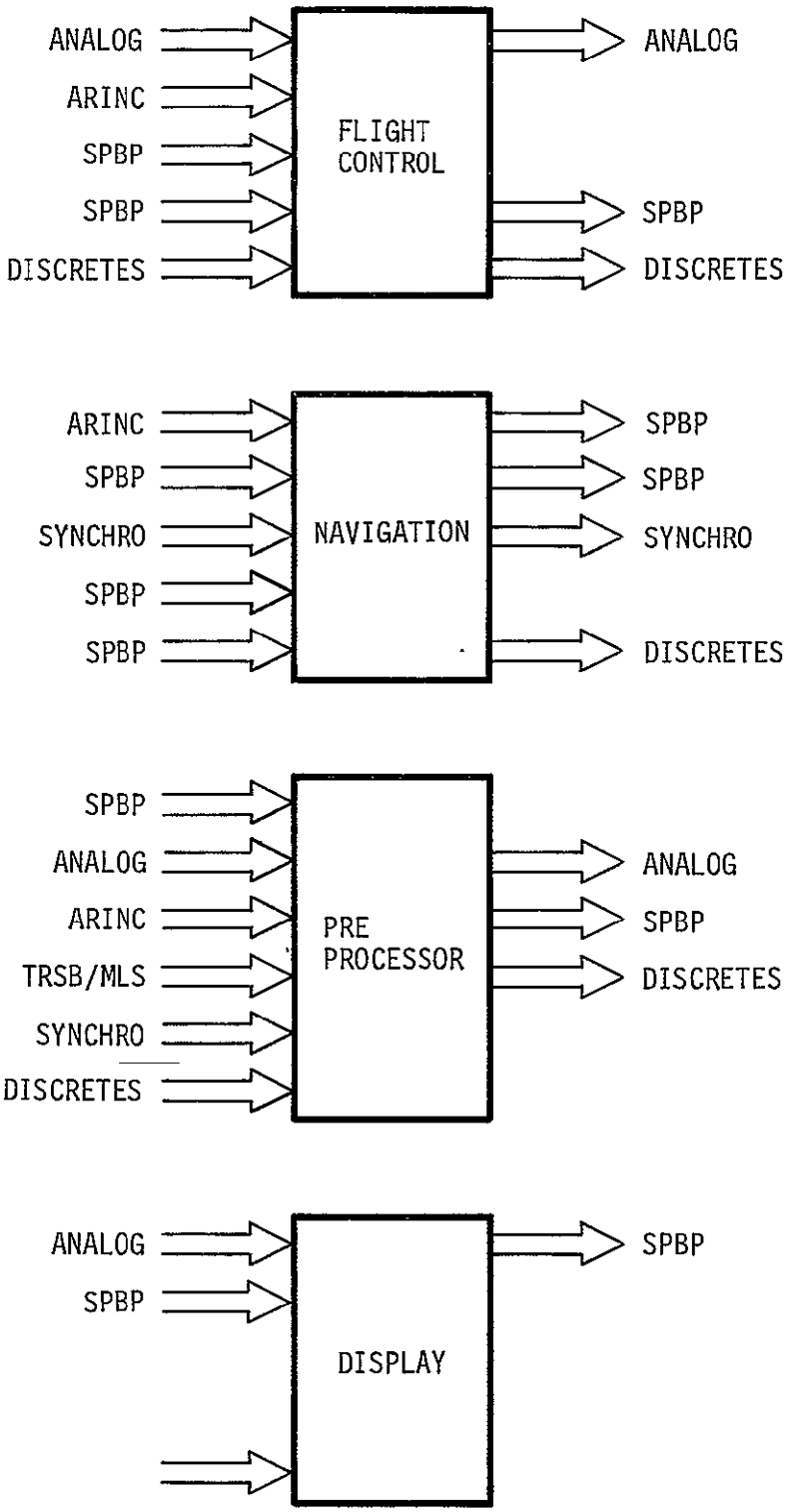

FIGURE XII-4 FLIGHT SUBSYSTEM INTERFACES

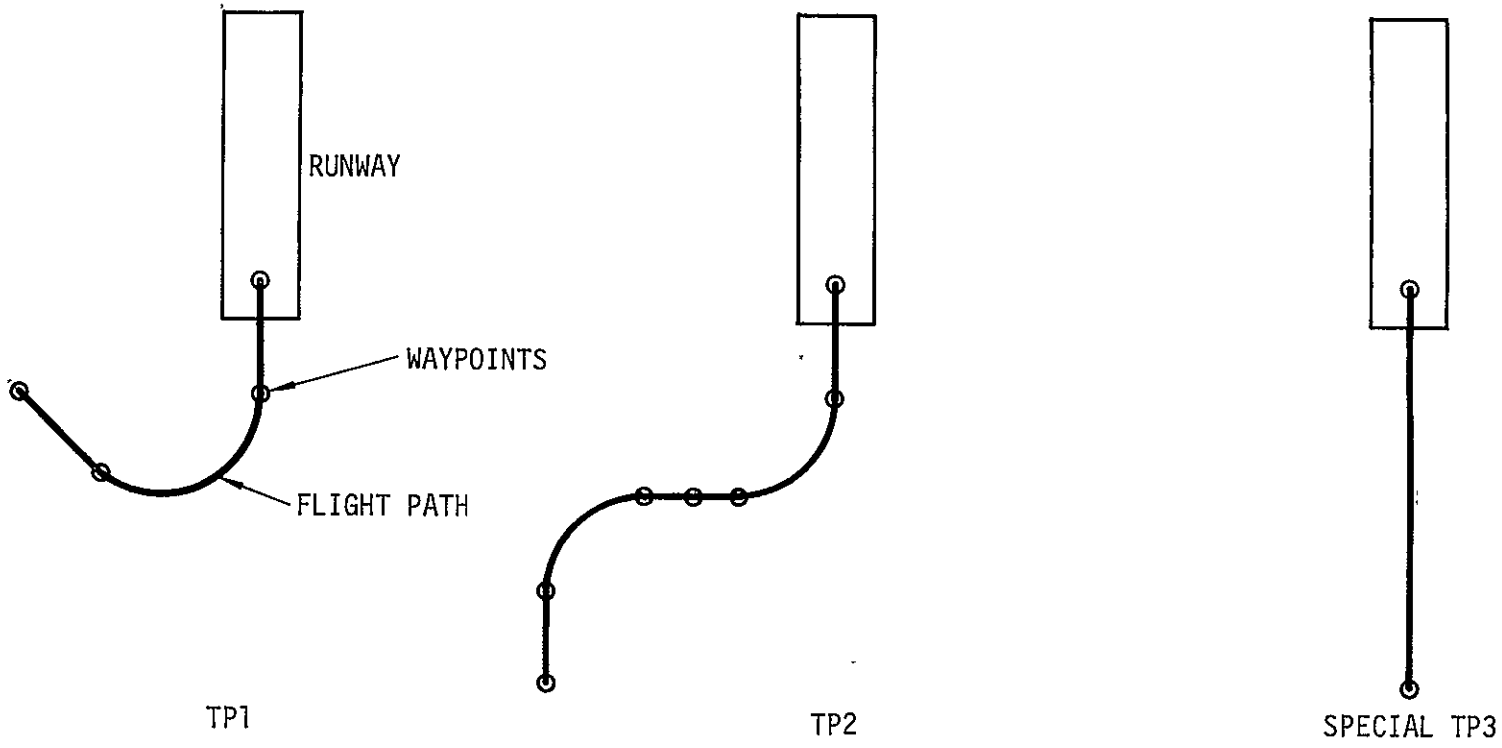

FIGURE XII-5 PERFORMANCE TEST PROFILES

XIII. SYSTEM DEVELOPMENT AND DEMONSTRATION FLIGHTS

By William F. White

SYSTEM DEVELOPMENT FLIGHTS

A chronological summary of flight testing leading up to the ICAO demonstration is given in Table XIII-1. Each flight number represents one day's flying, whether it was a single flight or several individual flights. Multiple flights are identified with alphabetical suffixes. Maintenance, ferry and other flights not directly related to the demonstration are not included. Unless otherwise specified, all flights took place at the NAFEC airport. Some preliminary antenna testing was done at Wallops Flight Center using a radar beacon, but the flights were primarily conducted for other purposes and are not listed here.

The initial (December) TRSB flight tests were conducted without the aircraft experimental avionics systems on board, since they were in the laboratory undergoing simulation testing. Guidance over the proposed ICAO demonstration flight paths was approximate, and was provided by a combination of visual ground references and radar vectoring. Development flights using the experimental avionics were delayed until late March due to TRSB ground system antenna modifications, which were not completed on schedule.

Once the TRSB-flight testing began in March the usual routine was a ferry flight to NAFEC each week, from two to four days of testing, and a return to Langley to analyze data and modify the system as required. The FAA-supplied TRSB equipment was installed upon the aircraft upon arrival at NAFEC and was removed before returning to Langley, due to the necessity for sharing equipment with other aircraft.

DEMONSTRATION FLIGHTS

Table XIII-2 gives a summary of flights during the demonstration period. For the ICAO observers, the normal schedule consisted of a short check flight each morning followed by two demonstration flights. During the second week, it was necessary to schedule three flights per day to accomodate all of the observers, and the check flights were discontinued.

TABLE XIII-1

SYSTEM DEVELOPMENT FLIGHTS

FLIGHT	DATE	OBJECTIVE	REMARKS
S082	12/17/75	Checkout of installed TRSB equipment	
S083	12/18/75	Coverage tests of C-band antennas	No computers aboard. Flew 4 candidate flight profiles using visual references
R088	2/19/76	Modified experimental systems c/o	Local area flight
R092	3/11/76	TRSB-modified software checkout	Local area flight
S095	3/23/76	Initial flight test using TRSB	Signal processing, displays, and RNAV coupled performance tested
S096	3/24/76	Coupled approaches including use of η, β in autoland control laws	First autolands achieved using INS accelerometers for filtering
S097	3/25/76	Same as S096	One radar altimeter patched out. Made autolands using both INS and body-mounted accelerometers.
S099	3/30/76	Repeat of S097A with corrected ICP gains, realigned and recalibrated body-mounted accelerometers	Autolands achieved using both INS and body-mounted accelerometers. Stopped when autopilot disengage button stuck.
S100	3/31/76	Obtain data base on options 3 and 4; try S turn approach; evaluate increased TRSB filter gains.	First full stop autoland and rollout achieved.
S101	4/1/76	Evaluate autoland system performance on ILS guidance	NCU problems required manual capture of localizer from forward flight deck.
S102	4/2/76	Repeat S101 with TRSB deviation signals from Bendix I.U. substituted for ILS.	Manually flown intercepts due to NCU problems.

TABLE XIII-1 continued

FLIGHT	DATE	OBJECTIVES	REMARKS
S103	4/13/76	Evaluate autoland performance with varied varied gains; K-band antenna test and taxi data	No $E1_2$ data obtained due to receiver problems
S104	4/14/76	Evaluate modified horizontal path gain scheduling; obtain data on the quality of navigation parameters from SKC-2000; lateral trim effects	Autothrottles not closing enough during flare. Lateral trim data obtained during ferry flight to Langley
S106	4/23/76	Evaluate modified horizontal guidance and delivery accuracy at final approach fix; lateral trim effects; obtain open loop $E1_2$ data; evaluate modified autoland control law and effect of SKC2000 gain; test telemetry system; get data on auto-throttle system; get data on autothrottle activity on glidepath.	First flight aborted due to NCU problems $E1_2$ receiver very weak during taxi tests and much of flight. Several AFD disconnects near touchdown due to loss of $E1_2$ data.
S107	4/24/76	Evaluate various NCU gains; get baseline data on ICAO flight profiles using best gains in all computers; evaluate $E1_2$ tracking; obtain open loop $E1_2$ flare data; evaluate autolands with manual throttle.	Still having $E1_2$ receiver problems starting early in flight. Apparently a heat problem.
R108	4/29/76	Check hardware spoiler feedback modification; obtain data on roll error gain change	
S108	4/29/76	Obtain open loop $E1_2$ flare data; $E1_1$ to $E1_2$ transition effects; baseline data on ICAO path performance using best gains	Overflow in ICP caused hardover pitchup at glidepath intercept. $E1_2$ altitude disagreed with radar altitude.

TABLE XIII-1 CONTINUED

FLIGHT	DATE	OBJECTIVES	REMARKS
S109	4/30/76	Compare $E1_2$ and radar altitude during flare; $E1_1$ to $E1_2$ transition at 900 feet; baseline data using best gain	ICP overflow problem again. Yaw damper failure cuased rolling and wallowing during approach and flare
S110	5/1/76	Compare $E1_2$ and radar flare performance evaluate overall performance using demonstration configuration and procedures	More pitch hardover problems; one flare engage at 500 feet altitude; lateral oscillations.
S111	5/2/76	Same as S110	Successfully accomplished $E1_2$ flares and landings
S114	5/7/76	Rehearsal of ICAO demonstration	Two 5-run flights completed.

TABLE XII-2 CONTINUED

DEMONSTRATION AND CHECKOUT FLIGHTS

FLIGHT	DATE	OBJECTIVES	REMARKS
S116B	5/11/76	Check flight after ferry trip to NAFEC	3 approaches; radar and $E1_2$ flares; S turn and 130°.
S117A	5/12/76	Check flight before demonstrative	1 each radar, $E1_2$ flare
S117B	5/12/76	ICAO Demonstration flight	$E1_2$ ground station inoperative, radar flares
S117C	5/12/76	ICAO Demonstration flight	$E1_2$ apparently repaired buy continued radar flares. One run aborted due to autopilot failure to couple
S118A	5/13/76	Check flight before demonstration	1 each radar, $E1_2$ flare
S118B	5/13/76	ICAO Demonstration flight	$E1_2$ flares
S118C	5/13/76	ICAO Demonstration flight	$E1_2$ flares
S121A	5/18/76	Check flight before demonstration	
S121B	5/18/76	Demonstration flight for media	Only 4 approaches required
S122A	5/19/76	Demonstration flight for industry and government officials	Quartering tailwinds gusting to 30 knots, turbulence
S122B	5/19/76	Same as S122A	Still high winds and turbulence
S122C	5/19/76	Same as S122A	Cancelled due high winds.
S123A	5/20/76	Same as S122A	Stopped after 3 approaches due passenger illness caused by turbulence.

TABLE XIII-2 CONTINUED

FLIGHT	DATE	OBJECTIVES	REMARKS
S123B	5/20/76	Demonstration flight for industry and government officials	Problems with El_2 ground station synchronization
S123C	5/20/76	Same as S123B	2 initial runs aborted. Synch problems caused shutdown of El_2. Demonstration completed using radar flares.

XIV. DATA ACQUISITION SYSTEM

By R. E. Campbell

INTRODUCTION

The data acquisition system (DAS) on the TCV B-737 is an airborne system operating in real time which acquires records and transmits signals representing parameters pertinent to a given test condition. The basis of the DAS is the Piloted Aircraft Data System (PADS), a system designed and fabricated by Langley Research Center. PADS combines onboard data recording with an L-Band telemetry down link for real time and/or safety-of-flight monitoring. For the TCV B-737 application, the PADS PCM encoder, which accepts only analog inputs, is supplemented by a digital data formatter to provide monitoring of the flight control computers. Moreover, the ARINC-561 output bus from the navigation computer unit is converted to Miller code and recorded, pilot display information is recorded on special video tape recorders, and an 8 channel oscillograph is installed to provide quick-look capability for selected flight control parameters.

Although the data recording capability outlined above is quite extensive, it was necessary to add the following capability to support the ICAO demonstration development. A parallel digital tape recorder was used to record MLS receiver outputs, an IRIG-B time-code generator was added for aircraft/MLS/tracker data time correlation, and three additional oscillographs were installed to provide extensive quick-look capability onboard the airplane. Finally, the L-Band telemetry link was modified to transmit, instead of the PADS PCM, the output of an FAA designed encoder containing MLS position data. This telemetry link was completed by utilizing the PADS ground based receiving system and by mounting antennas on a NAFEC phototheodolite tracker tower. The block diagram of the resulting DAS is shown in Figure XIV-1 and that of the telemetry link is shown in Figure XIV-2. This chapter contains a brief description of the major components of the DAS.

LIST OF ABBREVIATIONS

AFD	Aft Flight Deck
ARINC	Aeronautical Radio, Inc.
Bi-Ø	Bi-phase Encoding
CBW	Constant Bandwidth
CIU	Computer Interface Unit

LIST OF ABBREVIATIONS (Cont.)

DAS	Data Acquisition System
DM	Delayed Miller
DME	Distance Equipment
EADI	Electronic Attitude Director Indicator
EMI	Electro-magnetic Interference
FCC	Flight Control Computer
FFD	Forward Flight Deck
FM	Frequency Modulation
ICP	Incremental Computer Processor
ILS	Instrument Landing System
INS	Inertial Navigation System
IRIG	Inter-Range Instrumentation Group
Kbps	Thousand Bits Per Second
MFD	Multi-Function Display
MHz	Million Cycles Per Second
MLS	Microwave Landing System
NCDU	Navigation Control Display Unit
NCU	Navigation Computer Unit
NRZ	Non-Return to Zero
PADS	Piloted Aircraft Data System
PCM	Pulse Code Modulation
PCU	Pneumatic Control Unit
PROM	Programable Read Only Memory
sps	Samples Per Second
VCO	Voltage Controlled Oscillator
VOR	VFH Omni Range

EQUIPMENT DESCRIPTION

Piloted Aircraft Data System. PADS is a functionally flexible, physically modular data system designed and fabricated by the Langley Research Center to support a wide variety of data acquisition tasks on aircraft ranging in size and configuration from light, general aviation aircraft to large, commercial transports and helicopters. It is designed to provide quick access for ease of repair and is electrically compatible with all aircraft power systems. Its performance features include the following:

* 8 to 104 PCM channels; high (+5V) or low (±10MV) level analog inputs:
  9 bits resolution; data to 10 Hz; ±0.5% accuracy.

* Up to 40 high frequency channels (constant bandwidth FM); data to 400 Hz; high and low level inputs; 5% accuracy.

* L-Band telemetry; range up to 50 nautical miles.

* Time correlation of onboard measurements and ground station; Time in each PCM frame with 1 millisecond resolution.

* Voice and events channels for annotation of records.

* Built-in-checkout and calibration circuitry.

The PCM encoder is configured to accept and digitize 104 analog signals at a 40 sample per second rate. This provides a 5 Hz data frequency response for paramaters that originate in the navigation and guidance pallet, the flight control interface pallet and in several dedicated instrumentation transducers located throughout the airplane. A patch panel is provided on the DAS pallet so that the desired parameters for a given test may be selected. Table XIV-1 contains the list of parameters recorded for the ICAO-MLS development and the appendix describes the environmental qualifications of the PADS subsystems.

Signal Conditioning. Once selected, the signals are routed to the signal conditioning subsystem. This subsystem is the interface between the sensors, the power subsystem, the PCM, and the Calibrate Control Assembly. In addition, it modifies or conditions the outputs of the sensors, or other signal sources to conform to the input standards of the encoding equipment. The types of signal conditioning available in the subsystem include amplification or attenuation; impedance matching and buffering; biasing; filtering; and bridge circuit completion, sensivitity, and balance controls.

TABLE XIV-1. - PADS PCM PARAMETER LIST

CHANNEL	FUNCTION	ABBREVIATION	UNITS
7	Airspeed-Calibrated (CADC 3)	CAS 3	Knots
8	Angle of Attack - Cruise Calibration	ALPHA CR	Degrees
9	Angle of Attack - Approach Calibration	ALPHA AP	Degrees
10	Angle of Sideslip	BETA	Degrees
11	Spare		
12	Spare		
13	Heading-True (NCU)	HDGTRU	Degrees
14	Pitch Rate 1	PTCH RTE 1	Deg/Sec
15	Roll Rate 1	ROLL RTE 1	Deg/Sec
16	Yaw Rate	YAW RATE	Deg/Sec
17	CG Normal Acceleration	NORM ACC	Ft/Sec/Sec
18	CG Lateral Acceleration	LAT ACC	Ft/Sec/Sec
19	CG Longitudinal Acceleration	LONG ACC	Ft/Sec/Sec
20	Elevator PCU A	ELEV PCU A	Degrees
21	Aileron PCU B	AIL PCU B	Inches
22	Rudder Position (Servo)	RUD S/V 1	Degrees
23	Flap Position (TE)	T-E FLAP	Degrees
24	Throttle Handle Position 1 (FFD)	F TH HDL 1	Degrees
25	Column Force Sum 1	COL FRC S 1	Pounds
26	Wheel Force Sum 1	WHL FRC S 1	Pounds
27	Flap Handle Position (FFD)	F FLAP HDL	Degrees
28	Total Air Temperature	T.A.T.	Degrees C
29	Spare		
30	Spare		
31	Elevator PCU B	ELEV PCU B	Degrees
32	Stabilizer Trim Command (AFD)	A STB TRIM	Position
33	Aileron Trim Knob Position (AFD)	A AIL TRIM	Units
34	Rudder Trim Knob Position (AFD)	A RUD TRIM	Units

TABLE XIV-1. - PADS PCM PARAMETER LIST (Cont.)

CHANNEL	FUNCTION	ABBREVIATION	UNIT
35	Rudder Pedal Position (AFD)	A RUD PED	Inches
36	Pitch-Panel Mounted Controller	PMC PITCH	Inches
37	Roll-Panel Mounter Controller (AFD)	PMC ROLL	Degrees
38	Throttle Handle Position (AFD)	A TH HDL	Degrees
39	Flap Handle Position (AFD)	A FLAP HDL	Degrees
40	Stick Shaker	STK SHKR	Units
41	Speed Brake Handle Position (FFD)	F SPD BRK	Degrees
42	Nose Gear Position	N.G. POS	Position
43	DME Output	MDME	Feet
44	Radar Altitude 1 (SKC)	HRAD1	Feet
45	Altitude-Linear Pressure (CADC 2)	BARO ALT 2	Feet
46	Roll Attitude 2	ROLL 2	Degrees
47	ICP Test 4	ICP TEST 4	MU
48	Vertical Acceleration 2	VERT ACC 2	Ft/Sec/Sec
49	SKC Normal Acceleration	SKC AW	Ft/Sec/Sec
50	SKC Lateral Acceleration	SKC AV	Ft/Sec/Sec
51	SKC Longitudinal Acceleration	SKC AU	Ft/Sec/Sec
52	SKC Yaw Rate	SKC R	Ft/Sec
53	MLS Receiver Unfiltered Az Output	MAZU	Degrees
54	Baro Alt Fine (CADC 3)	BAR ALT F3	Feet
55	Spare		
56	ICP Test 1	ICP TEST 1	MU
57	Altitude Rate-Complimentary Filtered	HDOT CF	Deg/Sec
58	Altitude Rate-Baro 3	BAR HDOT 3	Ft/Sec
59	Spare		
60	Spare		
61	Stabilizer Position	STAB POS	Units
62	Elevator Command A	EL S CMD 1	Degrees

TABLE XIV-1. - PADS PCM PARAMETER LIST (Cont.)

CHANNEL	FUNCTION	ABBREVIATION	UNIT
63	Elevator Command B	EL S CMD 2	Degrees
64	Elevator Command C (MDL)	EL S CMD 3	Degrees
65	Combined Discrete 1	FCI DISC 1	Word
66	Combined Discrete 2	FCI DISC 2	Word
67	Combined Discrete 3	FCI DISC 3	Word
68	Flight Spoiler 7-2 (Right Outboard)	FLT SP 7 2	Degrees
69	Flight Spoiler 2-2 (Left Outboard)	FLT SP 2 2	Degrees
70	Flight Spoiler 7-1 (Right Outboard)	FLT SP 7 1	Degrees
71	Flight Spoiler 2-1 (Left Outboard)	FLT SP 2 1	Degrees
72	Altitude - Radio No. 1	RAD AL 1	Feet
73	Altitude - Radio No. 2	RAD AL 2	Feet
74	ICP Test 2	ICP TEST 2	MU
75	Rudder Command	RUD CMD 1	Degrees
76	Ground Speed	V GRD SPD	Knots
77	Cross Runway Velocity	XRWY VEL	Ft/Sec
78	Engine Pressure Ratio 2	EPR 2	Ratio
79	ICP Test 3	ICP TEST 3	MU
80	Combined Discrete 4	FCI DISC 4	Word
81	Cross Runway Velocity (SKC)	YDOTSK	Ft/Sec
82	ICP Test 6	ICP TEST 6	MU
83	Aileron Command 1	AIL CMD 1	Inches
84	Aileron Command 2	AIL CMD 2	Inches
85	Aileron Command 3 (MDL)	AIL CMD 3	Inches
86	Altitude Error (SKC)	DELHSK	Feet
87	Runway Centerline Deviation (SKC)	DELYSK	Feet
88	Altitude Rate (SKC)	MDOTSK	Ft/Sec
89	HRADI Minus HSK	DHTDZ	Feet
90	Engine Pressure Ratio 1	EPR 1	Ratio

TABLE XIV-1. - PADS PCM PARAMETER LIST (Cont.)

CHANNEL	FUNCTION	ABBREVIATION	UNIT
91	MLS Receiver Unfiltered EL-1 Output	MEL1U	Degrees
92	Drift Angle	DRIFT ANG	Degrees
93	Rudder Position	RUD POS	Degrees
94	Angle of Attack Vane-Safety Pilot	SP ALPHA	Degrees
95	Events	EVENTS	Events
96	ICP Test 5	ICP TEST 5	MU
97	Flight Spoiler 3 (Left Inboard)	FLT SPLR 3	Degrees
98	Flight Spoiler 6 (Right Inboard)	FLT SPLR 6	Degrees
99	Fuel Quantity - Total	TOTAL FUEL	Pounds
100	Pitch Attitude 2	PITCH 2	Degrees
101	Auto Stabilizer Trim POT A	ASTP A	Volts
102	Auto Stabilizer Trim POT B	ASTP B	Volts
103	Altitude (SKC)	HSKC	Feet
104	Throttle Handle Position 2 (FFD)	FTH HDL 2	Degrees
105	Elevator Position (LEFT)	ELEV POS L	Degrees
106	Aileron Position (LEFT)	AIL POS L	Degrees
107	MLS Receiver Unfiltered EL-2 Output	MEL2U	Degrees
108	Aileron PCU A	AIL PCU A	Inches
109	Aileron PCU Camout A	AIL CAM A	Inches
110	Aileron PCU Camout B	AIL CAM B	Inches

PCM Encoder. After signal conditioning, the analog signals are digitized by the PCM encoder and formatted into a serial data stream that is recorded on a wide band magnetic tape recorder. The PCM encoder also generates parity for each word, a NRZ (non-return to zero) data stream for telemetry and the NASA 36 bit time code used for onboard time correlation. To avoid errors due to tape speed variation caused bit jitter and to eliminate the need for DC tape recorder response, bi-phase coding is used for the PCM output data stream to be recorded. The bi-phase code has a transition density of at least one transition per bit time (Figure XIV-3) and requires a recorder bandwidth of

approximately twice the bit rate. This, coupled with the requirement to process 104 data channels at the 40 sample per second sample rate and 10 bit (including parity) word length, results in a PCM processing rate of 44.8 kilobits per second. Therefore, in this application, the tape recorder bandwidth must be 2 X 44.8 kilobits per second or 89.6 kHz.

Tape Recorder. The PADS onboard tape recorders are purchased items that meet the standards for Wideband 1 direct recording established by the Inter-Range Instrumentation Group (IRIG). The recorder used in this system has 14 tracks and a frequency response from 400 Hz to a maximum of 748 kHz. At a tape speed of 19.05 centimeters per second (7½ inches per second) the frequency response is 400 Hz to 93.5 kHz which meets the requirement for bandwidth outlined above. This tape speed provides a maximum record time of 120 minutes. Tape track assignments are shown in Table XIV-2.

TABLE XIV-2. - TAPE TRACK ASSIGNMENTS, ICAO-MLS

TRACK	DATA RECORDED
1	Time Code, NASA 36 Bit
2	MLS Sync Pulse
3	Spare
4	MLS Angle Receiver #1, Log Video
5	Digital Data Formatter, Bi-Ø PCM
6	MLS Angle Receiver #2, Log Video
7	Time Code, IRIG "B"
8	PADS, Bi-Ø PCM
9	NCU Signal/Clock, DM Code
10	PADS, Bi-Ø PCM
11	NCU Sync Channel
12	Time Code, NASA 36 Bit
13	Spare
14	Spare

Calibrator. Preflight calibration and checkout is accomplished by making use of the Calibration Control Assembly (Calibrator), a portable piece of ground equipment designed to work from 60 Hz commercial power or 115V, 400 Hz aircraft power. The unit will automatically calibrate all 104 PCM data channels in two minutes by generating a series of four calibrate commands. These commands, along with appropriate reference voltages, are received by the signal conditioning subsystem and used to generate zero and gain information that is processed by Langley Research Center's computerized data reduction facilities. The calibrator is also used to set time in the PCM time accumulator and to display the contents of individual PCM channels for pre-flight and post-flight calibration or troubleshooting.

Telemetry. The PADS telemetry subsystem was designed to accept a combination of PCM data and constant bandwidth FM subcarriers for telemetering both low and high frequency data to a monitoring ground station. The subsystem has three subassemblies: a premodulation processor (which contains frequency translators for the FM subcarriers, a PCM filter, and a summing amplifier), two transmitters, and two antennas. Reliable air-to-ground communication is obtained by the generation of a nearly omni-directional antenna pattern from the airplane and by the use of frequency and polarization diversity. Each antenna is coaxially fed by an individual transmitter, one transmitting at 1.4625 GHz and the other at 1.4805 GHz. The transmitters are standard, frequency modulated, commercial flight units with an output of eight to ten watts. Polarization diversity is accomplished by mounting the two inclined slot antennas on the top and bottom of the airplane. This results in complementary hemispherical patterns that exhibit a null in one pattern when the other is at a maximum. To make use of both frequency and polarization diversity, four receivers are required in the ground station.

Although normal PADS telemetry was not a requirement of the MLS demonstration development, one requirement was to telemeter MLS position data to the ground where real time plots were made of the difference between phototheodolite tracking and the onboard MLS position data. The source of this data was an FAA designed encoder which converted the digital outputs of the MLS receivers into a 5 kbps signal using an RS-232C format. Because of the relatively low frequency response (when compared to standard PADS PCM) of this signal and the fact that the PADS telemetry receivers do not have the DC response necessary for good recovery of a low frequency RS-232C signal, the PADS transmitter modulation technique was modified. The premodulation processor was deleted and replaced by a 54 kHz wideband voltage-controlled oscillator (VCO) and a related mixer/driver. The airborne system, coupled with the PADS ground receiving system (Figure XIV-2), yeilded virtually uninterrupted telemetry for the duration of the MLS demonstration development as well as for the ICAO demonstration itself.

Digital Data Formatter. The digital data formatter performs two functions: it contains the circuitry necessary to convert the NCU's ARINC-561 output bus to Miller code (Figure XIV-3) and it reformats data received from the flight control systems' computer interface units (CIU). ARINC-561 is a specification covering basic inertial navigation systems for commerical airlines. The NCU is programmed to output data in accordance with the standards and characteristics outlined in this specification. This output transmissions system consists of three two-wire circuits that contain the serial data (NRZ), word synchronization, and clock signals. The serial data signal consists of thirty-two 32-bit words (22 bits plus label and status code) in a binary 2's-complement format. The NCU performs navigation and guidance computations. Its primary sensor input is an LTN-51 inertial navigation system (INS) manufactured by Litton: however, it also receives signals from the air data computers, the DME's, ILS, MLS Preprocessor, and the magnetic compass. Navigation guidance system interfaces necessary for data recording are shown in Figure XIV-4. Selection of parameters for output is done under software control and may be varied in flight. A typical list of variables recorded is shown in Table XIV-3. The conversion of the output data to Miller code takes place within a converter in the formatter which combines the data and clock signals, and is necessary to make the NCU-generated data compatible with the PADS tape recording techniques.

TABLE XIV-3. - NCU PARAMETER LIST

LABEL	VARIABLE	SYMBOL	UNITS
300	Mode Word	MWORD	Octal
301	Runway Heading	RWYHDG	Deg/180
302	MLS Delta Latitude	MLSDLT	Degrees
303	MLS Delta Longitude	MLSDLG	Degrees
304	NCU Altitude *(CADC/MLS)	ALTCOR	Feet
305	NCU Ground Speed *(IDD/MLS)	GS	Knots
306	NCU Track Angle *(IDD/MLS)	TK	Degrees
307	HDOT Complementary Filtered *(Baro/MLS)	HDCF	Ft/sec
310	Velocity East (IDD)	IDDVE	Knots
311	MLS Along Track Acceleration	MLSATK	Ft/sec^2

TABLE XIV-3. - NCU PARAMETER LIST (Cont.)

312	XTK Distance	XTK	Feet
313	MLS X HAT	MLSXHT	Feet
314	MLS Y HAT	MLSYHT	Feet
315	IDD Altitude	IDDALT	Feet
316	IDD Track Angle	IDDTK	Deg/180
317	IDD Ground Speed	IDDGS	Knots
320	Velocity North (IDD)	IDDVN	Knots
321	Flight Path Angle	GAMMA	Deg/180
322	Wind Direction *(IDD/MLS)	WD	Deg/180
323	Wind Speed *(IDD/MLS)	WS	Knots
324	IDD ATK Acceleration	IDDATK	FPS2
325	Throttle Command	APC	Degrees
326	Track Angle Error	TKE	Degrees
327	Altitude Error	HER	Feet
330	Engine Pressure Ratio	EPR1	Units
331	F.P. Integrator	FWDPTH	Degrees
332	True Airspeed	TAS	Knots
333	East Velocity *(IDD/MLS)	VE	Knots
334	North Velocity *(IDD/MLS)	VN	Knots
335	MLS Z HAT	MLSZHT	Feet
336	Vertical Accel Command	VACMD	Ft/Sec2
337	Bank Angle Command	BACMD	Degrees

*Switched to MLS Da or Computed from MLS Data when MLS is valid.
IDD refers to data derived from Inertial/DME/DME computations.

The main function of the data formatter is to take parallel digital information from the CIU's and format that information into a PCM signal for data recording. The information available from the three CIU's consists of numeric sensor data, discrete data, and sensor failure codes. Because the numeric data is contained in sixteen-bit words and discrete data and sensor failure codes are made up of three-bit words, the output format is organized into 32 words, 48 bits long. This arrangement provides for 25 triplex sets of sensor data, 25 sensor failure code words, and 192 bits of discrete data. Data is available once for each algorithm pair time of the FCC's. Under PROM control it is possible to select (from the 64 FCC algorithm pair times) the data, sensor failure codes, and discretes required for analysis of a given test condition. A data formatter block diagram is shown in Figure XIV-5, and a typical parameter list is shown in Table XIV-4. The iteration rate is such that the recording of all data samples would be impossible at the desired tape speed of 19.05 cm/sec. To achieve an acceptable output bit rate, input data is averaged over eight iterations before being transferred to the output storage register. This averaging is accomplished by routing the data samples to serial input parallel adders. After each eight iterations, the adder contents are shifted right three places to divide by eight with the resulting data being equivalent to 20 samples per second. An output multiplexer then selects, in turn, the frame sync code, the numeric data, the sensor failure codes, and finally, the discretes. The output of the data formatter is a serial, bi-phase PCM data stream running at a rate of 32 kbps.

An integral part of the data formatter is a front panel display that provides inflight monitoring of performance variables being processed in the unit. The monitor is a synchronous decoder that gets its input directly from the output multiplexer and, therefore, is also useful for calibration and troubleshooting of the formatter. Six binary switches are used to select any desired 48 bit word for viewing on the three 5-digit octal displays available.

MLS Data Recording. The major additions to the DAS for the ICAO-MLS development provided for digital data recording, extensive onboard quick-look capability for MLS data, and made provision for time correlation between onboard data and NAFEC range tracking data. For digital recording, the FAA supplied a 7 track parallel digital tape recorder. The MLS variables available for digital recording were rigidly fixed (by the system) and are listed in Table XIV-5. This same digital data was sent to the preprocessor where additional data parameters were computed. Some of these parameters (Table XIV-5) were output on the 11 available analog channels, which consisted of 12 bit digital data converted to ±10V analog at the preprocessor cycle rate of 20 cps. This analog data was then routed to the PADS patch panel to be recorded along with other parameters and to the three preprocessor oscillographs for quick-look recording and inflight data analysis.

TABLE XIV-4. - DIGITAL DATA FORMATTER PARAMETER LIST

WORD	ALGORITHM	SENSOR/PARAMETER CIU A	CIU B	CIU C
1	16	Radio Altitude No. 1	Radio Altitude No. 2	
2	20	Vert Accel No. 1	Vert Accel No.2	Vert Accel No. 3
3	22	Altitude Rate No. 1	Altitude Rate No. 2	Altitude Rate No. 3
4	28	Pitch Attitude No. 1	Pitch Attitude No. 2	Pitch Attitude No. 3
5	30	Roll Attitude No. 1	Roll Attitude No. 2	Roll Attitude No. 3
6	32	Pitch Rate No. 1	Pitch Rate No. 2	Pitch Rate No. 3
7	34	Roll Rate No. 1	Roll Rate No. 2	Roll Rate No. 3
8	36	Column Force Mux 1	Column Force Mux 2	Column Force Mux 3
9	38	Wheel Force Mux 1	Wheel Force Mux 2	Wheel Force 3
10	40	Linear Airspeed 1	Linear Airspeed 2	Linear Airspeed 3
11	42	A/B Elevator PCU	Hardover	Elevator PCU Model
12	44	A/B Aileron PCU	Hardover	Aileron PCU Model
13	46	ASTP		
14	56	AFD Rud Ped Pos		
15	62	Rudder Servo Pos	Hardover	Rudder Servo Model
16	78			Altitude Rate-MLS
17	80	XTK Acceleration 1	XTK Acceleration 2	XTK Acceleration 3
18	82			Altitude-MLS
19	84			MLS Glideslope
20	86	Groudspeed No. 1	Groundspeed No. 2	Groundspeed No. 3
21	88	RWY Heading Error 1	RWY Heading Error 2	RWY Heading Error 3
22	90	Cross Runway Error 1	Cross Runway Error 2	Cross Runway Error 3
23	100			MLS Localizer
24	106			MLS Cross Runway Vel
25	120			MLS Vert Acceleration
26	-	Sensor Monitors		
27	-	Sensor Monitors		
28	-	Discrete Monitors		
29	-	Discrete Monitors		
30	-	Discrete Monitors		
31	-	Discrete Monitors		

TABLE XIV-5. - MLS DATA RECORDING

Parallel Digital Recorder

A. MLS Azimuth

1. Angle (Unfiltered)
2. Angle (Filtered)
3. Function Flag
4. Frame Flag

B. MLS Elevation

1. Angle (Unfiltered)
2. Angle (Filtered)
3. Function Flag
4. Frame Flag

C. MLS DME

1. Distance
2. Function Flag
3. Tracking Flag
4. Update Indicator

D. Range Time

Analog

1. Cross Runway Velocity
2. Altitude Error
3. Runway Centerline Deviation
4. Altitude Rate
5. Radio Altitude Minus Computed Altitude
6. MLS Receiver Unfiltered EL-1 Output
7. Computed Altitude
8. MLS Receiver Unfiltered EL-2 Output
9. Radar Altitude 1
10. MLS Receiver Unfiltered AZ Output
11. DME Output

MLS angle receiver log video outputs and Receiver No. 1 sync were recorded on three previously unused tracks of the PADS tape recorder and used for post flight diagnosis. Also recorded on the PADS recorder was an IRIG-B serial time code from a generator supplied by the FAA. Time synchronization is normally provided by the PADS internal NASA 36 bit time code generator. While quite adequate for the purpose intended, the lack of capability to utilize this code by facilities other than LRC necessitated the installation of the auxiliary IRIG-B generator. Both the PADS generator and the IRIG-B generator were synchronized to NAFEC range time at the beginning of each flight. The PADS generator provided range time to the PADS tape recorder and PCM, to the time displays throughout the airplane, and to the video recorders; the IRIG-B code was sent to the digital tape recorder and the PADS tape recorder while a slow code output was sent to the preprocessor oscillographs. MLS data recording interfaces are shown in Figure XIV-6.

Video Recording. The electronic display system is a complex, computer-controlled system employing both raster modulation and stroke writing for symbol generation. The pilot displays, an Electronic Attitude Director Indicator (EADI) and a Multi-Function Display (MFD), are essentially cathode ray tube X-Y plotters. For video recording, it is necessary that the X-Y information presented to the displays be translated to composite video signals. This is accomplished on the TCV B-737 by taking video pictures of the X-Y display information as it is displayed on two special monitors in the image converter pallet. As shown in Figure XIV-7, the camera outputs are routed through a video interface where a parallel BCD output of PADS time code is converted to a video symbology and added to each composite video signal. Also shown are the various inputs and interfaces necessary to generate the video data recordings.

REFERENCES

XIV-1. "Piloted Aircraft Data System". Memorandum for FED Technical Files No. 61. NASA-Langley Research Center. August 3, 1973.

XIV-2. "Data Formatter Manual", Document No. D6-32688. The Boeing Company, June, 1976.

APPENDIX - PADS ENVIRONMENTAL QUALIFICATIONS

All PADS subsystems have been qualified to the following environmental conditions:

* Vibration - Sine wave vibration requirements of Figure XIV-8 and the random vibration requirements of Figure XIV-9. Each unit was swept for 7.5 minutes up and 7.5 down the sine wave curve and 7.5 minutes duration on the curve of random vibration.

* Shock - 15g reached in 5.5 milliseconds with a total duration of 11.5 milliseconds in opposite directions along three mutually perpendicular axes.

* Altitude and Temperature - 50,000 feet at -67 degrees F to +160 degrees F at sea level. All units are qualified in still air.

In addition, each unit has been designed to meet the EMI requirements of MIL-STD 461/462 for Class I equipment and to operate in a relative humidity of 95 percent.

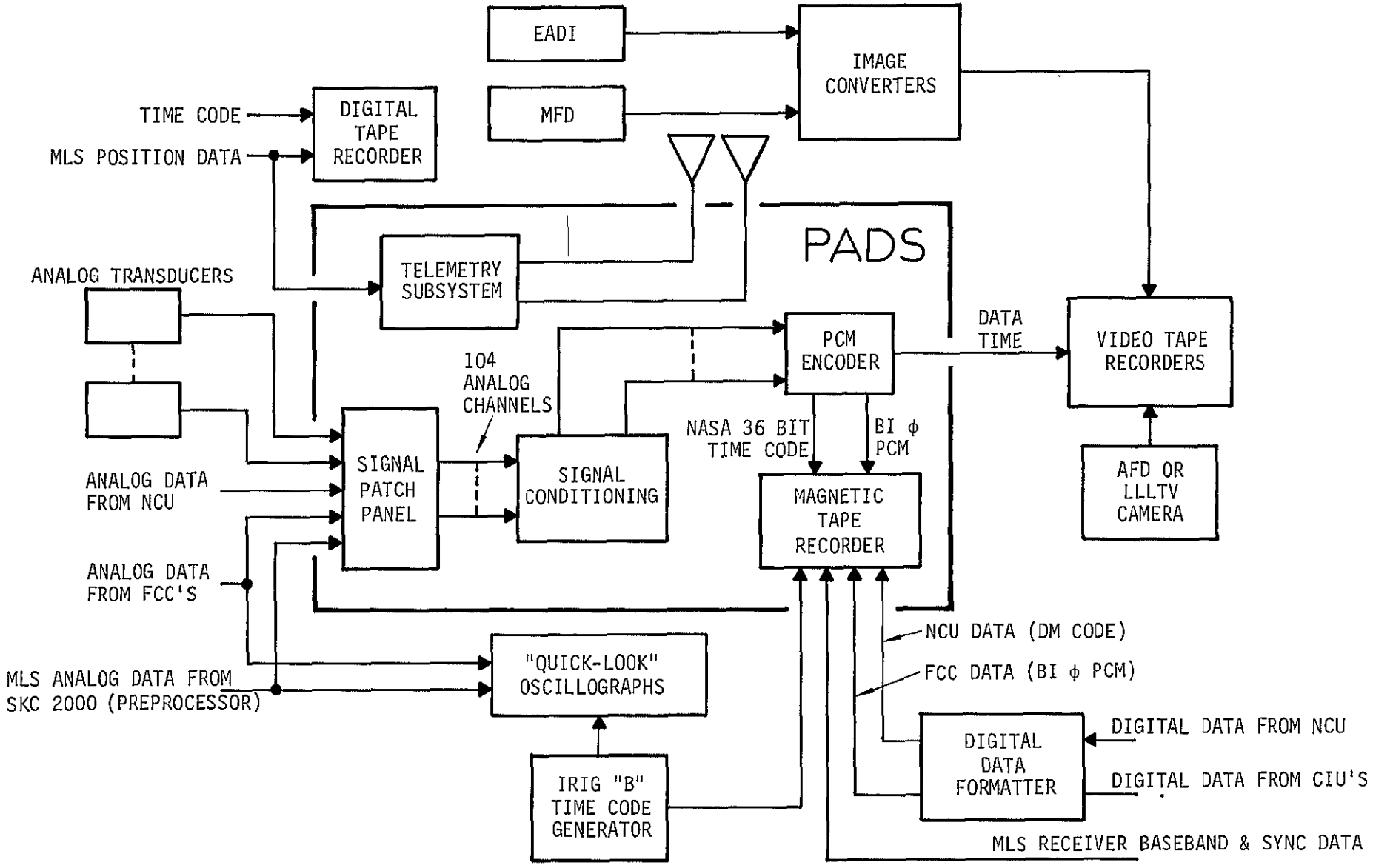

FIGURE XIV-1 ICAO-MLS DATA ACQUISITION

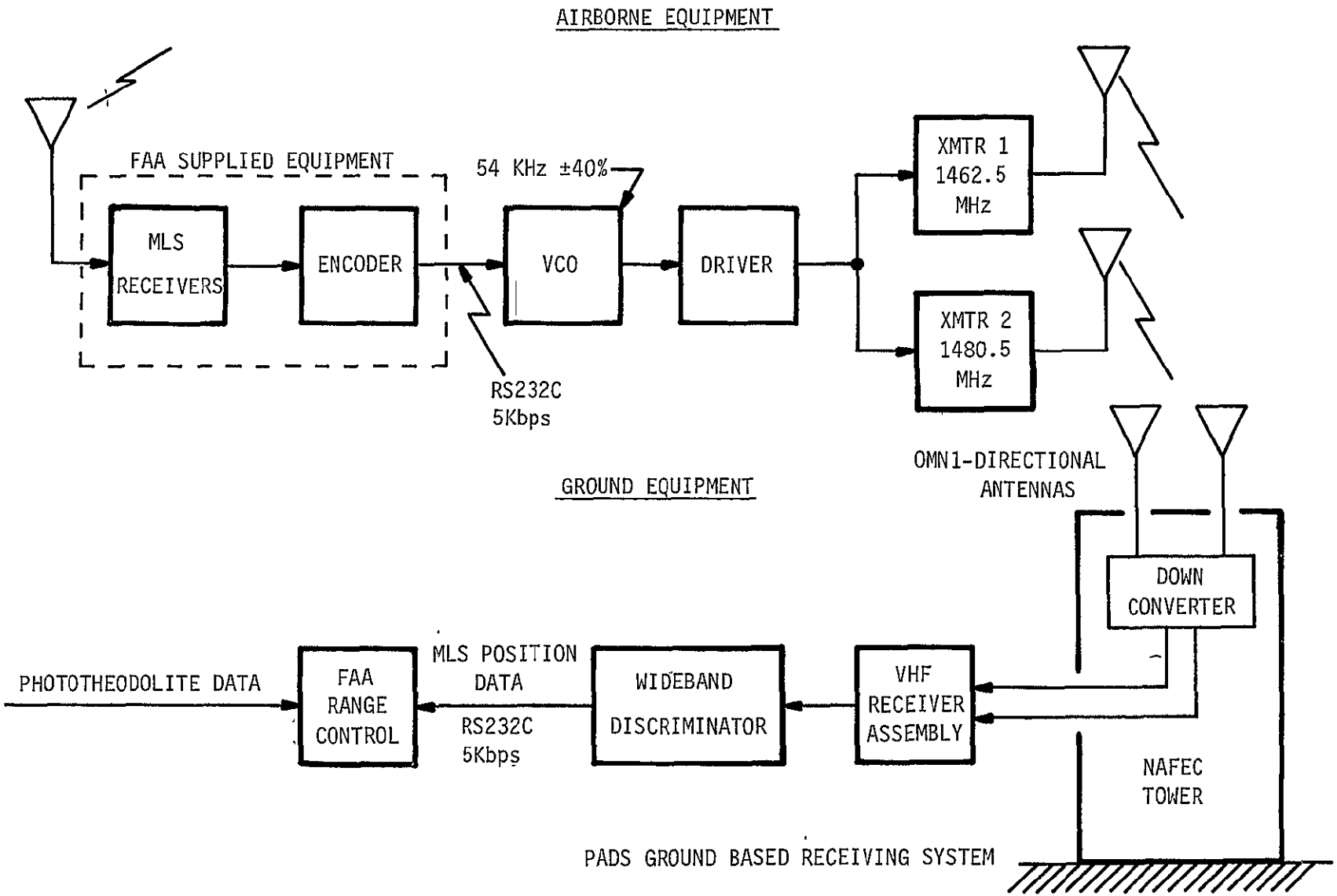

FIG. XIV-2 TELEMETRY LINK

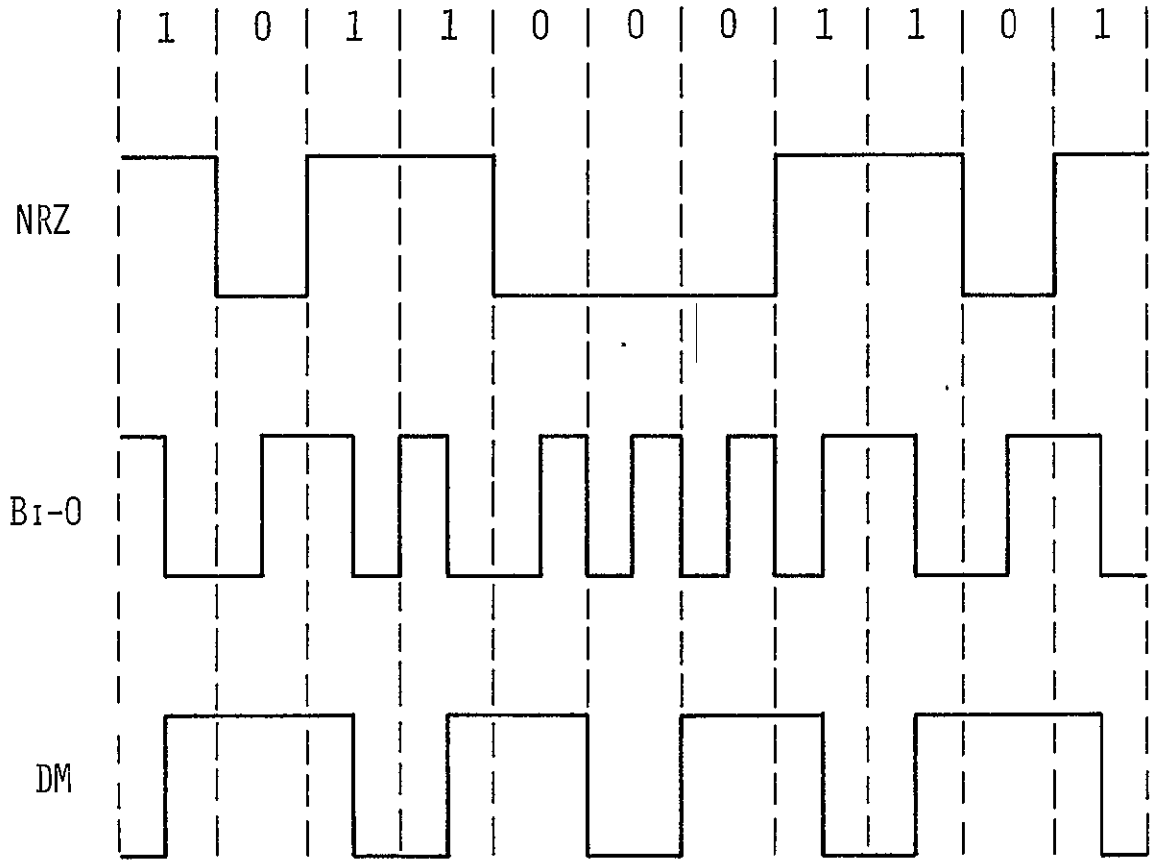

NRZ:
"ONE" IS REPRESENTED BY ONE LEVEL;
"ZERO" IS REPRESENTED BY THE OTHER LEVEL.

BI-Ø:
A TRANSITION OCCURS AT THE CNETER OF EVERY BIT PERIOD.
"ONE" IS REPRESENTED BY A CHANGE FROM HIGH TO LOW LEVEL; "ZERO" IS REPRESENTED BY A CHANGE FROM LOW TO HIGH LEVEL.

DM:
"ONE" IS REPRESENTED BY A TRANSITION AT MID-BIT TIME; "ZERO" FOLLOWED BY A "ZERO" IS REPRESENTED BY A TRANSITION AT THE END OF THE FIRST ZERO BIT.
PCM CODES

FIGURE XIV-3 PCM CODES

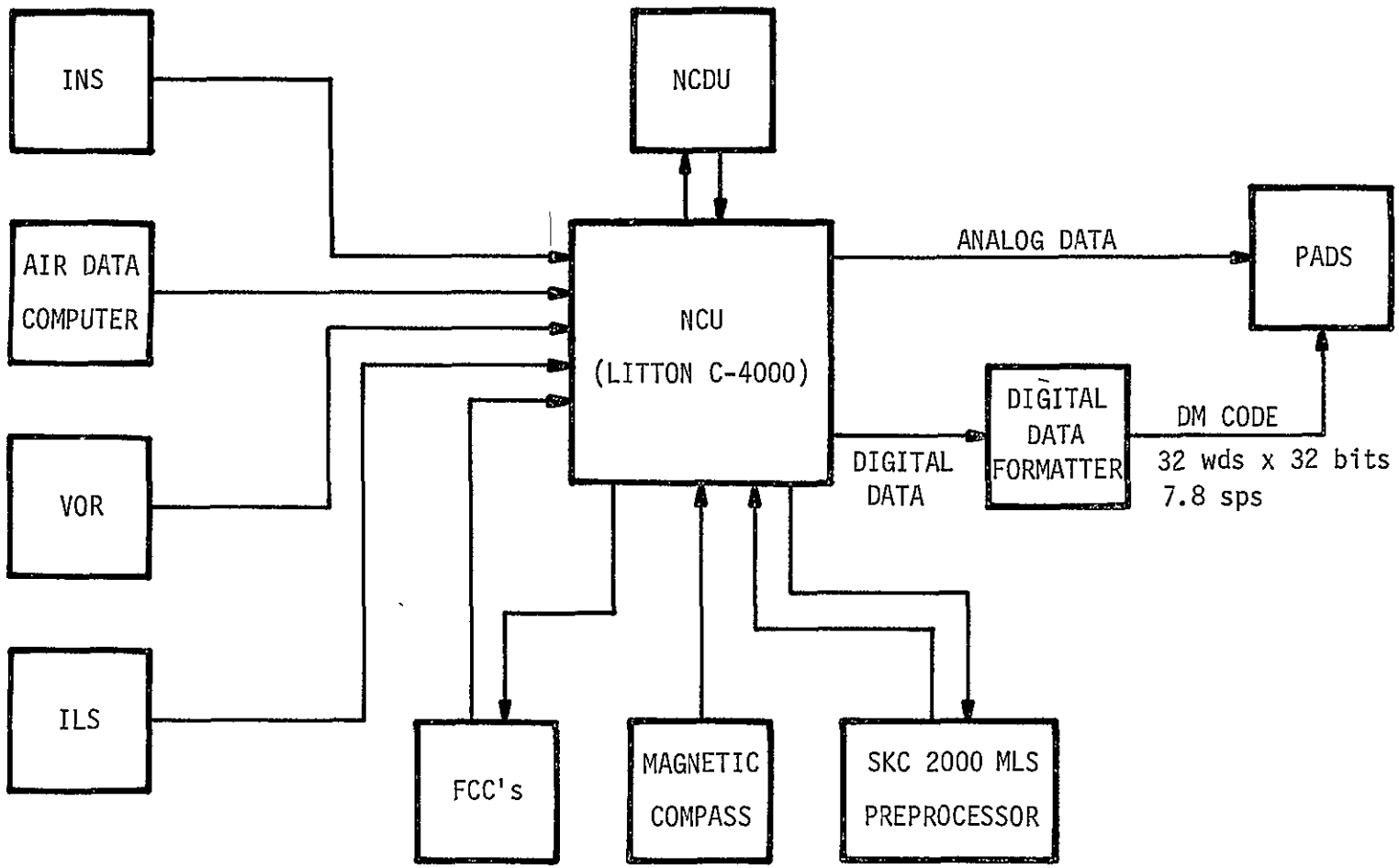

FIG. XIV-4 NAVIGATION/GUIDANCE DATA RECORDING

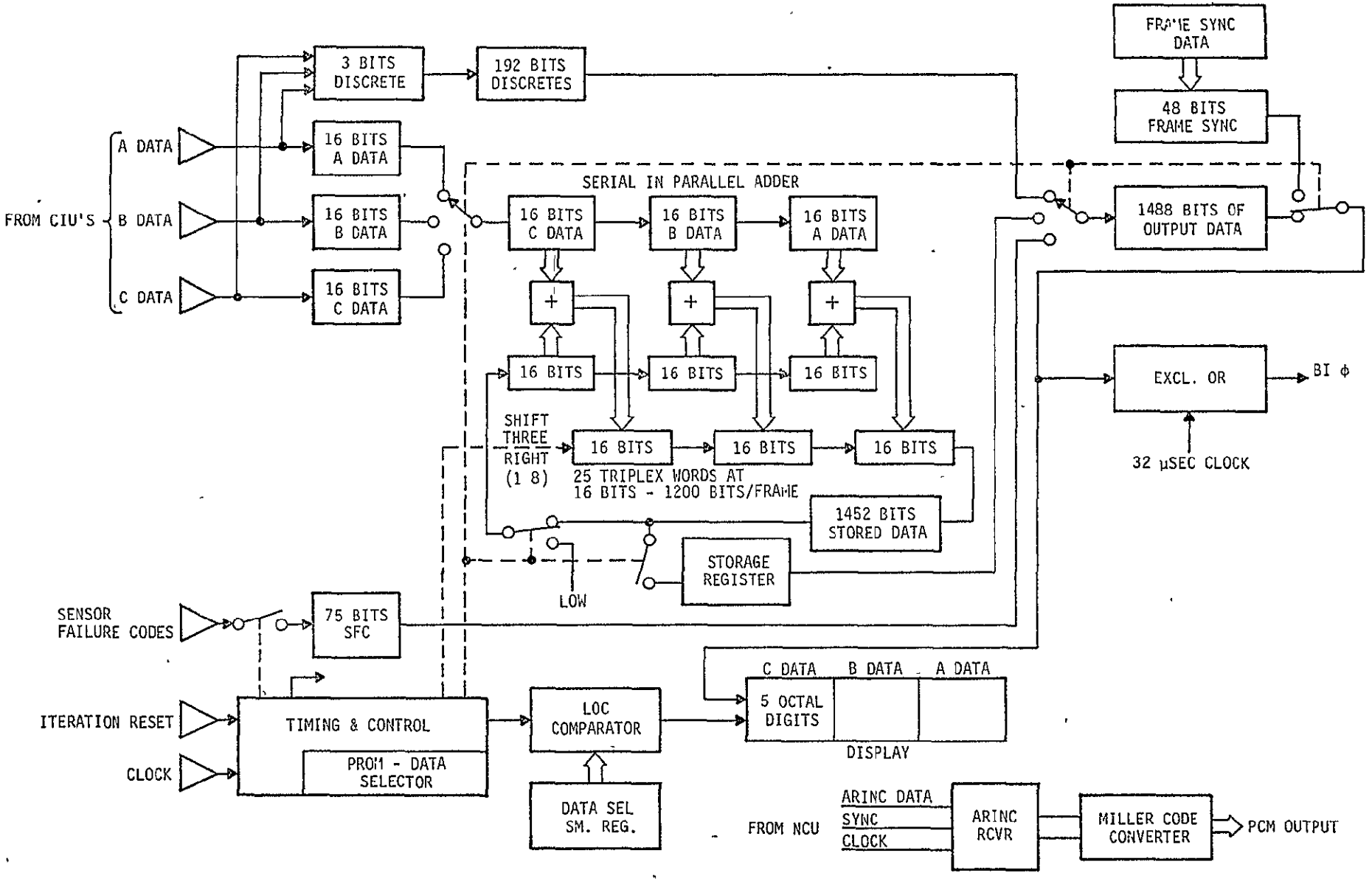

FIGURE XIV-5 DIGITAL DATA FORMATTER BLOCK DIAGAM

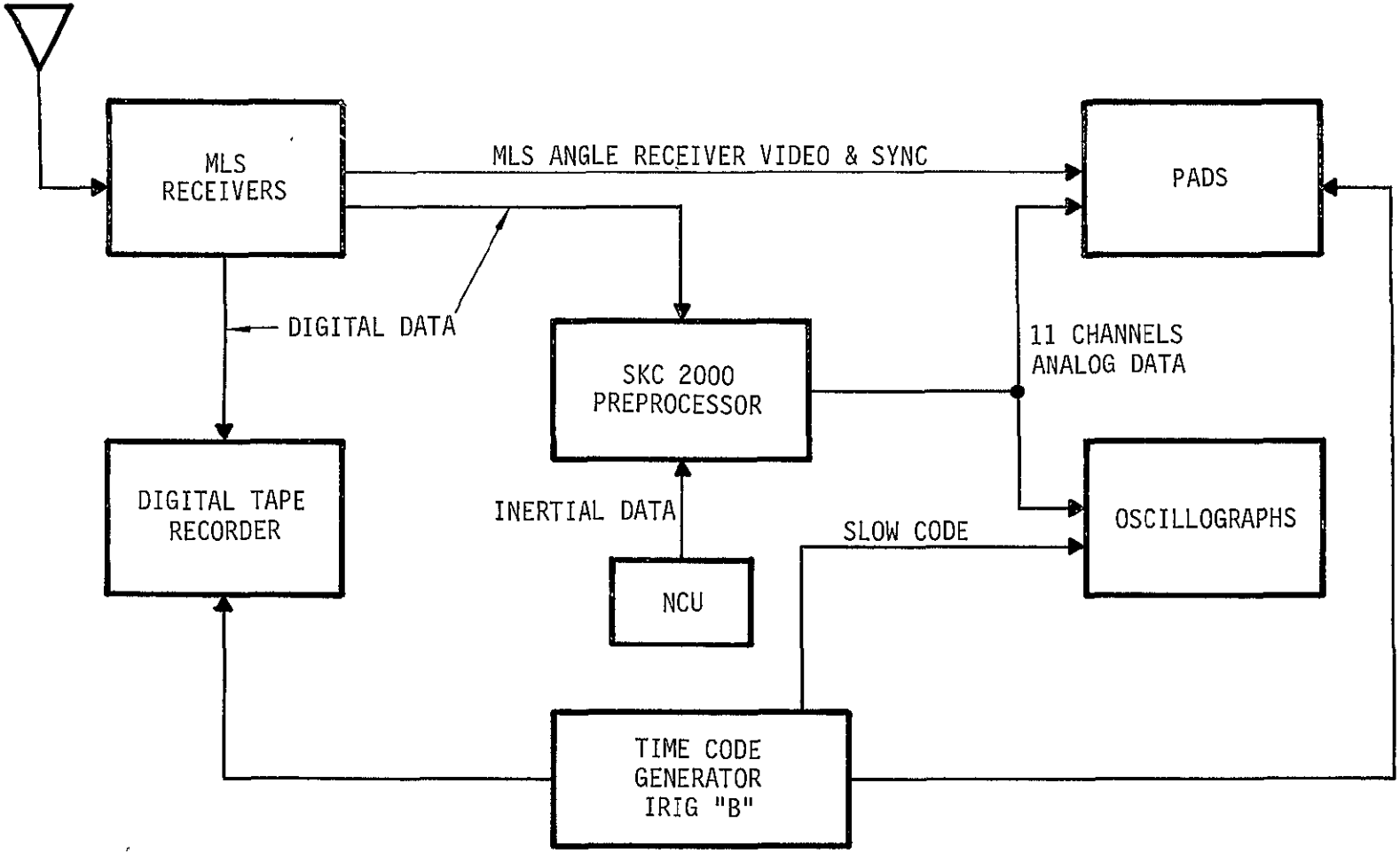

FIGURE XIV-6 MLS DATA RECORDING

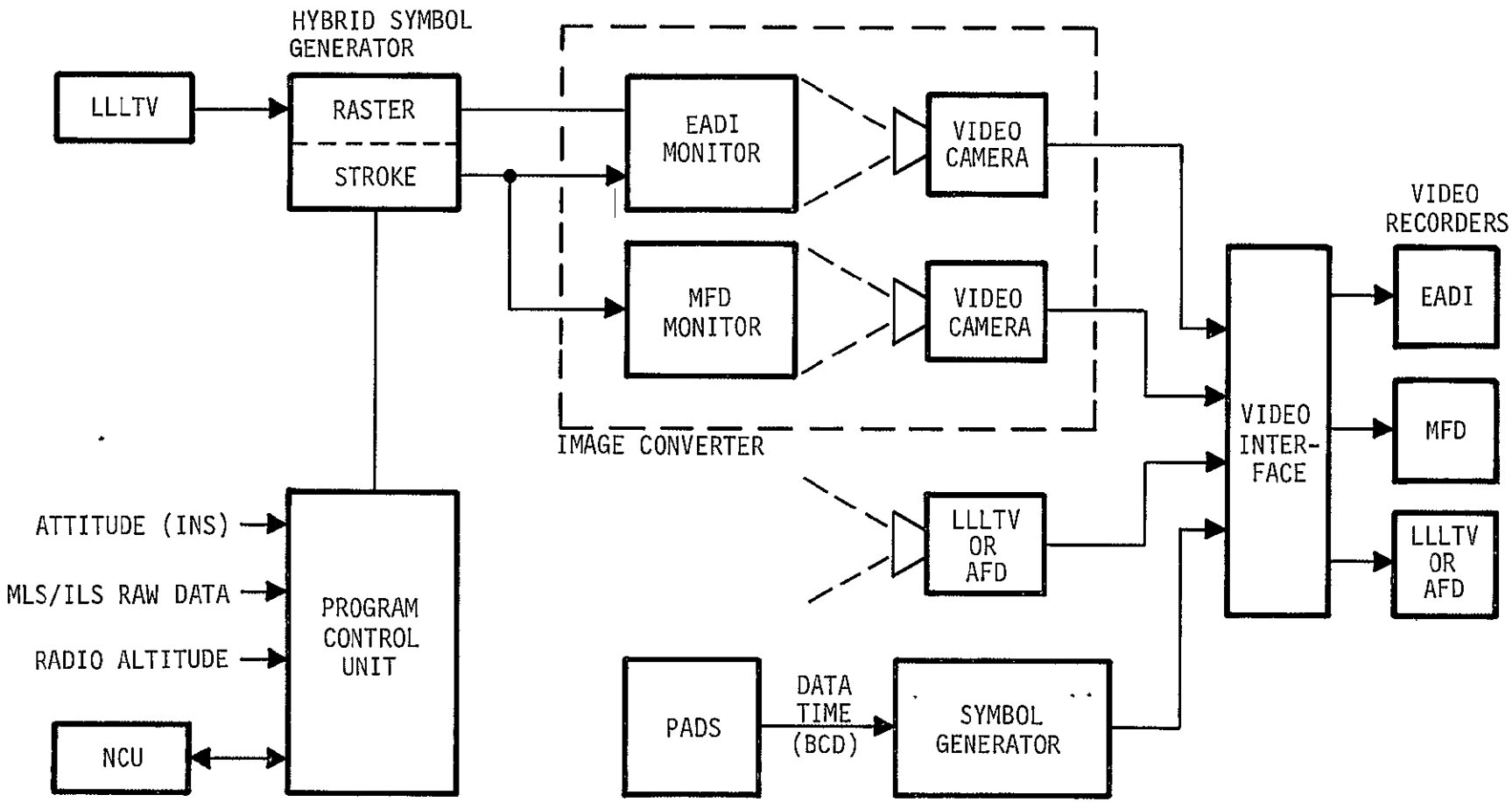

FIGURE XIV-7 VIDEO RECORDING

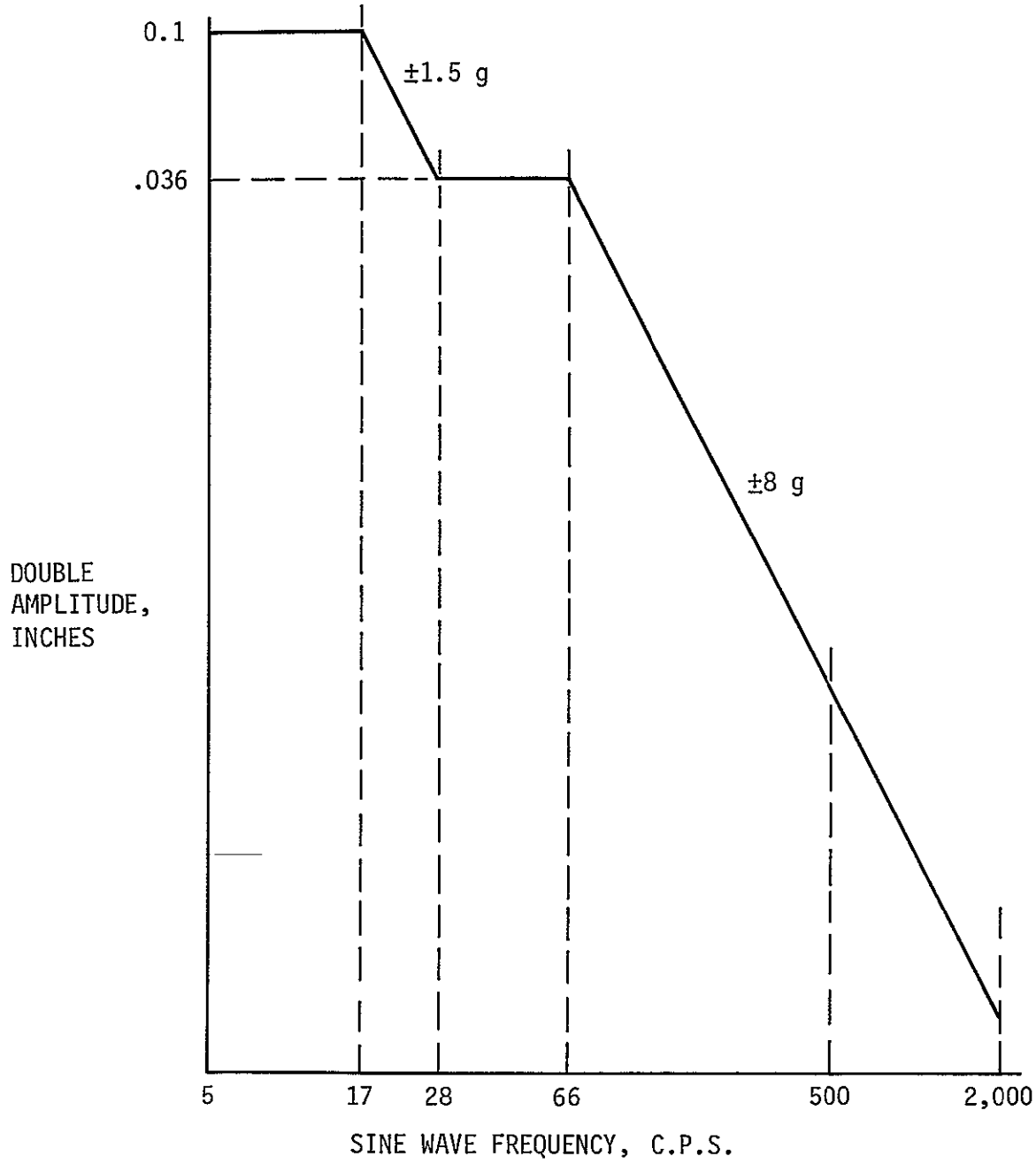

FIGURE XIV-8 SINE WAVE VIBRATION REQUIREMENTS

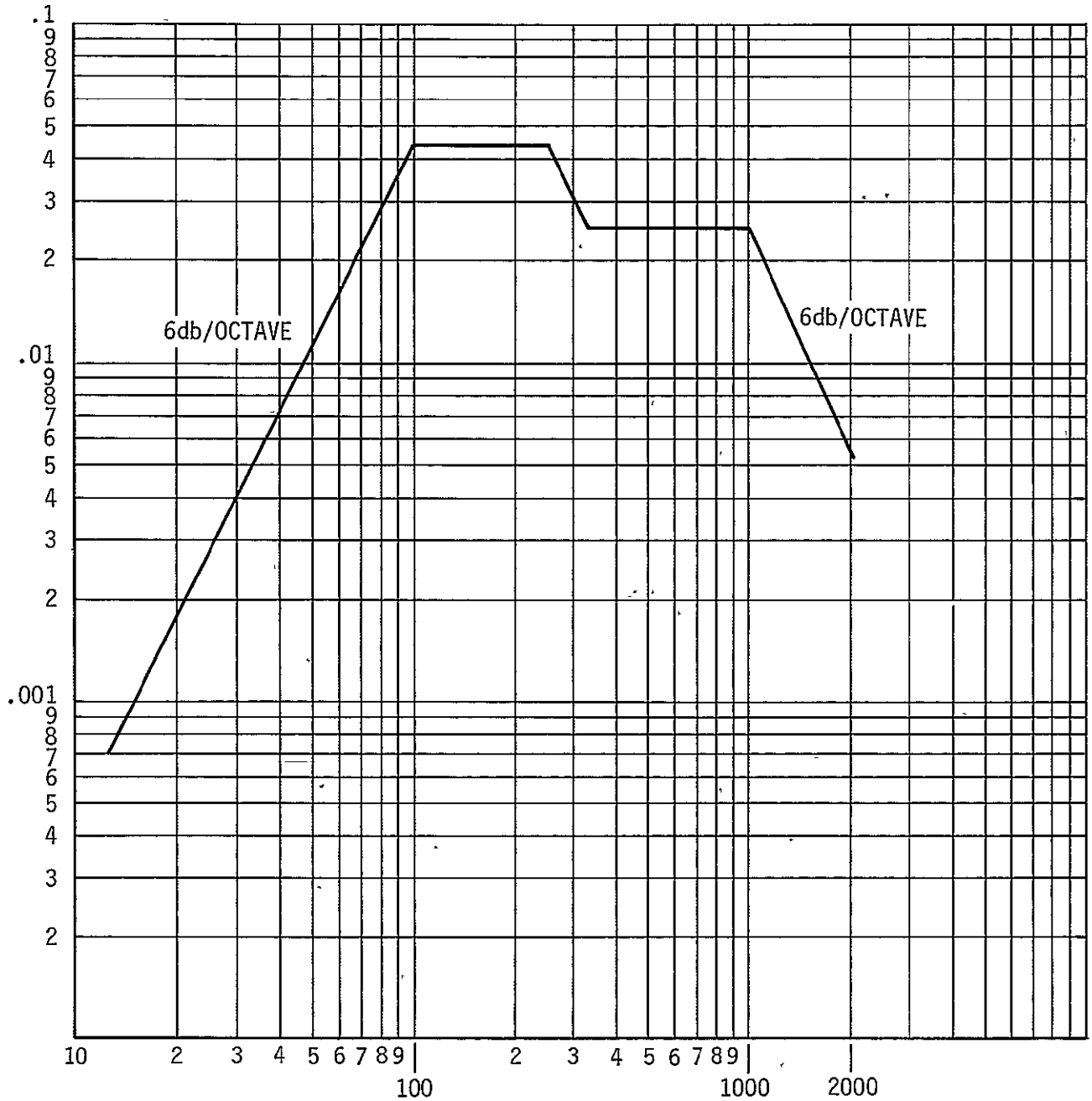

ABCISSA = FREQUENCY, HERTZ

ORDINATE = POWER SPECTRAL DENSITY, G^2/HZ

FIGURE XIV-9 RANDOM WAVE VIBRATION REQUIREMENTS

XV. GROUND TRACKING SYSTEMS

By Charles W. Meissner, Jr.

DISCUSSION

One of the most important measures of system performance was the ability of the airplane to fly a prescribed path in the MLS coverage volume. How closely the path was followed was determined by using the NAFEC ground tracking system. The tracking system consists of the Extended Area Instrumentation Radar (EAIR) for longer range tracking and phototheodolite triangulation for ranges closer than three or four miles from touchdown.

Extended Area Instrumentation Radar. The EAIR is a C-band radar that operated with a transponder aboard N515NA. The transponder was switched between antennas located on top and bottom of the fuselage. Loss of track was never a problem during the initial development flights, which is when the EAIR was used. NAFEC tracking system errors have been reported in FAA Report No. FAA-RD-74-207 entitled "Microwave Landing System Phase II Tracker Error Study". The EAIR has two-sigma errors of 0.055 degrees in azimuth, 0.043 degrees in elevation and 42.4 feet in range at the EAIR-to-phototheodolite switchover point, three to four miles from touchdown.

Phototheodolites. The later development flights made use of the greater accuracy available from the phototheodolite trackers. The phototheodolites are optical instruments which are manually trained on some identifiable feature of the aircraft. This feature was the top of the windshield divider in the case of N515NA. The photographic correction feature of the phototheodolite was never used since adequate accuracy was available without this extra step in data reduction.

GEOMETRY AND ACCURACY

The phototheodolite system two-sigma error curves indicate about 0.02 degrees for azimuth and elevation errors with the range error decreasing from about 30 feet at switchover to about 3 feet at touchdown. Unsmoothed phototheodolite data was used during the development flights since it was immediately available and the accuracy was sufficient to see changes in airplane path-following performance. Data was available as plot board plots and listings in the MLS coordinate system. This is a cartesian system with center at the MLS azimuth site and with the x-y plane normal to the local vertical at X_{MLS} = 6463 feet and Y_{MLS} = 766 feet. Z_{MLS} is increasing positive for increasing altitude. These points are shown on Figure XV-1 relative to the MLS runway. Also shown are the phototheodolite tower locations (P-8, P-29, P-36), the EAIR location and plan views of the demonstration flight profiles.

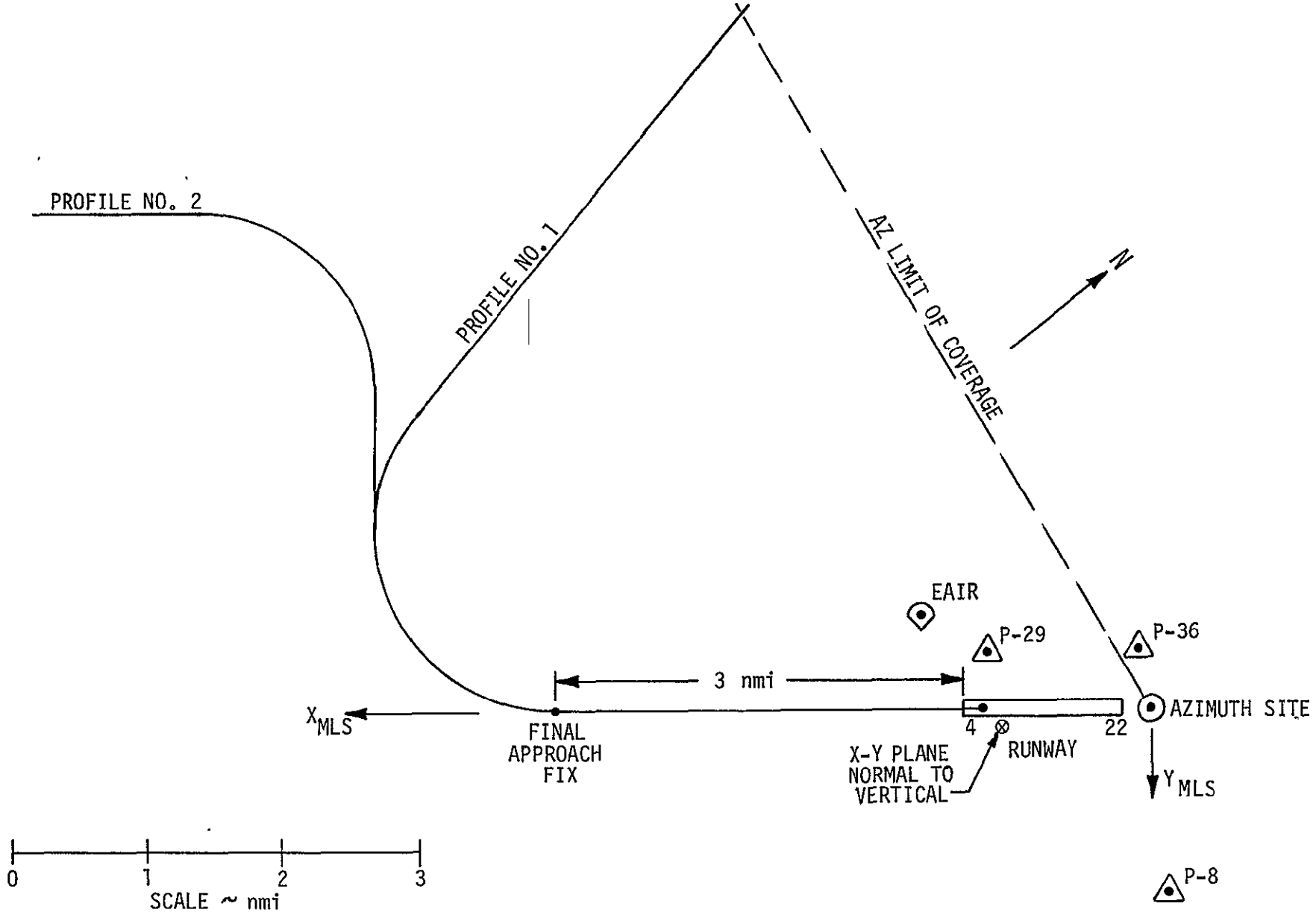

FIGURE XV-1 MLS COORDINATES AND TRACKING SYSTEM LOCATION

XVI. DIGITAL MLS DATA PROCESSING

By William F. White, William T. Bundick,
Stewart H. Irwin and Milton W. Skolaut, Jr.

INTRODUCTION

A digital recorder was used to record output data and status flags from the MLS angle and DME receivers. Prior to the beginning of flight tests a program was developed to process typical flight data tapes furnished by the FAA and provide a summary analysis of data reliability. During the flight testing phase, several other programs were developed using a minicomputer. Most of the processing was later transferred to the main computer center due to the necessity for converting the flight tapes into a format compatible with the minicomputer, and the time consumed in reading these tapes into the minicomputer using a relatively low-speed tape transport.

This chapter describes the processing used on the MLS digital data and on the phototheodolite tracking data with which it was compared, and provides illustrations of the output. For the flight data, the statistical analyses are from the December, 1975 antenna test flight. The plot examples are taken from the final approach of run 6 on flight S109. This flight used EL-1 elevation guidance down to an altitude of 900 feet, where it switched to EL-2 guidance. Flare and landing elevation guidance was from the radio altimeter.

TYPES OF PROCESSING

Summary Analyses. A Summary Analysis program was developed which divided the MLS data on the digital flight tapes into blocks according to time, with each block normally containing the data from a five second period. Within each block of data, the program counted and printed out the number of azimuth function flags, the number of azimuth data points which were flagged with a frame flag, and the times of the first and last data points in the block. The The program simultaneously provided the same information for the elevation, flare and DME functions. For the latter the program counted only new DME data points, that is, only DME data points which were accompanied by an update bit.

The results of the Summary Analysis program could be used to quickly spot periods of a flight where the MLS data was unreliable. Such periods were indicated by the presence of flags or by a departure from the nominal number of data points for a five second block. A missing angle data point corresponded to failure of the MLS angle receiver to decode a valid identification word during the preamble. It should be noted that the absence of only one or two data points within a five second block could not be reliably detected with the Summary Analysis program. A sample printout from this program is shown in

in Figure XVI-1.

Statistical Analysis. A minicomputer program was written to perform a function similar to the Summary Analysis program, but which could detect more types of data errors and listed each one along with the time at which it occurred. During a scan of the flight tape, the program listed each flag recorded. Deviations of more than 0.2^{o} from predicted angle values were designated outliers. Most of these points were accompanied by frame flags, but a few were not. Many of the latter cases were determined to be due to improper identification of the angle function, caused by incorrectly decoding the preamble. Also, missing data points (dropouts) were detected by the absence of an angle function at the expected time, as determined by the signal transmission format. This was easily determined since the signal timing jitter feature was not operating during the December flights.

The results of the analysis of the December antenna flights are given in Tables XVI-1 and XVI-2. No EL-2 analysis is available since at that time there was no Ku band capability aboard the aircraft. Further, the DME results are not included as the airborne equipment was malfunctioning and the range values were so erratic as to be meaningless during large portions of the flights. The results were broken down according to the type of flight pattern flown. The "Racetracks" column refers to patterns with a 180^{o} turn to final approach.

TABLE XVI-1. - STATISTICAL ANALYSIS OF AZIMUTH DATA

	ICAO Profiles	Racetracks
Number of recorded points	22,741	7,273
Missing data (dropouts)	9 (0.04%)	41 (0.6%)
Frame flags	3 (0.01%)	0
Function flags[1]	2	2
Incorrect identifications	2 (0.01%)	0
Outliers[2]	24 (0.1%)	0

1. Flags were caused by multipath interference on the ICAO profiles and dropouts on the racetrack patterns

2. Fluctuations in data due to multipath interference were the cause of all data tagged as outliers in this case

TABLE XVI-2. - STATISTICAL ANALYSIS OF ELEVATION DATA

	ICAO Profiles	Racetracks
Number of recorded points	67,325	18,132
Missing data (dropouts)	79 (0.12%)	51 (0.28%)
Frame flags	183 (0.27%)	81 (0.45%)
Function flags[1]	3	1
Incorrect identifications[2]	14 (0.02%)	8 (0.04%)
Outliers[3]	5 (0.01%)	0

1. Flag duration for each occurence was 0.38 to 0.40 seconds
2. Most of these were actually EL-2 signals and were flagged
3. Errors ranged from -2.4^{o} to $+0.95^{o}$

Statistical analyses were not done routinely on the development flights due to the necessity for modifying the program to account for the signal timing jitter. However, later spot checks of the data showed that the quality varied from time to time. In the tables above the azimuth signal was of the best quality but was affected by multipath interference, and the elevation signal showed numerous flags and dropouts. On some other flights the elevation data was much better than the azimuth data. In all cases there was more than 99% good data unless there was an equipment malfunction.

Filtering. The raw angle and range data was processed by an α-β tracking filter similar to the one used as a prefilter in the airborne computer. The equations used were:

$$\hat{x} = (1 - \alpha)x_p + \alpha x_o$$

$$\hat{v} = \hat{v} + (x_o - x_p)\beta/\Delta t$$

$$x_p = \hat{x} + \hat{v}\Delta t,$$

where x_o is the received value of angle or range, x_p is the predicted value for the next time interval, v is the rate of change of the variable, t is time, and the carat indicates an estimate of the variable.

In the case of dropouts or outliers, the missing or bad data point was replaced by the predicted value and the rate was assumed to be unchanged. Table XVI-3 gives the values of α and β used.

TABLE XVI-3. - MLS FILTERING CONSTANT USED

	AZIMUTH	ELEVATION	RANGE
ALPHA	0.11	0.051	0.031
BETA	0.0064	0.00133	0.000488

These values were chosen for assumed data rates of 13.5 Hz for the azimuth signal and 40 Hz for elevation and range.

Position Calculations. The aircraft position in the MLS-based rectangular coordinate system was calculated from both filtered and unfiltered data. In addition, it was calculated from both EL-1 and EL-2 data when both were available. The equations used were the same as those on board the aircraft. For the EL-1 calculations:

$$R = 6076.1\ R_{DME} + 7546.8$$

$$Y = -R \sin(AZ)$$

$$g = 7546.8 \sin^2(EL\text{-}1)$$

$$h = 5.70191 \times 10^7 \sin^2(EL\text{-}1) + Y^2 - R^2 \cos^2(EL\text{-}1) - 509.56\ Y \sin^2(EL\text{-}1)$$

$$X = g + (g^2 - h)^{1/2}$$

$$Z = (R^2 - X^2 - Y^2)^{1/2},$$

where R_{DME} is the DME range in nautical miles.

Calculations of position using EL-2 data were done in a similar fashion but with the following change in constants:

$$g = 5546.73 \sin^2(EL\text{-}2)$$

$$h = 3.08318 \times 10^7 \sin^2(EL\text{-}2) + Y^2 - R^2 \cos^2(EL\text{-}2) - 509.76\ Y \sin^2(EL\text{-}2)$$

Calculations of Δy and Δh. The cross-runway and height errors were computed from both MLS and phototheodolite data. The 0.88 foot offset of the azimuth antenna from the extended runway centerline was ignored, so that

$$\Delta y = -y$$

$$\Delta h = z - (x - 7546.8) \tan 3^{o}$$

Figure XVI-2 shows examples of Δy and Δh calculated from EL-1 data and Figure XVI-3 shows the corresponding plots for EL-2 data. The plots made from the real-time phototheodolite tracking data are given in Figures XVI-4 and XVI-5.

Calculation of η and β. The angular deviations from runway centerline (η) and glideslope (β) were calculated from the unfiltered data to preclude the possibility of phase shifts being caused by the filtering. This was not practical with Δy and Δh since the scaling used would have resulted in very noisy plots using the raw data. The quantities as calculated from MLS data were:

$$\eta = AZ$$

$$\beta = \tan^{-1} ((z + 11.76)/(x - 7546.8)) - 3^{o}$$

Figure XVI-6 is a plot of η and β made from EL-1 elevation data. The large spikes in the β plot are due to outliers, which were relatively common in the EL-1 data. Figure XVI-7 is the corresponding plot using EL-2 data.

For the phototheodolite data, it was necessary to calculate the azimuth angle by

$$AZ = \tan^{-1} (y/(x^2 + y^2)^{\frac{1}{2}})$$

The values of η and β were calculated in the same fashion as for the MLS data. Figures XVI-8 and XVI-9 are plots of η and β calculated from the tracking data.

Calculation of Height Above Touchdown. Height above the touchdown zone was calculated by the following equation:

$$h_{TD} = z - (6.12 + 38.25 \sin 3.5^{o}))$$

The 3.5^{o} angle was used as the average pitch attitude during approach and flare, since the actual pitch attitude data was not available soon enough after flights to be used. The use of a constant value caused h_{TD} to be too small during final approach, becoming somewhat too large during flare, and then again too small as the nosewheel dropped after touchdown. However, the errors were only a foot or two except during pitch maneuvers from turbulence or correction of guidance errors. Figures XVI-10 and XVI-11 show h_{TD} plots generated from filtered EL-1 and EL-2 data, respectively.

MLS TEST 2

TIME1	TO	TIME2	IDENTS AZ	EL1	EL2	BAZ	FLAGS AZ	EL1	EL2	BAZ	FR	DM1	DM2	UPD	FRAME FLAG IDENT FRAZ	FREL1	FREL2	FRBAZ
40228.723		40251.347	0	130	105	167	0	130	105	167	354	0	0	343	0	1	1	6
40251.445		40272.623	0	124	132	144	0	124	132	144	400	0	0	345	0	0	0	0
40272.740		40295.712	0	110	133	159	0	110	133	159	400	0	0	350	0	0	0	0
40295.846		40311.632	0	114	179	109	0	114	179	108	400	0	0	329	0	0	0	0
40311.986		40330.307	0	173	99	130	0	173	99	110	342	0	0	341	0	0	0	28
40330.819		40350.548	0	165	102	134	0	165	102	75	267	0	0	334	0	0	0	133
40350.600		40376.136	0	160	78	164	0	160	78	0	241	0	0	341	0	0	0	159
40376.287		40406.351	0	170	13	219	0	170	13	7	184	0	0	371	0	0	0	216
40406.398		40434.427	0	203	4	193	0	203	4	14	208	0	0	343	0	0	0	192
40434.838		40444.912	0	245	86	69	0	245	86	0	332	0	0	291	0	0	0	68
40444.943		40453.201	0	293	41	46	0	293	41	0	334	0	0	304	0	0	0	46
40453.232		40466.587	0	278	32	90	0	278	32	0	310	0	0	320	0	0	0	90
40466.630		40480.204	0	252	56	92	0	252	56	0	308	0	0	324	0	0	0	92
40480.221		40492.947	0	199	115	87	0	199	115	0	314	0	0	315	0	0	0	86
40492.990		40505.577	0	304	11	86	0	304	11	0	315	0	0	318	0	0	0	85
40505.638		40519.508	0	287	18	95	0	287	18	0	306	0	0	321	0	0	0	94
40519.539		40533.484	0	283	23	94	0	283	23	0	306	0	0	333	0	0	0	94
40533.498		40546.197	0	283	45	74	0	283	45	0	328	0	0	307	0	0	0	72
40544.208		40553.458	0	250	88	62	0	250	88	43	370	0	0	286	0	0	0	30
40553.477		40561.382	0	197	149	54	0	197	149	54	354	0	0	264	0	0	0	26
40561.461		40576.466	0	269	28	103	0	269	28	103	360	0	0	313	0	0	0	40
40576.519		40590.225	0	263	43	94	0	263	43	94	400	0	0	310	0	0	0	6
40590.236		40598.055	0	277	70	53	0	277	70	53	400	0	0	282	0	0	0	0
40598.060		40606.322	0	230	114	56	0	230	114	56	400	0	0	273	0	0	0	0
40606.348		40619.737	0	223	86	91	0	223	86	91	400	0	0	301	0	0	0	0
40619.846		40633.747	0	176	132	92	0	176	132	92	391	0	0	308	0	0	0	9
40633.768		40652.388	0	186	126	90	0	186	126	90	398	0	0	306	0	0	0	2
40652.339		40670.703	0	144	133	123	0	144	133	123	400	0	0	331	0	0	0	0
40670.724		40676.453	0	140	222	39	0	140	222	39	399	0	0	234	0	0	0	1
40676.601		40681.722	0	171	193	36	0	171	193	36	400	0	0	219	0	0	0	0
40681.727		40686.771	0	166	200	34	0	166	200	34	400	0	0	211	0	0	0	0
40686.792		40691.781	0	170	200	30	0	170	200	30	400	0	0	212	0	0	0	0
40691.786		40696.663	0	175	197	28	0	175	197	28	400	0	0	205	0	0	0	0
40696.669		40701.628	0	173	200	27	0	173	200	27	400	0	0	209	0	0	0	0
40701.633		40706.400	0	178	192	30	0	178	192	30	400	0	0	203	0	0	0	0
40706.412		40711.349	0	180	195	25	0	180	195	25	400	0	0	209	0	0	0	0
40711.354		40716.289	0	174	195	31	0	174	195	31	400	0	0	208	0	0	0	0
40716.309		40721.329	0	178	200	22	0	178	200	22	400	0	0	207	0	0	0	0
40721.350		40726.524	0	173	206	22	0	173	206	22	400	0	0	217	0	0	0	0
40726.569		40731.349	0	178	191	32	0	178	191	32	400	0	0	204	0	0	0	0
40731.372		40736.312	0	179	199	23	0	179	199	23	400	0	0	207	0	0	0	0
40736.363		40741.286	0	189	190	21	0	189	190	21	400	0	0	211	0	0	0	0
40741.291		40745.565	0	181	192	28	0	181	192	28	400	0	0	201	0	0	0	0
40745.687		40750.060	0	167	175	29	0	167	175	29	400	0	0	187	0	0	0	0
40750.083		40754.[illegible]	0	179	195	27	0	179	195	27	399	0	0	205	0	0	0	1
[illegible]		[illegible]	[illegible]	[illegible]	[illegible]	33	[illegible]	[illegible]	83	33	246	0	0	198	0	0	154	0

FIGURE XVI-1 SAMPLE OF SUMMARY ANALYSIS OUTPUT

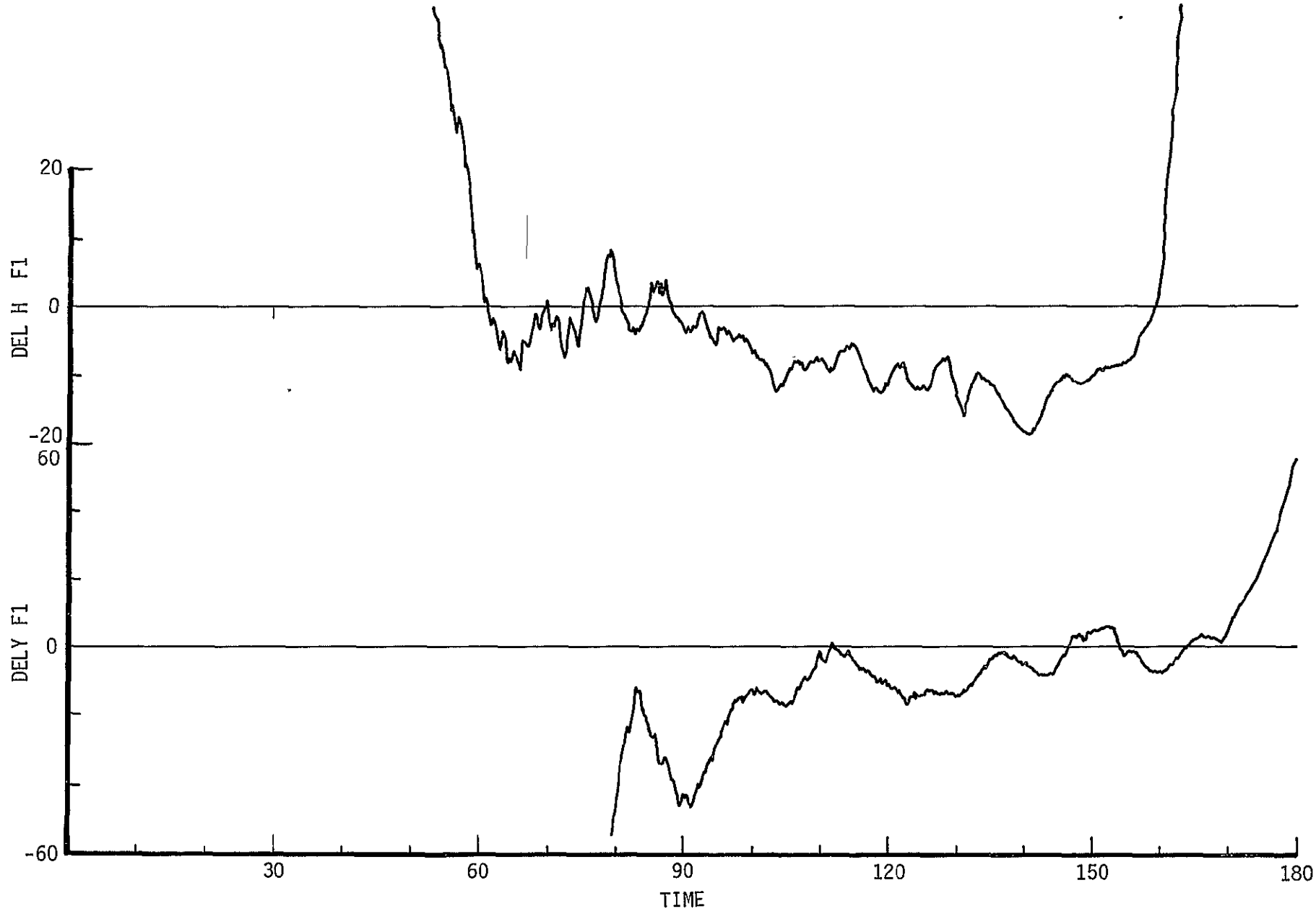

FIGURE XVI-2 ΔY AND ΔH CALCULATED USING FILTERED EL-1 DATA

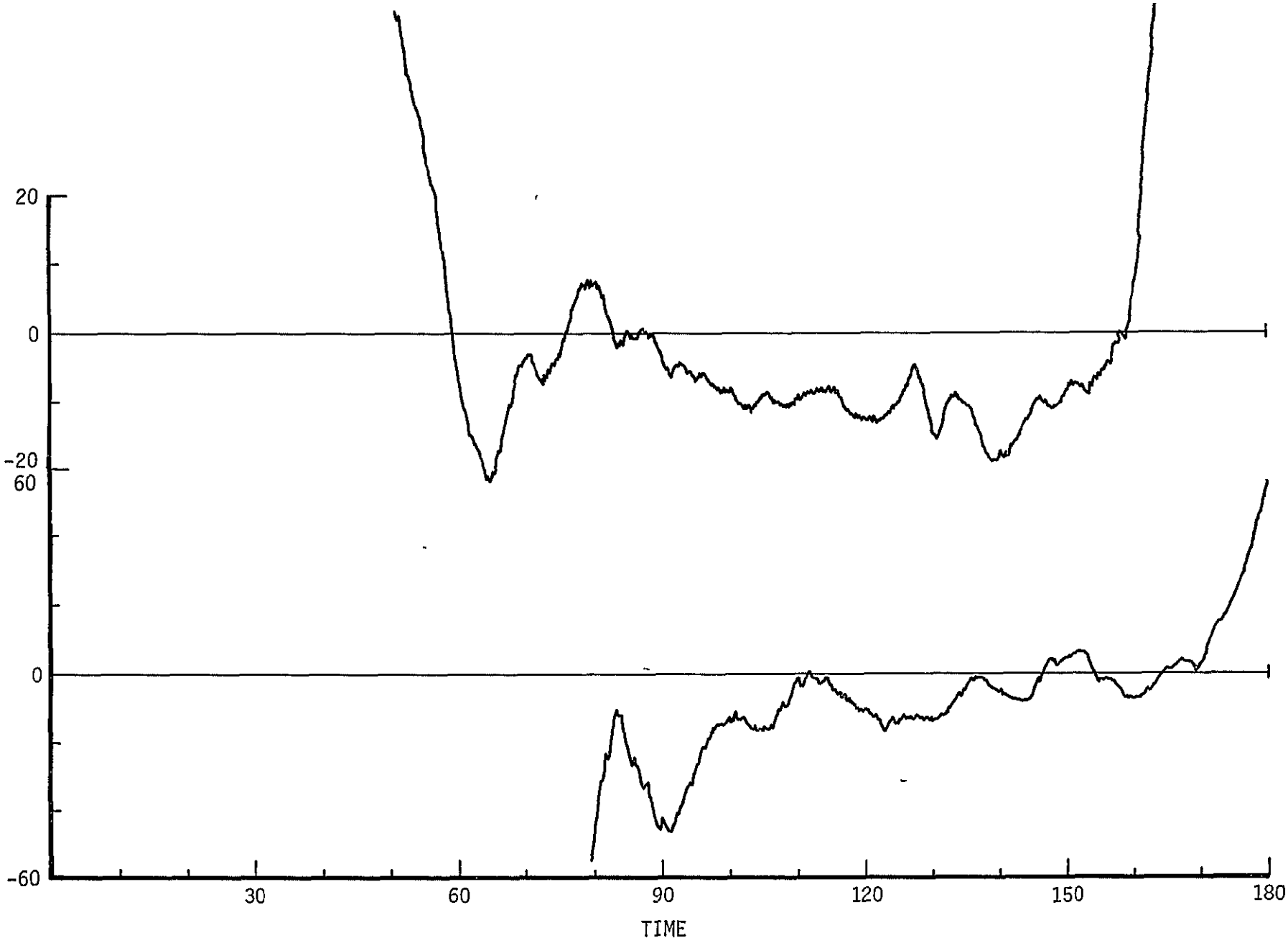

FIGURE XVI-3 ΔY AND ΔH CALCULATED USING FILTERED EL-2 DATA

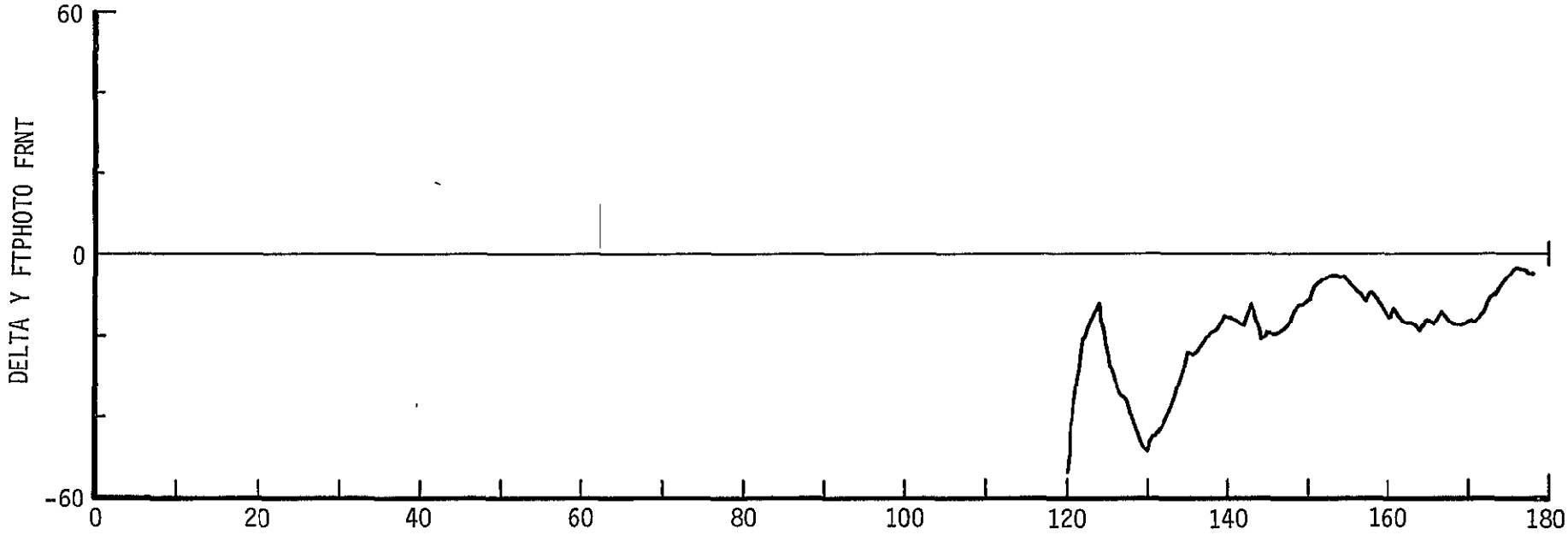

FIGURE XVI-4 ΔY CALCULATED FROM REAL TIME PHOTOTHEODOLITE DATA

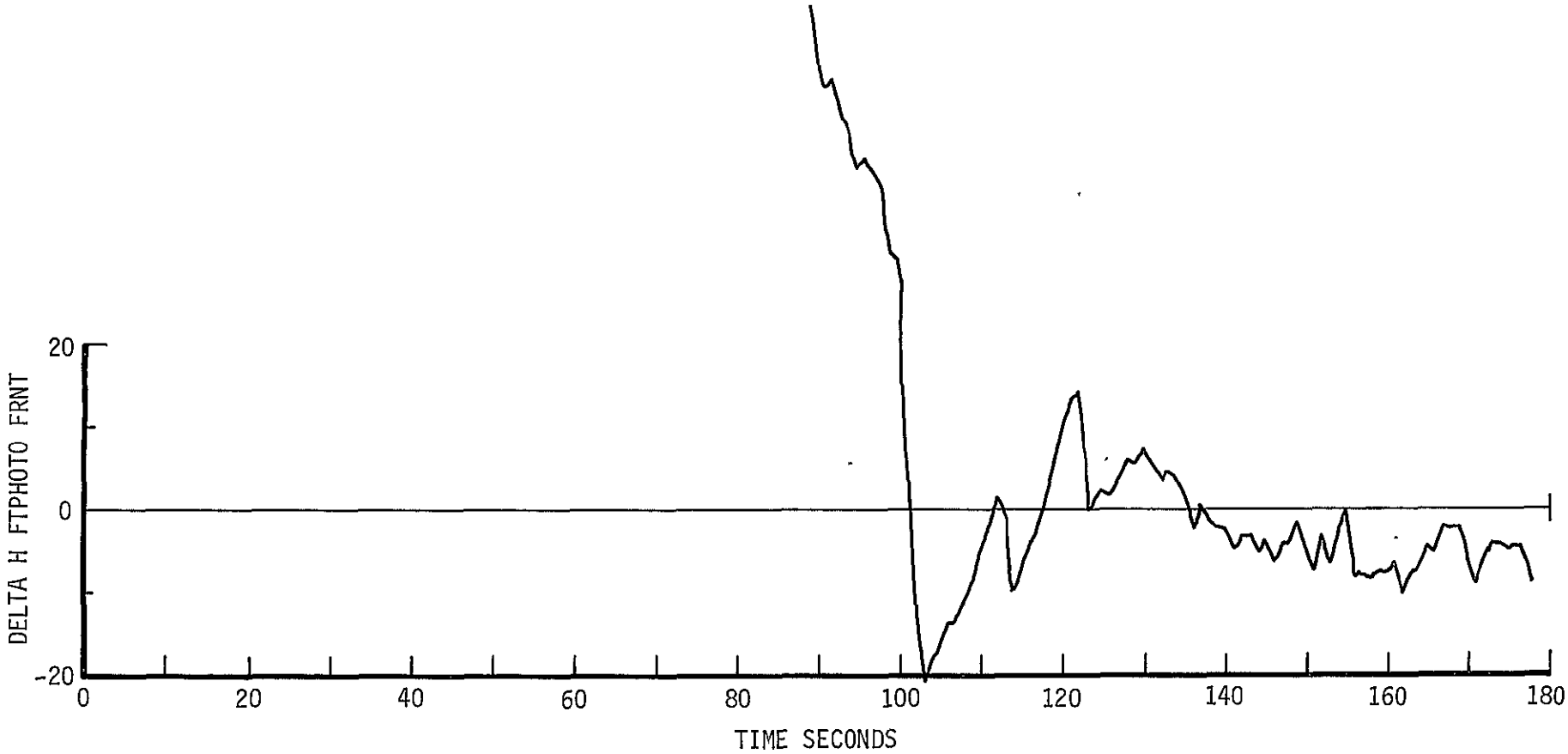

FIGURE XVI-5 ΔY CALCULATED FROM FEAL TIME POTOTHEODOLITE DATA

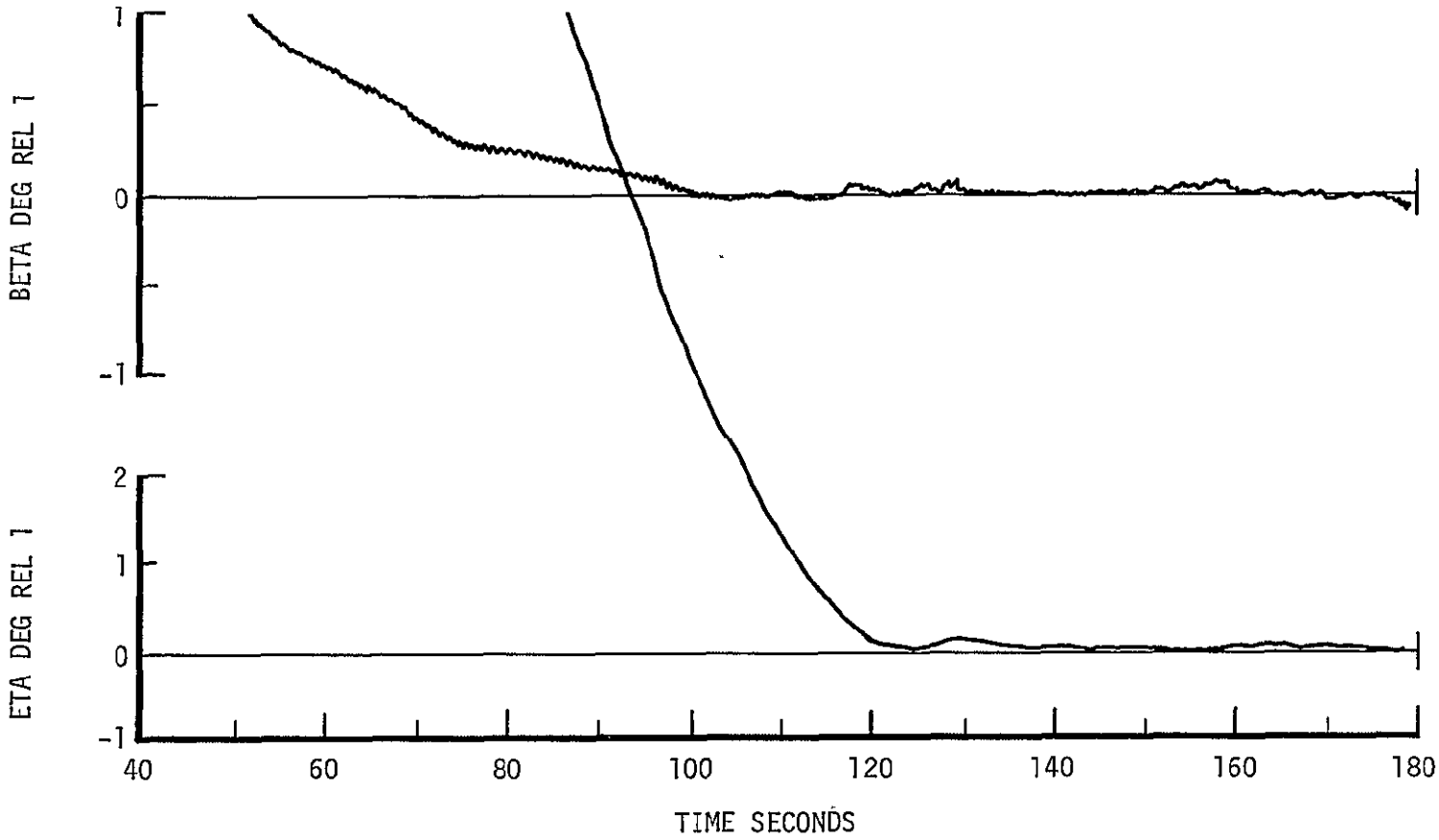

FIGHRE XVI-6 η AND β CALCULATED USING RAW EL-1 DATA

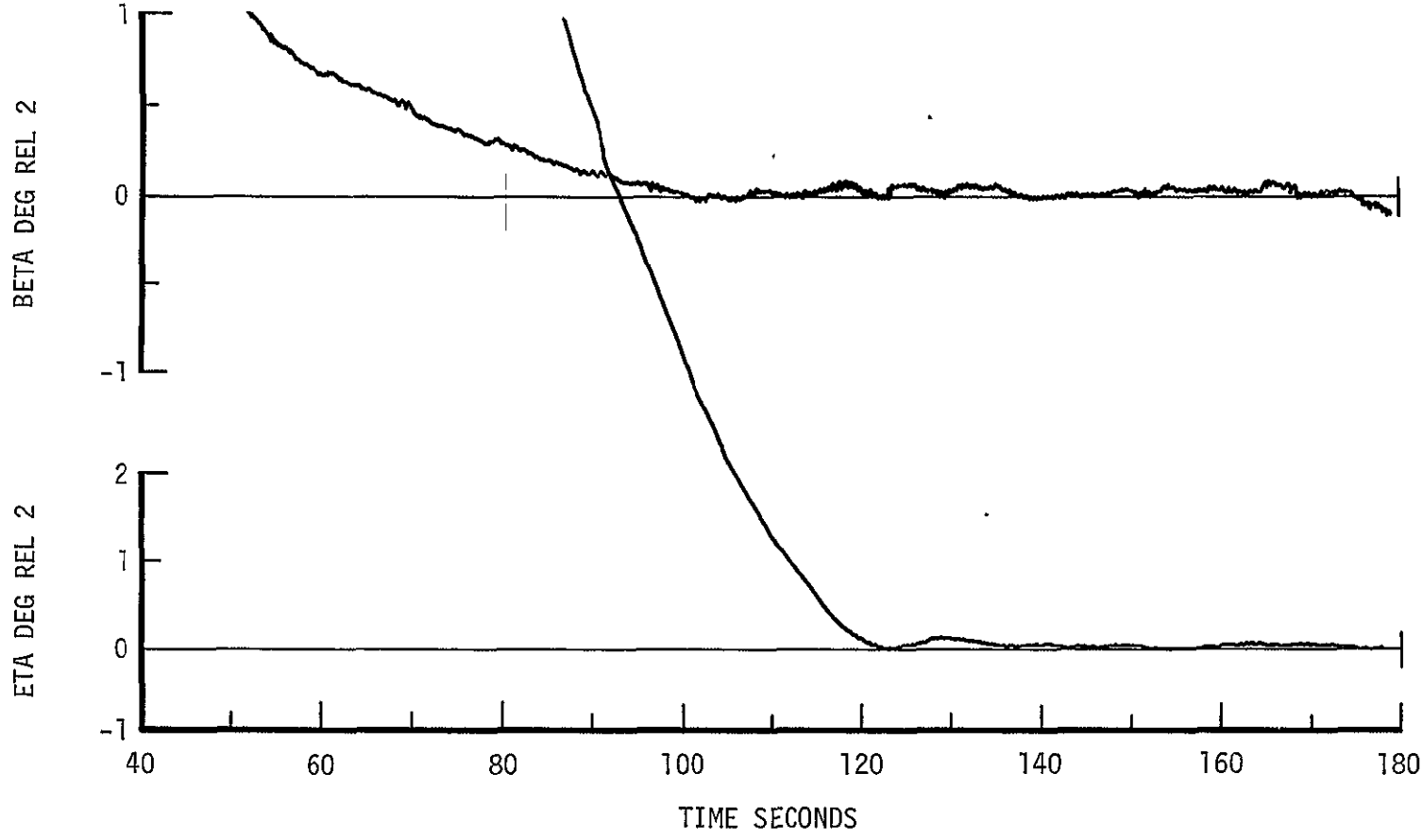

FIGURE XVI-7 η AND β CALCULATED USING RAW EL-2 DATA

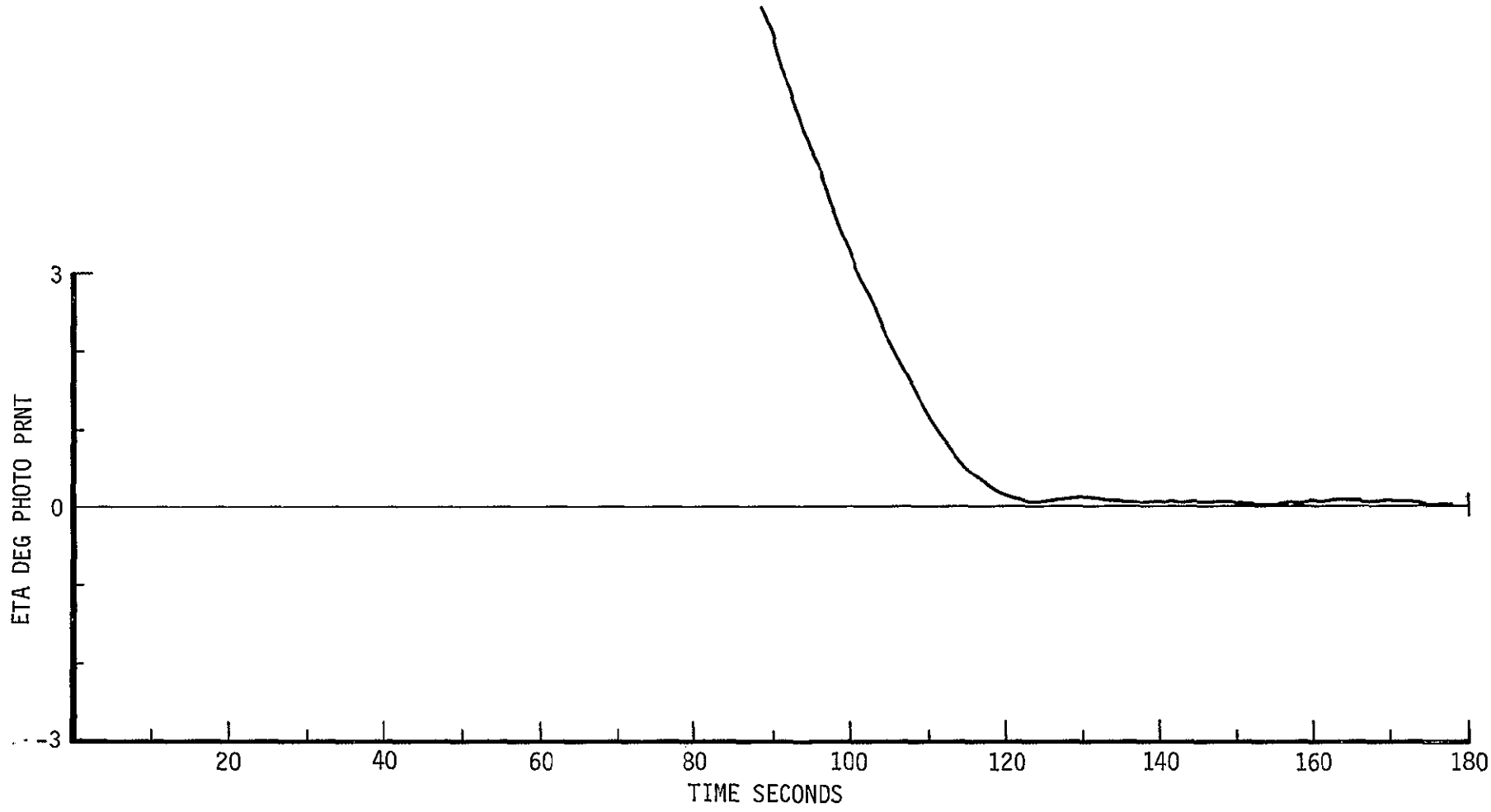

FIGURE XVI-8 n CALCULATED FROM REAL TIME PHOTOTHEODOLITE DATA

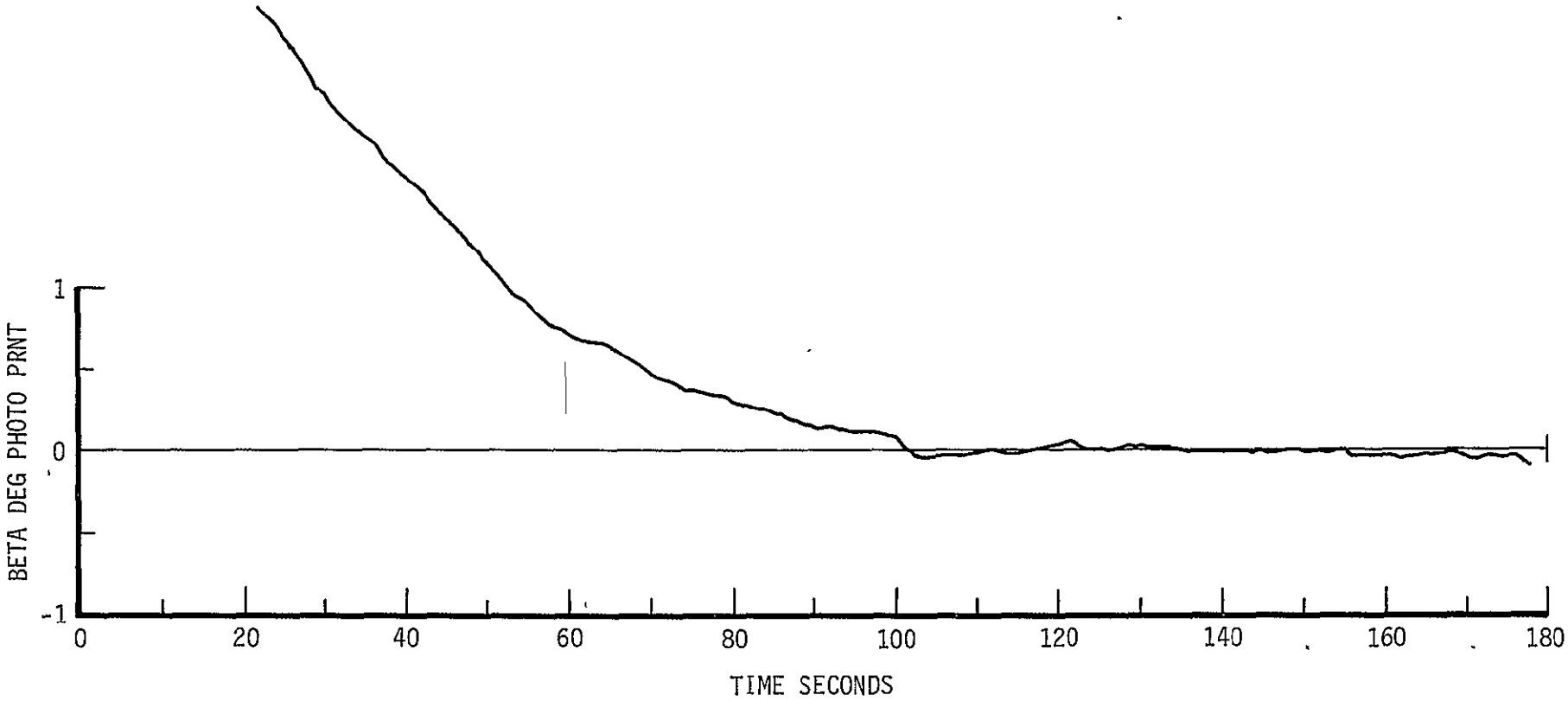

FIGURE XVI-9 β CALCULATED FROM REAL TIME PHOTOTHEODOLITE DATA

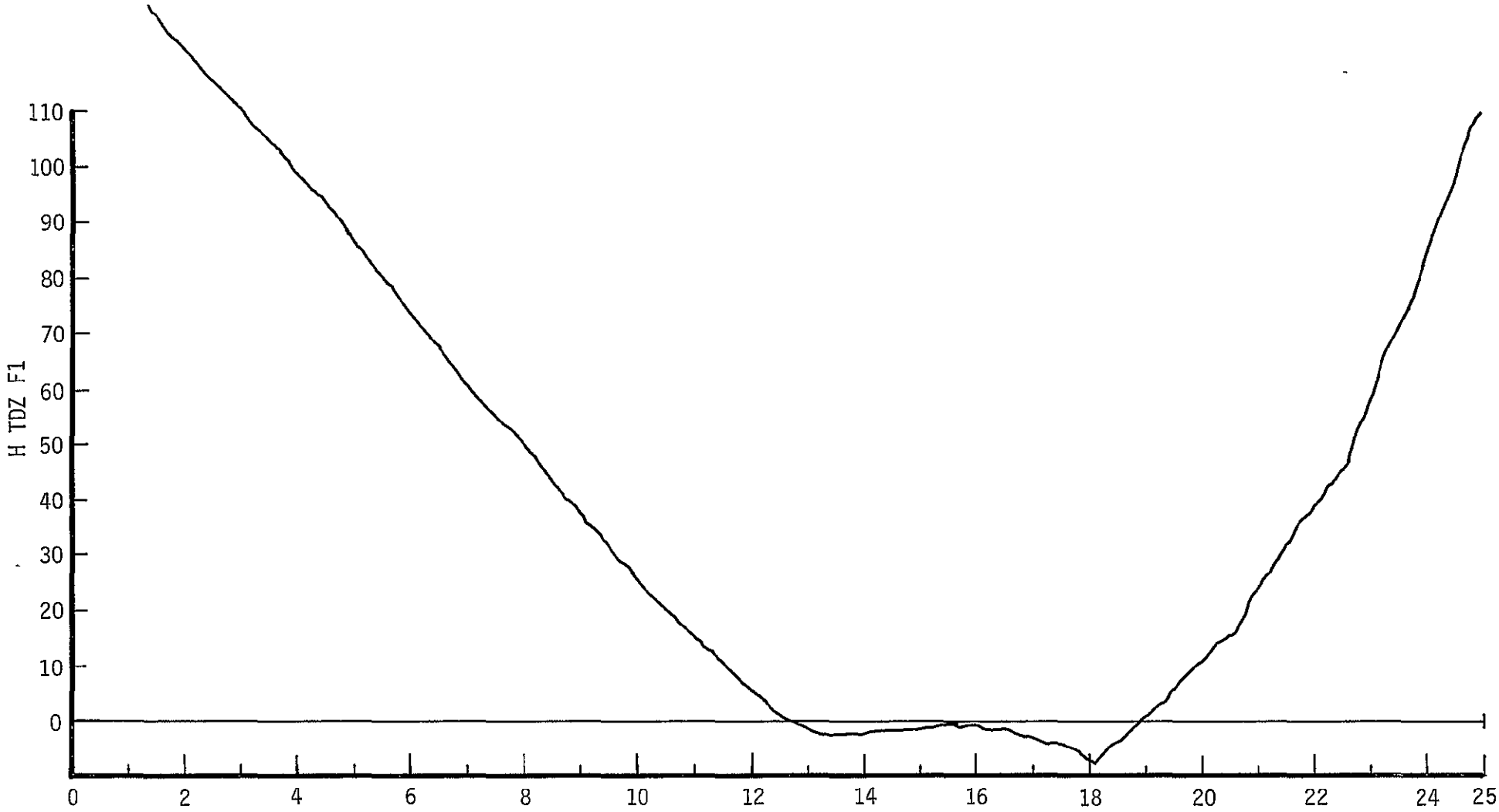

FIGURE XVI-10 H_{TD} CALCULATED USING FILTERED EL-1 DATA

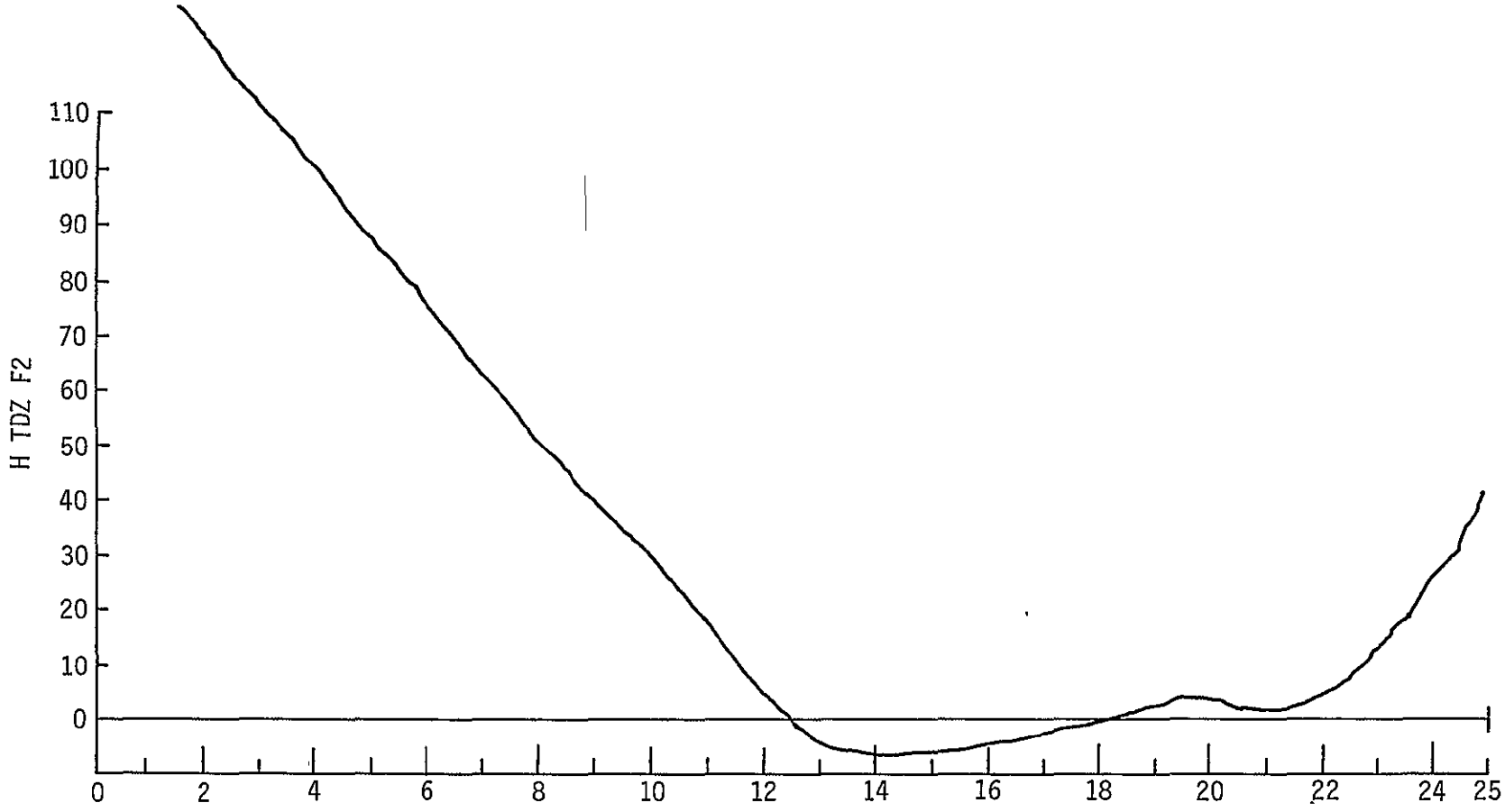

FIGURE XVI-11 H_{TD} CALCULATED USING FILTERED EL-2 DATA

XVII. - FLIGHT SYSTEM PERFORMANCE

by Thomas M. Walsh

INTRODUCTION

The demonstration of the U.S. National MLS to the All Weather Operations Panel (AWOP) of the International Civil Aviation Organization (ICAO) took place at the FAA's National Aviation Facilities Experimental Center (NAFEC) in May 1976. During this demonstration the MLS was utilized to provide the TCV B-737 research airplane with guidance for automatic control during transition from conventional to MLS area navigation in curved, descending flight and in flare, touchdown and roll-out. It is the purpose of this chapter to describe the operational aspects and performance achieved during the demonstration. Flight profiles, system configuration, and operating procedures used in the demonstrations are described, and performance results of the automatic flights are discussed.

The demonstrations to the ICAO of automatic flight performance of a transport type aircraft on complex MLS paths consisted of a large number of replicated flights in the same basic configuration. With these data as a basis, airplane flight performance can be analyzed statistically on an ensemble basis across similar runs, rather than along the time axis as is more customarily done with limited data replication. Mean and deviation type data are presented for airplane approach tracking parameters. Finally, these flights were conducted in rather adverse wind conditions. Hence, this atmospheric environment will also be described using three-dimensional wind vector characteristics computed from the extensive on-board sensor data.

APPROACH PATHS

The prescribed approach paths flown during the demonstration are shown in Figure XVII-1 and consist of two paths typical of the types of curved, three-dimensional complex paths which might be used to reduce overflight over noise-sensitive areas, or eliminate congestive or interfering flight traffic patterns. The first prescribed approach path was called the 130°-turn approach because of the curved, descending 130° left turn onto a short, three mile final approach. The second prescribed approach path consisted of two opposite 90° turns separated by a short intervening straight segment prior to the final approach turn, and was designated the S-turn approach. Both of these prescribed approach paths started at a nominal altitude of 4,000 feet and descended to the runway at a local 3° angle.

As seen in Figure XVII-1, take-off for the 130°-turn approach path was from runway 4 with the airplane controlled manually from the front cockpit —

during take-off. Shortly after take-off, control was shifted to the aft cockpit, where a manual control wheel steering (CWS) mode was selected by the AFD pilot. Prior to encountering the first way point, the AFD pilot selected a 3-D automatic area navigation (RNAV) mode for airplane control. This control mode used inertially smoothed DME/DME as the source of guidance information. Altitude was maintained at 4000 feet until the way point indicated by "Begin 3° descent" was passed. From this point the airplane continued descending 3° until flare was initiated. After crossing the Az boundary and approximately 15 seconds after crossing the EL1 boundary, the pilot received an indication of valid MLS data, at which time he selected the MLS RNAV mode which used MLS data as the source of guidance information. This latter event is noted as "MLS enable" in Figure XVII-1. Just prior to entering the final turn, the pilot selected Land Arm. The airplane continued to fly in the MLS RNAV mode until both selected glide slope and lateral path were acquired; then the control of the airplane was switched to autoland for control along the 3 nautical mile final approach. At an altitude consistent with the sink rate and altitude criteria of the flare laws in the autoland mode, flare was initiated. Flare was executed using EL2 and DME data as the source of vertical gudidance information on most of the touchdowns. On a few flights during the demonstration, a radio altimeter was used as the source of vertical guidance information for comparison purposes.

The events along the S-turn profile are very similar to the events of the 130°-turn profile. It may be noted that the S-turn profile resulted in a greater time period of MLS RNAV than did the 130°-turn profile. On touch-and-go approaches, control was switched from aft flight deck automatic control to front flight deck manual control for the take-off portion of repeat flights. On landings that continued to a full stop, roll-out was conducted in an automatic mode that used the Az beam for runway centerline guidance information.

A typical demonstration flight consisted of five approaches: four 130°-turns and one S-turn. Of these five approaches, the first four were touch-and-go landings while the final one was a full stop with roll-out guidance on the runway. All automatic approaches continued through flare, decrab, touchdown, and roll-out. In total, over 50 separate automatic approaches were conducted during this demonstration. It should be noted that approximately 150 additional automatic approaches were conducted at NAFEC during pre-demonstration development flights and post-demonstration flight experiments (Reference XVII-1). Over 40 manually controlled approaches were also flown after the demonstration using the advanced displays of the TCV B-737.

DATA ACQUISITION SYSTEMS

The TCV B-737 on-board, real-time data acquisition systems consisted of the Piloted Aircraft Data System (PADS), the Flight Control Computer (FCC) data formatter, and the Navigation Computer Unit (NCU) output bus. The TCV

B-737 PADS constitutes a general purpose data acquisition and retrieval system. For the MLS flight demonstrations, the PADS was configured to digitize at the rate of 40 samples/second. The basic word length is 10 bits per word. Data recorded on this data acquisition system originate in the MLS Processor, the NCU, the FCC, and several dedicated instrumentation transducers located throughout the airplane. The data formatter receives digital inputs from the Flight Control Computer Interface Unit (FCI) and reformats them into a serial digital signal that is recorded on wideband magnetic tape. Twenty-five different triplex sets of FCC sources are selectable for recording. The sample rate of this data acquisition system is approximately 20 samples/second with a 16 bit word length.

On-board data are also acquired from the data output bus of the NCU. This ARINC 561 format data bus is software controlled within the NCU. The sample rate of this system is approximately 8 samples/second with a word length of 24 bits. Outputs of these three data acquisition systems were recorded on wideband magnetic tape.

The NAFEC phototheodolite tracking system was employed to optically track the aircraft during the initial and final approach phases. Position information in an orthogonal coordinate system with origin located at the center of the MLS azimuth antenna array was derived from tracking elevation and azimuth angles from at least two and usually three tracking towers. These data were digitally filtered to reduced the noise level of the position information. The sample rate of the theodolite data is 10 position samples/second.

DATA ORGANIZATION AND PROCESSING

The MLS demonstration consisted of numerous flights on either of two specific prescribed approach paths, with the configuration of the TCV B-737 experimental systems remaining unchanged throughout. Because of the unusally large numbers of flights, it becomes meaningful to ask what the average values and statistical variations of the flight parameters were. In other words, the flight data acquired constituted a data base suitable for across-approach ensemble statistical analyses.

However, several fundamental obstacles had to be circumvented before statistical summarization. First, the time-referenced data describing any single approach were contained on four physically separate magnetic tapes at different sample rates. Data from these four sources had to be combined on a single storage device with a common time index. Secondly, after the data sources from a specific approach were correlated, there was still no means to readily align the data from separate approaches. Ground speeds were not the same from one approach to another. Consequently, a given time interval did not correspond to the same distance along the approach path from one approach to another.

Without a common independent or reference variable it was difficult to compare performance on one approach with that of another approach at an equivalent point on the prescribed approach path. To facilitate this comparison, an independent variable which was common to all approaches was defined.

The occurrence of most events during an approach was systematically correlated to the progress or position along the prescribed approach path. Since only two different prescribed approach paths were utilized during the demonstration flights, a reasonable independent variable with which to correlate data between flights on the same approach was the distance from the glide path intercept point along the prescribed path.

The value of this independent variable, L, was defined to be the point on the prescribed path closest to the actual tracked position as shown in Figure XVII-2. With the data subsequently referenced to points along the prescribed path, data corresponding to a particular point on the approach could be calculated by a linear interpolation. Consequently, for each of the two approach paths all the respective flight data could be compared at common spatial points. In addition, since all flights had identical final approach segments, this final data set consisted of all approaches combined. This process is illustrated graphically in Figure XVII-3.

To recapitulate, it was desired to compare performance data from similar approaches. To do this, the basic time-referenced data were transformed to a distance reference. The chosen distance reference was the scalar distance from the glide path intercept point (GPIP) along the prescribed approach path. With the resulting distance-referenced data base, statistical analyses of the flight data could be performed across the set of similar approaches at equivalent points along the prescribed approach paths. For example, the mean value of some variable at a specific distance from the GPIP could be readily calculated at relatively small intervals along the initial and final approach segments, resulting in mean and standard deviation descriptions that appear to be almost continuous along the prescribed approach path.

It is important to note that this across-run, ensemble approach was necessary because the system characteristics are not stationary in a statistical sense: gains, sensitivities, modes, and control laws vary with progression along the approach path.

PATH TRACKING PERFORMANCE

The automatic flight control system operation during the MLS portion of the approach consisted of two segments. The outer curved position prior to final approach was flown in an area navigation mode while the straight final approach through flare, touchdown, and roll-out was flown in an autoland mode. The guidance control laws associated with each of these

modes were substantially different. Concurrently, there are two sets of lateral and vertical deviation variables, one set corresponding to each of these two guidance modes.

Figure XVII-4 presents the lateral guidance signals for a typical 130°-turn approach culminating in a full stop landing. The upper trace is the lateral deviation from the prescribed path during the area navigation mode and the lower trace is a similar deviation for the autoland portion. It should be noted that these two quantities are defined with reversed signs, as indicated on the left of the figure. The independent variable is the along-path distance from the glide path intercept point, GPIP. The path length in this figure corresponds to the interval starting from about 8 nautical miles out and ending about 2/3 nautical miles past the GPIP. The change to autoland operation occurred at approximately L = 19,000 feet from the GPIP, shortly after completion of the turn to final.

The initial value of lateral deviation, XTK, at TRSB ENABLE (right-hand side) indicated an apparent error in tracking. This initial XTK deviation was the result of: (1) the transition from DME area navigation to the more accurate MLS area navigation, and (2) the initialization of the MLS Processor which produced transient MLS area navigation outputs. Frequently, in excess of 10,000 feet of path after TRSB ENABLE was required for the initialization transient for this particular filter to decay. This is exemplified in Figure XVII-4 by the rapid swing from an initial left (negative) XTK to a right (positive) XTK of approximately 125 feet.

Following the change to MLS autoland control laws, the lateral deviation is represented by the variable DELYSK. As illustrated in Figure XVII-4, the maximum values of DELYSK are much smaller than those of XTK. Also, the system dynamics indicated by the behaviour appear to be stiffer, with higher frequency components than are evident on the XTK signal. The tighter control of the airplane, as manifested by the decrease in the magnitude of the DELYSK guidance signal, was a result of the higher gains in the autoland localizer track control law.

Vertical path tracking performance for the same flight is shown in Figure XVII-5. As was the case for the lateral axis, two control laws were used during the MLS guidance portion of the approach. However, the point of transition from MLS area navigation to MLS autoland occurred earlier than in the lateral case. For this particular approach, transition occurred at approximately halfway around the 130° turn.

As in the lateral case, two variables represent vertical deviation: HER during area navigation and DELHSK during autoland operation. HER and DELHSK have reversed signs: positive HER means the airplane is below the prescribed approach path while positive DELHSK means the airplane is above the prescribed approach path, as indicated on the left side of Figure XVII-5. The disparity between the two vertical deviation variables at the transition point from one

control law to the other is primarily due to the difference in descent profiles. On the outer curved portion, the descent angle is 3^{o}, but measured with respect to the local vertical. On the inner portion, the descent angle is still 3^{o} but now measured along the extended runway centerline and with respect to the horizontal runway plane which is tangent to the earth's surface at the GPIP. The outer curved portion of the approach is above this 3^{o} glidepath angle, descending into it from the side during the turn to final. Consequently, the switch to autoland control laws prior to interception of the straight final approach course results in an apparent error above the course.

As stated previously, the demonstration flight series consisted of more than fifty approaches with more than forty of them being 130^{o}-turn approaches and about ten S-turn approaches. All valid tracking data for the 130^{o}-turn approaches were restructured and transformed to dependence on path length, as described earlier. With all similar approaches indexed in this manner the average deviation occurring at specific distances from the GPIP could be calculated. In fact, the average deviation was computed across the ensemble of 130^{o}-turn approaches at 200-foot intervals along the path starting at GPIP. This is shown for the outer segment of the 130^{o}-turn approach course in the upper portion of Figure XVII-6. In general, the beginning of valid data occurred at different points for the various individual approaches. Consequently, the right-hand side of Figure XVII-6 has greater variability (the progression of time along these approaches is from right to left). The lower portion of this figure shows the 2σ (twice the standard deviation) value of the deviation about the mean at the corresponding distances along the path. For distances further out than approximately 40,000 feet, the mean and 2σ values show the effects of MLS filter initialization transients. The mean deviation at 40,000 feet is about 60 feet to the right with a 2σ of almost 250 feet. However, during most of the 130^{o} turn to final the mean position is to the left side of path and somewhat closer. The tracking also becomes much less variable as indicated by the decrease of 2σ to about 70 feet. In other words, through the 130^{o} turn, the airplane tracked the computer path with a mean of less than 50 feet.

Similar data for the S-turn approach is shown in Figure XVII-7. Note immediately the absence of the initialization transient that was encountered for the 130^{o}-turn approach. Because of the particular geometry of the S-turn approach, the MLS signal processor received valid MLS data for a considerable distance prior to engagement of the MLS area navigation mode. Consequently, initial transients had subsided prior to the beginning of the MLS guidance usage. The mean and 2σ are somewhat less smooth locally because of perturbations of the mean lateral deviations. These deviations are generally less than 50 feet. The 2σ history also seems to be loosely correlated with the entries and exits of turns. In this case, the 2σ deviation about the mean is still generally 50 feet or less.

Mean and 2σ statistics for vertical deviation encountered on the 130^{o}-turn approach are shown in Figure XVII-8. From the right-hand side of this figure,

it appears that vertical error was also affected by either the filter initialization transient or the step increase in guidance accuracy, or both. Nevertheless, after the initial 6,000 to 8,000 feet, the maximum vertical position error is less than 20 feet and typically less than 10 feet. The 2σ value also remains less than 40 feet after the initial error decay.

Similar data for vertical deviation encountered during the S-turn approach are shown in Figure XVII-9. In general, the mean error and the 2σ deviation are smaller than the values resulting from the 130^{o}-turn approaches. The maximum mean vertical deviation is about 15 feet and occurs during the straight segment between the 90^{o} turns. The greatest 2σ deviation during the initial approach is about 30 feet from the mean. So far, both lateral and vertical deviation on the initial portions of both the 130^{o}-turn and S-turn approaches have been presented. The following paragraphs will consider these tracking deviations on the final approach segment.

Since the final approach segments of both approaches were identical, the data from both approach types were combined into a single data set. The lateral deviation variable for this segment is DELYSK which was computed in the MLS signal processor. This lateral deviation is presented in a slightly different form in Figure XVII-10. The center trace is the mean value as before. However, the 2σ value is added and subtracted from the mean giving both mean plus 2σ and mean minus 2σ traces. This is essentially the envelope within which the airplane normally remained. (The sign convention is reversed from that of XTK on the initial approach segment). At the right side of this figure the airplane has just completed the turn to final with an average overshoot to the right of less than 20 feet. The initial 2σ envelope is about 200 feet wide but collapses very rapidly to approximately 20 feet wide as the GPIP is neared. The distances of L = 3,800 and L = 2,000 feet correspond to heights of approximately 200 and 100 feet, respectively.

Careful examination of DELYSK at these positions reveals mean deviations of less than 7 feet and 5 feet, respectively, with associated 2σ dispersions of about 10 feet at both points.

The deviation variables presented thus far, XTK, HER, and DELYSK, were deviations computed from on-board receivers and sensors. As stated earlier, the ground-based theodolites at NAFEC were also employed to track the airplane.

In general, the independent theodolite tracking data agree well with the counterpart data generated on-board. The theodolite tracking data over the initial approach segments were often more variable than the on-board data largely because of weather-related obstructions to visibility and the absence of photo-correction to the theodolite data.

Figure XVII-11 presents the ground-tracked lateral deviation, DYA, for the final approach course. The sign convention of this variable is opposite that

of the on-board-computed DELYSK. Data over the final two nautical miles of the approach show very close correspondence between these two data sources. The on-ground data show a greater mean overshoot following the turn to final. Note also that the 2σ values increase substantially at about 16,000 feet from GPIP. This is probably due to an optical loss of the airplane by the ground tracking in this region during one or more of the approaches.

The final type of tracking data to be presented in this chapter is the vertical deviation of final approach as measured both on-board, DELHSK, and on-ground, DZA. These variables are shown in Figures XVII-12 and XVII-13, respectively. They exibit similar behaviour over the final two nautical miles or more. At the points corresponding to heights of 200 and 100 feet, mean deviations exibited by the on-board data appear to be less than a foot while the on-ground data show approximately three-foot deviations. In either case, the 2σ dispersion is less than 8 feet. The right-hand portion of these two figures show the vertical deviations during roughly the last half of the turn to final. Transition to the MLS vertical autoland mode occurred before intercept of the final approach course. Agreement between the two tracking variables is poorer during this portion of the turn to final. On-board data in Figure XVII-12 show an initial error above the prescribed path with a ramp-like correction back to path. This phenomenon is absent in the ground tracking data, Figure XVII-13. This completes the brief examination of the tracking performance of the NASA TCV B-737 during the flight demonstration of the MLS.

WIND ENVIRONMENT

These flights were conducted to demonstrate MLS performance to the ICAO. They were flown on a schedule contrained by demonstration considerations and were not flown simply for flight test data generation. Consequently, the flights were conducted in weather conditions more diverse and adverse than would normally have been encountered in engineering flight testing. As a result, it becomes important to quantify and characterize the wind environment so that its effect on the flight performance can be accounted for.

During the post-flight data processing the airplane's inertial velocity vector and the velocity vector relative to the air mass were computed. The vector difference between these is the wind velocity vector. Malfunction of one of the data systems precluded computation for about 40 percent of the flights. Figures XVII-14 and XVII-15 present the wind speed and direction during the final approach segment. Mean wind velocity at the start of the final approach is approximately 20 knots and decreases to about 15 knots in the vicinity of the runway threshold. Concurrently, the 2σ also decreases from about 15 knots to about 8 knots near the ground. Note that a wind velocity of 15 knots near the ground corresponds to a velocity exceeded only 15 percent of the time, according to the FAA and CAA certificatory documents (References XVII-2 and XVII-3).

Figure XVII-15 presents the corresponding mean and 2σ wind direction with respect to true north. The direction shown corresponds to the orientation of the wind vector, not the direction from which the wind is blowing. An average direction at low altitudes of about 50-60 degrees, as was the case during these flights, is especially significant since the runway direction was about 30°. Consequently, the average landing was flown with a left quartering tail-wind of about 15 knots. This is far above a normal situation; the FAA certificatory requirements on autoland systems are limited to 10 knots tail-wind at most.

CONCLUSIONS

This paper presents a brief summary of flight performance of the TCV B-737 Advanced Guidance and Control System (AGCS) operating in the MLS terminal area environment. The large number of flights in the same AGCS configuration during these demonstrations to the ICAO AWOP provided an unusual opportunity to analyze the flight performance on a statistical basis. In addition, the three dimensional navigation facility represented by the MLS presented another opportunity to examine flight on complex paths in the terminal area and to carefully assess the future operational potential of these kinds of flight paths for noise, congestion, and interference alleviation. Because of the extensive data gathering capabilities of the TCV B-737 in conjunction with the NAFEC theodolite, ground-based tracking facility, very thorough and accurate flight data recordings were available. A further unusual aspect of this MLS flight demonstration series was the presence of an exceptionally adverse atmospheric environment which was described quantitatively from the flight data.

Finally, the flight performance data presented in this paper represents only a small portion of the data resulting from these flights. Data from over fifty flights were recorded. From the extensive recorded data, thirty variables describing the airplane's flight performance were analyzed and are available. These data include navigation, guidance, control, and tracking variables from both on-board and ground-based sources, and a complete description of the atmospheric wind velocity vector throughout the initial and final approach regions. For each of these thirty variables, the mean, standard deviation, and histogram statistical descriptions are available. In addition, an individual along-path history of each variable for each of the 53 approaches is available.

Of equal importance to the automatic flight performance were the advanced displays that allowed the flight crew and observers to follow the flight situation and aircraft tracking performance very accurately from the aft flight deck of the TCV B-737 research airplane without outside reference (Reference XVII-1). Elements of these displays enabled the pilots to proceed after takeoff toward the initial waypoint of the flight profile, where automatic 3-D flight was initiated. During the initial phase of automatic 3-D navigation, elements

of the displays were driven by conventional navigation signals. Upon entering the MLS coverage region, MLS signals were used to drive the display elements for monitoring of the automatic control system performance during transition from conventional RNAV to MLS RNAV; curved, descending flight; final approach; flare; touchdown; and roll-out.

The flights demonstrated the utility of the wide area coverage of the MLS for curved, descending paths commencing with a standard RNAV approach into a terminal area and continuation of this approach throughout the MLS coverage area and onto the runway. The ability to fly precision curved navigation paths with use of MLS signals highlights the potential of this system for design of noise alleviation and high-capacity flight paths in a terminal area.

REFERENCES

XVII-1. Walsh, Thomas M.; Morello, Samuel A.; and Reeder, John P.: Review of Operational Aspects of Initial Experiments Utilizing the U. S. MLS. NASA SP-416, 1976.

XVII-2. "Automatic Landing Systems," FAA AC 20-57A, January 12, 1971.

XVII-3. "Airworthiness Requirements for Automatic Landing Including Landing in Restricted Visibility Down to Category 3," BCAR paper number 367, Issue 3, June 1970.

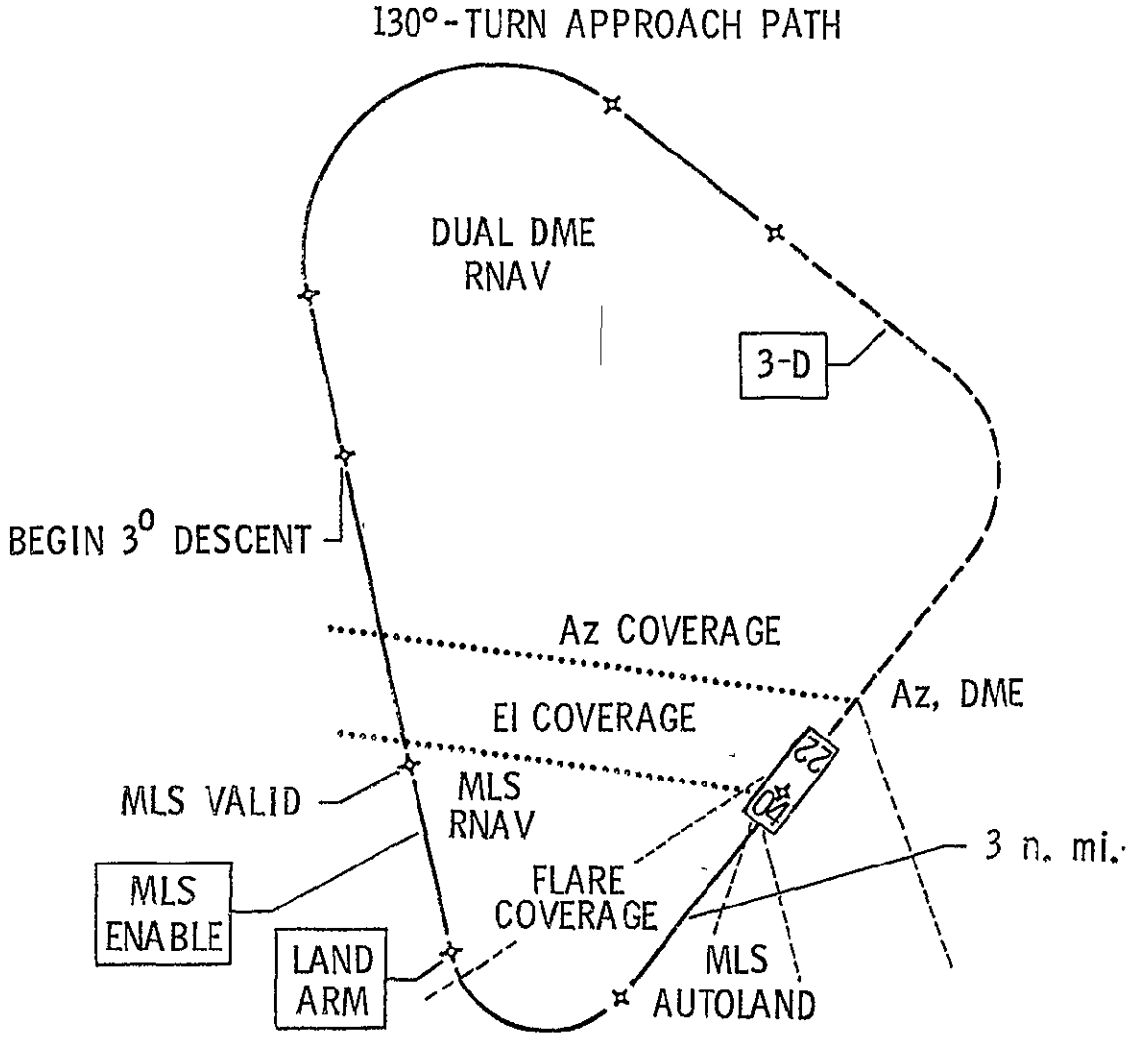

FIGURE XVII-1A MLS APPROACH PATHS

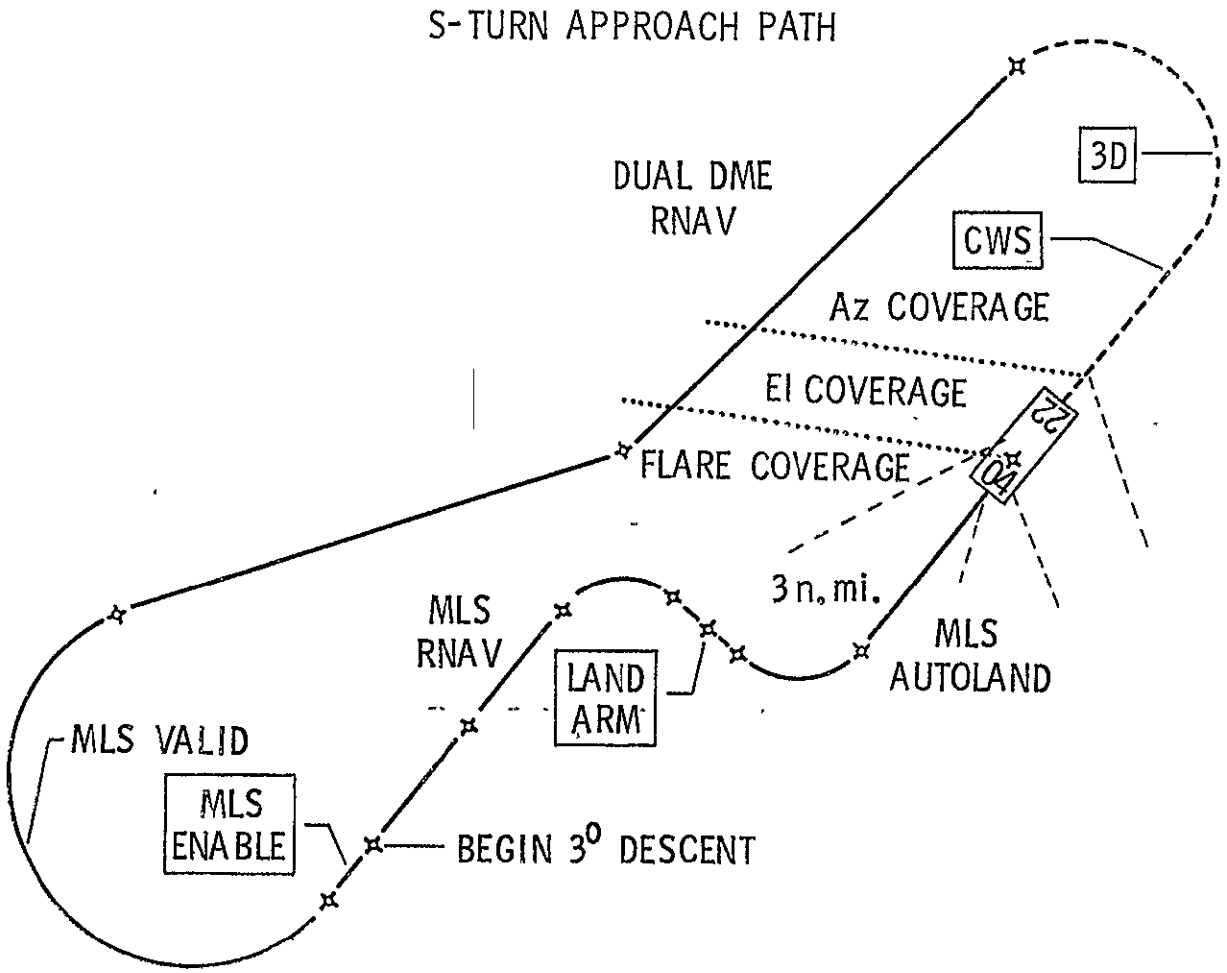

FIGURE XVII-1B MLS APPROACH PATHS

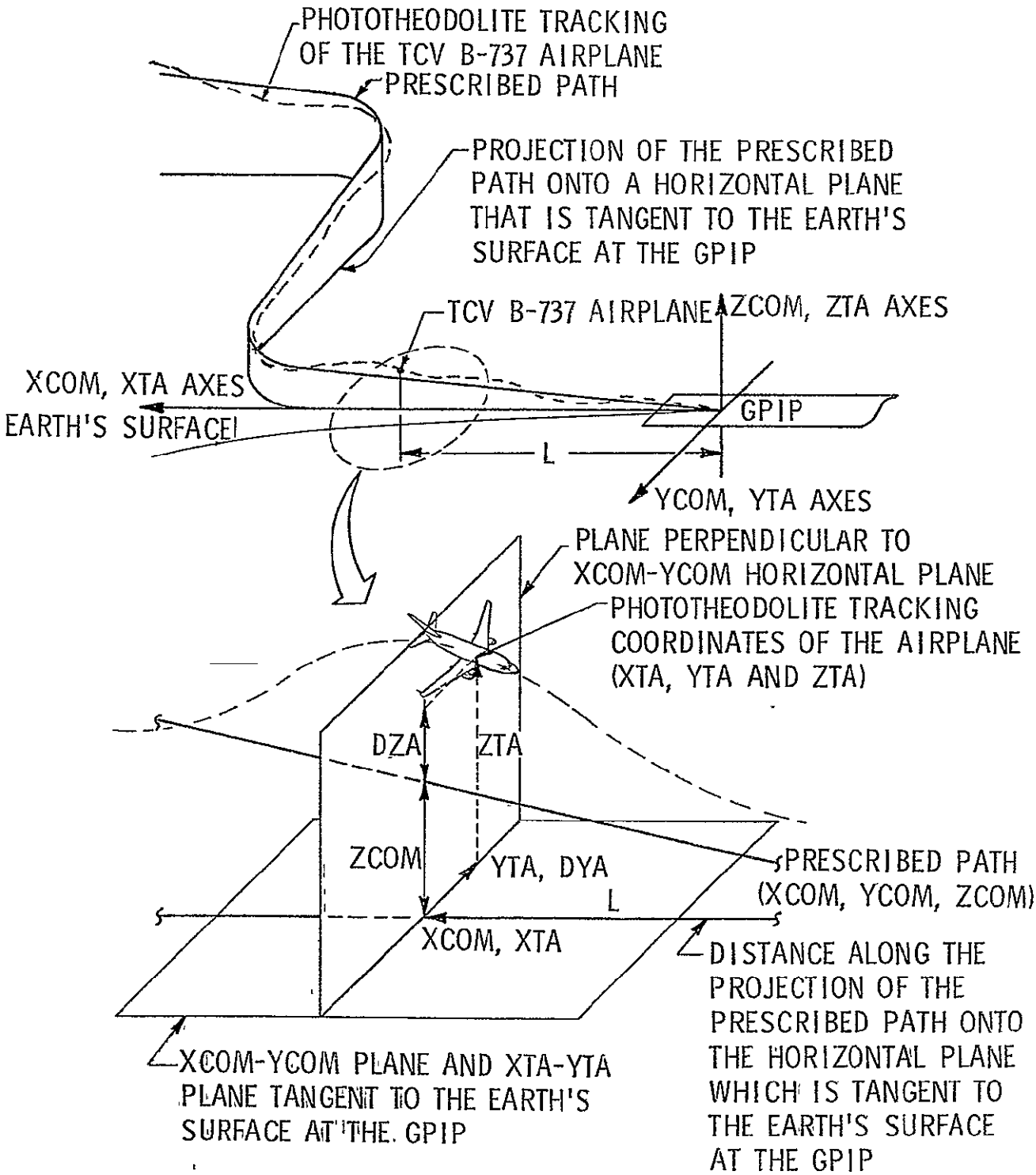

FIGURE XVII-2 DEFINITION OF L

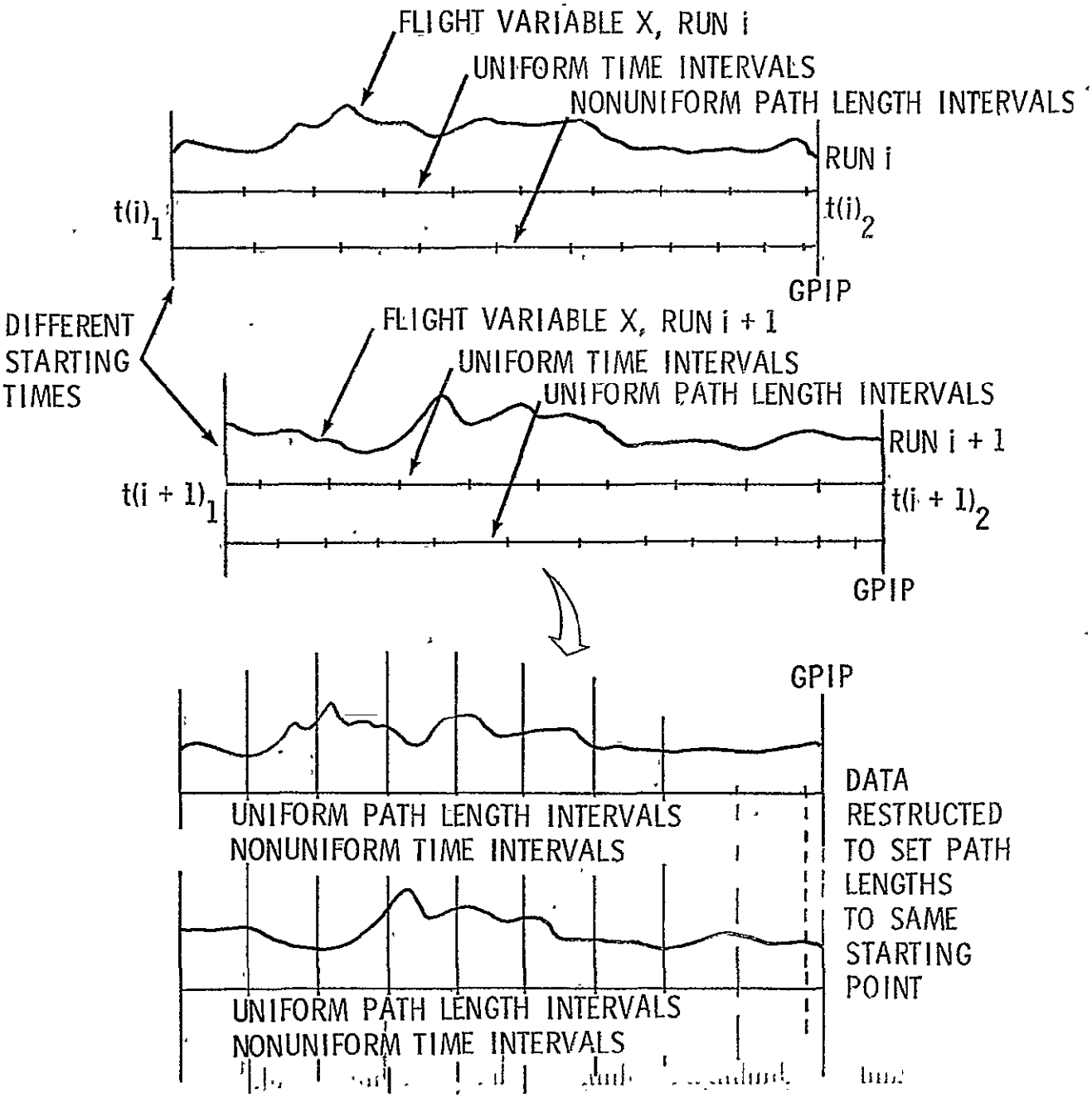

FIGURE XVII-3 FLIGHT DATA TRANSFORMATION FROM TIME TO PATH AND SUBSEQUENT RESTRUCTURED DATA ARRAY

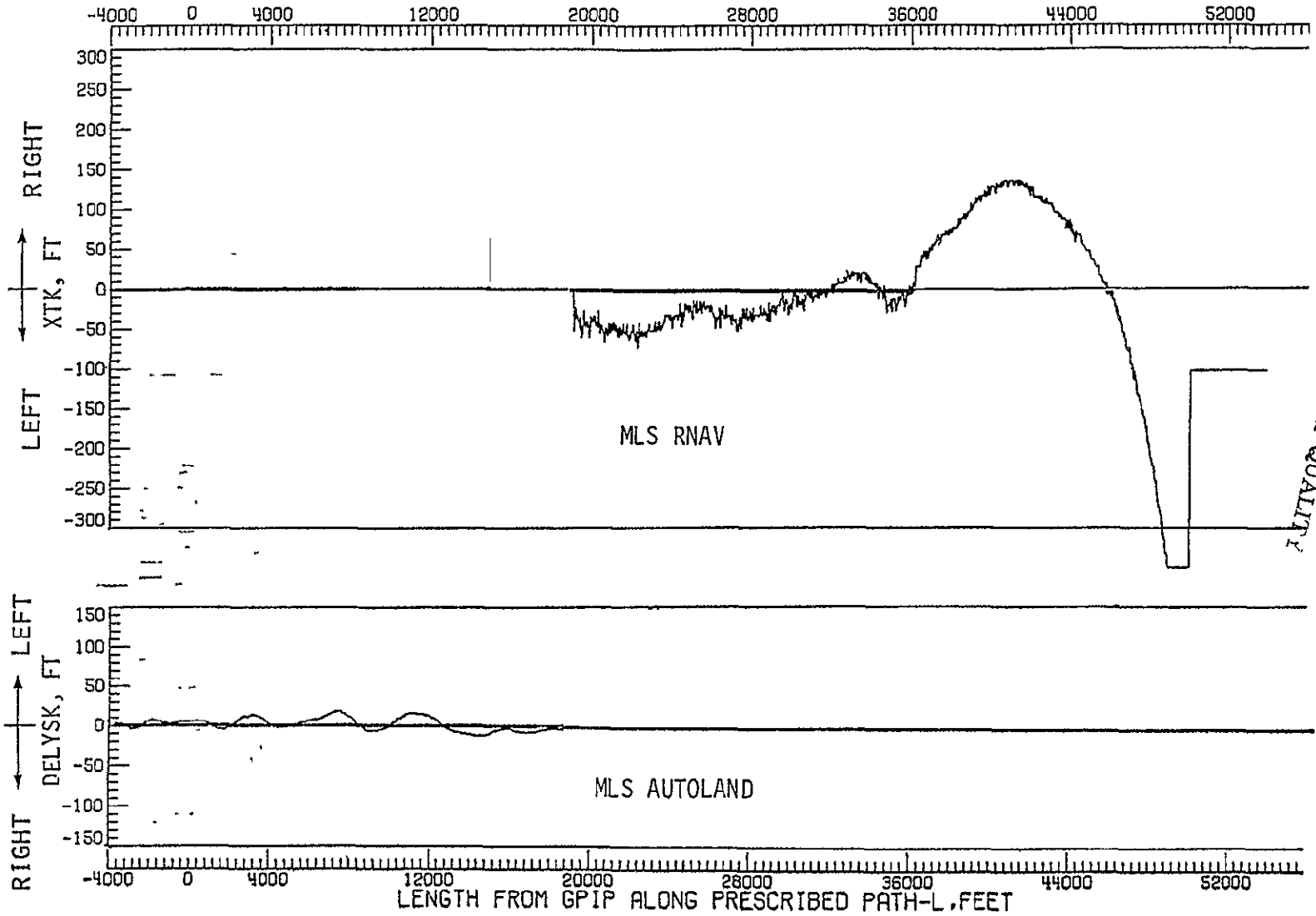

FIGURE XVII-4 L - HISTORY PLOTS OF XTK AND DELYSK, FLIGHT 122 RUN A5

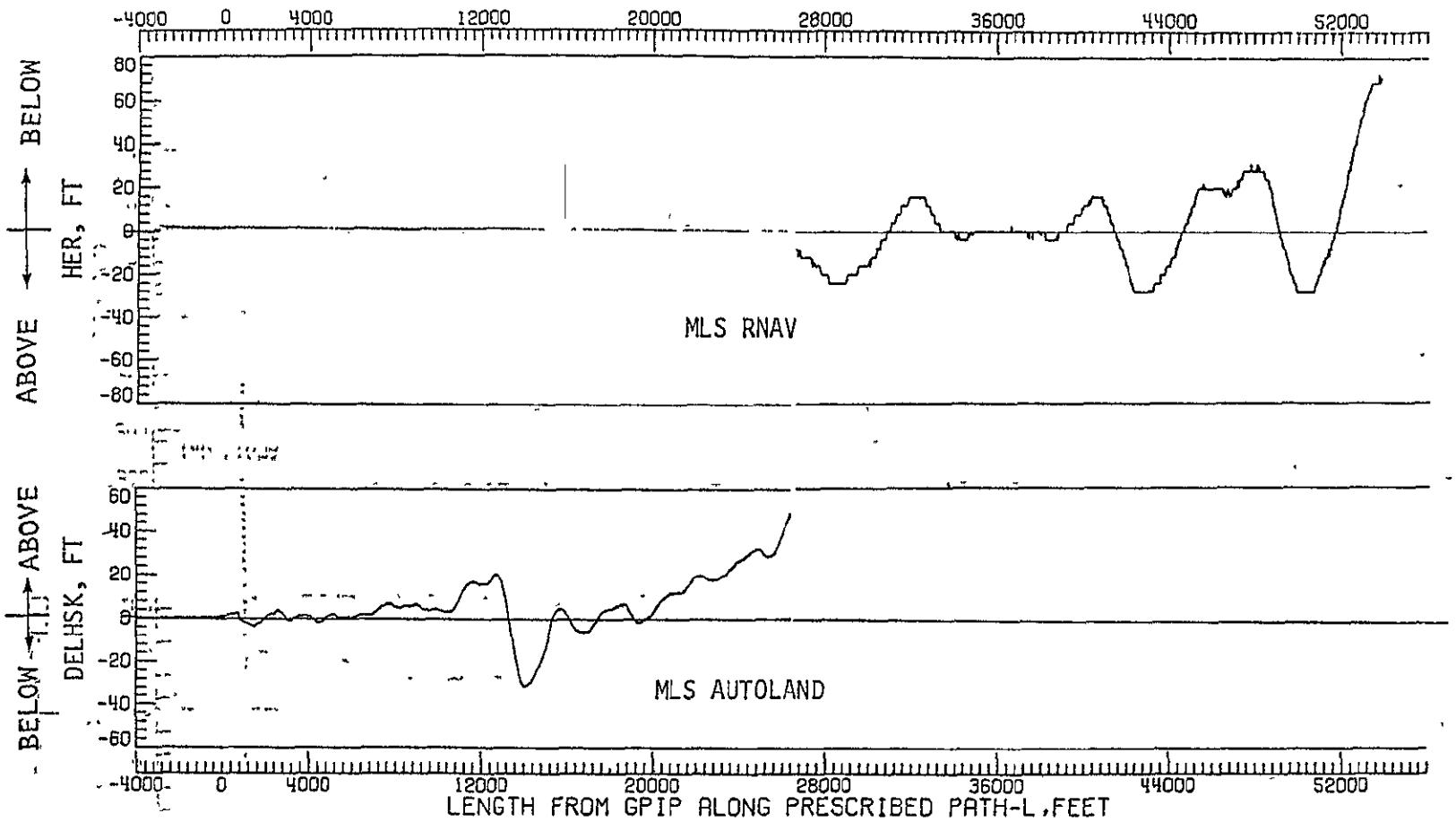

FIGURE XVII-5 L - HISTORY PLOTS OF HER AND DELHSK, FLIGHT 122 RUN A5

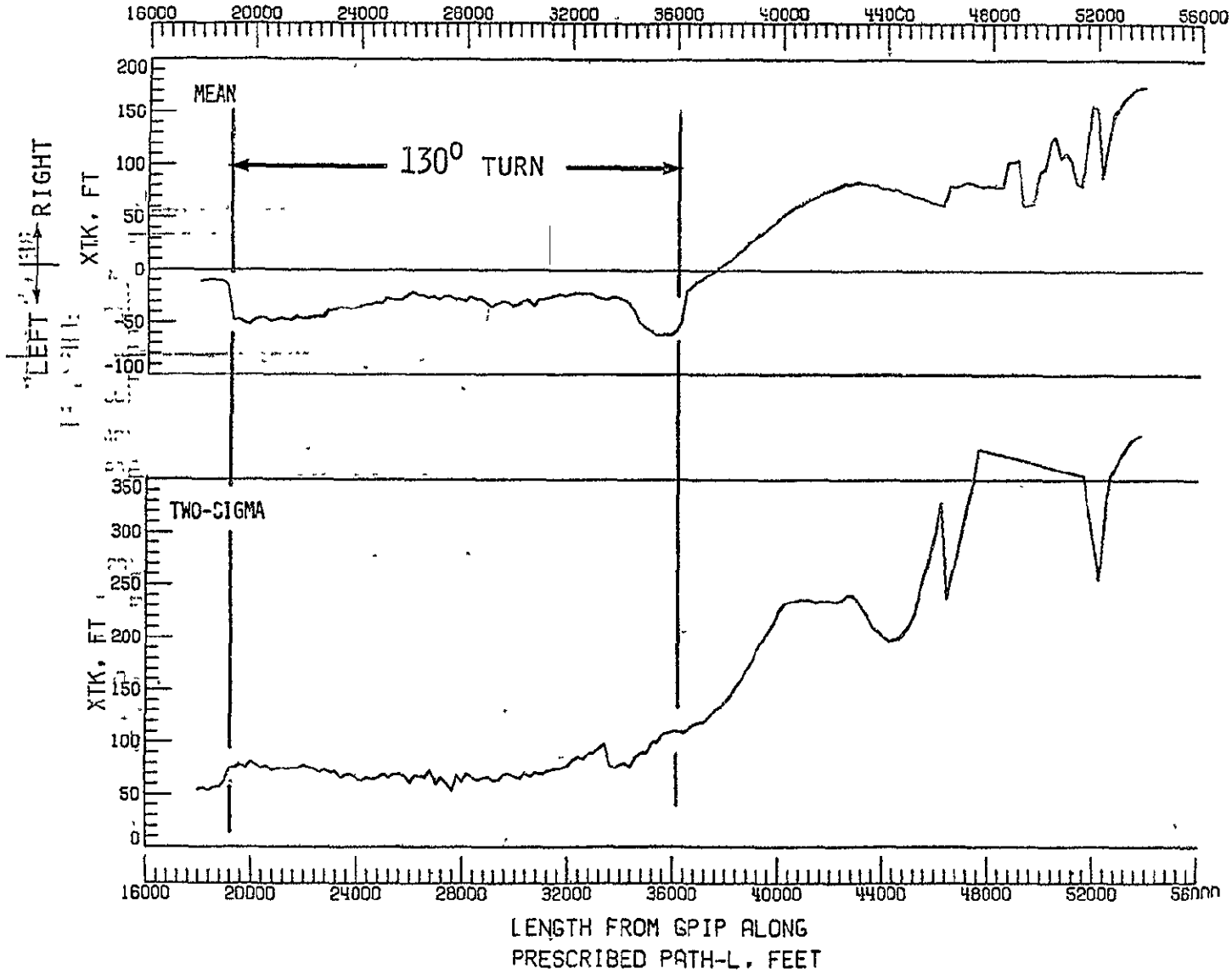

FIGURE XVII-6 XTK, MEAN AND TWO-SIGMA STATISTICS, 130 DEG TURN APPROACH

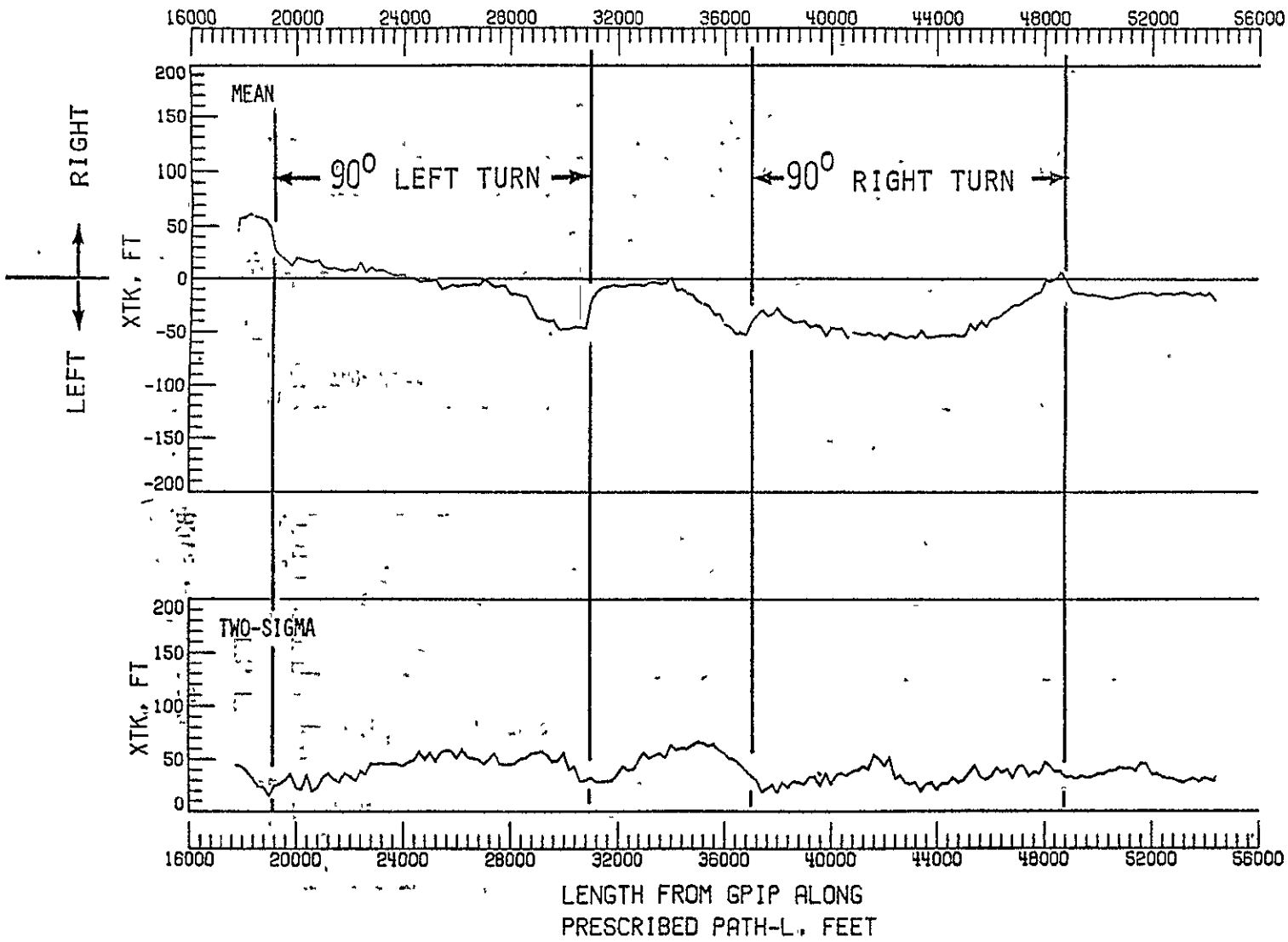

FIGURE XVII-7 XTK, MEAN AND TWO-SIGMA STATISTICS, S-TURN APPROACH

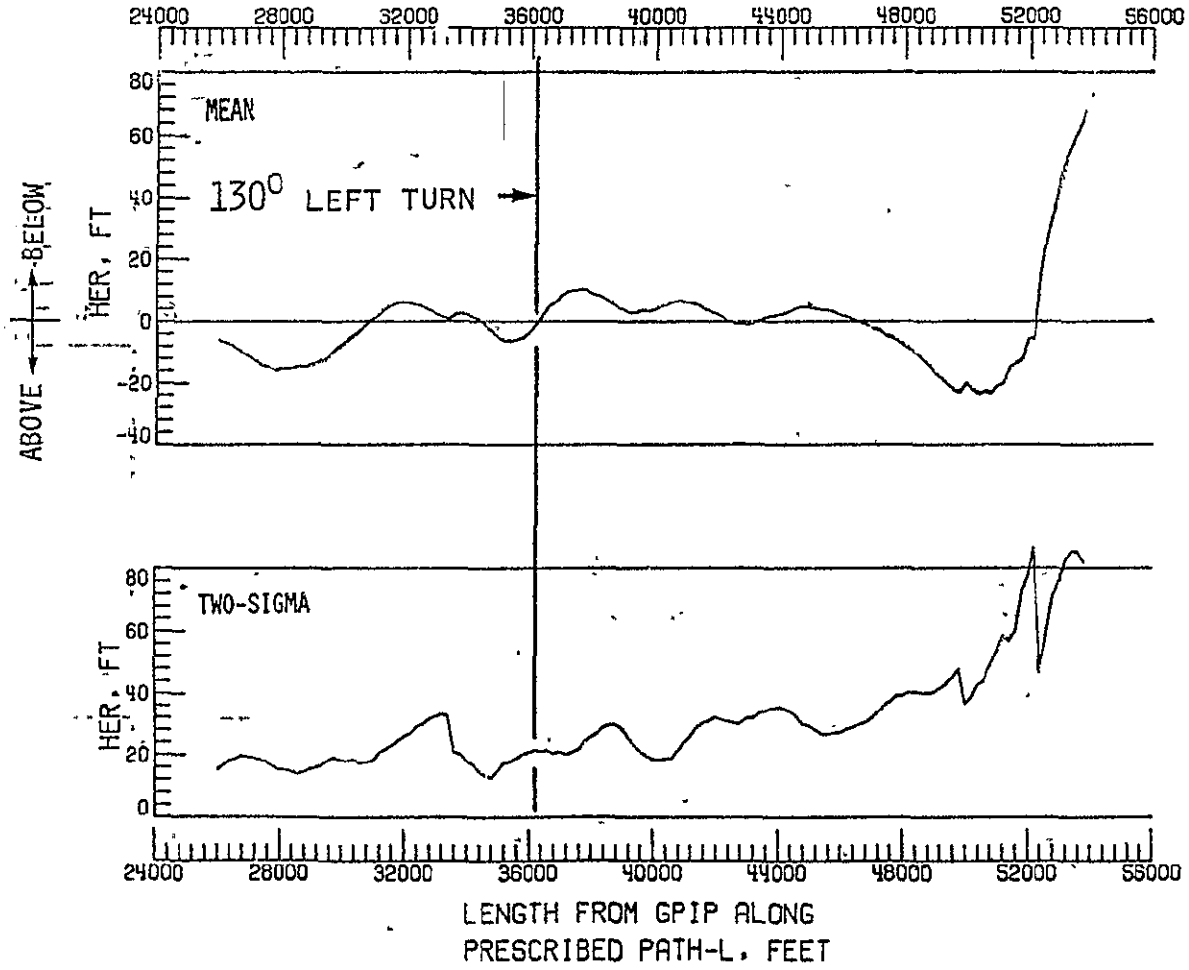

FIGURE XVII-8 HER, MEAN AND TWO-SIGMA STATISTICS, 130 DEG-TURN APPROACH

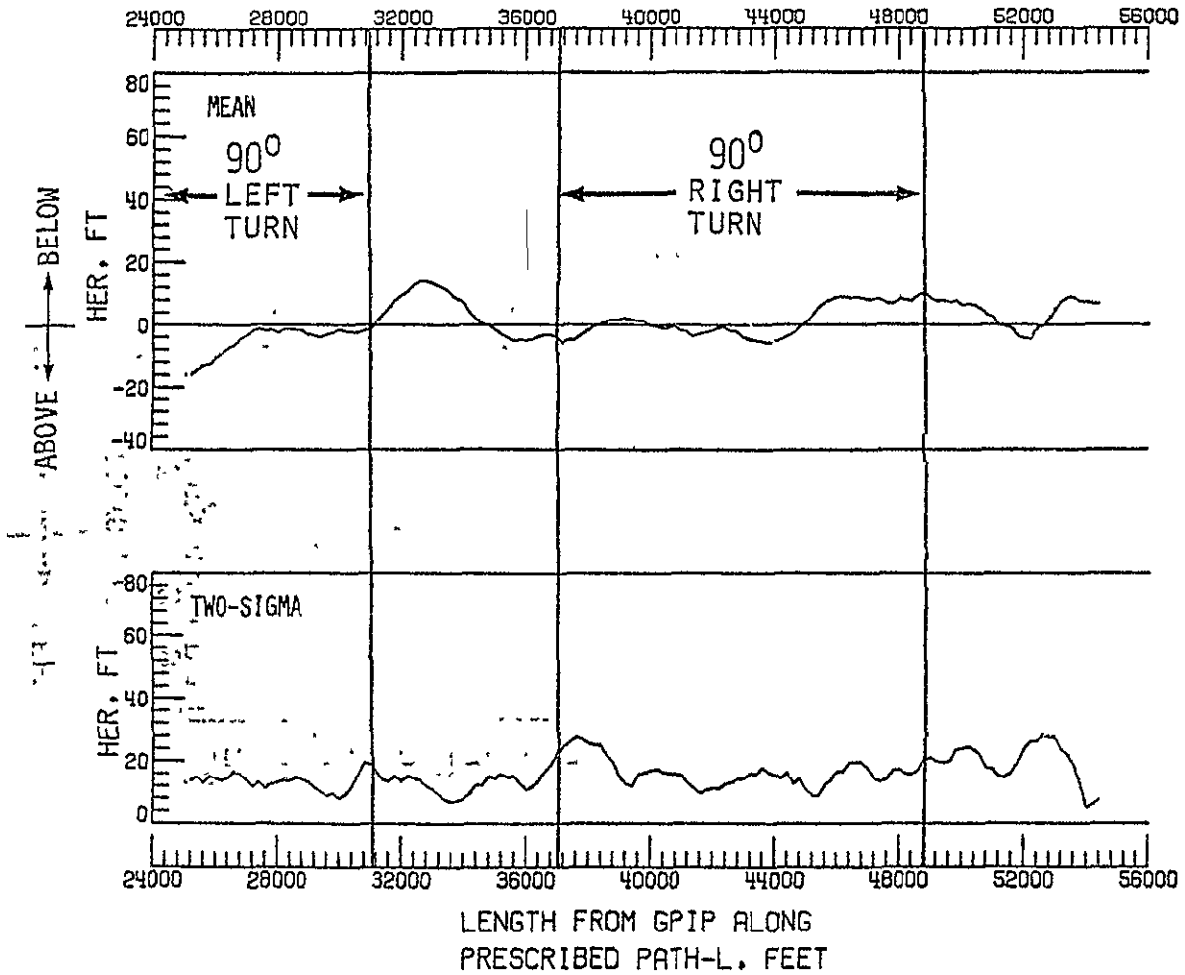

FIGURE XVII-9 HER, MEAN AND TWO-SIGMA STATISTICS, S-TURN APPROACH

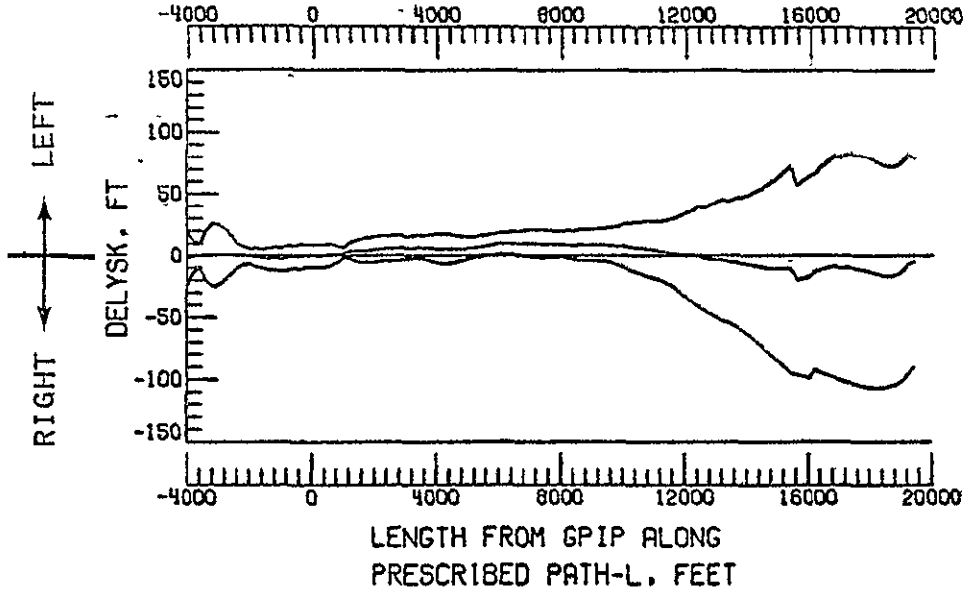

FIGURE XVII-10 DELYSK, MEAN AND MEAN ± TWO -SIGMA STATISTICS, FINAL APPROACH

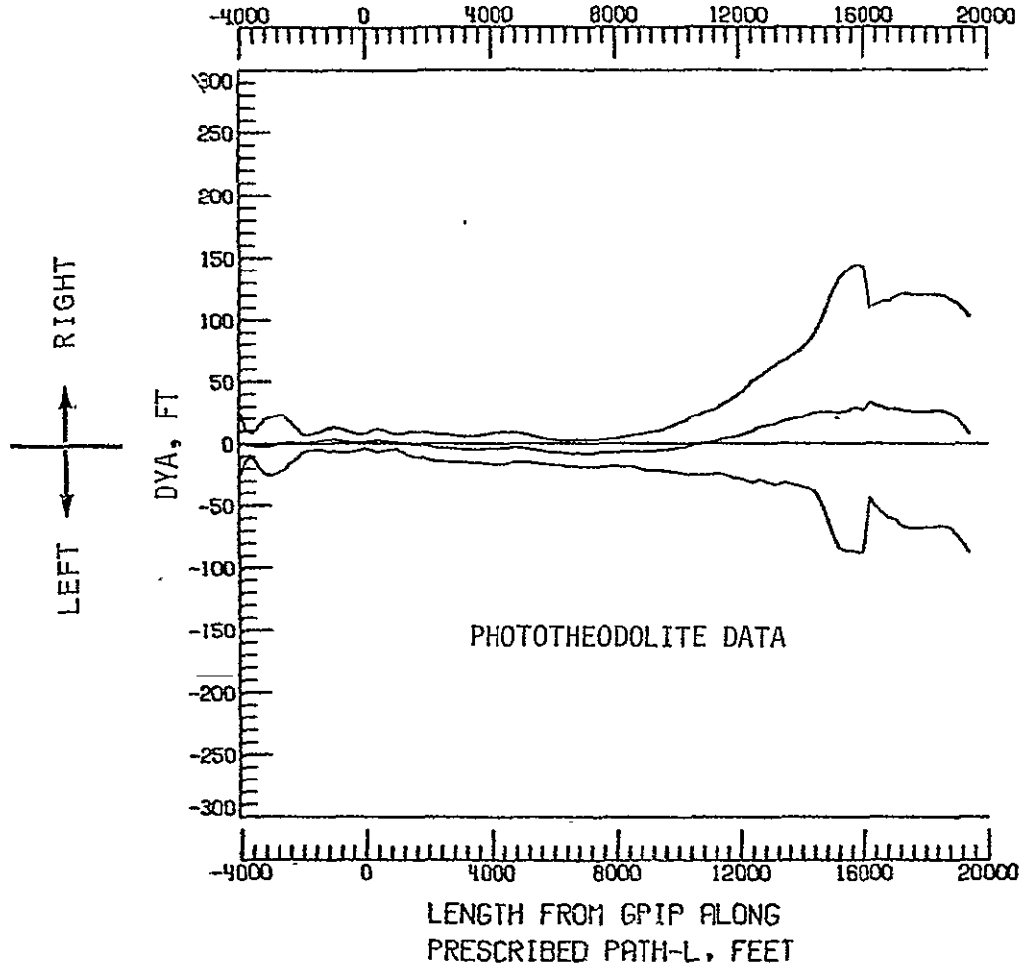

FIGURE XVII-11 DYA, MEAN AND MEAN ± TWO-SIGMA STATISTICS, FINAL APPROACH

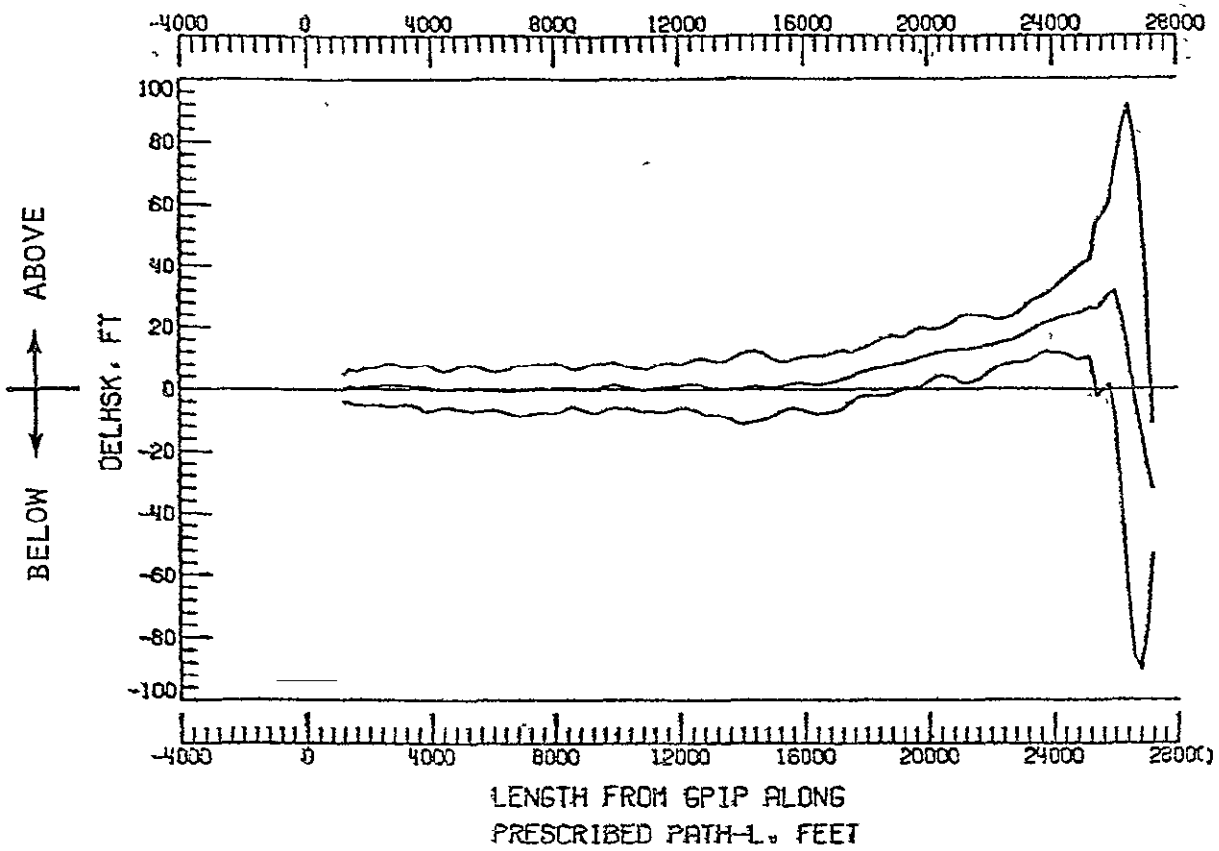

FIGURE XVII-12 DELHSK, MEAN AND MEAN ± TWO SIGMA STATISTICS, FINAL APPROACH

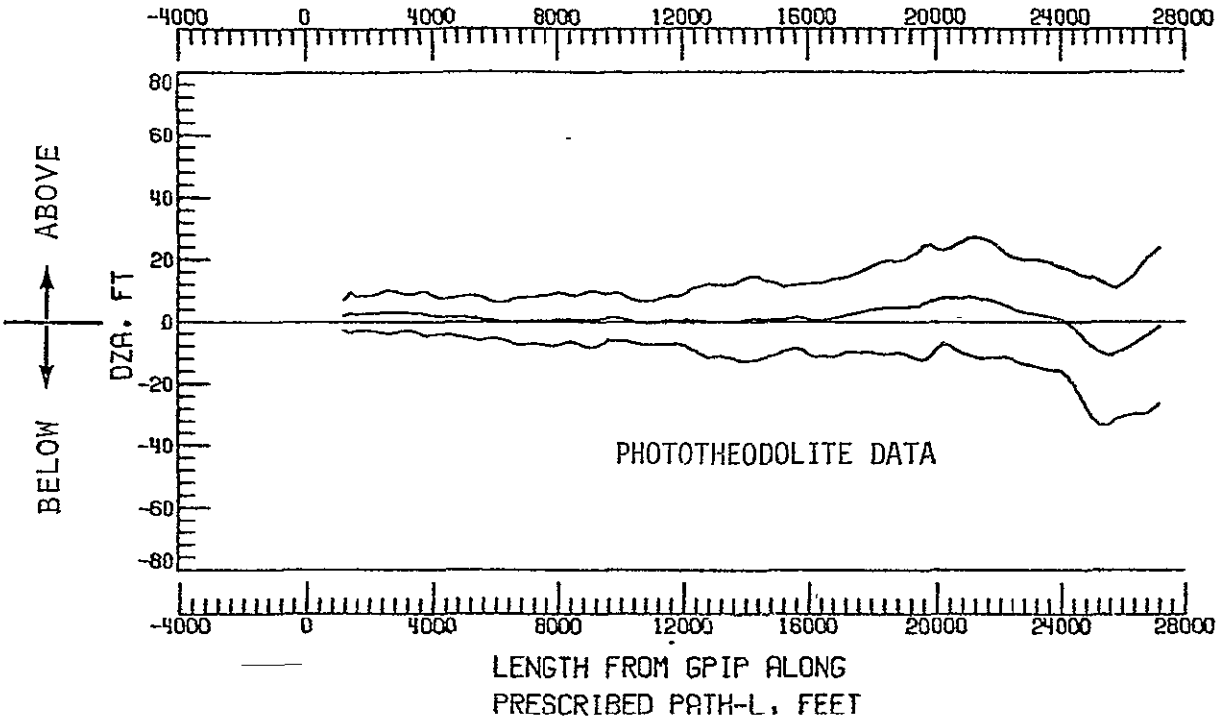

FIGURE XVII-13 DZA; MEAN AND MEAN ± TWO-SIGMA STATISTICS, FINAL APPROACH

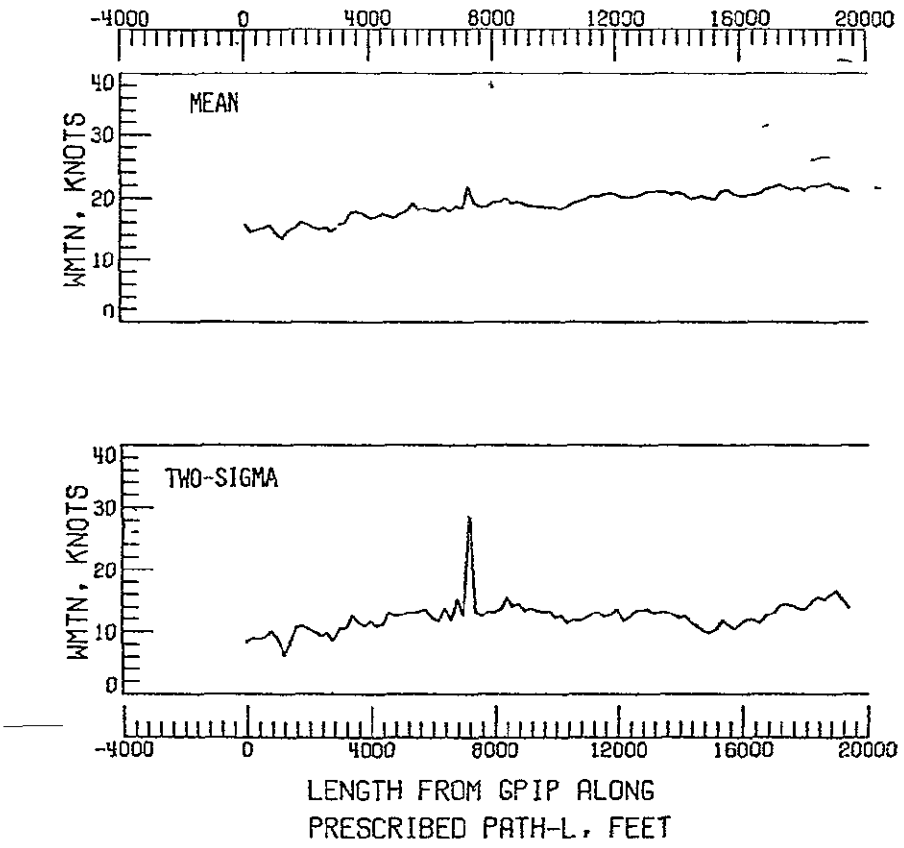

FIGURE XII-14 WMTN, MEAN AND TWO-SIGMA STATISTICS, FINAL APPROACH

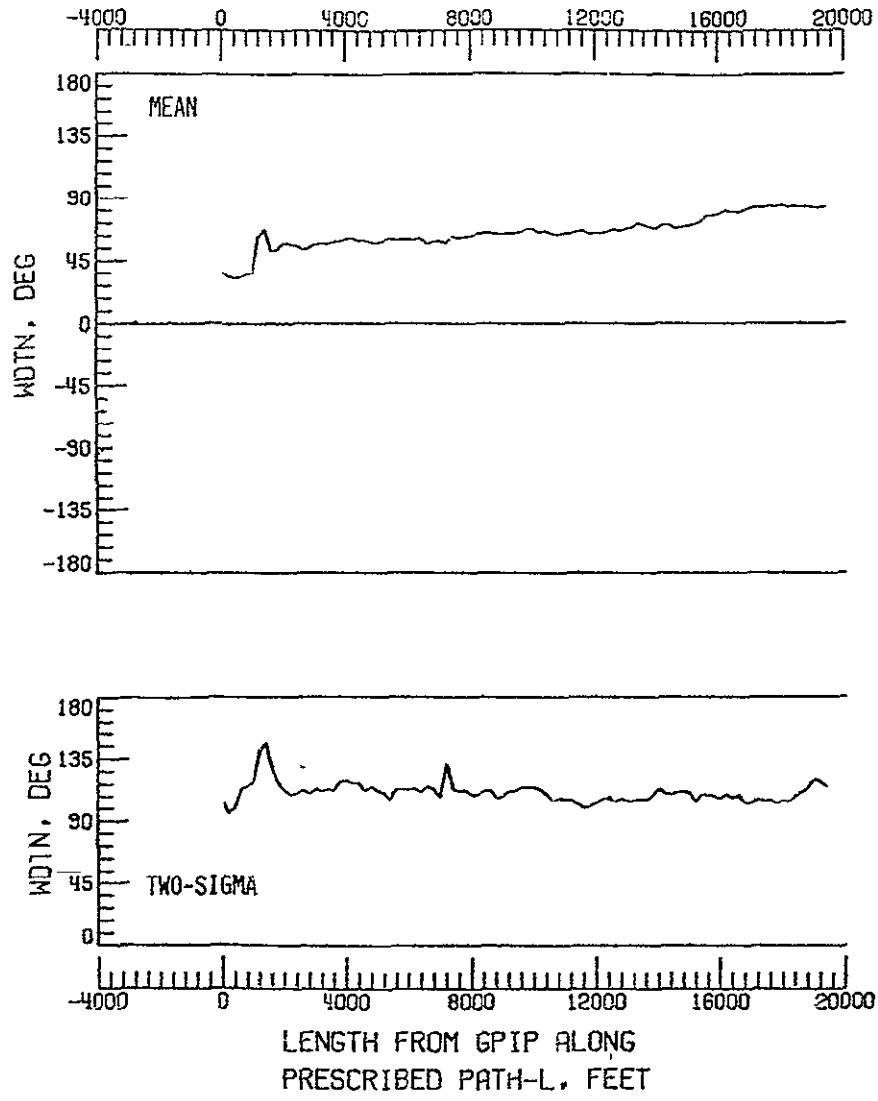

FIGURE XVII-15 WDTN, MEAN AND TWO SIGMA STATISTICS, FINAL APPROACH